Topics in the Stability of Localized Patterns for some Reaction-Diffusion Systems

by

Ignacio Rozada

B. Physics, Universidad Nacional Autónoma de México, 2004

M. Applied Mathematics, University of New Mexico, 2006

A THESIS SUBMITTED IN PARTIAL FULFILLMENT
OF THE REQUIREMENTS FOR THE DEGREE OF

Doctor of Philosophy

in

THE FACULTY OF GRADUATE STUDIES
(Mathematics)

The University Of British Columbia
(Vancouver)

May 2012

Abstract

In the first part of this thesis, we study the existence and stability of multi-spot patterns on the surface of a sphere for a singularly perturbed Brusselator and Schnakenburg reaction-diffusion model. The method of matched asymptotic expansions, tailored to problems with logarithmic gauge functions, is used to construct both symmetric and asymmetric spot patterns. There are three distinct types of instabilities of these patterns that are analyzed: self-replication instabilities, amplitude oscillations of the spots, and competition instabilities. By using a combination of spectral theory for nonlocal eigenvalue problems together with numerical computations, parameter thresholds for these three different classes of instabilities are obtained. For the Brusselator model, our results point towards the existence of cycles of creation and destruction of spots, and possibly to chaotic dynamics. For the Schnakenburg model, a differential-algebraic ODE system for the motion of the spots on the surface of the sphere is derived.

In the second part of the thesis, we study the existence and stability of mesa solutions in one spatial dimension and the corresponding planar mesa stripe patterns in two spatial dimensions. An asymptotic analysis is used in the limit of a large diffusivity ratio to construct mesa patterns in one spatial dimension for a general class of two-component reaction-diffusion systems that includes the well-known Gierer Meinhardt activator-inhibitor model with saturation (GMS model), and a predator-prey model. For such one-dimensional patterns, we study oscillatory instabilities of the pattern by way of a Hopf bifurcation and from a reduction to a limiting ODE-

PDE system. In addition, explicit thresholds are derived characterizing transverse instabilities of planar mesa-stripe patterns in two spatial dimensions. The results of our asymptotic theory as applied to the GMS and predator-prey systems are confirmed with full numerical results.

Table of Contents

List of Tables

List of Figures

Glossary

GMS	Gierer-Meinhardt model with saturation
RDE	reaction-difusion equations
ODE	ordinary differential equations
PDE	partial differential equations
BVAM	Barrio-Varea-Aragón-Maini model
BVP	Boundary value problem
NAS	Nonlinear algebraic system
NLEP	Nonlocal eigenvalue problem

Acknowledgments

I dedicate this thesis to my father, it was a long trip and he was always there with me.

I want to thank specially my advisor Michael Ward, for his support and his encouragement.

The faculty, staff and graduate students at UBC have been wonderful and it's been a great time.

I appreciate the financial support of the UBC and SEP graduate fellowships.

Chapter 1

Introduction

1.1 Historical perspective

The formal study of pattern formation mechanisms in the life sciences owes much to Alan Turing's seminal paper [60] on a mathematical model for a pattern-generating chemical reaction. The motivation behind the model was to shed light on the symmetry-breaking and differentiation mechanisms in biological organisms.

Turing's work presented a mechanism that can generate patterns from an initially homogeneous medium. By performing linear stability analysis, he showed it is possible to determine conditions for the existence of stable spatially-inhomogeneous solutions. In physical terms this means that under some conditions, a two-component chemical reaction can evolve into a stable non-trivial pattern. This new concept took many years to be accepted, despite early experimental evidence. In the 1950s the Russian chemist Boris Belousov [4] reported a self-oscillating chemical reaction, although he never managed to publish his findings in a peer-reviewed journal. His discovery eventually became known through one of his students, and the chemical reaction is now known as the Belousov-Zhabotinsky (BZ) reaction.

A mixing of two chemicals that does not lead to a dissipation in their gradients at first sight conflicts with the second law of thermodynamics; despite this seeming impossibility, similar mechanisms were soon discovered. The understanding of the physical mechanisms behind the reactions partly yielded Ilya Prigogine the 1977 Nobel prize in Chemistry [47].

In Turing's original paper, the basic model consists of a system of two nonlinear PDEs

$$\begin{aligned} U_t &= D_u \Delta U + F(U,V), \\ V_t &= D_v \Delta V + G(U,V), \end{aligned} \tag{1.1}$$

with U, V representing the concentration of two chemicals, D_u, D_v their diffusivities, and $F(U,V), G(U,V)$ the nonlinear reaction terms. The main insight was that under the right conditions, a spatially homogeneous solution of (1.1) could be destabilized by the presence of the diffusion terms. This process is now called diffusion-driven instability. One of the so-called Turing conditions for a diffusion-driven instability is that the ratio of the diffusion coefficients D_u/D_v be large. The rest of the conditions are also obtained through linear stability analysis (we work this out in detail for the Gierer-Meinhardt model with saturation (GMS model) in § 4.1).

In 1972, Gierer and Meinhardt [15] extended the idea of diffusion-driven instabilities with the observation that patterning occurs through the interaction between an auto-catalytic short range activator, and a long range inhibitor. This concept became extremely popular in biological modelling, and was subsequently applied to modelling skin pigment patterns in fish [25], fingerprints [5], colouring of marine shells [34], animal coat markings [36], and many others. In a much larger scale, models for interacting populations of predators and prey instead of chemicals were studied in 1972 [53], and more recently in [62], [2]. A survey of many reaction-diffusion models can be found in [37] and [29]).

While most of the early work was done in systems of one and two dimen-

sions, there soon started to be studies on how patterns were affected by growth and form (paraphrasing Thompson's classic, century old book on biological patterns [57]). Early studies on 1D systems that evolved on a growing domain ([12] [13] [3]) seemed to show that domain growth increased the robustness of pattern selection. Recent studies have incorporated domain growth to modelling limb development [35], and growth on plant tips [38]. Moreover, on a fundamental level, reworking Turing analysis on a general model with domain growth (making it non-autonomous) shows that diffusion-driven instabilities can occur in more general types of kinetics, beyond the activator-inhibitor framework [28].

Besides growth, curvature has been shown to have a profound effect on reaction diffusion models. Models on spheres range from simulations of Radiolaria structure [61], spherical tumour growth [10], to modelling plant tip growth on half-hemispheres [38], and single cell models [26] where bulk diffusion within the cell was coupled to diffusion along the boundary. In more general terms, it has been shown that the geometry of the domain, and specifically changes in curvature, can stabilize localized structures to critical points of the mean curvature [59].

Without question the Turing paradigm has been extremely successful. Applications range from single cell models up to herd dynamics and probabilistic models of criminal activity ([54]), overlapping multiple fields.

1.2 Mathematical perspective

As Turing models have grown more complex, incorporating domain growth and complicated topologies, there is a need for increasingly sophisticated mathematical tools capable of drawing insights from the models.

The key limitation of a Turing-type analysis is that it is linear in nature, and the fact that its pattern prediction capacity is severely hampered in both higher dimensions and in large domains. By virtue of its linearity, the Turing patterns predicted

will be close to the homogeneous solution. However, many physical and biological systems exhibit concentration gradients and localized structures that are far from equilibrium. These cannot be studied by relying on linear analysis. Furthermore, models in two and three spatial dimensions, have the complication that the pattern modes become degenerate. In these regimes, Turing analysis cannot predict the modes that will arise for specific parameter regimes. Gjorgjieva's work for a specific reaction-diffusion system on the surface of a sphere ([16], [17]) provides a good illustration of this phenomena.

Weakly nonlinear analysis has been used to successfully study the bifurcation structure leading from the Turing regime. However, its effectiveness is constrained to a region close to the Turing instability, and as such it provides poor results in regimes far from equilibrium.

In this thesis we will work with some of the classic reaction diffusion models: the Schnakenberg model [52], Brusselator [47], Gierer-Meinhardt [15], and a spatio-temporal predator-prey model [62]. The goal of our work is to develop analytical tools that are applicable to a wide variety of reaction-diffusion systems, and that provide insight into the existence and stability of solutions far from equilibrium, as well as on the dynamical processes that occur in those regimes. The models we used have been well studied and there is a large body of literature, in the case of the Brusselator going back to the seventies.

Starting from dimensionless versions of the models, we will perform an asymptotic analysis in the asymptotic limit of parameters that are either very large or small. We will develop particle-like solutions from matched asymptotic expansions in the singular limit, and construct solutions both for spot-type solutions, and for mesa-type patterns. The analytical results for these solutions and their stability properties will be verified with full numerical simulations.

1.3 Thesis outline

This thesis consists of two main parts.

The first part involves the study of spot patterns for the Brusselator and Schnakenberg models on the surface of a sphere. For both models we will construct localized spot-type solutions in the singular limit of small diffusivity using the method of matched asymptotic expansions. Away from the localized spatial regions where the spots are concentrated, the approximate solution will be shown to satisfy a linear elliptic problem where the spots are replaced by effective Coulomb singularities. This leads to a particle-like solution characterization of the asymptotically reduced problem. We will use a result from the theory of point vortices, for which extensive literature already exists ([21], [39], [41], [40], [8]) regarding a Neumann Green's function on the sphere that can be used to construct the solutions.

From analyzing the stability of the full nonlinear system for the case where all the spots have a common spot strength, we will derive a DAE that couples the strengths of the spots to their position on the sphere. The resulting problem is again related to point-vortices ([18], [6]), and the possible solutions are those of the Fekete problem [56], as well as the original Thomson atom model ([58], [1]).

Upon analyzing the stability properties of these solutions, we will derive analytical formulae for the thresholds of three distinct types of instabilities both by leading-order stability theory, through a related non-local eigenvalue problem [63], and by numerical calculation. These three instabilities all relate to instabilities of the amplitudes of the spots in a spot pattern, and they occur on a fast $O(1)$ time-scale. As discussed in Chapter 3, they have no direct counterpart with any translational-type instability mechanism for fluid point-vortices on the sphere.

In the second part of this thesis we will study reaction-diffusion models that admit mesa solutions, which consists of block-like patterns. Starting in one spatial dimension, we will analyze the bifurcation structure of these solutions, and study

the effect of a slowly growing domain on mesa-stability and mesa-splitting.

We will then consider the near-shadow regime, where the ratio of diffusivities of the two reaction components is very large. In this regime we will construct solutions far from equilibrium using the method of matched asymptotic expansions, and we will study the stability properties of these solutions.

Starting with the GMS model ([22],[23]), we will consider the case of multiple mesa solutions, and develop a general framework for other models. We will extend the 1-D solutions to 2-D planar stripe patterns, and then analyze transverse instabilities of these patterns. Our general framework for the analysis of transverse instabilities will also be applied to a Predator-Prey reaction-diffusion system, where we will compare our analytical predictions with results from full numerical simulations.

Chapter 2

The Brusselator Model on the Surface of the Sphere

In this chapter we study the existence and stability of localized spot patterns on the surface of the sphere for the Brusselator reaction-diffusion model. As surveyed in the introduction, there have been many studies characterizing weakly nonlinear patterns for the Brusselator that emerge from a linearized Turing-instability type analysis. The analysis of such weakly nonlinear patterns is rather complicated owing to the degeneracy of the Laplacian eigenfunctions on the surface of the sphere.

In contrast, in a singularly perturbed limit, the method of matched asymptotic expansions will be used to construct localized spot-type patterns for the Brusselator model. A precise asymptotic characterization of these patterns and the parameter ranges where they occur will be found, and the stability of these patterns analyzed. Three types of instabilities of these patterns will be discovered: a spot self-replication instability, a competition instability leading to the annihilation of spots, and a breather-type temporal instability of the spot amplitudes. Parameter ranges in terms of a phase diagram where these three instabilities occur will be determined.

The standard form of the Brusselator [47] model is given by

$$\begin{aligned} \frac{\partial U}{\partial t} &= \varepsilon^2 \nabla^2 U + E - (B+1)U + U^2 V, \\ \frac{\partial V}{\partial t} &= D\nabla^2 V + BU - U^2 V. \end{aligned} \tag{2.1}$$

The variable U is the short range activator component, and V is the long range inhibitor component.

We first give a formal scaling argument to determine the range of parameters with respect to ε for which spot patterns exist.

We start by letting $V = O(V_g)$ globally, with V_g the stationary homogeneous solution. For U we have different scalings near and away from spots; $U_{inn} = O(U_{inn})$ near a spot, and $U_{out} = O(U_{out})$ away from spots.

In the inner region, with $y = \varepsilon^{-1}(x - x_0)$, we need $O(U^2 V) = O(U)$ in order to have a construct a spot profile. Hence $U_{in} V_g = O(1)$, so that $U_{in} = O(1/V_g)$ in the inner region.

In the outer region, from the V equation in (2.1) we need that the nonlinear term, which will be localized near a spot, be approximated by a Delta function with the correct strength. As such we have $\int_\Omega U^2 V dx = O(\varepsilon^2 V_g U_{in}^2) = O(D V_g)$. Thus, $U_{in} = O(\varepsilon^{-1})$ and consequently $V_g = O(\varepsilon)$. Next, from the balance in the outer region that $D\Delta V = BU$, we get that $V_g = O(U_{out})$, which means that $U_{out} = O(\varepsilon)$. Finally, in the outer region we obtain from the U equation in (2.1) that E must balance $(B+1)U$, so that $E = O(U_{out})$ which yields $E = O(\varepsilon)$.

This very formal scaling analysis suggests that $U_{in} = O(1/\varepsilon)$, $U_{out} = O(\varepsilon)$, $V_g = O(\varepsilon)$, when $E = O(\varepsilon)$. Next, we use a non-dimensionalization based on these scalings in order to reduce the number of parameters in (2.1) and isolate our key bifurcation parameters.

We define the new variables u, v, and τ by

$$t = \tau T\,, \qquad U = \frac{\mu}{\varepsilon} u\,, \qquad V = \varepsilon\, v\,, \qquad E = \varepsilon\, E_0$$

In this way, (2.1) becomes

$$\begin{aligned} \frac{1}{T(B+1)} u_\tau &= \frac{\varepsilon^{\,2}}{B+1}\Delta u + \frac{\varepsilon^{\,2}}{B+1}\frac{E_0}{\mu} - u + \frac{\mu}{B+1} u^2 v, \\ \frac{1}{\mu^2 T} v_\tau &= \frac{D}{\mu^2}\Delta v + \frac{1}{\varepsilon^{\,2}}\left(\frac{B}{\mu} u - u^2 v\right). \end{aligned} \tag{2.2}$$

We now define $\varepsilon_{\,0}$, T, and μ by

$$\varepsilon_{\,0} = \frac{\varepsilon}{\sqrt{B+1}}\,, \qquad T = \frac{1}{B+1}\,, \qquad \mu = B\,.$$

Then, (2.2) transforms to

$$\begin{aligned} u_\tau &= \varepsilon_{\,0}^{\,2}\Delta u + \varepsilon_{\,0}^{\,2}\frac{E_0}{B} - u + \frac{B}{B+1} u^2 v, \\ \frac{(B+1)^2}{B^2} v_\tau &= \frac{D(B+1)}{B^2}\Delta v + \frac{1}{\varepsilon_{\,0}^{\,2}}\left(u - u^2 v\right), \end{aligned}$$

In this way, and upon replacing τ by t, we obtain the starting system for our analysis given by

$$u_t = \varepsilon_{\,0}^{\,2}\Delta u + \varepsilon_{\,0}^{\,2}\mathrm{E} - u + f u^2 v, \qquad \tau v_t = \mathcal{D}\Delta v + \frac{1}{\varepsilon_{\,0}^{\,2}}(u - u^2 v). \tag{2.3}$$

Here we have defined

$$f = \frac{B}{B+1}\,, \qquad \tau = \frac{1}{f^2}\,, \qquad \mathcal{D} = \frac{D(B+1)}{B^2}\,, \qquad \mathrm{E} = \frac{E_0}{B}\,. \tag{2.4}$$

We remark that in our non-dimensionalization, we chose not to scale v. If we were to additionally re-scale v, then we obtain (2.3) in which $\mathrm{E} = 1$ and with a slight re-definition of the other parameters $\mathcal{D}$ and τ. We choose instead to work with

(2.3) as it better isolates bifurcations due to changes in the parameter E_0.

We remark that the key bifurcation parameter f is defined conveniently in the narrow interval $(0,1)$. As $B \to \infty$ we get that $\tau \to 1$, $f \to 1$, $\mathrm{E} \to 0$, and $\mathcal{D} = O(1/B)$.

The system (2.3) on the surface of the sphere will be the starting point for our analysis. Without loss of generality we can let the sphere have radius one. When considering the system on the surface of the unit sphere it is understood that $\Delta \equiv \Delta_s$, where Δ is the Laplace-Beltrami operator given by

$$\Delta_s u \equiv \frac{1}{\sin^2\theta} u_{\phi\phi} + \frac{1}{\sin\theta}(\sin\theta\, u_\theta)_\theta\,, \quad 0 < \theta < \pi, \quad 0 < \phi < 2\pi.$$

2.1 The core problem and the construction of a quasi-equilibrium solution

We now construct a multi-spot quasi-equilibrium pattern for (2.3) in the limit $\varepsilon_0 \to 0$. For convenience we will re-label ε_0 by ε in the calculations below.

We first formulate the local (or inner) problem that determines the profile of an isolated spot. We center a spot at the angular coordinates $\phi = \phi_j$ and $\theta = \theta_j$, and we define

$$y_1 = \sin\theta_j \hat{\phi}, \quad y_2 = \hat{\theta}\,, \quad \text{with } \hat{\phi} = \frac{\phi - \phi_j}{\varepsilon}, \quad \hat{\theta} = \frac{\theta - \theta_j}{\varepsilon}\,.$$

Then, in the inner region near this spot we obtain, with an $O(\varepsilon)$ error, that

$$\Delta_s u = u_{y_1 y_1} + u_{y_2 y_2} + O(\varepsilon).$$

With this tangent-plane type-approximation to the sphere, we now construct a quasi-equilibrium spot pattern solution, with spots centred at (ϕ_j, θ_j) for $j =$

$1, \ldots, N$.

In the inner region near the j-th spot, we obtain to $O(\varepsilon)$ accuracy that (2.3) reduces to

$$\begin{aligned} &\Delta_y U_j - U_j + f U_j^2 V_j = 0, \qquad -\infty < y_1, y_2 < \infty, \\ &\mathcal{D}\Delta_y V_j + U_j - U_j^2 V_j = 0. \end{aligned} \tag{2.5}$$

Then, by rescaling

$$U_j = \sqrt{\mathcal{D}} u_j\,, \qquad V_j = v_j/\sqrt{\mathcal{D}}\,,$$

we can eliminate $\mathcal{D}$ and obtain the radially symmetric core problem for (u_j, v_j) in terms of the sole bifurcation parameter f:

$$\begin{aligned} &\Delta_\rho u_j - u_j + f u_j^2 v_j = 0, \qquad 0 < \rho < \infty, \\ &\Delta_\rho v_j + u_j - u_j^2 v_j = 0, \\ &u_j'(0) = v_j'(0) = 0, \\ &u_j \to 0 \text{ as } \rho \to \infty, \\ &v_j \sim S_j \log\rho + \chi(S_j; f) + 0(1), \quad \text{ as } \rho \to \infty, \end{aligned} \tag{2.6}$$

where we have defined $\rho = \sqrt{y_1^2 + y_2^2}$, and $\Delta_\rho \equiv \partial_{\rho\rho} + \frac{1}{\rho}\partial_\rho$.

The key feature in this problem is that we impose that $v_j \sim S_j \log\rho$ as $\rho \to \infty$, which is appropriate for $\Delta_\rho v_j = (u_j^2 v_j - u_j)$ owing to the fact that $u_j \to 0$ at infinity. The constant S_j is a parameter at this stage, but it will eventually be determined after the asymptotic matching of the inner and outer solutions. However, in terms of S_j and the bifurcation parameter f, the key function $\chi(S_j; f)$ must be computed numerically from the condition that $v_j - S_j \log\rho = O(1)$ as $\rho \to \infty$.

The boundary value problem (2.6) was solved for particular values of f and S_j by approximating this problem on a large but finite domain $0 \le \rho \le R$, where $R \gg 1$. In this way, we determined $\chi(S_j; f)$ by computing v_j at $\rho = R$. We took $R = 15$ in our computations. This calculation of $\chi(S_j; f)$ is of key importance for the rest of the analysis.

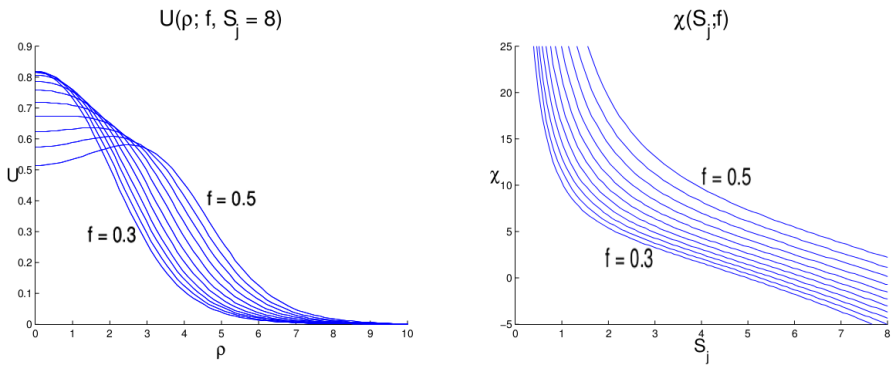

Figure 2.1: Left figure: the profile of the spot solution $u_j(\rho)$ for various values of f and fixed spot strength S_j. As f increases, u_j develops a volcano-shaped pattern that is commonly associated with splitting instabilities that occur in other systems such as the Gray-Scott model. Right figure: the nonlinear parameter $\chi(S_j; f)$ from the boundary condition in (2.6). The BVP was solved with Matlab's BVP5C routine. Each curve corresponds to a unique value of f, which ranges from 0.3 to 0.5.

There are a few identities that will be important later on. In the limit as $R \to \infty$, we have

$$\lim_{R\to\infty} \left(\int_0^R \rho \Delta_\rho v_j d\rho = \int_0^R (u_j^2 v_j - u_j)\rho d\rho \right),$$

and since $v_j \sim S_j \log \rho$, with $\rho(\Delta_\rho v_j) = (\rho v_{j\rho})_\rho$, we obtain

$$\lim_{R\to\infty} \int_0^R (\rho v_j')_\rho d\rho = \int_0^\infty (u_j^2 v_j - u_j)\rho d\rho = S_j \,. \tag{2.7}$$

In a similar way, we obtain from the u_j equation that

$$0 = \int_0^R \rho \Delta_\rho u_j d\rho = \int_0^\infty u_j \rho d\rho - f \int_0^\infty u_j^2 v_j \rho d\rho.$$

Combining this with (2.7), we conclude that

$$S_j = (1-f) \int_0^\infty u_j^2 v_j \rho d\rho. \tag{2.8}$$

Since we do not know the sign of v_j we cannot guarantee that $S_j > 0$. However, it is clear that as $f \to 1$ then $S_j \to 0$.

Next, we asymptotically match the far-field behaviours of the inner solutions near each spot to a certain global solution for v, which we will construct. In doing so, we will derive a nonlinear algebraic system of equations for the unknowns S_j, referred to as the "source strengths". Our asymptotic analysis has the key feature that it retains all of the logarithmic terms in $\nu \equiv -1/\log\varepsilon$ as $\varepsilon \to 0$, and so our asymptotic approximation for the solution and for the source strengths has an error that is algebraic, rather than logarithmic, in ε.

To determine the far-field behaviour of each inner solution we recall that $u = D^{1/2}u_j$ and $v = D^{-1/2}v_j$, with $v_j \sim S_j \log|y| + \chi + o(1)$ as $|y| \to \infty$. We let $\vec{x_j} = (\cos\phi_j \sin\theta_j, \sin\phi_j \sin\theta_j, \cos\theta_j)$ be a point on the unit sphere. Now, by Lemma A.1 in appendix A, we have that

$$|\vec{x} - \vec{x_j}| = \varepsilon\,|y| + o(1) \text{ as } \vec{x} \to \vec{x_j}, \text{ with } \vec{y} = (\hat{\phi}\sin\theta_j, \hat{\theta}),$$

and $\hat{\phi} = \frac{\phi - \phi_j}{\varepsilon}$, $\hat{\theta} = \frac{\theta - \theta_j}{\varepsilon}$. Thus, we obtain the far-field behaviour and matching condition

$$v \sim D^{-1/2}\left[S_j \log|x - x_j| + \frac{S_j}{\nu} + \chi(S_j; f)\right], \text{ as } x \to x_j; \quad \nu \equiv -\frac{1}{\log\varepsilon}.$$

This provides the singular behaviour of the outer solution for v.

Next, we study the outer solution for (2.3). Meanwhile, in the outer region away from $O(\varepsilon)$ neighborhoods of $\{\vec{x_1}, \ldots, \vec{x_n}\}$ we have that $\varepsilon^2\mathrm{E} - u + fu^2v = 0$. So the outer limit for u is $u \sim \varepsilon^2\mathrm{E} + O(\varepsilon^2)$.

We have then that the outer and inner solutions for $\mathcal{U}$ are, respectively,

$$u_{out} = \varepsilon^2_0\mathrm{E}, \qquad \text{and} \qquad u_{in} = \mathcal{D}^{1/2}u_j(\varepsilon^{-1}|x - x_j|),$$

whereas the inner approximation for v is $v \sim \mathcal{D}^{-1/2}v_j$. By combining the global

and local parts, we get a uniformly valid approximation for u given by

$$u \sim \varepsilon^{\,2}\mathrm{E} + \sum_{j=1}^{N} (\mathcal{D}^{1/2} u_j(\varepsilon^{\,-1}|x - x_j|) + \ldots).$$

We then must estimate the term $\varepsilon^{\,-2}(u - u^2 v)$ in the v-equation of (2.3) in the sense of distributions. The evaluation of this term requires care to retain both the local contribution near each spot and the global contribution arising from the non-vanishing outer solution for u of order $O(\varepsilon^{\,2})$. In the sense of distributions we obtain

$$\begin{aligned} \frac{1}{\varepsilon^{\,2}}(u - u^2 v) &\sim E + 2\pi \mathcal{D}^{1/2} \int_0^\infty (u_j - u_j^2 v_j)\rho d\rho \; \delta\,(x - x_j), \\ &\sim E - 2\pi \mathcal{D}^{1/2} S_j \delta\,(x - x_j). \end{aligned}$$

By using this result, together with the matching condition for v as given above, we obtain that the outer problem for v is

$$\begin{aligned} &\Delta_s v + \frac{\mathrm{E}}{\mathcal{D}} = \frac{2\pi}{\sqrt{\mathcal{D}}} \sum_{j=1}^{N} S_j \delta\,(x - x_j) \quad \text{in } \Omega\,, \\ &v \sim \mathcal{D}^{-1/2} \left[S_j \log|x - x_j| + \frac{S_j}{\nu} + \chi \right] + o(1) \quad \text{as } x \to x_j, \end{aligned} \tag{2.9}$$

for $j = 1, \ldots, N$, where Ω is the surface of the unit sphere. A key feature in this problem is that by pre-specifying the form of the non-singular $O(1)$ term in each singularity condition, we will obtain a nonlinear algebraic system for the source strengths $S_1, \ldots, S_N$.

To solve this problem we introduce the Neumann Green's function $G(x; x_0)$ defined as the unique solution to

$$\Delta_s G = \frac{1}{4\pi} - \delta\,(x - x_0)\,, \qquad \int_S G\, dx = \int_0^{2\pi} \int_0^{\pi} G \sin\theta \, d\theta \, d\phi = 0. \tag{2.10}$$

Here G is 2π periodic in ϕ, is smooth at the poles $\theta = 0, \pi$, and the integral condition eliminates an arbitrary constant in G and thus specifies it uniquely . It is well known ([19], [20], [21]) that

$$G = -\frac{1}{2\pi}\log|x - x_0| + R, \qquad R = \frac{1}{4\pi}(2\log 2 - 1)\,. \tag{2.11}$$

We can write the solution to (2.9) in terms of G as

$$v = -\frac{2\pi}{\sqrt{\mathcal{D}}}\sum_{j=1}^{N} S_j G(x; x_j) + \frac{\bar{v}}{\sqrt{\mathcal{D}}}, \tag{2.12}$$

where $\bar{v}$ is an arbitrary constant that must be determined as part of the analysis. To verify that (2.12) has the correct strength of the logarithmic singularity, we calculate

$$\Delta_s v = -\frac{2\pi}{\sqrt{\mathcal{D}}}\sum_{j=1}^{N} S_j \Delta_s G = -\frac{2\pi}{\sqrt{\mathcal{D}}}\sum_{j=1}^{N} S_j\left(\frac{1}{4\pi}\right) + \frac{2\pi}{\sqrt{\mathcal{D}}}\sum_{j=1}^{N} S_j \delta\left(x - x_j\right).$$

This leads to the condition that the sum of the source strengths are related to E by

$$\sum_{j=1}^{N} S_j = \frac{2\mathrm{E}}{\sqrt{\mathcal{D}}}.$$

As $x \to x_i$, the matching condition in (2.9) together with the explicit solution for v in (2.12) yields that

$$-\frac{2\pi}{\sqrt{\mathcal{D}}}\left[-\frac{S_i}{2\pi}\log|x - x_i| + S_i R\right] - \frac{2\pi}{\sqrt{\mathcal{D}}}\sum_{\substack{j=1\\ j\neq i}}^{N} S_j G_{ij} + \frac{\bar{v}}{\sqrt{\mathcal{D}}}$$
$$\sim \mathcal{D}^{-1/2}\left[S_i \log|x - x_i| + \frac{S_i}{\nu} + \chi\right],$$

for $i = 1, \ldots, N$. This results in a system of $N + 1$ nonlinear algebraic system

Nonlinear algebraic system (NAS) for S_i and $\bar{v}$,

$$\begin{aligned} \frac{S_i}{\nu} + 2\pi\left(S_i R + \sum_{j\neq i}^{N} S_j G_{ij}\right) + \chi(S_i; f) = \bar{v}, \qquad i = 1, \ldots, N, \\ \sum_{i=1}^{N} S_i = \frac{2\mathrm{E}}{\sqrt{\mathcal{D}}}. \end{aligned} \tag{2.13}$$

Here $G_{ij} = G(x_i; x_j)$ is to be computed from (2.11)

Before casting this system into a more convenient form, we make a few remarks. Firstly, the nonlinearity in (2.13) arises from the $\chi(S_i; f)$ term. For a given set of spot locations $x_1, \ldots, x_N$, we can compute $S_1, \ldots, S_N$ and $\bar{v}$. This then determines the quasi-equilibrium pattern. For each S_j our numerical results indicate that there is a unique solution to the core problem (2.6). The outer solution for v will be given by (2.12). Due to the intractability in solving this system analytically, the solvability of this system must (typically) be explored numerically.

Next, we decompose the G_{ij} terms in the NAS to re-cast this system into a more convenient form. We write $G_{ij} = \frac{1}{2\pi} L_{ij} + R$, where $R = \frac{1}{4\pi}(2\log 2 - 1)$ (see (2.11)), and where we have labelled $L_{ij} \equiv \log|x_i - x_j|$. We calculate that

$$\begin{aligned} S_i R + \sum_{j\neq i}^{N} S_j \left(-\frac{1}{2\pi} L_{ij} + R\right) &= -\frac{1}{2\pi} \sum_{j\neq i}^{N} S_j L_{ij} + \sum_{j=1}^{N} S_j R, \\ &= -\frac{1}{2\pi} \sum_{j\neq i}^{N} S_j L_{ij} + \frac{2R\mathrm{E}}{\sqrt{\mathcal{D}}}, \end{aligned}$$

so that (2.13) becomes

$$S_i - \nu \sum_{j\neq i}^{N} S_j L_{ij} + \frac{\nu R_0 \mathrm{E}}{\sqrt{\mathcal{D}}} + \nu\chi(S_i; f) = \nu\bar{v}, \qquad R_0 \equiv 4\pi R = 2\log 2 - 1\,, \tag{2.14}$$

for $i = 1, \ldots, N$.

To write this system in matrix form, we introduce

$$\vec{S} = \begin{pmatrix} S_1 \\ \vdots \\ S_N \end{pmatrix}, \qquad \vec{e} = \begin{pmatrix} 1 \\ \vdots \\ 1 \end{pmatrix}, \qquad \vec{\chi} = \begin{pmatrix} \chi(S_1; f) \\ \vdots \\ \chi(S_N; f) \end{pmatrix},$$
$$\mathcal{G} = \begin{pmatrix} 0 & L_{12} & \cdots & L_{1N} \\ L_{21} & \ddots & & \vdots \\ \vdots & & & \\ L_{N1} & \cdots & & 0 \end{pmatrix}, \tag{2.15}$$

so that the system for the source strengths becomes

$$(I - \nu\mathcal{G})\vec{S} + \nu\vec{\chi} = \left(\nu\bar{v} - \frac{\nu R_0 \mathrm{E}}{\sqrt{\mathcal{D}}}\right)\vec{e}.$$

We multiply by $\vec{e}^T$ and use the fact that $\vec{e}^T\vec{S} = \frac{2\mathrm{E}}{\sqrt{\mathcal{D}}}$, and $\vec{e}^T\vec{e} = N$. This yields

$$\frac{2\mathrm{E}}{\sqrt{\mathcal{D}}} - \vec{e}^T\nu\mathcal{G}\vec{S} + \nu\vec{e}^T\vec{\chi} = \nu\bar{v}N - \frac{\nu R_0 \mathrm{E}}{\sqrt{\mathcal{D}}}N,$$

which allows us to solve for $\bar{v}$ as

$$\bar{v} = \frac{2\mathrm{E}}{\sqrt{D}N\nu} + \frac{R_0\mathrm{E}}{\sqrt{\mathcal{D}}} + \frac{\vec{e}^T\vec{\chi}}{N} - \frac{\vec{e}^T\mathcal{G}\vec{S}}{N}. \tag{2.16}$$

By eliminating $\bar{v}$ in (2.13) we obtain

$$\vec{S} + \nu\left(\frac{\vec{e}\vec{e}^T}{N}\mathcal{G} - \mathcal{G}\right)\vec{S} + \nu\left(\vec{\chi} - \frac{1}{N}\vec{e}\vec{e}^T\vec{\chi}\right) = \frac{2\mathrm{E}}{\sqrt{\mathcal{D}}N}\vec{e}.$$

We now define the matrix

$$\mathcal{E}_0 \equiv \frac{1}{N}\vec{e}\vec{e}^T = \frac{1}{N}\begin{pmatrix} 1 & \cdots & 1 \\ \vdots & & \vdots \\ 1 & \cdots & 1 \end{pmatrix}.$$

With this we can conclude that the solution to (2.13) satisfies

$$\vec{S} + \nu(I - \mathcal{E}_0)\mathcal{G}\vec{S} + \nu(I - \mathcal{E}_0)\vec{\chi} = \frac{2\mathrm{E}}{\sqrt{\mathcal{D}}N}\vec{e}, \tag{2.17a}$$

and that

$$\bar{v} = \frac{2\mathrm{E}}{\sqrt{D}N\nu} + \frac{R_0\mathrm{E}}{\sqrt{\mathcal{D}}} + \frac{1}{N}(\vec{e}^T\vec{\chi} - \vec{e}^T\mathcal{G}\vec{S}). \tag{2.17b}$$

We remark that the nonlinear algebraic system in (2.17) is decoupled. One first solves for $S_1, \ldots, S_N$ in (2.17a), and then the result is used to calculate $\bar{v}$ in (2.17b). By using the numerical values computed from the core problem for $\chi(S; f)$ (see Figure 2.1), one can solve (2.17a) for various spot configurations.

The specific form (2.17a) of the nonlinear algebraic system is the one that is used in the analysis below.

2.2 Stability analysis of the quasi-equilibrium pattern

In this section we study the stability of the N-spot quasi-equilibrium solution constructed in the previous section to $O(1)$ time-scale instabilities. The $O(1)$ time-scale of such instabilities is fast in comparison with the expected slow dynamics of the spots with speed $O(\varepsilon^2)$. Therefore, in the stability analysis we "freeze" the locations of the spots and then characterize whether the resulting quasi-equilibrium pattern is unstable to fast $O(1)$ time-scale instabilities. There are three distinct types of instabilities that can occur and will be discussed. We remark that our stability analysis is accurate to all logarithmic orders in ν. A leading-order stability analysis is given in a later section.

We begin with the nondimensionalized system from (2.3) on Ω written as

$$u_t = \varepsilon^2 \Delta u + \varepsilon^2 \mathrm{E} - u + f u^2 v,$$
$$\tau v_t = \mathcal{D} \Delta v + \frac{1}{\varepsilon^2}(u - u^2 v)$$

where Ω is the surface of the unit sphere.

We recall that the quasi-equilibrium solution, as constructed in the previous section, satisfies

$$u_{qe} \sim \varepsilon^2 \mathrm{E} + \sum_{j=1}^{N} \sqrt{\mathcal{D}} u_j(\varepsilon^{-1}|x - x_j|),$$
$$v_{qe} \sim \begin{cases} \frac{1}{\sqrt{\mathcal{D}}} v_j & \text{for } |x - x_j| = O(\varepsilon) \\ -\frac{2\pi}{\sqrt{D}} \sum_{j=1}^{N} S_j G(x; x_j) + \frac{\bar{v}}{\sqrt{\mathcal{D}}} & \text{for } |x - x_j| \gg O(\varepsilon) \end{cases}$$

We linearize around this solution by writing

$$u = u_{qe} + e^{\lambda t}\psi, \qquad v = v_{qe} + e^{\lambda t}\eta,$$

to obtain that the perturbation satisfies

$$\begin{aligned} \varepsilon^2 \Delta_s \psi - \psi + 2 f u_{qe} v_{qe} \psi + f u_{qe}^2 \eta = \lambda \psi, \\ \mathcal{D} \Delta_s \eta + \frac{1}{\varepsilon^2}(\psi - 2 u_{qe} v_{qe} \psi - u_{qe}^2 \eta) = \tau \lambda \eta. \end{aligned} \tag{2.18}$$

For the inner solution, we consider the local coordinates near the j-th spot

$$\hat{\phi} = \frac{\phi - \phi_j}{\varepsilon}, \quad \hat{\theta} = \frac{\theta - \theta_j}{\varepsilon}; \quad y_1 = \sin\theta_j \hat{\phi}, \quad y_2 = \hat{\theta}.$$

We re-write the Laplace-Beltrami operator in the local coordinate system to get

$$\begin{aligned} \psi_{j_{y_1 y_1}} + \psi_{j_{y_2 y_2}} - \psi_j + 2 f u_j v_j \psi_j + f \mathcal{D} u_j^2 \eta_j = \lambda \psi_j, \\ \mathcal{D}(\eta_{j_{y_1 y_1}} + \eta_{j_{y_2 y_2}}) + \psi_j - 2 u_j v_j \psi_j - \mathcal{D} u_j^2 \eta = \tau \lambda \eta_j \varepsilon^2, \end{aligned} \tag{2.19}$$

since in the inner region we have $u_{qe}v_{qe} \simeq u_j v_j$. We now define $N_j = \mathcal{D}\eta_j$, and we assume that $\tau\lambda \ll O(\varepsilon^{-2})$, which leads to the eigenvalue problem

$$\begin{aligned} \psi_{j_{y_1y_1}} + \psi_{j_{y_2y_2}} - \psi_j + 2f u_j v_j \psi_j + f u_j^2 N_j &= \lambda\psi_j, \\ N_{j_{y_1y_1}} + N_{j_{y_2y_2}} + \psi_j - 2u_j v_j \psi_j - u_j^2 N_j &= 0, \end{aligned} \tag{2.20}$$

on $-\infty < y_1, y_2 < \infty$.

In deriving this system we used $\Delta_s\psi = \psi_{y_1y_1} + \psi_{y_2y_2} + O(\varepsilon)$, and neglected the $O(\varepsilon)$ error term. In addition, we recall that u_j and v_j are obtained by solving the radially symmetric core problem (2.6), and that they depend on S_j and f. Finally, we note that due to the $-\psi_j$ term in the ψ_j equation, it is consistent to impose that $\psi_j \to 0$ as $\rho^2 = y_1^2 + y_2^2 \to \infty$, provided that $\lambda > -1$. However, the boundary conditions on N_j will depend on the type of eigenfunction that we are seeking.

We now look for a separation of variable solution of the form

$$\psi_j = \hat{\psi}_j(\rho)e^{iwm}, \qquad N_j = \hat{N}_j(\rho)e^{iwm},$$

where $w = \tan^{-1}(y_2/y_1)$ and $m = 0, 1, 2, \ldots$ ($e^{2\pi im} = 1\ \forall m$), provides a periodicity condition for the perturbation in the tangent plane. Overall, this results in a local polar coordinate system on the tangent plane to the sphere at the j-th spot location. In terms of these variables, (2.20) becomes a radially symmetric problem with parameter m:

$$\begin{aligned} &\hat{\psi}_j'' + \frac{1}{\rho}\hat{\psi}_j' - \frac{m^2}{\rho}\hat{\psi}_j - (1+\lambda)\hat{\psi}_j + 2f u_j v_j \hat{\psi}_j + f u_j^2 \hat{N}_j = 0 \\ &\hat{N}_j'' + \frac{1}{\rho}\hat{N}_j' - \frac{m^2}{\rho}\hat{N}_j + \hat{\psi}_j - 2u_j v_j \hat{\psi}_j - u_j^2 \hat{N}_j = 0, \quad 0 < \rho < \infty, \\ &\hat{\psi}_j'(0) = \hat{N}_j'(0) = 0, \quad \hat{\psi}_j \to 0 \text{ as } \rho \to \infty. \end{aligned} \tag{2.21}$$

We need only consider the modes $m = 0, 2, 3, 4, \ldots$, since $m = 1$ corresponds to the translation mode associated with the neutral eigenvalue $\lambda = 0$.

2.2.1 Case I: $m = 2, 3, \ldots$

We now look for solutions to the eigenvalue problem generated by non-radially symmetric perturbations near the j-th spot ($m = 2, 3, \ldots$). Due to the $-m^2\hat{N}_j/\rho^2$ term in the $\hat{N}_j$ equation we can impose an algebraic decay as $\hat{N}_j \to \infty$. Thus we can append to (2.21) the condition $\hat{N}_j \to 0$ as $\rho \to \infty$.

This implies that non-radially symmetric eigenfunctions are largely local instabilities, and are only coupled together through the NAS for $S_1, \ldots, S_N$.

We proceed to solve the eigenvalue problem. For particular values of f, we compute u_j and v_j from the core problem. Despite the boundary condition being set at infinity, the solution converges exponentially fast, and it became clear that discretizing (2.21) for $0 < \rho < 14$ would result in convergence to machine precision. We first solve for $\hat{N}_j$ in the second equation, using centred differences for the first and second derivatives, and upon substituting this into the first equation we can approximate $\hat{\psi}_j$ and the eigenvalue λ by the solution of a matrix eigenvalue problem.

In Figure 2.2 we show the eigenvalues as a function of the parameter S_j for modes $m = 2, 3, 4$ for a specific value of f. In addition, we give the value of the pairs (f, S_j) for which $\lambda = 0$ for the $m = 2$ mode. The figure agrees with the expectation that the solution becomes unstable at the range where u_j attains a volcano-like profile (shown in Figure 2.1)

The results indicate that if the source strength exceeds some critical value S_c, which depends on f, then the spot becomes unstable to a mode $m = 2$ linear instability. This linear instability is of peanut-splitting type and is the trigger for a nonlinear spot self-replication event.

To illustrate this phenomena, in Figure 2.3 we show numerical results computed from the full PDE system for a one-spot initial condition for the parameter

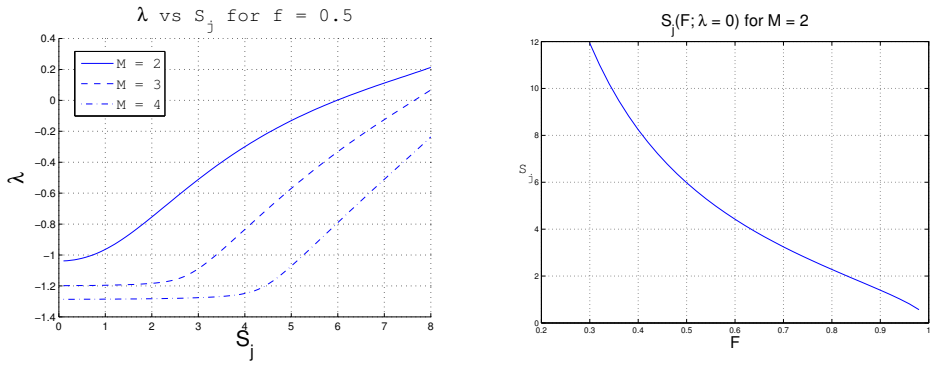

Figure 2.2: The figure on the left shows the eigenvalue λ as the source strength S_j increases for the case $f = 0.5$. This figure is representative of what we saw for various values of f. The figure on the right tracks the values of (f, S_j) that result in the critical case $\lambda = 0$ for $m = 2$.

values $f = 0.7$ and $\varepsilon = 0.1$. The numerical method used to obtain these results is described at the end of next chapter on the 2-D Schakenburg mode. In the first row of this figure where $\mathcal{D} = 0.35$, we have that $S > S_c$ and so there is a peanut-splitting linear instability. This instability is shown to lead to spot self-replication. Alternatively, for $\mathcal{D} = 0.45$, then $S < S_c$ and, as shown in the second row of this figure, there is no spot self-replication.

2.2.2 Case II: The splitting case, $m = 0$

The case $m = 0$ corresponds to a locally radially symmetric perturbation near the j-th spot. The key difference, as compared with the $m = 2, 3, \cdots$ case, is that without the $-m^2 N_j/\rho^2$ term we cannot impose that $N_j \to 0$ as $\rho \to \infty$. Instead, we must allow for logarithmic growth in the far-field. Returning to the eigenvalue problem (2.21), we impose the far-field behaviour

$$N_j \sim c_j \log \rho, \qquad \text{as } \rho \to \infty.$$

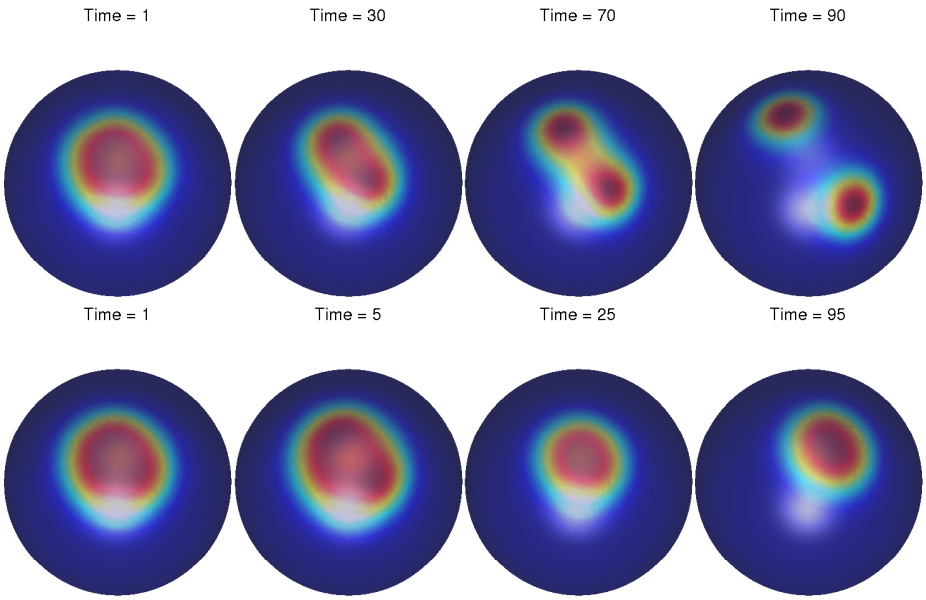

Figure 2.3: Full numerical simulation on a sphere, $u(\vec{x})$ for $f = 0.7$ and $\varepsilon = 0.1$. The splitting case has $\mathcal{D} = 0.35$, whereas the non-splitting case has $\mathcal{D} = 0.45$.

The constants c_j for $j = 1, \ldots, N$ will be determined later from a global matrix problem that couples all local eigenvalue problems near each of the spots.

Since the eigenvalue problem is linear and homogeneous, we can write

$$\psi = c_j \tilde{\psi}_j(\rho), \qquad N = c_j \bar{N}_j(\rho),$$

so that (2.21) becomes

$$\begin{aligned}
&\tilde{\psi}_j'' + \frac{1}{\rho}\tilde{\psi}_j' - (1+\lambda)\tilde{\psi}_j + 2f u_j v_j \tilde{\psi}_j + f u_j^2 \tilde{N}_j = 0, \qquad 0 < \rho < \infty, \\
&\tilde{N}_j'' + \frac{1}{\rho}\tilde{N}_j' + \tilde{\psi}_j - 2u_j v_j \tilde{\psi}_j - u_j^2 \tilde{N}_j = 0, \qquad 0 < \rho < \infty, \\
&\tilde{\psi}_j'(0) = \tilde{N}_j'(0) = 0; \qquad \tilde{\psi}_j \to 0 \quad \text{and} \quad \tilde{N}_j \to \log\rho + \tilde{B}_j + o(1) \text{ as } \rho \to \infty.
\end{aligned} \tag{2.22}$$

From this system, the term $\tilde{B}_j = \tilde{B}_j(S_j, f, \lambda)$ must be computed numerically by solving the complex-valued BVP. Numerically solving it is not as straightforward as in the uncoupled $m = 0$ case; this was done carefully in § 2.2.6.

In addition, since $\tilde{N}_j$ does not tend to zero at infinity, the local eigenvalue problems near each spot will all be coupled together. This is in contrast to the $m \neq 0$ case for non-radially symmetric perturbations studied earlier, which are largely local instabilities.

We observe that the $\tilde{N}_j$ equation can be written as

$$\left(\rho \tilde{N}_j'\right)' + \rho\left(\tilde{\psi}_j(1 - 2u_j v_j) - u_j^2 \tilde{N}_j\right) = 0\,.$$

We can integrate this equation from $0 < \rho < \infty$ with $\tilde{N}_j \sim \log\rho$ as $\rho \to \infty$, to get

$$1 = \int_0^\infty \left(\tilde{\psi}_j(1 - 2u_j v_j) - u_j^2 \tilde{N}_j\right) \rho d\rho.$$

Then, by using the fact that $\tilde{\psi}_j = \psi_j/c_j$, $\tilde{N}_j = N_j/c_j$, we obtain the identity

$$c_j = \int_0^\infty \left(\psi_j(1 - 2u_j v_j) - u_j^2 N_j\right) \rho d\rho. \tag{2.23}$$

Next, we derive an equation in the outer region for η. The far-field condition of the inner solution near the j-th spot is needed. We had previously defined $\eta_j = N_j/\mathcal{D} = c_j\tilde{N}_j/\mathcal{D}$. As $\rho \to \infty$ we have $\tilde{N}_j \sim \log\rho + \tilde{B}_j + o(1)$, with $\rho = (y_1^2 + y_2^2)^{1/2}$. Therefore, in terms of outer variables we obtain the matching condition that

$$\eta_j \sim \frac{c_j}{\mathcal{D}}\left[\log|x - x_j| + \frac{1}{\nu} + \tilde{B}_j\right], \quad \text{as } x \to x_j, \tag{2.24}$$

where$\nu = -1/\log\varepsilon$.

Now, from (2.18) we obtain in the outer region from the ψ equation that

$$-\psi_{out} + 2fu_e v_e \psi_{out} + fu_e^2 \eta_{out} = \lambda_{out}\psi_{out}.$$

Since, in the outer region, we have $u_e = O(\varepsilon^{\,2})$, $v_e = O(1)$, and $\eta_{out} = O(1)$, we obtain that $\psi_{out} = O(\varepsilon^{\,4}) \ll 1$.

From the η equation in (2.18) we obtain that the outer approximation for η satisfies

$$\mathcal{D}\Delta_s \eta + \frac{1}{\varepsilon^{\,2}}\left(\psi + 2u_e v_e \psi - u_e^2 \eta\right) = \tau\lambda\eta. \tag{2.25}$$

We then must estimate the coefficient of $\varepsilon^{\,-2}$ in (2.25). In the outer region we use $u_e = O(\varepsilon^{\,2})$, $v_e = O(1)$, $\eta_{out} = O(1)$, and $\psi_{out} = O(\varepsilon^{\,4}) \ll 1$, to estimate $\varepsilon^{\,-2}(-u_e^2\eta_{out}) = O(\varepsilon^{\,2}\eta)$ and $\varepsilon^{\,-2}\left(\psi + 2u_e v_e \psi\right) = \varepsilon^{\,-2}\left(O(\varepsilon^{\,4}) - O(\varepsilon^{\,2} v_e \psi_{out})\right) = O(\varepsilon^{\,2}) + O(\varepsilon^{\,4})$. Therefore, both of these terms are negligible in the outer region.

The estimate above shows that we need only consider the local contributions near each spot. The global contribution from the non-trivial background state of u_e is negligible with regards to their contribution on the outer solution for η. To calculate the contribution from the local terms near the j-th spot we use (2.23) to obtain

$$\frac{1}{\varepsilon^{\,2}}\left(\psi + 2u_e v_e \psi - u_e^2 \eta\right) \to 2\pi \sum_{j=1}^{N} \int_0^{\infty} \left(\psi_j(1 - 2u_j v_j) - u_j^2 \eta_j\right) \rho d\rho \delta\left(x - x_j\right)$$

$$= -2\pi \sum_{j=1}^{N} c_j \delta\left(x - x_j\right).$$

In this way, we obtain from (2.24) and (2.25) that the outer solution for η

satisfies

$$\begin{aligned}
&\Delta_s \eta - \frac{\tau\lambda}{\mathcal{D}}\eta = 2\pi \sum_{j=1}^{N} c_j \delta\left(x - x_j\right), \\
&\eta \sim \frac{c_j}{\mathcal{D}}\left(\log|x - x_j| + \frac{1}{\nu} + \tilde{B}_j\right), \quad \text{as } x \to x_j, \quad \text{for } j = 1, \ldots, N.
\end{aligned} \tag{2.26}$$

Next, we will represent the solution to this problem in terms of a Green's function, and from it we will obtain a homogeneous linear algebraic system of the form

$$\mathcal{M}\vec{c} = \vec{0}, \qquad \text{where} \qquad \mathcal{M} = \mathcal{M}(S_1, \ldots, S_N, \lambda, f, \mathcal{D}).$$

The condition for the existence of a non-trivial solution for $\vec{c} = (c_1, \ldots, c_N)^T$ is that

$$\det \mathcal{M} = 0.$$

This condition effectively leads to a transcendental equation for any discrete eigenvalues λ.

Before deriving this system, we obtain a key identity that is helpful for obtaining stability thresholds. By differentiating the core problem (2.6) with respect to S_j we get

$$\begin{aligned}
&(\partial_{s_j} u_j)'' + \frac{1}{\rho}(\partial_{s_j} u_j)' - (\partial_{s_j} u_j) + 2f u_j v_j (\partial_{s_j} u_j) + f u_j^2 (\partial_{s_j} v_j) = 0, \\
&(\partial_{s_j} v_j)'' + \frac{1}{\rho}(\partial_{s_j} v_j)' + (\partial_{s_j} u_j) - 2u_j v_j (\partial_{s_j} u_j) + u_j^2 (\partial_{s_j} v_j) = 0, \\
&v_j \sim \log\rho + \partial_{s_j}\chi(S_j; f), \quad \text{as } \rho \to \infty.
\end{aligned} \tag{2.27}$$

By comparing this problem with (2.22) we obtain the key identity

$$\tilde{B}_j(S_j, f, \lambda = 0) = \partial_{s_j}\chi(S_j; f) \equiv \chi'(S_j; f). \tag{2.28}$$

In solving (2.26) we will identify two separate two cases. The case $\tau = 0$,

where the solution will depend on the Neumann Green's function for a sphere, and the case where $\tau \neq 0$, for which we will identify a new Green's function on a sphere that is related to Legendre functions.

2.2.3 Case A: The competition case, $m \geq 2$ and $\tau = 0$

For this case, (2.26) reduces to

$$\begin{aligned} &\Delta_s \eta = 2\pi \sum_{j=1}^{N} c_j \delta\left(x - x_j\right), \\ &\eta \sim \frac{c_j}{\mathcal{D}} \left(\log|x - x_j| + \frac{1}{\nu} + \tilde{B}_j \right), \quad \text{as } x \to x_j, \quad \text{for } j = 1, \ldots, N. \end{aligned} \tag{2.29}$$

In terms of this Neumann Green's function of (2.10) and (2.11), the solution to (2.29) is

$$\eta = -\frac{2\pi}{\mathcal{D}} \sum_{j=1}^{N} c_j G(x; x_j) + \frac{\bar{\eta}}{\mathcal{D}}, \tag{2.30}$$

where $\bar{\eta}$ is a constant to be found. We then calculate that

$$\begin{aligned} \Delta_s \eta = -\frac{2\pi}{\mathcal{D}} \sum_{j=1}^{N} c_j \Delta_s G(x; x_j) &= -\frac{2\pi}{\mathcal{D}} \sum_{j=1}^{N} c_j \left(\frac{1}{4\pi} - \delta\left(x - x_j\right) \right) \\ &= -\frac{1}{2\mathcal{D}} \sum_{j=1}^{N} c_j + \frac{2\pi}{\mathcal{D}} \sum_{j=1}^{N} c_j \delta\left(x - x_j\right). \end{aligned}$$

Upon comparing this with (2.29), we require that the following solvability condition be satisfied:

$$\sum_{j=1}^{N} c_j = 0. \tag{2.31}$$

Next, by letting $x \to x_i$ in (2.30) and comparing it with (2.29), we obtain

$$\begin{aligned}\eta &= -\frac{2\pi}{\mathcal{D}}\left(-\frac{c_i}{2\pi}\log|x-x_i| + c_i R + \sum_{j\neq i} c_j G_{ij}\right) + \frac{\bar{\eta}}{\mathcal{D}} \\ &\sim \frac{c_i}{\mathcal{D}}\left(\log|x-x_i| + \frac{1}{\nu} + \tilde{B}_i\right).\end{aligned}$$

This yields a linear system of the form

$$-2\pi\nu\left(c_i R + \sum_{j\neq i}^{N} c_j G_{ij}\right) + \nu\bar{\eta} = c_i\left(1 + \eta\hat{B}_i\right).$$

We then use $G_{ij} = -\frac{1}{2\pi}L_{ij} + R$, with $L_{ij} = \log|x_i - x_j|$, to write this linear system as

$$-2\pi\nu\left(c_i R + \sum_{j\neq i}^{N} c_j R - \frac{1}{2\pi}\sum_{j\neq i}^{N} c_j L_{ij}\right) + \nu\bar{\eta} = c_i\left(1 + \eta\hat{B}_i\right).$$

Then, by using the solvability condition $\sum_{j=1}^{N} c_j = 0$, we can simplify the system above to an $N+1$ dimensional system

$$\nu\sum_{j\neq i}^{N} c_j L_{ij} + \nu\bar{\eta} = c_i\left(1 + \eta\hat{B}_i\right), \quad i = 1,\ldots,N\,; \quad \sum_{j=1}^{N} c_j = 0, \tag{2.32}$$

for the $N+1$ unknowns $\bar{\eta}$ and c_j for $j = 1,\ldots,N$.

To rewrite (2.32) in matrix form, we define

$$\mathcal{B} = \begin{pmatrix} \tilde{B}_1 & & 0 \\ & \ddots & \\ 0 & & \tilde{B}_N \end{pmatrix}, \qquad \vec{e} = \begin{pmatrix} 1 \\ \vdots \\ 1 \end{pmatrix}, \qquad \vec{c} = \begin{pmatrix} c_1 \\ \vdots \\ c_N \end{pmatrix},$$
$$\mathcal{G} = \begin{pmatrix} 0 & L_{12} & \cdots & L_{1N} \\ L_{21} & \ddots & & \vdots \\ \vdots & & & \\ L_{N1} & \cdots & & 0 \end{pmatrix}, \tag{2.33}$$

so that the matrix formulation of (2.32) is

$$\nu\mathcal{G}\vec{c} + \nu\bar{\eta}\vec{e} = \vec{c} + \nu\mathcal{B}\vec{c}, \qquad e^T\vec{c} = 0. \tag{2.34}$$

Pre-multiplying by $\vec{e}^T$ allows us to solve for $\bar{\eta}$ as

$$\bar{\eta} = \frac{1}{N}\left(\vec{e}^T\mathcal{B}\vec{c} - \vec{e}^T\mathcal{G}\vec{c}\right).$$

Upon substituting $\bar{\eta}$ back into (2.34) we get

$$\nu\mathcal{G}\vec{c} + \frac{\nu}{N}\vec{e}\left(\vec{e}^T\mathcal{B}\vec{c} - \vec{e}^T\mathcal{G}\vec{c}\right) = \vec{c} + \nu\mathcal{B}\vec{c}.$$

Finally, we define the matrix $\mathcal{E}_0$ as

$$\mathcal{E}_0 \equiv \frac{1}{N}\vec{e}\vec{e}^T = \frac{1}{N}\begin{pmatrix} 1 & \cdots & 1 \\ \vdots & & \vdots \\ 1 & \cdots & 1 \end{pmatrix},$$

and then re-arrange the system above to get that $\vec{c}$ is an eigenvector of the matrix problem

$$\mathcal{M}\vec{c} = \vec{0}, \qquad \mathcal{M} \equiv \left(\frac{1}{\nu}I + (I - \mathcal{E}_0)(\mathcal{B} - \mathcal{G})\right).$$

In summary, we conclude that $\vec{c} = (c_1, \ldots, c_N)^T$ are eigenvectors for the homo-

geneous linear system $\mathcal{M}\vec{c} = \vec{0}$, where $\mathcal{M} = \mathcal{M}(\lambda)$ since $\mathcal{B}_{jj} = \tilde{B}_j(\lambda)$. We refer to this system as the *globally coupled eigenvalue problem*.

The condition $\det \mathcal{M} = 0$, which yields a transcendental equation for λ, determines the discrete eigenvalues for the case $\tau = 0$. In general, solving $\det \mathcal{M} = 0$ requires the determination of $\tilde{B}_j = \tilde{B}_j(\lambda, S_j, f)$ as defined in (2.22). Recall that the source strengths $S_1, \ldots, S_N$ terms must be computed from the nonlinear system given by

$$\vec{S} + \nu(I - \mathcal{E}_0)G\vec{S} + \nu(I - \mathcal{E}_0)\vec{\chi} = \frac{2}{\sqrt{\mathcal{D}}N}\vec{e}. \tag{2.35}$$

2.2.4 Threshold calculation

Although it is difficult to compute the discrete eigenvalues of the *globally coupled eigenvalue problem*, it is a relatively simple matter to calculate the stability threshold for eigenvalues entering $\mathrm{Re}(\lambda) > 0$ through the origin $\lambda = 0$ by using the identity of (2.28). Near the end of section § 2.2.5 we prove that eigenvalues that cross into $\mathrm{Re}(\lambda) > 0$ have no imaginary components when $\mathrm{Re}(\lambda) = 0$.

Recall that when $\lambda = 0$ we have

$$\tilde{B}_j(0, S_j, f) = \chi'(S_j; f).$$

Therefore, when $\lambda = 0$ we do not need to compute $\tilde{B}_j(0, S_j, f)$ from (2.22). It is simply provided by the core problem through the numerical estimation of $\chi'(S_j; f)$. Therefore, when $\lambda = 0$, the matrix $\mathcal{B}$ is known, and we need to solve

$$\det \mathcal{M} = 0, \qquad \text{with} \quad \mathcal{M} \equiv \frac{1}{\nu}I + (I - \mathcal{E}_0)(\mathcal{B} - \mathcal{G}), \quad \nu = -\frac{1}{\log \varepsilon},$$

together with (2.35).

We now calculate this threshold explicitly for the special case where all the

spots have a common source strength, i.e., $S_c \equiv S_1 = \cdots = S_N$. This will occur whenever $\vec{e} = (1, \ldots, 1)^T$ is an eigenvector of $\mathcal{G}$, so that

$$\mathcal{G}\vec{e} = \kappa_1 \vec{e}, \tag{2.36}$$

for some κ_1. In particular, such a cyclic matrix structure will always occur for a two spot pattern, since

$$\mathcal{G} = \begin{pmatrix} 0 & L_{12} \\ L_{21} & 0 \end{pmatrix},$$

and $L_{12} = L_{21}$. A cyclic matrix structure also occurs for other symmetric arrangements of spots, such as N equally-spaced spots lying on a ring of constant latitude on the sphere. In addition, in general the cyclic structure of the Green's matrix will also hold when the spot locations are at the elliptic Fekete points, i.e. at the spot configuration that minimizes

$$-\sum_{i=1}^{N} \sum_{\substack{j=1 \\ j \neq i}}^{N} \log |x_i - x_j| .$$

This minimization problem is also called the Thomson problem [58], which consists of finding the optimal distribution of N equally charged particles on the surface of a sphere

Assuming that (2.36) holds, we then have that $\vec{S} = S_c \vec{e}$, and from (2.35) we have that $S_c = \frac{2}{\sqrt{\mathcal{D}}N}$. Similarly, for $\mathcal{M}$ we calculate

$$\mathcal{M} = \frac{1}{\nu} I + \chi'(S_c)(I - \mathcal{E}_0) - (I - \mathcal{E}_0)\mathcal{G}.$$

We want to find conditions that guarantee that $\mathcal{M}$ will be a singular matrix.

Lemma 2.1 *Consider the eigenvalue problem*

$$\mathcal{G}\vec{b} = k\vec{b}, \qquad \text{for } k_1, \ldots, k_N, \text{ and eigenvectors } \vec{b}_1, \ldots, \vec{b}_N.$$

Assume that $\mathcal{G}\vec{e} = k_1\vec{e}$, so that $\vec{b}_1 = \vec{e}$. Then we must have

$$\mathcal{G}\vec{b}_j = k_j\vec{b}_j, \quad j = 2, \ldots, N, \quad \text{with } \vec{b}_j^T\vec{e} = 0, \quad \text{for } j = 2, \ldots, N.$$

Proof Since $\mathcal{G}$ is a symmetric matrix by Green's reciprocity theorem, then the eigenspace must be orthogonal. We do need the dimension of the nullspace of $(\mathcal{G} - k_1 I)$ to be equal to one, so that k_1 is a simple eigenvalue of $\mathcal{G}$. ∎

Claim 1 *$\vec{b}_j$, for $j = 2, \ldots, N$, and $\vec{e}$ are eigenvectors of $\mathcal{M}$.*

Proof We have that

$$\mathcal{M}\vec{b}_j = \frac{1}{\nu}\vec{b}_j + \chi'(S_c)(I - \mathcal{E}_0)\vec{b}_j - (I - \mathcal{E}_0)\mathcal{G}\vec{b}_j, \quad \text{for } j = 2, \ldots, N,$$

with $\mathcal{G}\vec{b}_j = k_j\vec{b}_j$ and $\mathcal{E}_0\vec{b}_j = \frac{1}{N}\vec{e}\vec{e}^T\vec{b}_j = 0$, for $j = 2, \ldots, N$.

This shows that

$$\mathcal{M}\vec{b}_j = \frac{1}{\nu}\vec{b}_j + \chi'(S_c)\vec{b}_j - k_j\vec{b}_j = \left(\frac{1}{\nu} + \chi'(S_c) - k_j\right)\vec{b}_j.$$

In addition, we have that $(I - \mathcal{E}_0)\vec{e} = 0$, and $\mathcal{G}\vec{e} = k_1\vec{e}$. Therefore, the other eigenvector of $\mathcal{M}$ is

$$\mathcal{M}\vec{e} = \frac{1}{\nu}\vec{e} + \chi'(S_c)(I - \mathcal{E}_0)\vec{e} - (I - \mathcal{E}_0)\mathcal{G}\vec{e} = \frac{1}{\nu}\vec{e}. \quad ∎$$

Therefore we can conclude that $\vec{b}_2, \ldots, \vec{b}_N$ and $\vec{e}$ are the eigenvectors of $\mathcal{M}$.

Requiring that $\det \mathcal{M} = 0$ then yields $N-1$ algebraic equations of the form

$$\frac{1}{\nu} + \chi'(S_c) - k_j = 0, \quad \text{for } j = 2, \ldots, N, \tag{2.37}$$

where k_j for $j = 2, \ldots, N$ are any of the eigenvalues of $\mathcal{G}$ corresponding to the $N-1$ dimensional subspace perpendicular to $\vec{e}$.

2.2.5 Stability threshold

Suppose that $\mathcal{G}\vec{e} = k_1\vec{e}$, which implies a condition on the spot configuration $x_1, \ldots, x_N$ when $N > 2$. The cyclic structure always holds for $N = 2$. Then there exists a solution to (2.35) with a common source strength S_c, given by

$$S_c = \frac{2}{\sqrt{\mathcal{D}}N}.$$

From Figure 2.2 we know that self-replication occurs if $S_c^* > \Sigma_2(f)$, with Σ_2 the critical value where $\lambda = 0$ for the $m = 2$ mode. Alternatively, we know that there exists an instability with a sign-fluctuating eigenfunction whenever

$$\frac{1}{\nu} + \chi'(S_c) - k_j = 0, \quad \text{for some } j \text{ in } j = 2, \ldots, N.$$

We now make some remarks. The eigenfunction is sign-fluctuating because $\vec{c} = \vec{b}$ is one of the vectors for which $\vec{b}^T\vec{e} = 0$. Recall $\psi = c_j\hat{\psi}_j(\rho), \vec{c} = (c_1, \ldots, c_N)^T$, and that ψ is a perturbation of the quasi-equilibrium solution for u. We also note that k_j only depends on the number of spots N and their locations. From Figure 2.1, we know that $\chi'(S_c)$ is a negative concave down curve when S_c is small enough, with $\chi'(S_c) \to \infty$ as $S_c \to 0^+$. We define $\sigma_j = \frac{1}{\nu} + \chi'(S_c) - j_j$, with $\nu = -\frac{1}{\log \varepsilon}$. For $\nu \ll 1$ we have $\sigma_j \sim \frac{1}{\nu} > 0$ (to leading order). On the other hand, as $\mathcal{D} \to \infty$, we have that $S_c \to 0^+$, and thus $\chi'(S_c) \to -\infty$. Therefore, for $\mathcal{D}$ small enough we will eventually have $\sigma_j = 0$, with $k_j = \max_{2 \le j \le N}\{k_j\}$.

Principal Result 2.2.1 *As $\mathcal{D}$ is increased, i.e. as S_c is decreased, the smallest value of $\mathcal{D}$ for which $\lambda = 0$ is given by the root of the transcendental equation*

$$\frac{1}{\nu} - k_j = -\chi'(S_c), \quad S_c = \frac{2}{\sqrt{\mathcal{D}}N}, \tag{2.38}$$

where $k_j = \max_{2\leq j\leq N} k_j$, and $\mathcal{G}\vec{b_j} = k_j\vec{b_j}$, with $\vec{b_j}^T\vec{e} = 0$.

This criterion defines a threshold S_c^*, and since χ depends on f and N, then $S_c^* = S_c^*(f, N)$. In Figure 2.4 we compute the competition instability threshold for

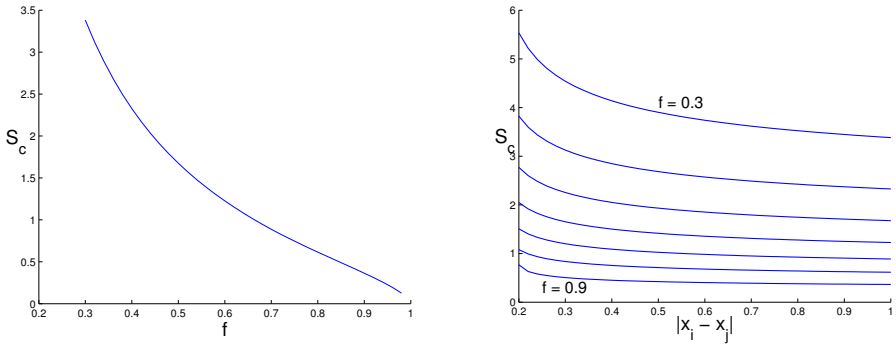

Figure 2.4: Competition instability threshold, i.e., stability with respect to the $m = 0$ mode when $\tau = 0$. The figure on the left is for two spots located at opposite poles of the sphere, and the figure on the right computes the threshold as a function of the distance between the spots (for fixed values of f).

two spots with common spot-strength S_c. The figure on the left considers the case of two spots located at opposite ends on a sphere, as a function of f. Since $S_c = 2/\sqrt{\mathcal{D}}N$ the profile of the curve f vs $\mathcal{D}_c$ would be monotonically increasing. If we are below any of the curves in these figures we would predict that a competition instability will occur.

The figure on the right computes the competition instability threshold for two spots at varying distances from each other, for fixed values of f. The result shows that the critical spot-strength S_c increases the closer the spots are to each other, and

equivalently $\mathcal{D}_c$ will decrease as they approach each other.

The key quantity determining the competition instability threshold is the largest eigenvalue of $\mathcal{G}$ in the subspace perpendicular to $\vec{e}$. For equally spaced spots, the matrix $\mathcal{G}$ has exactly two eigenvalues which can be calculated analytically. For the more general case of N spots, this must be done numerically.

We summarize our stability results so far as follows: Suppose that the spot locations are such that $\mathcal{G}\vec{e} = k_1\vec{e}$, so that they have a common source strength S_c. Then,

- If $S_c > \Sigma_2(f)$, a peanut-splitting linear instability occurs, which numerically is shown to lead to spot self-replication.
- If $S_c = S_c^*(f;N)$ then $\lambda = 0$, and in fact we predict that if $S_c < S_c^*(f;N)$, which corresponds to $\mathcal{D}$ too large, then there will exist a real positive eigenvalue with sign-fluctuating eigenfunction.

The interaction between these two thresholds could lead to the following scenario: Consider an initial condition of N homogeneously spaced (equally spaced if $N \leq 4$, or in a Fekete distribution for $N > 4$) spots on the surface of a sphere, and suppose that $\mathcal{D}$ is such that $S_c^* < \Sigma_2(f)$.

Suppose that there are N initial spots with a common source strength and that S_c exceeds the spot self-replication threshold Σ_2. Then, we predict that the N spots will split, self-replicating into $2N$ spots.

Suppose that now, for the $2N$ spots, their value of $S_c = \frac{2}{\sqrt{\mathcal{D}}(2N)}$ now satisfies $S_c < S_c^*(f;N)$. Then a sign-fluctuating instability will occur, which will annihilate some of the $2N$ spots, bringing the system back to a state for which the new S_c value exceeds the self-replication value.

This scenario may be too simplistic in that we are neglecting any motion of the

spots. More specifically, we cannot guarantee that the spots will remain equally spaced for all time. Thus, the Green's matrix equally may not be cyclic for all time. There is also the possibility that after the self-replication event the sign-fluctuating instability annihilates a different number of spots.

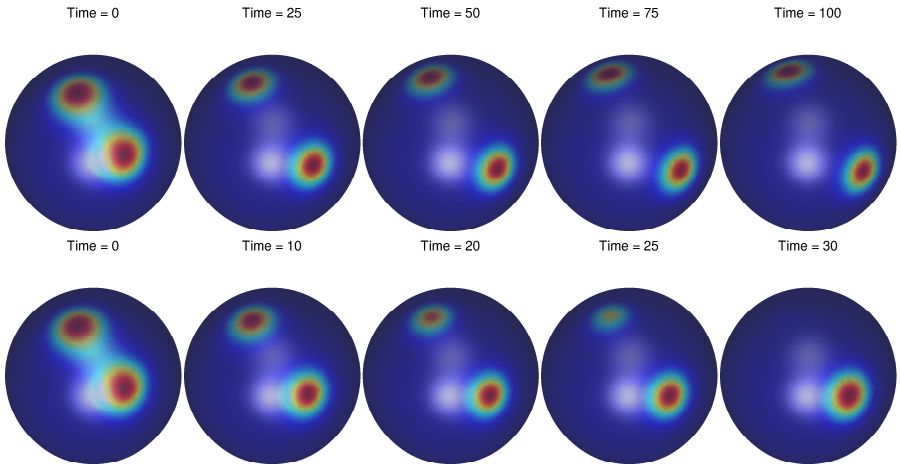

Figure 2.5: Full numerical simulation of the Brusselator model on a sphere ($u(\vec{x})$). A competition instability can be observed for the lower row ($\mathcal{D} = 1.2$), which is not triggered in the top row ($\mathcal{D} = 0.8$). Both scenarios have $f = 0.7, \varepsilon = 0.1$.

In the full numerical computations of the Brusselator exhibited in Figure 2.5 we show a competition instability that occurs for a two-spot pattern when the diffusivity $\mathcal{D}$ is large enough. The other parameter values are given in the caption of this figure. As mentioned earlier, the analytical estimate above does not account for the motion of the spots, and this complicates the determination of a threshold.

For the case $\tau = 0$ that we have been studying, we now would like to prove for the common source-strength case $S_c = S_1 = S_2 = \cdots = S_N$ that it is impossible for eigenvalues to enter the half-plane $\mathrm{Re}(\lambda) > 0$ except from $\lambda = 0$. In other words, we want to rule out Hopf bifurcations.

For this case, we label $\tilde{B}_j(\lambda, S_j, f) = \tilde{B}_c(\lambda, S_c, f)$ for all $j = 1, \ldots, N$. Then $\mathcal{M} = \frac{1}{\nu} + \tilde{B}_c(\lambda, s_c, f)(I - \mathcal{E}_0) - (I - \mathcal{E}_0)\mathcal{G}$. Recall that when $\mathcal{G}\vec{e} = k_1\vec{e}$, then $\mathcal{M}\vec{e} = \frac{1}{\nu}\vec{e}$. Alternatively, for $\mathcal{G}\vec{b} = k_j\vec{b}_j$, with $\vec{b}_j^t\vec{e} = 0$, then $\mathcal{M}\vec{b}_j = \left(\frac{1}{\nu} + \tilde{B}_c(\lambda, S_c, f) - k_j\right)\vec{b}_j$.

Thus, the eigenvalues λ are the roots of the transcendental equations

$$\frac{1}{\nu} + \tilde{B}_c(\lambda, S_c, f) - k_j = 0, \qquad j = 2, \ldots, N. \tag{2.39}$$

We aim to show that it is impossible for $\lambda = i\lambda_I$, with $\lambda_I > 0$, to be a solution to (2.39) for any $j = 2, \ldots, N$. This would prove that eigenvalues can only enter the unstable right-half plane along the real axis. Letting $\lambda = i\lambda_I$, and separating (2.39) into real and imaginary parts we conclude that any such Hopf bifurcation must satisfy

$$\text{Im}[\tilde{B}_c(i\lambda_I, S_c, f)] = 0, \qquad \text{Re}[\tilde{B}_c(i\lambda_I, S_c, f)] = -\frac{1}{\nu} + k_j. \tag{2.40}$$

Recall that $\tilde{B}_c(i\lambda_I, S_c, f)$ is computed from (2.22), which we write as

$$\begin{aligned} \mathcal{L}_\rho\tilde{\psi} - \tilde{\psi} + 2fu_cv_c\tilde{\psi} + fu_c^2\tilde{N} &= i\lambda_i\tilde{\psi}, \\ \mathcal{L}_\rho\tilde{N} + \tilde{\psi}(1 - 2u_cv_c) - u_c^2\tilde{N} &= 0, \\ \tilde{\psi} \to 0, \text{ as } \rho \to \infty, \\ \tilde{N} \sim \log\rho + \tilde{B}_c + o(1) \text{ as } \rho \to \infty, \end{aligned} \tag{2.41}$$

with $\mathcal{L}_\rho = \partial_{\rho\rho} + \frac{1}{\rho}\partial_\rho$, and (u_c, v_c) the solutions to the core problem.

If we now separate $\tilde{\psi}$ and $\tilde{N}$ in terms of their real and imaginary components as

$$\tilde{\psi} = \tilde{\psi}_R + i\tilde{\psi}_I, \qquad \tilde{N} = \tilde{N}_R + i\tilde{N}_I,$$

then from (2.41) we get

$$\begin{aligned}
\mathcal{L}_\rho\tilde{\psi}_R - \tilde{\psi}_R + 2fu_cv_c\tilde{\psi}_R + fu_c^2\tilde{N}_R &= -\lambda_I\tilde{\psi}_I,\\
\mathcal{L}_\rho\tilde{N}_R + \tilde{\psi}_R(1-2u_cv_c) &= u_c^2\tilde{N}_R,\\
\tilde{\psi}_R \to 0,\ \text{as } \rho\to\infty, \qquad \tilde{N}_R &\to \log\rho + \text{Re}(\tilde{B}_c) + o(1),\ \text{as } \rho\to\infty,\\
\mathcal{L}_\rho\tilde{\psi}_I - \tilde{\psi}_I + 2fu_cv_c\tilde{\psi}_I + fu_c^2\tilde{N}_I &= -\lambda_I\tilde{\psi}_R,\\
\mathcal{L}_\rho\tilde{N}_I + \tilde{\psi}_I(1-2u_cv_c) &= u_c^2\tilde{N}_I,\\
\tilde{\psi}_I \to 0,\ \text{as } \rho\to\infty, \qquad \tilde{N}_I &\to \text{Im}(\tilde{B}_c) + o(1),\ \text{as } \rho\to\infty.
\end{aligned}$$

There is no solution to $\mathcal{L}_\rho\tilde{N}_I = u_c^2\tilde{N}_I - \tilde{\psi}_I(1-2u_cv_c)$ for which $\tilde{N}_I \to 0$ as $\rho\to\infty$. The best one can say is that $\tilde{N}_I$ is bounded at infinity. In fact, in solving

$$u'' + \frac{1}{\rho}u' = f(\rho), \qquad 0<\rho<\infty, \quad u'(0)=0,$$

then $u \sim \left(\int_0^\infty yf(y)dy\right)\log\rho + o(1)$ at infinity. The logarithmic term vanishes only if $\left(\int_0^\infty yf(y)dy\right) = 0$. Therefore, we conclude that

$$\text{Im}[\tilde{B}_c(i\lambda_I, S_c, f)] \neq 0,$$

which contradicts the first equation in (2.40). We conclude that a Hopf bifurcation is impossible for the case $\tau = 0$ when the Green's matrix is cyclic. Instabilities for this case can only be triggered by eigenvalues crossing into $\text{Re}(\lambda) > 0$ along the real axis in the $\lambda-$plane.

2.2.6 Case B: The Hopf bifurcation case, $m \geq 2$ and $\tau > 0$

For the case $\tau > 0$, we will show that Hopf bifurcations in the spot amplitudes are possible. For this case, we return to (2.26), which we write as

$$\begin{aligned} \Delta_S \eta - \frac{\tau\lambda}{\mathcal{D}}\eta &= 2\pi \sum_{j=1}^{N} c_j \delta(x - x_j), \\ \eta &\sim \frac{c_j}{\mathcal{D}}\left[\log|x - x_j| + \frac{1}{\nu} + \tilde{B}_j\right] \qquad \text{as } x \to x_j, \quad j = 1, \ldots, N. \end{aligned}$$

We define $G_\lambda(x; x_0)$ to be the unique solution to

$$\begin{aligned} \Delta_S G_\lambda - \frac{\tau\lambda}{\mathcal{D}} G_\lambda &= -\delta(x - x_0), \\ G_\lambda(x; x_0) &\sim -\frac{1}{2\pi}\log|x - x_0| + R_\lambda + o(1), \quad x \to x_0\,. \end{aligned} \tag{2.42}$$

Here G_λ is 2π periodic in ϕ, and smooth in $\theta = 0, \pi$.

An explicit formula for G_λ can be written in terms of Legendre functions. We notice by symmetry that R_λ is independent of x_0. The solution for η is

$$\eta = -\frac{2\pi}{\mathcal{D}} \sum_{j=1}^{N} c_j G_\lambda(x; x_j).$$

Now, as $x \to x_i$, we obtain for each $i = 1, \ldots, N$ that the matching condition

$$\frac{2\pi}{\mathcal{D}}\left[-\frac{c_i}{2\pi}\log|x - x_i| + c_i R_\lambda + \sum_{j \neq i}^{N} c_j G_{\lambda ij}\right] \sim \frac{c_i}{\mathcal{D}}\left[\log|x - x_i| + \frac{1}{\nu} + \tilde{B}_i\right],$$

must hold. By matching the $O(1)$ terms, we conclude that

$$c_i + 2\pi\nu\left(c_i R_\lambda + \sum_{j \neq i}^{N} c_j G_{\lambda ij}\right) + \nu\tilde{B}_i c_i = 0\,. \qquad i = 1, \ldots, N. \tag{2.43}$$

For this case it is no longer holds that we can write for any x on sphere that

$$G_\lambda(x;x_j) = -\frac{1}{2\pi}\log|x-x_j| + \text{ constant},$$

where the constant is independent of x. In fact, there must be terms of the form $|x-x_0|^2\log|x-x_0|$, etc. As such, we can only write (2.43) as

$$I\vec{c}+2\pi\nu\mathcal{G}_\lambda\vec{c}+\nu\tilde{B}\vec{c}=0, \qquad \vec{c}=\begin{pmatrix} c_1 \\ \vdots \\ c_N \end{pmatrix}, \quad \mathcal{G}_\lambda = \begin{pmatrix} R_\lambda & & G_{\lambda ij} \\ & \ddots & \\ G_{\lambda ij} & & R_\lambda \end{pmatrix}, \tag{2.44}$$

where the $\mathcal{G}_\lambda$ matrix has common entries along its diagonal that are independent of the spot locations. In addition,

$$\tilde{B} = \begin{pmatrix} \tilde{B}_1 & & 0 \\ & \ddots & \\ 0 & & \tilde{B}_N \end{pmatrix}.$$

Thus we conclude that λ must be such that the matrix problem

$$\tilde{\mathcal{M}}\vec{c}=0, \qquad \tilde{\mathcal{M}} \equiv I + 2\pi\nu\mathcal{G}_\lambda + \nu\tilde{B} \tag{2.45}$$

has a non-trivial solution, i.e., that $\det\tilde{\mathcal{M}} = 0$.

Next, we consider the case where the spots have a common source strength S_c, with $S_c = S_1 = \cdots = S_N$. Then,

$$\tilde{B} = \tilde{B}_c(\lambda; S_c, f)I,$$

so that

$$\tilde{\mathcal{M}} = I + 2\pi\nu\mathcal{G}_\lambda + \nu\tilde{B}_c I.$$

In terms of the matrix spectrum of $\mathcal{G}_\lambda$

$$\mathcal{G}_\lambda \vec{b}_{j\lambda} = k_{j\lambda}\vec{b}_{j\lambda} \quad \text{for } j = 1, \ldots, N,$$

it follows that

$$\tilde{\mathcal{M}}\vec{b}_{j\lambda} = \left(1 + 2\pi\nu k_{j\lambda} + \nu\tilde{B}_c\right)\vec{b}_{j\lambda}.$$

We conclude that $\det \tilde{\mathcal{M}} = 0$ when

$$1 + 2\pi\nu k_{j\lambda} + \nu\tilde{B}_c = 0, \qquad j = 1, \ldots, N. \tag{2.46}$$

We remark that as τ increases it is impossible for eigenvalues to enter $\text{Re}(\lambda) > 0$ along the real axis by crossing through $\lambda = 0$. This is because $\mathcal{G}_\lambda$ depends only on the product $\tau\lambda$, which vanishes when $\lambda = 0$. Secondly, in (2.46) we recall that $\tilde{B}_c(\lambda; S_c, f)$ is obtained from the solution to

$$\begin{aligned} \mathcal{L}_\rho\tilde{\psi} - \tilde{\psi} + 2fu_cv_c\tilde{\psi} + fu_c^2\tilde{N} &= \lambda\tilde{\psi}, \\ \mathcal{L}_\rho\tilde{N} + \tilde{\psi}(1 - 2u_cv_c) &= u_c^2\tilde{N}, \\ \tilde{\psi} \to 0, \quad \tilde{N} \sim \log\rho + \tilde{B}_c(\lambda, S_c, f) + o(1) &\text{ as } \rho \to \infty. \end{aligned} \tag{2.47}$$

We remark that $\tilde{\psi}$ and $\tilde{N}$ are complex-valued when $\lambda = \lambda_R + i\lambda_I$ is complex. However, given a complex-valued λ we can readily solve this BVP by separating the solution into real and imaginary parts and then identifying $\text{Re}[\tilde{B}_c]$ and $\text{Im}[\tilde{B}_c]$.

Now, we look for a Hopf bifurcation that occurs at some value $\tau = \tau_{Hj}$, for $j = 1, \ldots, N$. The stability threshold τ_H is defined by

$$\tau_h = \min_j\{\tau_{Hj}\}.$$

We predict that the N-spot solution is stable to an oscillatory profile instability if $0 < \tau < \tau_H$. Thus, we define $\lambda = i\lambda_{Ij}$ and $\tau = \tau_{Hj}$, and we need to compute λ_{Ij}

and τ_{Hj} for which

$$\begin{aligned} \nu^{-1} + 2\pi \text{Re}[k_{j\lambda}] + \text{Re}[\tilde{B}(i\lambda_I, S_c, f)] = 0, \\ 2\pi \text{Im}[k_{j\lambda}] + \text{Im}[\tilde{B}(i\lambda_I, S_c, f)] = 0. \end{aligned} \tag{2.48}$$

In order to compute the numerical solution to (2.48), for fixed locations $x_1, \ldots, x_N$ for which we have a common source strength S_c, the following steps were taken:

(i) We need to calculate the Green's function $G_\lambda(x; x_j)$ that satisfies

$$\begin{aligned} \Delta_s G_\lambda - \frac{i\lambda_{Ij}\tau_{Hj}}{\mathcal{D}} G_\lambda = -\delta(x - x_j), \\ G_\lambda \sim -\frac{1}{2\pi} \log|x - x_j| + R_\lambda, \quad \text{as } x \to x_j. \end{aligned}$$

For this we use the result in the appendix of [11], that connects this equation to the Legendre function of first kind of complex order σ, $P_\sigma(z)$. We have that the solution to

$$\Delta_s G_h + \sigma(\sigma + 1) G_h = -\delta(\vec{x} - \vec{x_0}), \tag{2.49}$$

with $\vec{x}$ on the sphere and where G_h is 2π periodic and smooth at $\phi = 0, 2\pi$ is given by

$$G_h(x; x_0) = -\frac{1}{4\sin(\pi\sigma)} P_\sigma(-\vec{x} \cdot \vec{x_0}),$$

when σ not an integer.

As $z \to -1^+$, we have that (see the appendix of [11])

$$P_\sigma(z) \sim \frac{\sin(\pi\sigma}{\pi} \left[\log\left(\frac{1+z}{2}\right) + 2\gamma + 2\Phi(\sigma + 1) + \pi \cot(\pi\sigma) \right].$$

Here γ is Euler's constant, $\Phi(z)$ is the Psi or digamma function $\Phi(z) = \Gamma'(z)/\Gamma(z)$, with $\Gamma(z)$ the gamma function.

Numerically, we evaluated the complex digamma function terms on Maple

and the rest of the routine was done in Matlab. Now, as $\vec{x} \to \vec{x_0}$, we have

$$G_h(x; x_0) \sim -\frac{1}{2\pi} \log |\vec{x} - \vec{x_0}| + R_h,$$

where

$$R_h \equiv -\frac{1}{4\pi} \left[-2 \log 2 + 2\gamma + 2\Phi(\sigma + 1) + \pi \cot(\pi\sigma) \right].$$

Therefore, in order to obtain $G_\lambda(\vec{x}; \vec{x_j})$ and R_λ, we simply need to set

$$\sigma(\sigma + 1) = -\frac{i\lambda_I \tau}{\mathcal{D}},$$

and solve for σ. We obtain

$$\sigma = -\frac{1}{2} + \sqrt{\frac{1}{4} - \frac{i\lambda_I \tau}{\mathcal{D}}},$$

and we must choose the principal branch $\text{Re}\left(\sqrt{1/4 - i\lambda_I \tau/\mathcal{D}}\right) > 0$ on account of the requirement that $\sigma = 0$ when $\tau = 0$.

(ii) Once we have identified $G_\lambda(x_i; x_j)$ for $i \neq j$ and R_λ, we build the complex-valued matrix

$$\mathcal{G}_\lambda = \begin{pmatrix} R_\lambda & & G_{\lambda ij} \\ & \ddots & \\ G_{\lambda ij} & & R_\lambda \end{pmatrix}$$

and calculate the complex-valued eigenvalues $k_{\lambda j}$ for $j = 1, \ldots, N$ of this matrix.

We remark that $\mathcal{G}_\lambda$ is symmetric, but not Hermitian when $\lambda = i\lambda_I$, since $G_{\lambda ij} \neq \overline{G_{\lambda ji}}$. Thus, the $k_{\lambda j}$ eigenvalues are in general complex-valued.

(iii) We next calculate the real and imaginary parts of $\tilde{B}(i\lambda_I, S_c, f)$ from the complex BVP (2.47).

(iv) For each eigenvalue $k_{\lambda j}$ we do a 2×2 matrix Newton update on the nonlinear system from (2.46).

Figure 2.6 shows the results of the full numerical simulation. We used an initial approximation obtained by using $\mathcal{D} = 100$ (as outlined in the procedure described below), and we did a continuation on $\mathcal{D}$ to obtain the Hopf bifurcation threshold for smaller values of $\mathcal{D}$.

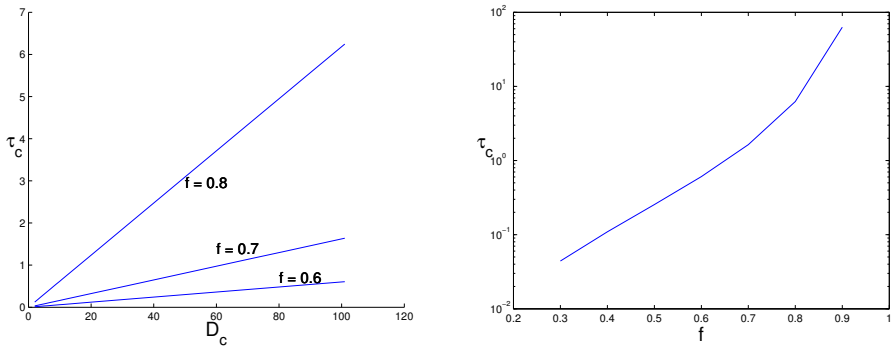

Figure 2.6: The Hopf bifurcation threshold for varying $\mathcal{D}$ (left), and as a function of f when $\mathcal{D} = 100$.

An important remark is that the Newton update is on the two variables (τ, λ_I), and without a good starting guess it is very hard to converge to a solution. However, it is possible to find a good initial guess when considering $\mathcal{D} \gg 1$.

If we let $\varepsilon = \frac{\lambda_I \tau}{\mathcal{D}}$, with $\varepsilon \ll 1$, we need to solve

$$\Delta_s G - i\varepsilon G = -\delta(\vec{x} - \vec{x_0}).$$

We do an asymptotic expansion $G \sim \frac{G_0}{\varepsilon} + G_1 + \cdots$, and we get that G_0 is a constant, and that G_1 satisfies

$$\Delta_s G_1 - iG_0 = -\delta(\vec{x} - \vec{x_0}).$$

By integrating over the sphere, and using the explicit formula for the Green's func-

tion in (2.11), we have

$$G_0 = -\frac{i}{4\pi}, \qquad G_1 = -\frac{1}{2\pi}\log|\vec{x} - \vec{x_0}| + R_1, \qquad R_1 = \frac{1}{4\pi}(2\log 2 - 1).$$

For the one spot case, the eigenvalue of the Green's matrix will simply be the regular part, and therefore we have the approximation $k_\lambda = G_0/\varepsilon + R_1$. This effectively decouples (2.48), and we can find the other variable by a bisection algorithm. The approximation also serves as an independent check with the full solution of the Green's function in (2.49). With the initial condition variables, the difference between the asymptotic approximation to G and the full Legendre solution is of less than three decimal digits in both the real and imaginary parts.

In particular, we used $\mathrm{Re}(k_\lambda) = \frac{1}{4\pi}(2\log 2 - 1) \simeq 0.03074$, and solved the first equation in (2.48). At each iteration we had to solve the complex BVP version of (2.47) on both sides of the bisection bracket. After a few iterations we found an initial estimate $(\lambda = 0.8489380, \tau = 1.621877)$, which we finally used as the seed to the Newton algorithm.

Finding the threshold for smaller values of $\mathcal{D}$ is simply a matter of performing numerical continuation.

In the N-spot case one of the eigenvectors will correspond to $\vec{e}$ since

$$\mathcal{G}_\lambda \vec{e} = k_{\lambda 1}\vec{e}$$

should hold. This eigenvalue corresponds to a synchronous oscillatory instability of the spot amplitudes.

2.3 Leading-order theory

In the previous section, an asymptotic method based on accounting for all logarithmic terms in ν was developed in order to construct quasi-equilibrium spot patterns and to analyze their stability. However, the implementation of this theory required some numerical computations, and so the overall approach can be considered a hybrid analytical-numerical theory.

In this section, we will formulate a leading-order-in-ν theory for the existence and stability of an N-spot quasi-equilibrium solution for the regime where

$$\mathcal{D} = \frac{\mathcal{D}_0}{\nu}, \qquad \nu = -\frac{1}{\log \varepsilon}, \qquad \text{and} \quad \mathcal{D}_0 = O(1).$$

With this approach we will obtain explicit analytical results for the profile of each spot and for the competition instability threshold.

For this range of $\mathcal{D}$, the equilibrium problem is

$$\begin{aligned} \varepsilon^2 \Delta_s u + \varepsilon^2 \mathrm{E} - u + f u^2 v = 0, \\ \mathcal{D}_0 \Delta_s v + \frac{\nu}{\varepsilon^2}\left(u - u^2 v\right) = 0. \end{aligned} \tag{2.50}$$

We now construct a leading-order quasi-equilibrium solution using the method of matched asymptotic expansions. We begin with the inner problem.

2.3.1 Inner problem

We let $\hat{\phi} = \varepsilon^{-1}(\phi - \phi_j)$ and $\hat{\theta} = \varepsilon^{-1}(\theta - \theta_j)$, where $y_1 = \sin\theta_j \hat{\phi}$ and $y_2 = \hat{\theta}$. Then, with $\rho = (y_1^2 + y_2^2)^{1/2}$, we obtain the following local problem on $\rho > 0$:

$$\begin{aligned} \Delta_\rho U_j - U_j + f U_j^2 V_j = 0, \qquad \Delta_\rho \equiv \partial_{\rho\rho} + \frac{1}{\rho}\partial_\rho, \\ \Delta_\rho V_j + \frac{\nu}{\mathcal{D}_0}(U_j - U_j^2 V_j) = 0. \end{aligned}$$

Now, for $\nu \ll 1$, we expand

$$U_j = U_{j0} + \nu U_{j1} + \ldots, \qquad V_j = V_{j0} + \nu V_{j1} + \ldots$$

We obtain that V_{j0} is a constant, and that U_{j0} satisfies

$$\Delta_\rho U_{j0} - U_{j0} + f V_{j0} U_{j0}^2 = 0,$$

so that $U_{j0} = \frac{1}{f V_{j0}^2} w(\rho)$, where w on $\rho > 0$ satisfies

$$\begin{aligned} \Delta_\rho w - w + w^2 = 0, \qquad \rho > 0, \\ w(0) > 0, \qquad w'(0) = 0, \qquad w \to 0 \quad \text{as } \rho \to \infty. \end{aligned} \tag{2.51}$$

Here $w = w(\rho)$ is called the "ground-state" solution. Figure 2.7 shows the numerical solution for $w(\rho)$, as computed with Matlab's BVP5C routine.

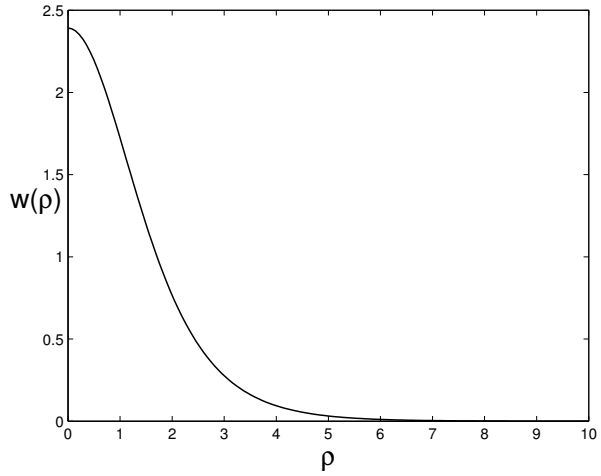

Figure 2.7: Numerical solution to the ground-state BVP $\Delta_\rho w - w + w^2 = 0$.

At next order the equation for V_{j1} is

$$\Delta_\rho V_{j1} = \frac{1}{\mathcal{D}_0}(U_{j0}^2 V_{j0} - U_{j0}) = \frac{1}{\mathcal{D}_0}\left(\frac{1}{f^2 V_{j0}} w^2 - \frac{1}{f V_{j0}} w\right).$$

Therefore, $V_{j1} \sim A_{j1} \log|y|$ as $|y| \to \infty$, where

$$A_{j1} \equiv \frac{1}{\mathcal{D}_0 f V_{j0}}\left(\frac{1}{f}\int_0^\infty \rho w^2 d\rho - \int_0^\infty \rho w d\rho\right).$$

However, from integrating (2.51) we see that $\int_0^\infty \rho w d\rho = \int_0^\infty \rho w^2 d\rho$. Thus, we conclude that

$$U_j \sim U_{j0} = \frac{1}{f V_{j0}} w(\rho), \qquad V_j \sim V_{j0} + \nu V_{j1} + \ldots,$$

with

$$\Delta_\rho V_{j1} = \frac{1}{\mathcal{D}_0 f V_{j0}}\left(\frac{1}{f} w^2 - w\right),$$

and $V_{j1} \sim A_{j1} \log\rho + o(1)$ as $\rho \to \infty$, where

$$A_{j1} = \frac{b}{\mathcal{D}_0 f V_{j0}}\left(\frac{1}{f} - 1\right), \qquad b = \int_0^\infty \rho w^2 d\rho\,.$$

Thus, if we set $\rho = \varepsilon^{-1}|x - x_j|$, we obtain the matching condition

$$V_j \sim V_{j0} + A_{j1}\nu \log|x - x_j| + A_{j1} \qquad \text{as } x \to x_j.$$

We remark that since $\Delta_\rho V_{j1} = g(\rho)$ for some known function $g(\rho)$, and $V_{j1} = V_{j1}(\rho)$ with $V_{j1}'(0) = 0$, we can impose that $V_{j1} - \left(\int_0^\infty z g(z) dz\right)\log\rho \to 0$ as $\rho \to \infty$. This follows because we can always add a constant to the solution for V_{j1} as it is a linear differential equation.

2.3.2 Outer expansion

In the outer region we obtain $u \sim \varepsilon^2 \mathrm{E}$, and so for $|x - x_j| \gg O(\varepsilon)$ we get the global contribution

$$\frac{\nu}{\varepsilon^2}(u - u^2 v) \simeq \nu \mathrm{E} + O(\varepsilon^2 v).$$

In contrast, the local contribution from the $x = x_j$ region is

$$\begin{aligned}
\frac{\nu}{\varepsilon^2}(u - u^2 v) &\sim 2\pi\nu \int_0^\infty (U_{j0} - U_{j0}^2 V_{j0}) \rho d\rho \, \delta(x - x_j), \\
&\sim 2\pi\nu \int_0^\infty \left(\frac{1}{f V_{j0}} w - \frac{1}{f^2 V_{j0}} w^2 \right) \rho d\rho \, \delta(x - x_j), \\
&\sim \frac{2\pi\nu}{f V_{j0}} \left(1 - \frac{1}{f} \right) \int_0^\infty \rho w^2 d\rho \, \delta(x - x_j).
\end{aligned}$$

Thus, in terms of A_{j1} computed previously, the local contribution from the j-th spot is

$$\frac{\nu}{\varepsilon^2}(u - u^2 v) \sim -2\pi \mathcal{D}_0 \nu A_{j1} \delta(x - x_j),$$

where

$$A_{j1} = \frac{1}{\mathcal{D}_0 f V_{j0}} \left(\frac{1}{f} - 1 \right) \left(\int_0^\infty \rho w^2 d\rho \right).$$

By combining the local and global contributions, we obtain the outer problem

$$\begin{aligned}
\Delta_s v + \frac{v\mathrm{E}}{\mathcal{D}_0} &= 2\pi\nu \sum_{j=1}^N A_{j1} \delta(x - x_j), \\
v \sim V_{j0} + A_{j1} + \nu A_{j1} \log|x - x_j| \qquad &\text{as } x \to x_j, \quad j = 1, \ldots, N \,.
\end{aligned} \tag{2.52}$$

Our goal now is to determine a nonlinear algebraic system for V_{j0} for $j = 1, \ldots, N$. Upon integrating (2.52) over the sphere, we obtain the solvability condition

$$\frac{\mathrm{E}}{\mathcal{D}_0} = \frac{1}{2} \sum_{j=1}^N A_{j1} \,.$$

In terms of an as yet unknown constant $\overline{v}$, the solution to (2.52) is

$$v = -2\pi\nu \sum_{j=1}^{N} A_{j1} G(x; x_j) + \overline{v}, \tag{2.53}$$

where G is the Neumann Green's function for the unit sphere.

Now, equating the leading terms in v as $x \to x_i$ with the non-singular terms in (2.52) as $x \to x_i$, we obtain that

$$v \sim \overline{v} + O(\nu) = V_{j0} + A_{j1} + O(\nu), \qquad i = 1, \ldots, N.$$

Thus, our leading-order-in-ν theory yields that

$$\begin{aligned} \overline{v} &= V_{j0} + A_{j1}, \qquad j = 1, \ldots, N, \\ \frac{\mathrm{E}}{\mathcal{D}_0} &= \frac{1}{2} \sum_{j=1}^{N} A_{j1}, \\ \text{with} \quad A_{j1} = \frac{\mathcal{B}}{V_{j0}}, &\qquad \mathcal{B} \equiv \frac{1}{\mathcal{D}_0 f} \left(\frac{1}{f} - 1 \right) \int_0^\infty \rho w^2 d\rho > 0. \end{aligned} \tag{2.54}$$

Next, we solve this leading order system (2.54) for V_{j0}.

We have $\overline{v} \equiv H(V_{j0}) = V_{j0} + \frac{\mathcal{B}}{V_{j0}}$, where $\overline{v}$ is a constant independent of j. A simple plot of $H(V_{j0})$ versus V_{j0} shows that $H \to \infty$ as $V_{j0} \to 0^+$ and as $V_{j0} \to +\infty$. Furthermore, $H(V_{j0})$ has a unique critical point at $V_{j0} = \sqrt{\beta}$ with $H'' > 0$ for all $V_{j0} > 0$. Therefore, by looking for intersections of $H(V_{j0})$ with the constant $\overline{v}$, we conclude that there are only two possible values of V_{j0}, which we label as V_{j0s} and V_{j0b}.

2.3.3 Case I: $V_{j0s} = V_{j0b}$, symmetric spot quasi-equilibrium

For a collection of N spots, suppose that we take a common value for V_{j0} for each spot. Then $V_{j0} = V_0$, and we have $A_{j1} = \frac{\mathcal{B}}{V_0}$, and $\frac{\mathrm{E}}{\mathcal{D}_0} = \frac{1}{2}\frac{\mathcal{B}}{V_0}N$. Hence, $V_0 = \frac{\mathcal{D}_0\mathcal{V}N}{2\mathrm{E}}$ is the common value, and we calculate $\overline{v} = V_0 + \frac{\mathcal{B}}{V_0}$. Given that $H(V_0)$ is a concave-up curve for $V_0 > 0$, we will be either to the left or to the right of the minimum at $V_0 = \sqrt{\mathcal{B}}$.

This construction yields to leading-order in ν an N-spot pattern with spots of equal height. For this symmetric pattern, the quasi-equilibrium solution has the form

$$\begin{aligned} u &\sim \varepsilon^2\mathrm{E} + \sum_{j=1}^{N} \frac{1}{fV_0} w\left(\varepsilon^{-1}|x - x_j|\right), \\ \text{where} \quad V_0 &= \frac{\mathcal{D}_0\mathcal{B}N}{2\mathrm{E}}, \qquad \mathcal{B} \equiv \frac{1}{\mathcal{D}_0 f}\left(\frac{1}{f} - 1\right)\int_0^\infty \rho w^2 d\rho. \end{aligned} \tag{2.55}$$

Notice that $\mathcal{B} > 0$ since $0 < f < 1$. Thus, V_0 is independent of $\mathcal{D}_0$.

2.3.4 Case II: Asymmetric spot equilibria

In the remainder of this chapter we will focus on symmetric spot patterns. However, we now briefly mention that one can also construct asymmetric patterns where the spots have different amplitudes. To see this suppose that we have M_1 small amplitude spots with $V_{j0} = V_{0b}$ for $j = 1, \ldots, M_1$, and M_2 large amplitude spots with $V_{j0} = V_{0s}$ for $j = M_1 + 1, \ldots, N$, where $M_2 = N - M_1$. We note that since $U_{j0} \sim \frac{1}{fV_{j0}} w$, a large value of V_{j0} yields a small-amplitude spot, and vice versa.

The small and large spots must be such that

$$\overline{v} = V_{0b} + \frac{\mathcal{B}}{V_{0b}} = V_{0s} + \frac{\mathcal{B}}{V_{0s}}.$$

Then, by Using $A_{j1} = \frac{\mathcal{B}}{V_{j0}}$ from (2.54), we obtain

$$\frac{\mathrm{E}}{\mathcal{D}_0} = \frac{1}{2}\sum_{j=1}^{N} A_{j1} = \frac{\mathcal{B}}{2}\left(\frac{M_1}{V_{0b}} + \frac{M_2}{V_{0s}}\right).$$

Therefore, we conclude that V_{0b}, V_{0s} satisfy the coupled nonlinear algebraic problem

$$\frac{\mathrm{E}}{\mathcal{D}_0} = \frac{\mathcal{B}}{2}\left(\frac{M_1}{V_{0b}} + \frac{(N-M_1)}{V_{0s}}\right), \qquad V_{0b} + \frac{\mathcal{B}}{V_{0b}} = V_{0s} + \frac{\mathcal{B}}{V_{0s}}. \tag{2.56}$$

This yields two equations for the two unknowns V_{0b} and V_{0s}.

Now, the system (2.56) is not solvable for all values of $\mathcal{D}_0$. At the coalescence point where $V_{0s} = V_{0b} = \sqrt{\mathcal{B}}$, we have that

$$\mathcal{D}_{0ASY} = \frac{2\mathrm{E}}{\sqrt{\mathcal{B}}N}, \qquad \mathcal{B} = \frac{b(1-f)}{\mathcal{D}_0 f^2}.$$

At this particular value of $\mathcal{D}$, solution branches of asymmetric quasi-equilibrium patterns bifurcate off of the symmetric solution branch. If $\mathcal{D}_0 > \mathcal{D}_{0ASY}$ the system (2.56) should not be solvable. This construction indicates that there exists asymmetric spot equilibria to leading-order in ν when

$$\mathcal{D} \sim \frac{\mathcal{D}_0}{\nu}, \qquad \text{and} \quad \mathcal{D}_0 < \mathcal{D}_{0ASY}.$$

2.4 Derivation from the S-formulation

In this section we show how to independently recover the leading-order results in the previous section by considering the limit as $S_j \to 0$ of the S-formulation of §2.1. Near the j-th spot we recall from (2.5) that

$$U_j = \mathcal{D}^{1/2} u_j, \qquad V_j = \mathcal{D}^{-1/2} v_j,$$

so that (u_j, v_j) satisfy (see (2.6))

$$\begin{aligned} \Delta_\rho u_j - u_j + f u_j^2 v_j = 0, \qquad & u_j \to 0 \text{ as } \rho \to \infty, \\ \Delta_\rho v_j + u_j - u_j^2 v_j = 0, \qquad & v_j \sim S_j \log \rho + \chi(S_j) \text{ as } \rho \to \infty. \end{aligned} \tag{2.57}$$

and where the S_i for $i = 1, \ldots, N$ satisfy (2.14), written again as

$$\begin{aligned} & S_i - \nu \sum_{j \neq i}^{N} S_j L_{ij} + \frac{\nu R_0 \mathrm{E}}{\sqrt{\mathcal{D}}} + \nu \chi(S_i; f) = \nu \overline{v}, \quad i = 1, \ldots, N\,, \\ & L_{ij} \equiv \log |x_i - x_j|, \qquad \sum_{i=1}^{N} S_i = \frac{2\mathrm{E}}{\sqrt{\mathcal{D}}}, \qquad R_0 = 2 \log 2 - 1. \end{aligned} \tag{2.58}$$

We want now to expand the system as $S_j \to 0$ when $\mathcal{D} = \mathcal{D}_0/\nu \gg 1$. As such, we must consider the following side problem, which will determine the asymptotics of $\chi(S_i; f)$ as $S_i \to 0$:

2.4.1 Core problem: Small S-asymptotics

For $S \to 0$, we now calculate u, v, and χ for

$$\begin{aligned} \Delta_\rho u - u + f u^2 v = 0, \qquad & u \to 0 \text{ as } \quad \rho \to \infty, \\ \Delta_\rho v + u - u^2 v = 0, \qquad & v \sim S \log \rho + \chi \text{ as } \quad \rho \to \infty. \end{aligned}$$

We write $u = S\tilde{u}$, $v = \tilde{v}/S$, and $\chi = \tilde{\chi}/S$ to obtain

$$\begin{aligned} \Delta_\rho \tilde{u} - \tilde{u} + f \tilde{u}^2 \tilde{v} = 0, \qquad & \tilde{u} \to 0 \text{ as } \quad \rho \to \infty, \\ \Delta_\rho \tilde{v} + S^2(\tilde{u} - \tilde{u}^2 \tilde{v}) = 0, \qquad & \tilde{v} \sim S^2 \log \rho + \tilde{\chi} \text{ as } \quad \rho \to \infty. \end{aligned}$$

This suggests that we should seek an approximate solution for $S \ll 1$ in the

form

$$\tilde{u} = \tilde{u}_0 + S^2\tilde{u}_1 + S^4\tilde{u}_2 + \cdots ,$$
$$\tilde{v} = \tilde{v}_0 + S^2\tilde{v}_1 + S^4\tilde{v}_2 + \cdots ,$$
$$\tilde{\chi} = \tilde{\chi}_0 + S^2\tilde{\chi}_1 + S^4\tilde{\chi}_2 + \ldots .$$

Upon substituting this expansion into the problem for $(\tilde{u}, \tilde{v})$ and collecting powers of S^2 we obtain the following sequence of problems:

$$\begin{aligned} \Delta_\rho\tilde{u}_0 - \tilde{u}_0 + f\tilde{u}_0^2\tilde{v}_0 = 0, \qquad \tilde{u}_0 \to 0 \quad \text{as} \quad \rho \to \infty, \\ \Delta_\rho\tilde{v}_0 = 0, \qquad \tilde{v}_0 \to \tilde{\chi}_0, \quad \text{as} \quad \rho \to \infty \end{aligned} \tag{2.59}$$

$$\begin{aligned} \Delta_\rho\tilde{u}_1 - \tilde{u}_1 + 2f\tilde{u}_0\tilde{v}_0\tilde{u}_1 = -f\tilde{u}_0^2\tilde{v}_1, \qquad \tilde{v}_1 \to 0 \quad \text{as} \quad \rho \to \infty, \\ \Delta_\rho\tilde{v}_1 = -\tilde{u}_0 + \tilde{u}_0^2\tilde{v}_0, \qquad \tilde{v}_1 \to \log\rho + \tilde{\chi}_1 \quad \text{as} \quad \rho \to \infty. \end{aligned} \tag{2.60}$$

In addition, we obtain that $\tilde{v}_2$ satisfies

$$\Delta_\rho\tilde{v}_2 = -\tilde{u}_1 + 2\tilde{u}_0\tilde{v}_0\tilde{u}_1 + \tilde{u}_0^2\tilde{v}_1 , \tag{2.61}$$

with $\tilde{v}_2$ bounded as $\rho \to \infty$.

We conclude that

$$\tilde{u}_0 = \frac{1}{f\tilde{v}_0}w, \qquad \tilde{v}_0 = \tilde{\chi}_0, \tag{2.62}$$

where w is the ground-state solution satisfying $\Delta_\rho w - w + w^2 = 0$.

Notice that since $w \to 0$ at infinity, then $\int_0^\infty \rho w d\rho = \int_0^\infty \rho w^2 d\rho$. Next, the solvability condition from the $\tilde{v}_1$ equation yields that

$$\lim_{\rho\to\infty} \rho\tilde{v}_{1\rho} = \int_0^\infty \left(-\tilde{u}_0 + \tilde{u}_0^2\tilde{v}_0\right)\rho d\rho,$$

with $\tilde{v}_{1\rho} = 1/\rho$ as $\rho \to \infty$. Thus, from (2.62) we obtain that

$$1 = -\frac{1}{f\tilde{v}_0}\int_0^\infty \rho w d\rho + \frac{1}{f^2\tilde{v}_0}\int_0^\infty \rho w^2 d\rho.$$

Then, since $\int_0^\infty \rho w d\rho = \int_0^\infty \rho w^2 d\rho$, we conclude that

$$\tilde{v}_0 = \tilde{\chi}_0 = \frac{b(1-f)}{f^2}, \quad \text{with} \quad b = \int_0^\infty \rho w^2 d\rho \approx 4.9343. \tag{2.63}$$

The numerical value for b was obtained from the numerical computation of the ground state shown in Figure 2.7. With the leading-order terms calculated, the problem for the second-order terms $\tilde{u}_1$, $\tilde{v}_1$ can then be written as

$$\begin{aligned} &\Delta_\rho \tilde{u}_1 - \tilde{u}_1 + 2w\tilde{u}_1 = -\frac{1}{f\tilde{v}_0^2} w^2 \tilde{v}_1, \qquad \tilde{u}_1 \to 0 \quad \text{as} \quad \rho \to \infty, \\ &\Delta_\rho \tilde{v}_1 = \frac{1}{\tilde{v}_0}\left(\frac{w^2}{f^2} - \frac{w}{f}\right), \qquad \tilde{v}_1 \sim \log\rho + \tilde{\chi}_1, \quad \text{as} \quad \rho \to \infty. \end{aligned} \tag{2.64}$$

Next, the solvability condition for the $\tilde{v}_2$ equation (2.61) yields that

$$\int_0^\infty (2\tilde{u}_0\tilde{v}_0 - 1)\tilde{u}_1 \rho d\rho + \int_0^\infty \tilde{u}_0^2 \tilde{v}_1 \rho d\rho = 0.$$

Upon using $\tilde{u}_0 = \frac{1}{f\tilde{v}_0} w$ this becomes

$$\int_0^\infty \left(\frac{2w}{f} - 1\right)\tilde{u}_1 \rho d\rho + \frac{1}{f^2\tilde{v}_0^2}\int_0^\infty w^2 \tilde{v}_1 \rho d\rho = 0. \tag{2.65}$$

We now integrate multiply the equation for $\tilde{u}_1$ in (2.64) by f^{-1} and integrate to obtain

$$\frac{1}{f}\int_0^\infty \rho\Delta_\rho \tilde{u}_1 d\rho - \frac{1}{f}\int_0^\infty \rho\tilde{u}_1 d\rho + \frac{1}{f}\int_0^\infty 2w\tilde{u}_1 \rho d\rho = -\frac{1}{f^2\tilde{v}_0^2}\int_0^\infty w^2\tilde{v}_1\rho d\rho.$$

Upon combining this with (2.65) we obtain

$$\int_0^\infty \left(\frac{2w}{f} - 1\right) \tilde{u}_1 \rho d\rho = \int_0^\infty \frac{2w}{f} \tilde{u}_1 \rho d\rho - \int_0^\infty \frac{1}{f} \tilde{u}_1 \rho d\rho + \int_0^\infty \frac{1}{f} \rho \Delta_\rho \tilde{u}_1 d\rho.$$

Since $\tilde{u}_1'(0) = 0$ and $\tilde{u}_1 \to 0$ as $\rho \to \infty$, the last integral vanishes upon integration, and so the equation above reduces to

$$\left(\frac{1}{f} - 1\right) \int_0^\infty \tilde{u}_1 \rho d\rho = 0.$$

Since $0 < f < 1$, we conclude that

$$\int_0^\infty \tilde{u}_1 \rho d\rho = 0. \tag{2.66}$$

We now show how this equation determines $\tilde{\chi}_1$.

We return to (2.64). The solution can be written in the form

$$\tilde{v}_1 = \tilde{\chi}_1 + \frac{1}{\tilde{v}_0 f^2} \tilde{v}_{1p},$$

where $\tilde{v}_{1p}$ is the unique solution on $0 < \rho < \infty$ to

$$\begin{aligned} &\Delta_\rho \tilde{v}_{1p} = \tilde{v}_{1p}'' + \frac{1}{\rho} \tilde{v}_{1p}' = w^2 - fw, \\ &\tilde{v}_{1p} \sim \tilde{v}_0 f^2 \log \rho + o(1) \quad \text{as} \quad \rho \to \infty\,; \qquad \tilde{v}_{1p}'(0) = 0. \end{aligned} \tag{2.67}$$

The uniqueness of $\tilde{v}_{1p}$ follows from the condition that $\tilde{v}_{1p} - \tilde{v}_0 f^2 \log \rho \to 0$ as $\rho \to \infty$. In terms of $\tilde{v}_{1p}$, the equation for $\tilde{u}_1$ in (2.64) becomes

$$L\tilde{u}_1 \equiv \Delta_\rho \tilde{u}_1 - \tilde{u}_1 + 2w\tilde{u}_1 = -\frac{\tilde{\chi}_1}{f\tilde{v}_0^2} w^2 - \frac{w^2}{\tilde{v}_0^3 f^3} \tilde{v}_{1p}.$$

Now, since $Lw = w^2$, as seen from $Lw = \Delta w - w + 2w^2 = -w^2 + 2w^2 = w^2$,

we can decompose $\tilde{u}_1$ as

$$\tilde{u}_1 = -\frac{\tilde{\chi}_1}{f\tilde{v}_0^2} w - \frac{1}{\tilde{v}_0^3 f^3}\tilde{u}_{1p}, \tag{2.68}$$

where $\tilde{u}_{1p}$ satisfies

$$\Delta_\rho \tilde{u}_{1p} - \tilde{u}_{1p} - 2w\tilde{u}_{1p} = w^2\tilde{v}_{1p}. \tag{2.69}$$

In summary, on $0 < \rho < \infty$, let $\tilde{v}_{1p}$ and $\tilde{u}_{1p}$ satisfy the coupled system

$$\begin{aligned} &\Delta_\rho \tilde{v}_{1p} = w^2 - fw; \qquad \tilde{v}_{1p} \sim \tilde{v}_0 f^2 \log\rho + o(1) \quad \text{as } \rho \to \infty, \\ &\Delta\tilde{u}_{1p} - \tilde{u}_{1p} + 2w\tilde{u}_{1p} = w^2\tilde{v}_{1p}, \qquad \tilde{u}_{1p} \to 0 \quad \text{as } \rho \to \infty. \end{aligned} \tag{2.70}$$

Then, $\tilde{v}_1$ and $\tilde{u}_1$ are given by

$$\tilde{v}_1 = \tilde{\chi}_1 + \frac{1}{\tilde{v}_0 f^2}\tilde{v}_{1p}, \qquad \tilde{u}_1 = -\frac{\tilde{\chi}_1}{f\tilde{v}_0^2} w - \frac{1}{\tilde{v}_0^3 f^3}\tilde{u}_{1p}. \tag{2.71}$$

Finally, we determine $\tilde{\chi}_1$. We substitute $\tilde{u}_1$ into the solvability condition (2.66) to obtain

$$0 = \int_0^\infty \rho\tilde{u}_1 d\rho = -\frac{\tilde{\chi}_1}{f\tilde{v}_0^2}\int_0^\infty \rho w d\rho - \frac{1}{\tilde{v}_0^3 f^3}\int_0^\infty \rho\tilde{u}_{1p} d\rho.$$

Therefore,

$$\tilde{\chi}_1 \int_0^\infty \rho w d\rho = -\frac{1}{\tilde{v}_0 f^2}\int_0^\infty \rho\tilde{u}_{1p} d\rho.$$

However, since

$$\int_0^\infty \rho w d\rho = \int_0^\infty \rho w^2 d\rho = b, \qquad \text{and} \qquad \tilde{v}_0 = \frac{(1-f)}{f^2}\int_0^\infty \rho w^2 d\rho,$$

we get

$$\tilde{\chi}_1 = -\frac{1}{b^2(1-f)}\int_0^\infty \rho\tilde{u}_{1p} d\rho. \tag{2.72}$$

This determines $\tilde{\chi}_1$ in terms of $\tilde{u}_{1p}$.

We can further simplify (2.72) by using (2.70). The goal is to obtain a formula for $\tilde{\chi}_1$ where the parameter dependence on f appears explicitly rather than implicitly through $\tilde{u}_{1p}$. To obtain such a result, we use $w^2 = w - \Delta w$ to write the problem for $\tilde{v}_{1p}$ as

$$\begin{aligned}
&\Delta_\rho(\tilde{v}_{1p} + w) = (1-f)w, \\
&\tilde{v}_{1p} + w \sim (1-f)b\log\rho + o(1) \quad \text{as} \quad \rho \to \infty.
\end{aligned}$$

This suggests that we can introduce $\tilde{v}_{1Q}$ by $\tilde{v}_{1p} + w = (1-f)\tilde{v}_{1Q}$, where $\tilde{v}_{1Q}$ satisfies the parameter-independent problem

$$\begin{aligned}
&\Delta_\rho \tilde{v}_{1Q} = w, \qquad \rho \geq 0, \\
&\tilde{v}'_{1Q}(0) = 0\,; \qquad \tilde{v}_{1Q} \to b\log\rho + o(1)\,, \quad \text{as} \quad \rho \to \infty.
\end{aligned}$$

Now, from the problem for $\tilde{u}_{1p}$ we obtain $\tilde{v}_{1p} = -w + (1-f)\tilde{v}_{1Q}$, so that

$$L\tilde{u}_{1p} = w^2(-w + (1-f)\tilde{v}_{1Q}).$$

This suggests that we decompose $\tilde{u}_{1p}$ as $\tilde{u}_{1p} = -\tilde{u}_{1pI} + \tilde{u}_{1pII}(1-f)$, where

$$L\tilde{u}_{1pI} = w^3, \qquad L\tilde{u}_{1pII} = w^2\tilde{v}_{1Q}.$$

Finally, from (2.72) we get

$$\tilde{\chi}_1 = \frac{1}{b^2(1-f)}\int_0^\infty \rho\tilde{u}_{1pI}d\rho - \frac{1}{b^2}\int_0^\infty \rho\tilde{u}_{1pII}d\rho\,,$$

where the two integral terms are independent of f. We summarize the calculation of the asymptotics for $S \to 0$ of the solution to the core problem as follows:

For $S \to 0$, we obtain that $U = \mathcal{D}^{1/2}u$, $V = D^{-1/2}v$, with

$$\begin{aligned} u &\sim S\left[\tilde{u}_0 + S^2\tilde{u}_1 + \ldots\right], \\ v &\sim S\left[\tilde{v}_0 + S^2\tilde{v}_1 + \ldots\right], \\ \chi &\sim \frac{1}{S}\left[\tilde{\chi}_0 + S^2\tilde{\chi}_1 + \ldots\right]. \end{aligned} \tag{2.73}$$

Here $b = \int_0^\infty \rho w^2 d\rho$, w is the solution of the ground-state problem $\Delta_\rho w - w + w^2 = 0$, and

$$\begin{aligned} \tilde{u}_0 &= \frac{1}{f\tilde{v}_0}w, \qquad \tilde{u}_1 = -\frac{\tilde{\chi}_1}{f\tilde{v}_0^2}w - \frac{1}{\tilde{v}_0^3 f^3}\left[-\tilde{u}_{1pI} + (1-f)\tilde{u}_{1pII}\right], \\ \tilde{v}_0 &= \frac{b(1-f)}{f^2}, \qquad \tilde{v}_1 = \tilde{\chi}_1 + \frac{1}{\tilde{v}_0 f^2}\left[-w + (1-f)\tilde{v}_{1Q}\right], \\ \tilde{\chi}_0 &= \frac{b(1-f)}{f^2}, \qquad \tilde{\chi}_1 = \frac{1}{b^2(1-f)}\int_0^\infty \rho\tilde{u}_{1pI}d\rho - \frac{1}{b^2}\int_0^\infty \rho\tilde{u}_{1pII}d\rho. \end{aligned} \tag{2.74}$$

Moreover, $\tilde{v}_{1Q}$ is the unique solution to

$$\begin{aligned} &\Delta_\rho\tilde{v}_{1Q} = w, \qquad 0 < \rho < \infty, \\ &\tilde{v}'_{1Q}(0) = 0, \qquad \tilde{v}_{1Q} \to b\log\rho + o(1), \quad \text{as} \quad \rho \to \infty, \end{aligned} \tag{2.75}$$

while $\tilde{u}_{1pI}$ and $\tilde{u}_{1pII}$ are the unique solutions of

$$\begin{aligned} &L\tilde{u}_{1pI} \equiv \Delta_\rho\tilde{u}_{1pI} - \tilde{u}_{1pI} + 2w\tilde{u}_{1pI} = w^3, \qquad \tilde{u}_{1pI} \to 0 \quad \text{as} \quad \rho \to \infty, \\ &L\tilde{u}_{1pII} = w^2\tilde{v}_{1Q}, \qquad \tilde{u}_{1pII} \to 0 \quad \text{as} \quad \rho \to \infty. \end{aligned} \tag{2.76}$$

Remark

(i) Notice that $\tilde{v}_{1Q}, \tilde{u}_{1pI}, \tilde{u}_{1pII}$ do not depend on any parameters (such as f). Hence we need only compute $\int_0^\infty \rho\tilde{u}_{1pI}d\rho, \int_0^\infty \rho\tilde{u}_{1pII}d\rho$ once in order to determine $\tilde{\chi}_1$. This was the motivation for introducing this decomposition from (2.72)

(ii) The leading order theory yields

$$U \sim \frac{\mathcal{D}^{1/2} S f}{b(1-f)} w, \qquad V \sim \frac{\mathcal{D}^{-1/2}}{S} \frac{b(1-f)}{f^2}, \tag{2.77}$$

and the two term expansion for χ is

$$\chi \sim \frac{1}{S} \frac{b(1-f)}{f^2} + \tilde{\chi}_1 S + \dots \tag{2.78}$$

(iii) Recall now that (2.58) holds:

$$S_i - \nu \sum_{j \neq i}^{N} S_j L_{ij} + \frac{\nu R_0 \mathrm{E}}{\sqrt{\mathcal{D}}} + \nu \chi(S_i; f) = \nu \overline{v}, \ , \quad i = 1, \dots, N$$

$$\sum_{i=1}^{N} S_i = \frac{2\mathrm{E}}{\sqrt{\mathcal{D}}}.$$

We now assume $\mathcal{D} = \mathcal{D}/\nu$ where $\nu = -1/\log \varepsilon$. Thus, $\sum_{i=1}^{N} S_i = O(\nu^{1/2})$, which indicates that $S_i = O(\nu^{1/2})$. We then use $\chi_i \sim \frac{b(1-f)}{f^2 S_i}$ to obtain, with $S_i \to 0$ that

$$S_i - O(\nu) + \frac{\nu b(1-f)}{f^2 S_i} \simeq \nu \overline{v}, \qquad \sum_{i=1}^{N} S_i = \frac{2\nu^{1/2}}{\sqrt{\mathcal{D}_0}}.$$

We then put $S_i = \nu^{1/2} \tilde{S}_i$ and $\overline{v} = \nu^{-1/2} \overline{v}_0$, which leads to the reduced problem

$$\tilde{S}_i + \frac{b(1-f)}{f^2 \tilde{S}_i} = \overline{v}_0, \qquad \sum_{i=1}^{N} \tilde{S}_i = \frac{2}{\sqrt{\mathcal{D}_0}} \mathrm{E}. \tag{2.79}$$

Substituting into (2.77), we get

$$U \sim \frac{w}{f v_i}, \qquad V \sim v_i \equiv \frac{1}{\tilde{S}_i \sqrt{\mathcal{D}_0}} \frac{b(1-f)}{f^2}, \tag{2.80}$$

which holds near the i-th spot. We then solve for S_i in terms of v_i and substitute into (2.79) to obtain after some algebra that

$$\begin{aligned} v_i + \left(\frac{b(1-f)}{\mathcal{D}_0 f^2}\right)\frac{1}{v_i} &= \frac{1}{\sqrt{\mathcal{D}_0}}\overline{v}_0, \qquad i = 1, \ldots, N, \\ \sum_{i=1}^{N} \frac{1}{v_i} &= \frac{2f^2}{b(1-f)}\mathrm{E}, \end{aligned} \tag{2.81}$$

with $U \sim \frac{2}{f v_i} w$ near the i-th spot (from (2.80)).

Notice that this is precisely the same system derived in (2.54), where

$$\mathcal{B} = \frac{b(1-f)}{\mathcal{D}_0 f^2}, \qquad b = \int_0^\infty \rho w^2 d\rho.$$

We conclude that we can recover the leading-order terms in the expansion in ν from the small S-asymptotics of the core problem.

2.5 Leading-order stability theory

For $\mathcal{D} = \mathcal{D}_0/\nu$, the time-dependent Brusselator system on the surface of the unit sphere is

$$\begin{aligned} u_t &= \varepsilon^2 \Delta_s u + \varepsilon^2 \mathrm{E} - u + f u^2 v, \\ \nu\tau v_t &= \mathcal{D}_0 \Delta_s v + \frac{\nu}{\varepsilon^2}(u - u^2 v)\,. \end{aligned}$$

Now we linearize around the quasi-equilibrium solution by writing

$$u = u_e + e^{\lambda t}\psi, \qquad \text{and } v = v_e + e^{\lambda t}\eta\,,$$

so that

$$\begin{aligned} \varepsilon^2\Delta_s\psi - \psi + 2fu_ev_e\psi + fu_e^2\eta = \lambda\psi, \\ \Delta_s\eta + \frac{\nu}{\varepsilon^2\mathcal{D}_0}(\psi - 2u_ev_e\psi - u_e^2\eta) = \frac{\tau\nu\lambda}{\mathcal{D}_0}\eta. \end{aligned} \tag{2.82}$$

We will consider the regime where $\tau = O(1)$.

We look for radially symmetric solutions in the inner region near the j-th spot. In this inner region we use $u_e \sim \frac{1}{fv_j}w,\ \ v_e \sim v_j$ to obtain for $\rho = |y|$ that

$$\Delta_\rho\Psi_j - \Psi_j + 2w\Psi_j + \frac{1}{fv_j^2}w^2\eta(x_j) = \lambda\Psi_j, \qquad \rho \geq 0. \tag{2.83}$$

Now, from the equation for η we have

$$\Delta_y\eta + \frac{\nu}{\mathcal{D}_0}\left(-\Psi_j + 2u_ev_e\Psi_j + -u_e^2\eta\right) = O\left(\frac{\lambda\tau\nu\varepsilon^2}{\mathcal{D}_0}\right).$$

Assuming that $\tau \ll O(\varepsilon^{-2})$, we use $u_ev_e = w/f$ to obtain

$$\Delta_y\eta = \frac{\nu}{\mathcal{D}_0}\left(-\Psi_j + \frac{2}{f}w\Psi_j + \frac{w^2}{f^2v_j^2}\eta\right). \tag{2.84}$$

Now we expand $\eta = \eta_j + \nu\eta_{j1} + \ldots$, with $\eta_j = \eta(x_j)$. We obtain that η_{j1} satisfies

$$\Delta_y\eta_{j1} = \frac{1}{\mathcal{D}_0}\left(-\Psi_j + \frac{2}{f}w\Psi_j + \frac{w^2}{f^2v_j^2}\eta_j\right).$$

The far-field asymptotic behaviour of the solution is readily calculated as

$$\eta_{j1} \sim \frac{1}{\mathcal{D}_0} A_j \log\rho, \qquad \text{as } \rho \to \infty,$$
$$A_j = \int_0^\infty \left(-\Psi_j + \frac{2}{f} w\Psi_j + \frac{w^2}{f^2 v_j^2}\eta_j \right) \rho d\rho,$$
$$A_j = \int_0^\infty \left(\frac{2}{f} w\Psi_j - \Psi_j \right) \rho d\rho + \frac{\eta_j}{f^2 v_j^2} b, \qquad b = \int_0^\infty \rho w^2 d\rho.$$

This shows that we have the far-field behaviour $\eta \sim \eta_j + \frac{\nu}{\mathcal{D}_0} A_j \log\rho$ as $\rho \to \infty$. To determine the matching condition to the outer solution, we use $\rho = \varepsilon^{-1}|x - x_j|$, and re-write this far-field behaviour in terms of the outer variable as

$$\eta \sim \eta_j + \frac{A_j}{\mathcal{D}_0} + \frac{\nu A_j}{\mathcal{D}_0} \log|x - x_j|, \qquad \text{as } x \to x_j. \tag{2.85}$$

Now, in the outer region we estimate for $x \approx x_j$ that

$$\frac{1}{\varepsilon^2}(\psi - 2u_e v_e \psi - u_e^2 \eta) \to \left(\int_0^\infty \left(\Psi_j - \frac{2}{f}\Psi_j - \frac{1}{f^2 v_j^2} w^2 \eta_j \right) \rho d\rho \right) \delta(x - x_j).$$

Thus, we obtain that the outer solution for $\eta(x)$, valid for $|x - x_j| \gg O(\varepsilon)$, satisfies

$$\Delta_s \eta - \frac{\lambda\tau\nu}{\mathcal{D}_0}\eta = \frac{2\pi\nu}{\mathcal{D}_0} \sum_{i=1}^N A_i \delta(x - x_i), \tag{2.86}$$

with singularity behaviour (2.85) at each x_j.

We now expand the solution to this problem for $\nu \ll 1$. We get

$$\eta = \overline{\eta} + \nu\eta_1 + \ldots, \qquad \text{with} \quad \overline{\eta} = \eta_j + \frac{A_j}{\mathcal{D}_0}, \quad j = 1, \ldots, N,$$

where $\overline{\eta}$ is a constant. At next order, η_1 satisfies

$$\Delta_s \eta_1 = \frac{\tau\lambda\overline{\eta}}{\mathcal{D}_0} + \frac{2\pi}{\mathcal{D}_0}\sum_{i=1}^{N} A_i \delta(x - x_i).$$

The solvability condition for this problem, as obtained by integrating it over the sphere, is

$$\frac{4\pi\tau\lambda\overline{\eta}}{\mathcal{D}_0} + \frac{2\pi}{\mathcal{D}_0}\sum_{i=1}^{N} A_i = 0.$$

In this way, we obtain that

$$-\overline{\eta}\tau\lambda = \frac{1}{2}\sum_{i=1}^{N} A_i, \qquad \overline{\eta} = \eta_j + \frac{A_j}{\mathcal{D}_0}, \quad j = 1, \ldots, N. \tag{2.87}$$

Next, we recall that

$$A_j = \int_0^\infty \left(\frac{2}{f} w \Psi_j - \Psi_j\right) \rho d\rho + \frac{\eta_j}{f^2 v_j^2} b, \tag{2.88}$$

so that combining it with (2.87) we get

$$\eta_j + \frac{A_j}{\mathcal{D}_0} = -\frac{1}{2\tau\lambda}\sum_{i=1}^{N} A_i, \qquad j = 1, \ldots, N. \tag{2.89}$$

We then write both (2.88) and (2.89) in matrix form. For (2.89) we write

$$\vec{\eta} + \frac{\vec{A}}{\mathcal{D}_0} = -\frac{N}{2\tau}\mathrm{E}_0 \vec{A}, \qquad \mathrm{E}_0 = \frac{1}{N}\vec{e}\vec{e}^{\,T}, \tag{2.90}$$

where $\vec{e} = (1, \ldots, 1)^T$. Next, for (2.88) we first define

$$\vec{J} = \int_0^\infty \left(\frac{2}{f} w \vec{\Psi} - \vec{\Psi}\right) \rho d\rho, \qquad \vec{\Psi} = \begin{pmatrix} \Psi_1 \\ \vdots \\ \Psi_N \end{pmatrix}, \qquad \vec{\eta} = \begin{pmatrix} \eta_1 \\ \vdots \\ \eta_N \end{pmatrix},$$

and introduce the matrix

$$\mathcal{H} = \begin{pmatrix} 1/f^2v_1^2 & & 0 \\ & \ddots & \\ 0 & & 1/f^2v_N^2 \end{pmatrix}.$$

With this notation we can rewrite (2.88) as

$$\vec{A} = \vec{J} + b\mathcal{H}\vec{\eta}. \tag{2.91}$$

Then, upon combining (2.90) and (2.91), we obtain that $\vec{\eta}$ satisfies the matrix problem

$$\left(I + \frac{b}{\mathcal{D}_0}\mathcal{H} + \frac{Nb\mathrm{E}_0}{2\tau\lambda}\mathcal{H}\right)\vec{\eta} = -\left(\frac{1}{\mathcal{D}_0}I + \frac{N}{2\tau\lambda}\mathrm{E}_0\right)\vec{J}. \tag{2.92}$$

We then write (2.83) in matrix form as

$$\Delta_\rho\vec{\Psi} - \vec{\Psi} + 2w\vec{\Psi} + fw^2\mathcal{H}\vec{\eta} = \lambda\vec{\Psi}, \tag{2.93}$$

where $\vec{\eta}$ is given in terms of nonlocal terms via (2.92).

The system (2.92)) and (2.93) is a vector nonlocal eigenvalue problem for $\vec{\Psi}$. We will obtain an explicit nonlocal eigenvalue problem from it for the case of symmetric spot patterns where the spots have a common source strength. Recall from (2.55) that for such symmetric patterns we have

$$v_j = v \equiv \frac{\mathcal{D}_0\mathcal{B}N}{2}, \qquad \mathcal{B} = \frac{1}{\mathcal{D}_0 f^2}(1-f)b,$$

for all j, so that

$$\begin{aligned} f^2v_j^2 = \left(\frac{f\mathcal{D}_0\mathcal{B}N}{2}\right)^2 &= \left(\frac{\mathcal{D}_0 fN}{2}\frac{1}{\mathcal{D}_0 f^2}(1-f)b\right)^2, \\ &= \frac{N^2(1-f)^2}{4f^2}b^2, \qquad \text{for } j = 1,\ldots,N. \end{aligned} \tag{2.94}$$

For this symmetric case, $\mathcal{H} = \frac{1}{f^2v^2}I$ where f^2v^2 is given in (2.94). Thus (2.92)

and (2.93) become

$$\left(I+\frac{b}{\mathcal{D}_0 f^2 v^2}I+\frac{Nb}{2\tau\lambda}\frac{1}{f^2v^2}\mathrm{E}_0\right)\vec{\eta}=-\left(\frac{1}{\mathcal{D}_0}I+\frac{N}{2\tau\lambda}\mathrm{E}_0\right)\vec{J}. \tag{2.95}$$

$$\Delta_\rho\vec{\Psi}-\vec{\Psi}+2w\vec{\Psi}+\frac{w^2}{fv^2}\vec{\eta}=\lambda\vec{\Psi}. \tag{2.96}$$

We then write $\vec{\eta}=-\mathcal{A}\vec{J}$, where $\mathcal{A}$ is given by

$$\mathcal{A}=\left(I+\frac{b}{f^2v^2\mathcal{D}_0}I+\frac{Nb}{2\tau\lambda f^2v^2}\mathrm{E}_0\right)^{-1}\left(\frac{1}{\mathcal{D}_0}I+\frac{1}{\mathcal{D}_0}I+\frac{N}{2\tau\lambda}\mathrm{E}_0\right),$$

Therefore, (2.96) becomes the vector Nonlocal eigenvalue problem (NLEP)

$$\Delta_\rho\vec{\Psi}-\vec{\Psi}+2w\vec{\Psi}-\frac{w^2}{fv^2}\mathcal{A}\vec{J}=\lambda\vec{\Psi}. \tag{2.97}$$

Our final step in the analysis is to diagonalize this vector NLEP to obtain a scalar NLEP. To do so, we write the eigenvectors of $\mathcal{A}$ as $\mathcal{A}\vec{q_j}=\mu_j\vec{q_j}$, so that in matrix form

$$\mathcal{A}=Q\Lambda Q^{-1},\qquad Q=\begin{pmatrix}| & & |\\ q_1 & \cdots & q_N\\ | & & |\end{pmatrix},\qquad \Lambda=\begin{pmatrix}\mu_1 & & 0\\ & \ddots & \\ 0 & & \mu_N\end{pmatrix}.$$

Letting $\vec{\Psi}=Q\hat{\vec{\Psi}}$, we can diagonalize the vector NLEP as

$$Q\Delta_\rho\hat{\vec{\Psi}}-Q\hat{\vec{\Psi}}+2wQ\hat{\vec{\Psi}}-\frac{fw^2}{f^2v^2}Q\Lambda Q^{-1}\int_0^\infty\left(\frac{2}{f}wQ\hat{\vec{\Psi}}-Q\hat{\vec{\Psi}}\right)\rho d\rho=\lambda Q\hat{\vec{\Psi}}.$$

Multiplying by Q^{-1} we obtain that $\hat{\vec{\Psi}}$ satisfies any one of the N scalar NLEPs

$$\Delta_\rho\hat{\vec{\Psi}}-\hat{\vec{\Psi}}+2w\hat{\vec{\Psi}}-\frac{fw^2}{f^2v^2}\Lambda\int_0^\infty\left(\frac{2}{f}w\hat{\vec{\Psi}}-\hat{\vec{\Psi}}\right)\rho d\rho=\lambda\hat{\vec{\Psi}}.$$

This leads to the study of the scalar NLEP

$$\begin{aligned} \Delta_\rho \tilde{\Psi} - \tilde{\Psi} + 2w\tilde{\Psi} - \frac{fw^2}{f^2v^2}\mu_j \int_0^\infty \left(\frac{2}{f} w\tilde{\Psi} - \tilde{\Psi}\right) \rho d\rho = \lambda \tilde{\Psi}, \\ \tilde{\Psi} \to 0, \qquad \text{as} \quad \rho \to \infty, \end{aligned} \tag{2.98}$$

where μ_j, for $j = 1, \ldots, N$ is any eigenvalue of the matrix $\mathcal{A}$ defined by

$$\mathcal{A} = \left(I + \frac{b}{f^2v^2\mathcal{D}_0} I + \frac{Nb}{2\tau\lambda f^2v^2} \mathrm{E}_0\right)^{-1} \left(\frac{1}{\mathcal{D}_0} I + \frac{N}{2\tau\lambda} \mathrm{E}_0\right). \tag{2.99}$$

In contrast to the NLEP's derived previously for other reaction-diffusion systems such as the Gierer-Meinhardt or Gray-Scott models, this NLEP involves two separate nonlocal terms. Before calculating μ_j we will write (2.98) in a standard form involving only one nonlocal term as

$$\Delta_\rho \tilde{\Psi} - \tilde{\Psi} + 2w\tilde{\Psi} - \gamma w^2 \frac{\int_0^\infty \rho w \tilde{\Psi} d\rho}{\int_0^\infty \rho w^2 d\rho} = \lambda \tilde{\Psi}, \quad 0 < \rho < \infty, \tag{2.100}$$

for some $\gamma = \gamma(\lambda)$. This is the standard form for which Wei (e.g. [63]) has many rigorous results on the spectrum of the NLEP that are used to obtain explicit criteria for stability.

To write (2.98) in standard form we define I_1 and I_2 by $I_1 = \int_0^\infty \rho w \tilde{\Psi} d\rho$ and $I_2 = \int_0^\infty \rho \tilde{\Psi} d\rho$. Then we can write (2.98) as

$$\Delta_\rho \tilde{\Psi} - \tilde{\Psi} + 2w\tilde{\Psi} - \frac{2w^2\mu_j}{f^2v^2} I_1 + \frac{w^2\mu_j}{fv^2} I_2 = \lambda \tilde{\Psi}. \tag{2.101}$$

Multiplying by ρ and integrating yields

$$-I_2 + 2I_1 - \frac{2\mu_j b}{f^2v^2} I_1 + \frac{b\mu_j}{fv^2} I_2 = \lambda I_2.$$

Upon solving for I_2 in terms of I_1 we get

$$I_2 = \zeta I_1, \qquad \zeta = \frac{2(\mu_j b - f^2 v^2)}{\mu_j b f - f^2 v^2 (\lambda + 1)},$$

so that by eliminating I_1 in (2.101) we obtain

$$\Delta_\rho \tilde{\Psi} - \tilde{\Psi} + 2w\tilde{\Psi} - \frac{2w^2 \mu_j b}{f^2 v^2} \left(1 - \frac{f}{2}\zeta\right) \left(\frac{I_1}{b}\right) = \lambda \tilde{\Psi}.$$

Now, since $I_1/b = \int_0^\infty \rho w \tilde{\Psi} d\rho / \int_0^\infty \rho w^2 d\rho$, we can now write (2.98) in the standard form (2.100), with

$$\gamma = \frac{2\mu_j b}{f^2 v^2} \left(1 - \frac{f\zeta}{2}\right), \tag{2.102}$$

where ζ is defined by

$$\zeta = \frac{2(\mu_j - f^2 v^2/b)}{\mu_j f - (\lambda + 1) f^2 v^2 / b}. \tag{2.103}$$

The next step is to simplify the coefficient γ in (2.102), and calculate the eigenvalues μ_j. To simplify γ, we use (2.94) to define φ as

$$\varphi = \frac{f^2 v^2}{b} = \frac{N^2}{4f^2}(1 - f)^2 b, \qquad b = \int_0^\infty \rho w^2 d\rho \,. \tag{2.104}$$

Then

$$\begin{aligned} \gamma &= 2\mu_j \left(\frac{b}{f^2 v^2}\right) \left(1 - \frac{f(\mu_j - f^2 v^2/b)}{\mu_j f - (\lambda + 1) f^2 v^2 / b}\right), \\ &= \frac{2\mu_j}{\varphi} \left[\frac{\varphi(f - (\lambda + 1))}{\mu_j f - \varphi(\lambda + 1)}\right] = 2\mu_j \left(\frac{f - (\lambda + 1)}{\mu_j f - \varphi(\lambda + 1)}\right). \end{aligned}$$

Therefore, we have that the NLEP in (2.98) has multiplier γ given by

$$\gamma = 2\mu_j \left(\frac{f - (\lambda + 1)}{\mu_j f - \varphi(\lambda + 1)}\right), \qquad \varphi \equiv \frac{N^2}{4f^2}(1 - f)^2 b. \tag{2.105}$$

Finally, we will calculate the eigenvalues μ_j of $\mathcal{A}$ as defined in (2.99). In terms of $\varphi = f^2v^2/b$, as given in (2.104), we can write $\mathcal{A}$ as

$$\mathcal{A} = \left(I + \frac{1}{\varphi\mathcal{D}_0}I + \frac{N}{2\tau\lambda\varphi}\mathrm{E}_0\right)^{-1}\left(\frac{1}{\mathcal{D}_0}I + \frac{N}{2\tau\lambda}\mathrm{E}_0\right).$$

We write $\mathcal{A}\vec{q} = \mu\vec{q}$ so that

$$\left(\frac{1}{\mathcal{D}_0}I + \frac{N}{2\tau\lambda}\mathrm{E}_0\right)\vec{q} = \mu\left(I + \frac{1}{\varphi\mathcal{D}_0}I + \frac{N}{2\tau\lambda\varphi}\mathrm{E}_0\right)\vec{q}.$$

In this form, the eigenvectors and eigenvalues are easy to detect. It turns out that there are only two distinct eigenvalues.

- Let $\vec{q} = \vec{e}$, and recall that $\mathrm{E}_0\vec{e} = \vec{e}(\vec{e}^T\vec{e})/N = \vec{e}$. Thus, with $\vec{q} = \vec{e}$, we have

  $$\left(\frac{1}{\mathcal{D}_0} + \frac{N}{2\tau\lambda}\right)\vec{e} = \mu\left(I + \frac{1}{\varphi\mathcal{D}_0}I + \frac{N}{2\tau\lambda\varphi}\right)\vec{e}.$$

  Thus, we obtain that for $\vec{q} = \vec{e}$, representing the synchronous mode of instability, the corresponding eigenvalue is

  $$\mu = \frac{\frac{1}{\mathcal{D}_0} + \frac{N}{2\tau\lambda}}{I + \frac{1}{\varphi\mathcal{D}_0}I + \frac{N}{2\tau\lambda\varphi}} = \frac{\varphi(N + 2\tau\lambda/\mathcal{D}_0)}{N + 2\tau\lambda(\varphi + 1/\mathcal{D}_0)}. \tag{2.106}$$

- Let $\vec{q} = \vec{b}$, with $\vec{b}^T\vec{e} = 0$. There exists $N - 1$ such independent vectors. These are the competition instability modes. Then

  $$\left(\frac{1}{\mathcal{D}_0}I + \frac{N}{2\tau\lambda}\mathrm{E}_0\right)\vec{b} = \mu\left(I + \frac{1}{\varphi\mathcal{D}_0}I + \frac{N}{2\tau\lambda\varphi}\mathrm{E}_0\right)\vec{b}.$$

  However, $\mathrm{E}_0\vec{b} = 0$, and so $\mathcal{D}_0^{-1} = \mu\,(1 + 1/\varphi\mathcal{D}_0)$. Therefore, with $\vec{q} = \vec{b}$ and $\vec{b}^T\vec{e} = 0$, then

  $$\mu = \frac{\varphi}{1 + \varphi\mathcal{D}_0}\,. \tag{2.107}$$

This completes the determination of the NLEP. Next, we derive specific stability criteria from the determination of the spectrum of this NLEP.

2.5.1 Stability thresholds

(I) We consider the competition instability threshold for $N \geq 2$. From (2.105) and (2.107) we obtain

$$\gamma = \frac{2\varphi}{1+\varphi\mathcal{D}_0}\left(\frac{f-(\lambda+1)}{\frac{\varphi f}{1+\varphi\mathcal{D}_0}-\varphi(\lambda+1)}\right) = \frac{2\left[f-(\lambda+1)\right]}{f-(\lambda+1)(1+\varphi\mathcal{D}_0)}. \quad (2.108)$$

Since $0 < f < 1$, it is readily seen that γ is analytic in the right half-plane $\mathrm{Re}(\lambda) > 0$.

The NLEP for this competition instability is

$$\Delta_\rho\tilde{\Psi} - \tilde{\Psi} + 2w\tilde{\Psi} - \gamma w^2\frac{\int_0^\infty \rho w\tilde{\Psi}d\rho}{\int_0^\infty \rho w^2 d\rho} = \lambda\tilde{\Psi}, \quad (2.109)$$

with γ as given in (2.108). Notice that this NLEP is not self-adjoint and that $\gamma = \gamma(\lambda)$.

Wei's result (Theorem 1.4 in [63]) proves if γ is a constant, independent of λ, then $\mathrm{Re}(\lambda) > 0$ if and only if $\gamma < 1$. Therefore, when γ is a constant the stability threshold is precisely $\gamma = 1$. However, in our case, $\gamma = \gamma(\lambda)$ as given in (2.108). In Appendix B, we prove that there exists a real positive eigenvalue when $\gamma(0) < 1$. Hence, we have instability when $\gamma(0) < 1$. In addition, if $\gamma(0) = 1$ then $\tilde{\Psi} = w$ is an eigenfunction corresponding to $\lambda = 0$. This follows since if we set $\lambda = 0$ and $\tilde{\Psi} = w$ then

$$\Delta_\rho w - w + 2w^2 - \gamma w^2\frac{\int_0^\infty \rho w^2 d\rho}{\int_0^\infty \rho w^2 d\rho} = 0\cdot w.$$

If $\gamma(0) = 1$, we use $\Delta_\rho w - w + 2w^2 - \gamma w^2 = \Delta w - w + w^2 = 0$ to establish the identity.

Therefore, to determine an instability threshold we set $\gamma(0) < 1$ to obtain that $\varphi \mathcal{D}_0 > 1 - f$. Upon recalling the definition of φ in (2.105), we obtain our main leading-order-in-ν stability result:

Principal Result 2.5.1 *Let $\mathcal{D} = \mathcal{D}_0/\nu$, $\tau = O(1)$. Then, to leading order in ν, an N-spot symmetric solution with $N \geq 2$ is unstable to a competition instability when*

$$\mathcal{D}_0 > \mathcal{D}_{0c} \equiv \frac{4f^2}{N^2(1-f)b}, \qquad b = \int_0^\infty \rho w^2 d\rho. \tag{2.110}$$

Remark

(i) As shown below in (2.118)., this threshold agrees precisely with the leading-order term in the stability threshold as obtained from expanding for $S \to 0$ the results from our S-formulation involving summing logarithmic terms.

(ii) Notice that as $f \to 1^-$, then $\mathcal{D}_{0c}$ increases. However, as N increases, then $\mathcal{D}_{0c}$ decreases. If $\mathcal{D}_0$ is too large, then a competition instability is triggered. This is an overcrowding type of instability.

(iii) To leading-order, the stability threshold is the same for all competition modes. However, in (2.118) below we will be able to determine the correction term in this instability threshold, which yields $N - 1$ distinct competition instability thresholds. In addition, this correction term will involve the locations of the spots on the surface of the sphere.

(iv) The proof of this instability result is given in Appendix B.

Although it is relatively easy to obtain an instability threshold, it is substantially more difficult to prove a stability result for the parameter range $\mathcal{D}_0 < \mathcal{D}_{0c}$. The difficulty stems from the fact that $\gamma = \gamma(\lambda)$ and that one must account for complex eigenvalues. We have been unable to prove a stability result for this range of $\mathcal{D}_0$.

(II) We now consider the synchronous instability threshold. The NLEP for synchronous instabilities is

$$\Delta_\rho \tilde{\Psi} - \tilde{\Psi} + 2w\tilde{\Psi} - \gamma w^2 \frac{\int_0^\infty \rho w \tilde{\Psi} d\rho}{\int_0^\infty \rho w^2 d\rho} = \lambda \tilde{\Psi}, \qquad \rho > 0,$$
$$\tilde{\Psi}'(0) = 0, \qquad \tilde{\Psi} \to 0 \qquad \text{as} \quad \rho \to \infty,$$

with $\gamma = \gamma(\lambda)$ defined by

$$\gamma = 2\mu \left(\frac{f - (\lambda + 1)}{\mu f - \varphi(\lambda + 1)} \right). \tag{2.111}$$

Here from (2.106) μ is given by

$$\mu = \frac{\varphi(N + 2\tau\lambda/\mathcal{D}_0)}{N + 2\tau\lambda(\varphi + 1/\mathcal{D}_0)}, \qquad \varphi \equiv \frac{N^2}{4f^2}(1 - f)^2 b.$$

Now suppose that $\tau = 0$. Then, $\mu = \varphi$ and hence

$$\gamma = 2\varphi \frac{(f - (\lambda + 1))}{(\varphi f - \varphi(\lambda + 1))} = 2.$$

Hence, when $\tau = 0$, then $\gamma = 2 > 1$ independent of λ. Wei's result (Theorem 1.4 in [63]) then guarantees that $\mathrm{Re}(\lambda) < 0$ and we have stability. By a perturbation argument we conclude that we must have stability when $\tau > 0$ is sufficiently small.

In addition, we notice that τ only enters through the product $\tau\lambda$. If we set $\lambda = 0$, then $\gamma = 2 > 1$ independent of all the other parameters. This proves that an eigenvalue cannot enter the unstable right half-plane $\mathrm{Re}(\lambda) > 0$ through crossing the origin $\lambda = 0$ as τ is increased. Therefore, an instability if it occurs must arise through a Hopf bifurcation as τ is increased.

As shown in Appendix B, the NLEP

$$\mathcal{L}_0 \tilde{\psi} - \gamma w^2 \frac{\int_0^\infty \rho w \tilde{\psi} d\rho}{\int_0^\infty \rho w^2 d\rho} = \lambda \tilde{\psi}\,,$$

where $\mathcal{L}_0\tilde{\psi} \equiv \Delta_\rho\tilde{\psi} - \tilde{\psi} + 2w\tilde{\psi}$ is equivalent to finding the roots of $g(\lambda) = 0$, where

$$g(\lambda) = \frac{1}{\gamma(\lambda)} - \frac{\int_0^\infty \rho w(\mathcal{L}_0 - \lambda)^{-1} w^2 d\rho}{\int_0^\infty \rho w^2 d\rho}. \tag{2.112}$$

As such, for the competition instability modes, we obtain from (2.108) that

$$\frac{1}{\gamma} = \frac{(f - (\lambda+1)(1+\varphi\mathcal{D}_0))}{2[f - (\lambda+1)]}. \tag{2.113}$$

In addition, for the synchronous instability mode we obtain that

$$\frac{1}{\gamma} = \frac{\mu f - \varphi(\lambda+1)}{2\mu[f - (\lambda+1)]} = \frac{f - (\varphi/\mu)(\lambda+1)}{2[f - (\lambda+1)]}, \tag{2.114}$$

where

$$\mu = \frac{\varphi(N + 2\tau\lambda/\mathcal{D}_0)}{N + 2\tau\lambda(\varphi + 1/\mathcal{D}_0)}.$$

2.6 Stability theory; Small S-Analysis from Summing Log Formulation

In this section we re-derive and then improve upon our leading-order stability results of the previous section by expanding the stability formulation of § 2.2 for small source strengths. As shown previously, when $\mathcal{D} = O(1/\nu)$, then the source strengths tend to zero. Consequently, the stability formulation of § 2.2 can be simplified in this limit.

We will separate our analysis into two cases: $\tau = 0$ for which we can obtain an explicit two-term result for the instability threshold, and $\tau > 0$ where we can recover the NLEP problem.

2.6.1 Case A; $\tau = 0$

We consider the competition instability threshold for the case where $\tau = 0$. Recall that the leading-order result is given in (2.110). We will now derive a 2-term expansion for this threshold for the case of a symmetric spot pattern where $S_c = S_1 = \ldots = S_N$.

We recall from the threshold calculation in § 2.2, that $\lambda = 0$ when $\det \mathcal{M} = 0$, where

$$\mathcal{M} = \frac{1}{\nu} I + (I - \mathrm{E}_0)(\mathcal{B} - \mathcal{G}),$$

and

$$\mathcal{B} = \begin{pmatrix} \chi'(S_1) & & 0 \\ & \ddots & \\ 0 & & \chi'(S_N) \end{pmatrix}, \quad \mathrm{E}_0 = \frac{1}{N} \begin{pmatrix} 1 & \cdots & 1 \\ \vdots & & \vdots \\ 1 & \cdots & 1 \end{pmatrix}, \quad \mathcal{G} = \begin{pmatrix} 0 & & L_{ij} \\ & \ddots & \\ L_{ji} & & 0 \end{pmatrix},$$

with $L_{ij} = \log|x_i - x_j|$ for $i \neq j$, and where $S_1, \ldots, S_N$ satisfies

$$\vec{S} + \nu(I - \mathrm{E}_0)\mathcal{G}\vec{S} + \nu(I - \mathrm{E}_0)\vec{\chi} = \frac{2}{\sqrt{\mathcal{D}}N}\vec{e}. \tag{2.115}$$

For the symmetric case where $S_1 = \ldots = S_N = S_c$, and $\mathcal{G}\vec{e} = k_1\vec{e}$, then $S_c = 2/\sqrt{\mathcal{D}}N$ is the exact solution to (2.115) for all ν, and $\det \mathcal{M} = 0$ reduces to (see (2.38))

$$\begin{aligned} \frac{1}{\nu} - k_J &= -\chi'(S_c), \\ \mathcal{G}\vec{b_j} = k_j\vec{b_j}, \qquad \vec{b_j}^T\vec{e} &= 0, \qquad \text{for } j = 2, \ldots, N. \end{aligned} \tag{2.116}$$

Now suppose that $\mathcal{D} = \mathcal{D}_0/\nu$, with $\nu = -1/\log\varepsilon$. Then we estimate $S_c = \frac{2}{\sqrt{\mathcal{D}_0}N}\nu^{1/2} \ll 1$. Hence, we must determine an expansion for $\chi'(S)$ when $S \ll 1$.

To do so, we recall from (2.74) that

$$\chi(S) \sim \frac{d_0}{S} + d_1 S + O(S^3) \qquad \text{as} \quad S \to 0, \tag{2.117a}$$

$$d_0 \equiv \frac{b(1-f)}{f^2}, \qquad d_1 \equiv \frac{1}{b^2}\left[\frac{1}{(1-f)}\int_0^\infty \rho \tilde{u}_{1pI} d\rho - \int_0^\infty \rho \tilde{u}_{1pII} d\rho\right], \tag{2.117b}$$

where $b = \int_0^\infty \rho w^2 d\rho$. Here $\tilde{u}_{1pI}$ and $\tilde{u}_{1pII}$ are the unique solutions of (2.76) (see § 2.3).

Thus, $\chi'(S) \sim -\frac{d_0}{S^2} + d_1$ as $S \to 0$, so that (2.116) becomes

$$\frac{1}{\nu} - k_j = \frac{d_0}{S_c^2} - d_1 + \dots .$$

We solve this relation for S_c as

$$S_c = \frac{\nu d_0}{1 + \nu(d_1 - k_j)}, \qquad \nu = -1/\log\varepsilon.$$

However, $S_c^2 = \frac{4}{\mathcal{D}_0 N^2}\nu$. Thus, the critical values $\mathcal{D}_{0c}$ of $\mathcal{D}_0$ where $\lambda = 0$ are given by

$$\mathcal{D}_{0c} = \frac{4}{N^2 d_0}\left[1 + \nu(d_1 - k_j)\right],$$

where k_j for $2 \le j \le N$ are any one of the eigenvalues of $\mathcal{G}$ with eigenvector perpendicular to $\vec{e}$. The largest such value of k_j will set the instability threshold.

We summarize our result as follows.

Principal Result 2.6.1 *Suppose that the spot locations $\{x_1, \dots, x_N\}$ are such that $\mathcal{G}$ is a cyclic matrix so that $\mathcal{G}\vec{e} = k_1\vec{e}$. Consider a symmetric quasi-equilibrium solution with $S_1 = \dots = S_N = S_c = \frac{2}{\sqrt{\mathcal{D}N}}$. Then, for $\mathcal{D} = O(-\log\varepsilon)$, with $\mathcal{D} = \mathcal{D}_0/\nu$, the smallest value of $\mathcal{D}_0$, labelled by $\mathcal{D}_{0c}$, for which a competition instability occurs (i.e. $\lambda = 0$ with a sign-fluctuating eigenfunction $\vec{c}_J$) is at the*

threshold

$$\mathcal{D}_{0c} = \frac{4}{N^2 d_0}\left[1 + \nu(d_1 - k_J)\right] \tag{2.118}$$

where

$$k_J = \max_{2\le j\le N}\{k_j\}, \quad \mathcal{G}\vec{b_j} = k_j\vec{b_j}, \quad \vec{b_j}^T\vec{e} = 0, \quad \textit{for } j = 2,\ldots,N,$$

and d_0, d_1 *are given in* (2.117b)*.*

Remark

(i) The leading-order result is the same as was derived by NLEP theory in (2.110). However, we are able to obtain the next correction term to the leading-order result as given in (2.118). This correction term depends on a perturbation of the solution to the core problem as manifested in the parameter d_1, as well as on the locations of the spots.

(ii) The sign-fluctuating eigenvector is $\vec{b}_j \equiv \vec{c}_j$.

(iii) The limitation of this simple calculation is that it provides a threshold for $\lambda = 0$, but does not give a rigorous instability result for $\mathcal{D} > \mathcal{D}_{0c}$

2.6.2 Case B, $\tau \neq 0$

Next, we consider the case where $\tau \neq 0$. Again we consider an N-spot pattern with spots such that $\mathcal{G}\vec{e} = k_1\vec{e}$. Then $S_1 = \ldots = S_N = S_c = 2/\sqrt{\mathcal{D}}N$.

In (2.46) we showed that the stability threshold when $\det\mathcal{M} = 0$ is equivalent to

$$\nu^{-1} + 2\pi k_{j\lambda} + \tilde{B}_c = 0, \qquad \text{for } j = 1,\ldots,N, \tag{2.119}$$

where $\nu = -1/\log\varepsilon$, and $k_{j\lambda}$ are the eigenvalues of the matrix $\mathcal{G}_\lambda$ defined in (2.44), written as

$$\mathcal{G}_\lambda \vec{b}_{j\lambda} = k_{j\lambda}\vec{b}_{j\lambda}, \qquad j = 1, \ldots, N.$$

Recall that the entries in this matrix are obtained from the Green's function $G(x; x_0)$ of (2.42), written as the solution to

$$\begin{aligned} \Delta G_\lambda - \frac{\tau\lambda}{\mathcal{D}} G_\lambda &= -\delta(x - x_0), \\ G_\lambda(x - x_0) \sim -\frac{1}{2\pi}\log|x - x_0| + R_\lambda + o(1) &\quad \text{as } x \to x_0. \end{aligned} \tag{2.120}$$

In the derivation leading to (2.119) we required that $\lambda \neq 0$. The constant $\tilde{B}_c$, which depends on λ and S_c, is obtained from the solution on $0 < \rho < \infty$ to

$$\begin{aligned} \mathcal{L}_\rho\tilde{\psi} - \tilde{\psi} + 2fuv\tilde{\psi} + fu^2\tilde{N} &= \lambda\tilde{\psi}, \\ \mathcal{L}_\rho\tilde{N} - \tilde{N}u^2 + \tilde{\psi}(1 - 2uv) &= 0, \\ \tilde{\psi} \to 0 \qquad &\text{as } \rho \to \infty, \\ \tilde{N} \to \log\rho + \tilde{B}_c \qquad &\text{as } \rho \to \infty, \end{aligned} \tag{2.121}$$

where u, v satisfy the core problem (2.57).

Since $\mathcal{D} = O(-\log\varepsilon\,)$, then $S_c \ll 1$. As such, we must now calculate $\tilde{B}_c$ for $S_c \to 0$. We start with the (2.121) system. As $S_c \to 0$ we recall from (2.73) and (2.74) that

$$u \sim u_c \sim \frac{S_c}{fv_0}w, \qquad v_c \sim \frac{v_0}{S_c}, \qquad u_c v_c \sim \frac{w}{f}.$$

Therefore (2.121) becomes

$$\begin{aligned} \mathcal{L}_\rho\tilde{\psi} - \tilde{\psi} + 2w\tilde{\psi} + \frac{S_c^2}{fv_0^2}w^2\tilde{N} &= \lambda\tilde{\psi}, \\ \mathcal{L}_\rho\tilde{N} + \tilde{\psi}\left(1 - \frac{2w}{f}\right) &= \frac{S_c^2}{f^2v_0^2}w^2\tilde{N}, \\ \tilde{N} \to \log\rho + \tilde{B}_c, \qquad \tilde{\psi} \to 0, &\quad \text{as} \quad \rho \to \infty. \end{aligned} \tag{2.122}$$

Next, we introduce $\hat{N}$ and $\hat{B}_c$ by

$$\tilde{N} = \hat{N}/S_c^2, \qquad \tilde{B}_c = \hat{B}_c/S_c^2, \tag{2.123}$$

so that (2.122) becomes

$$\begin{aligned} \mathcal{L}_\rho \tilde{\psi} - \tilde{\psi} + 2w\tilde{\psi} + \frac{1}{f v_0^2} w^2 \hat{N} &= \lambda \tilde{\psi}, \\ \mathcal{L}_\rho \hat{N} &= S_c^2 \left[\tilde{\psi} \left(\frac{2w}{f} - 1 \right) + \frac{w^2}{f^2 v_0^2} \hat{N} \right], \\ \hat{N} \to \hat{B}_c + S_c^2 \log \rho, \qquad \tilde{\psi} &\to 0, \quad \text{as} \quad \rho \to \infty. \end{aligned} \tag{2.124}$$

We now expand the solution for $S_c \ll 1$ as

$$\hat{N} = \hat{B}_c + S_c^2 \hat{N}_1 + \dots.$$

Then we obtain with $\mathcal{L}_0 \tilde{\psi} \equiv (\mathcal{L}_\rho - 1 + 2w)\tilde{\psi}$ that

$$(\mathcal{L}_0 - \lambda)\tilde{\psi} = -\frac{1}{f v_0^2} w^2 \hat{B}_c,$$

so that

$$\tilde{\psi} = -\frac{1}{f v_0^2} \hat{B}_c (\mathcal{L}_0 - \lambda)^{-1} w^2. \tag{2.125}$$

In terms of $\tilde{\psi}$, it follows that $\hat{N}_1$ from (2.124) satisfies

$$\begin{aligned} \mathcal{L}_\rho \hat{N}_1 &= \tilde{\psi} \left(\frac{2w}{f} - 1 \right) + \frac{w^2}{f^2 v_0^2} \hat{B}_c, \\ \hat{N}_1 &\sim \log \rho \qquad \text{as} \quad \rho \to \infty. \end{aligned}$$

Upon integrating this equation, we obtain the solvability condition

$$\lim_{\rho \to \infty} (\rho \hat{N}_1') = \int_0^\infty \tilde{\psi} \left(\frac{2w}{f} - 1 \right) \rho d\rho + \int_0^\infty \hat{B}_c \, \frac{w^2}{f^2 v_0^2} \rho d\rho,$$

which becomes

$$\frac{2}{f}\int_0^\infty \tilde{\psi} w \rho d\rho - \int_0^\infty \tilde{\psi}\rho d\rho + \frac{\hat{B}_c b}{f^2 v_0^2} = 1. \tag{2.126}$$

Now we calculate $\int_0^\infty \tilde{\psi}\rho d\rho$. We integrate the equation for $\tilde{\psi}$ in (2.124) to get

$$\int_0^\infty \rho \mathcal{L}_\rho \tilde{\psi} d\rho - \int_0^\infty \tilde{\psi}\rho d\rho + 2\int_0^\infty w\tilde{\psi}\rho d\rho + \frac{\hat{B}_c}{f v_0^2}\int_0^\infty w^2 \rho d\rho = \lambda \int_0^\infty \tilde{\psi}\rho d\rho.$$

Since the first integral is equal to zero, this reduces to

$$\int_0^\infty \tilde{\psi}\rho d\rho = \frac{2}{\lambda+1}\int_0^\infty w\tilde{\psi}\rho d\rho + \frac{\hat{B}_c b}{f v_0^2(\lambda+1)}. \tag{2.127}$$

Then, we combine (2.126) and (2.127) to obtain

$$\frac{\hat{B}_c b}{f^2 v_0^2}\left(1 - \frac{f}{\lambda+1}\right) + \left(\frac{2}{f} - \frac{2}{\lambda+1}\right)\int_0^\infty w\tilde{\psi}\rho d\rho = 1. \tag{2.128}$$

To simplify this expression we recall from (2.63) that $v_0 = b(1-f)/f^2$. Therefore, we get

$$\frac{f^2 v_0^2}{b} = \frac{b(1-f)^2}{f^2} \equiv \alpha. \tag{2.129}$$

Then, (2.128) can be written as

$$\frac{\hat{B}_c}{2\alpha} + \frac{1}{f}\int_0^\infty w\tilde{\psi}\rho d\rho = \frac{(\lambda+1)}{2(\lambda+1-f)}. \tag{2.130}$$

Next, we use $\tilde{\psi} = -\frac{1}{f v_0^2}\hat{B}_c(\mathcal{L}_0 - \lambda)^{-1} w^2$ from (2.125) to get

$$\frac{\hat{B}_c}{2\alpha} - \frac{\hat{B}_c}{f^2 v_0^2}\int_0^\infty \rho w(\mathcal{L}_0 - \lambda)^{-1} w^2 d\rho = \frac{(\lambda+1)}{2(\lambda+1-f)}.$$

Now, upon multiplying the integral term top and bottom by b and then using (2.129)

for $f^2 v_0^2/b$, we get

$$\frac{\hat{B}_c}{2\alpha} - \frac{\hat{B}_c}{\alpha}\frac{\int_0^\infty \rho w(\mathcal{L}_0 - \lambda)^{-1} w^2 d\rho}{\int_0^\infty \rho w^2 d\rho} = \frac{(\lambda+1)}{2(\lambda+1-f)}, \tag{2.131}$$

which can be written as

$$\frac{\hat{B}_c}{2\alpha} - \frac{\hat{B}_c}{\alpha}\mathcal{F}(\lambda) = \frac{(\lambda+1)}{2(\lambda+1-f)}.$$

Finally, we write this problem as finding the roots of $g(\lambda) = 0$, where

$$\begin{aligned} g(\lambda) &= \frac{1}{2}\left[\frac{f-(\lambda+1)(1-\alpha/\hat{B}_c)}{f-(\lambda+1)}\right] - \mathcal{F}(\lambda), \qquad \text{where} \\ \mathcal{F}(\lambda) &\equiv \frac{\int_0^\infty w\rho(\mathcal{L}_0-\lambda)^{-1}w^2 d\rho}{\int_0^\infty \rho w^2 d\rho}. \end{aligned} \tag{2.132}$$

This is an NLEP once we determine $\hat{B}_c$. We recall from (2.123) that $\hat{B}_c = S_c^2 \tilde{B}_c$ as $S_c \to 0$, where $S_c = 2\nu^{1/2}/\sqrt{\mathcal{D}_0}N$ is the common source strength.

Our goal is to verify that the roots $g(\lambda) = 0$ in (2.132) are the same as those obtained by the leading-order NLEP theory, as given in (2.112)-(2.114).

To establish this relationship we must determine $\hat{B}_c$. To do so, we first need to approximate the matrix $\mathcal{G}_\lambda$ when $\mathcal{D} = \mathcal{D}_0/\nu \gg 1$. For $\mathcal{D} = \mathcal{D}_0/\nu$ and $\lambda \neq 0$, then G_λ satisfies

$$\Delta_s G_\lambda - \frac{\tau\lambda\nu}{\mathcal{D}_0} G_\lambda = -\delta(x - x_0), \qquad (\lambda \neq 0).$$

For $\nu = 0$ this problem has no solution. Therefore, for $\lambda \neq 0$ and $\nu \ll 1$ we must expand the solution as

$$G_\lambda = \frac{a}{\nu} + G_0 + O(\nu) + \ldots,$$

for some unknown constant a. At next order, we obtain that

$$\Delta_s G_0 = \frac{a\tau\lambda}{\mathcal{D}_0} a - \delta(x - x_0), \qquad \int_\Omega G_0 dx = 0.$$

We remark that the integral constraint for G_0 arises from a solvability condition on the $O(\nu)$ correction term. By the divergence theorem we conclude that $a = \frac{\mathcal{D}_0}{4\pi\tau\lambda}$. Thus, for $\nu \ll 1$, we have that

$$G_\lambda(x; x_0) \sim \frac{\mathcal{D}_0}{4\pi\tau\lambda\nu} + G_0 + O(\nu),$$

where G_0 is the Neumann Green's function satisfying

$$\Delta_s G_0 = \frac{1}{4\pi} - \delta(x - x_0), \qquad \int_\Omega G_0 dx = 0\,,$$

with $G_0 \sim -\frac{1}{2\pi}\log|x - x_0| + R_0$ as $x \to x_0$.

Then $R_\lambda \sim \frac{\mathcal{D}_0}{4\pi\tau\lambda\nu} + R_0$, and we can write the $\mathcal{G}_\lambda$ matrix as

$$\mathcal{G}_\lambda = \frac{\mathcal{D}_0 N}{4\pi\tau\lambda\nu}\mathrm{E}_0 + O(1), \qquad \mathrm{E}_0 = \frac{1}{N}\begin{pmatrix} 1 & \cdots & 1 \\ \vdots & & \vdots \\ 1 & \cdots & 1 \end{pmatrix}, \tag{2.133}$$

which is valid for $\tau\lambda \neq 0$.

The eigenvalues and eigenvectors of $\mathcal{G}_\lambda$ are as follows:

- Since $\mathrm{E}_0\vec{e} = \vec{e}$, then

$$\mathcal{G}_\lambda\vec{e} = k_1\vec{e}, \qquad k_1 = \frac{\mathcal{D}_0 N}{4\pi\tau\lambda\nu}.$$

- Since $\mathrm{E}_0\vec{b} = 0$, whenever $\vec{b}^T\vec{e} = 0$, then $\mathcal{G}_\lambda\vec{b} = 0$. There are $N - 1$ such independent vectors.

Then, we obtain from (2.119) that the threshold condition for stability is either

$$\tilde{B}_c + \nu^{-1} = 0 \qquad \text{whenever} \quad \vec{b}^T \vec{e} = 0, \tag{2.134}$$

or,

$$\tilde{B}_c + \frac{1}{\nu}\left(\frac{\mathcal{D}_0 N}{2\tau\lambda} + 1\right) = 0, \qquad \text{when} \quad \mathcal{G}_\lambda \vec{e} = k_1 \vec{e}. \tag{2.135}$$

The condition (2.134) represents the competition modes, whereas the condition (2.135) corresponds to the synchronous modes.

We first consider the synchronous mode. We have from (2.135) that

$$\tilde{B}_c + \frac{1}{\nu}\left(\frac{\mathcal{D}_0 N}{2\tau\lambda} + 1\right) = 0.$$

However, since $\tilde{B}_c = \hat{B}_c / S_c^2$, with $S_c = 2\nu^{1/2}/\sqrt{\mathcal{D}_0} N$, we obtain that

$$\hat{B}_c = -\frac{2}{\tau\lambda N^2}\left(N + \frac{2\tau\lambda}{\mathcal{D}_0}\right).$$

Now, in the NLEP (2.132) we calculate with $\alpha = b(1-f)^2/f^2$ (see (2.129)) that

$$\frac{\alpha}{\hat{B}_c} = -\frac{b(1-f)^2 N^2}{4f^2} \frac{2\tau\lambda}{N + 2\tau\lambda/\mathcal{D}_0},$$

Next, we recall the definition of φ in (2.104) to obtain

$$1 - \frac{\alpha}{\hat{B}_c} = 1 + \frac{2\tau\lambda\varphi}{N + 2\tau\lambda/\mathcal{D}_0} = \frac{N + 2\tau\lambda/\mathcal{D}_0 + 2\tau\lambda\varphi}{N + 2\tau\lambda/\mathcal{D}_0}.$$

We then compare this with (2.114) and conclude that

$$1 - \frac{\alpha}{\hat{B}_c} \equiv \frac{\varphi}{\mu},$$

where μ is defined in (2.114).

Finally, we substitute this last expression into (2.132) to obtain

$$g(\lambda) = \frac{1}{2}\left[\frac{f-(\lambda+1)(\varphi/\mu)}{f-(\lambda+1)}\right] - \mathcal{F}(\lambda),$$

in agreement with (2.114).

Next, we consider the competition modes. We have from (2.134) that $\tilde{B}_c = -\nu^{-1}$. Now $\tilde{B}_c = \hat{B}_c/S_c^2$, so that

$$\hat{B}_c = -S_c^2/\nu = -4/\mathcal{D}_0 N^2,$$

since $S_c = 2\nu^{1/2}/\sqrt{\mathcal{D}_0}N$.

We then calculate that

$$\frac{\alpha}{\hat{B}_c} = -\frac{b(1-f)^2}{f^2}\left(\frac{\mathcal{D}_0 N^2}{4}\right) = -\mathcal{D}_0\frac{b(1-f)^2N^2}{4f^2} = -\varphi\mathcal{D}_0,$$

with $\varphi = N^2(1-f^2)b/4f^2$. This shows that (2.132) becomes

$$g(\lambda) = \frac{1}{2}\left[\frac{f-(\lambda+1)(1+\mathcal{D}_0\varphi)}{f-(\lambda+1)}\right] - \mathcal{F}(\lambda),$$

which agrees precisely with the NLEP in (2.113).

We summarize the result of this section as follows. Let $\tau > 0$ with $\tau = O(1)$. Assume that $\mathcal{D} = \mathcal{D}_0/\nu$. Then, the small S asymptotics of the stability theory in the summing logs formulation of § 2.2 agrees with the NLEP as derived directly in section § 2.5.

Finally, we remark that an advantage of the stability theory of § 2.2 is that it is accurate to all orders in ν. However, in order to implement the theory, numerical methods are needed and therefore it is difficult to obtain full analytical results. In contrast, for the leading-order NLEP stability theory we can obtain an explicit instability threshold in terms of $\mathcal{D}_0$ for the competition mode (see (2.110)), while

the small S-asymptotics of the stability theory of § 2.2 provides a higher order correction term (see (2.118)). However, for both stability formulations, numerical methods are needed to compute any Hopf bifurcation threshold in terms of τ.

Chapter summary

In this chapter we derived a localized spot-type solution for the Brusselator model, and we analyzed its stability. By means of three different methods: a full nonlinear derivation that results in a DAE system, an asymptotic expansion in ν, and through the derivation of an NLEP for which stability results exist, we were able to derive thresholds for a competition instability, a spot-splitting instability, and an oscillatory Hopf instability. We corroborated the analytic thresholds with full numerical simulations.

The DAE system obtained by uncoupling the fully nonlinear problem in a system with symmetric spot strengths was shown to have solutions that are connected to the classic Fekete/Thomson problem of distributing Coulomb charges on the surface of a sphere.

In the next chapter we will apply similar techniques to the Schnakenberg model and will also derive a set of differential equations for the slow motion of the spots.

Chapter 3

The Schnakenberg Model on the Surface of the Sphere

Reaction-diffusion systems have been previously proposed to model skin pigmentation patterns on a species of Angelfish ([25], [43]). Despite its origin as a mechanism to explain pattern formation on such two-dimensional manifolds, for analytical and computational simplicity most previous work has been done for either the case of one spatial dimension or for weakly nonlinear patterns near a spatially homogeneous equilibrium state. Our goal is to analytically characterize localized patterns for the Schnakenberg model on the surface of the sphere.

The Schnakenberg model [52] on a sphere of radius L is a two-component reaction-diffusion system given in non-dimensional form by

$$\begin{aligned} \mathcal{V}_t - D_v \Delta_s \mathcal{V} &= f(\mathcal{U}, \mathcal{V}) \equiv b - \mathcal{V} + \mathcal{U}\mathcal{V}^2 \,, \\ \mathcal{U}_t - D_u \Delta_s \mathcal{U} &= g(\mathcal{U}, \mathcal{V}) \equiv a - \mathcal{U}\mathcal{V}^2 \,. \end{aligned} \tag{3.1}$$

Here Δ_s is the Laplace-Beltrami operator for a sphere of radius L. This system is one of the more robust pattern generators among reaction-diffusion systems, while

remaining amenable to analysis due to the algebraic simplicity of the kinetics [37]. The problem is connected with physical applications in which the constant terms (a, b) could represent source terms that couple a dynamical problem in the interior of the sphere with a diffusion process on the surface of the sphere ([11], [42]).

The standard Turing analysis of linearizing a reaction-diffusion system around a spatially homogeneous equilibrium state is of somewhat limited use for characterizing patterns on the surface of the sphere. The difficulty is that mode predictability becomes severely hampered by the fact that the Laplacian eigenfunctions responsible for small amplitude spatially inhomogeneous patterns have a high degree of degeneracy on the surface of the sphere. This can be readily seen by linearizing around the homogeneous solution.

For the Schnakenberg system, the spatially homogeneous base state is $\mathcal{V}_e = a + b$ and $\mathcal{U}_e = a/(a + b)^2$. We linearize (3.1) around this spatially homogeneous base state to obtain the linearized problem

$$\phi_t = \mathcal{J}\phi + D\Delta_s\phi, \qquad \mathcal{D} = \frac{1}{L^2}\begin{pmatrix} D_v & 0 \\ 0 & D_u \end{pmatrix}, \quad \mathcal{J} = \begin{pmatrix} f_{\mathcal{V}} & f_{\mathcal{U}} \\ g_{\mathcal{V}} & g_{\mathcal{U}} \end{pmatrix}_{\mathcal{U}_e,\mathcal{V}_e}. \tag{3.2}$$

Here ϕ is a two-vector, L is the radius of the sphere, and Δ_s now denotes the standard surface Laplacian on the unit sphere.

Upon separating variables, it follows that the spatial eigenfunctions are the well-known spherical harmonics Y satisfying

$$\Delta_s Y + k^2 Y = 0, \tag{3.3}$$

given explicitly in terms of Legendre polynomials as

$$Y_l^m(\theta, \phi) = c_l^m P_l^{|m|}(\cos\theta)\exp(im\phi), \;\; l = 0, 1, 2, \ldots, \quad |m| \le l\,, \;\; k^2 = l(l{+}1). \tag{3.4}$$

Here l and m are called the degree and the order of the spherical harmonic, respectively. With the exception of the simple eigenvalue $k = 0$, the other nonzero

eigenvalues $k^2 = l(l+1)$ with $l > 0$ are $2l+1$-fold degenerate, in the sense that there are $2l+1$ independent eigenfunctions, characterized by the order m in $|m| \leq l$, corresponding to this eigenvalue. As l increases, the set of eigenfunctions becomes increasingly degenerate.

A Turing stability analysis for the linearization of the Schnakenberg system on the surface of the sphere is a standard exercise and was done in [16]. In this 2-D case, the interval in k^2 where an instability of the spatially homogeneous base state occurs scales like $O(L^2)$, where L is the radius of the sphere. Thus, for large sphere radii, there will be a large number of Laplacian eigenvalues in this interval. This fact, together with the intrinsic degeneracy of the spherical harmonic eigenspace for larger eigenvalues, implies that mode prediction will only be accurate for small sphere radii (i.e. corresponding to low values of l). To illustrate this mode degeneracy, in [16] a table of values is given for the eigenvalue ranges as a function of increasing values of the radius of the sphere for the Schnakenberg system with $a = 0.95$ and $b = 0.07$.

This shows that a standard linear Turing-type stability theory is not particularly well-suited for predicting small amplitude patterns on the surface of the sphere when the sphere has a large radius. The eigenpairs of the Laplacian become rather degenerate as the radius of the sphere increases, and mode determination becomes a very difficult issue. Although there have been some previous weakly nonlinear normal-form type theories for reaction-diffusion systems on a sphere near bifurcation points, showing the emergence of different solution branches from a single bifurcation point, it is in general difficult to determine which branch is the most stable and to determine its basin of attraction [30]. For the Brusselator model this has been done in [38].

Rather than adopting this weakly nonlinear viewpoint, our approach is to seek "particle-like" solutions consisting of localized spots to the fully nonlinear Schnakenberg system on the surface of the sphere. Our analysis relies on the assumption of an asymptotically large diffusion coefficient ratio. In this asymptotic limit, our goal is to characterize the existence, stability, and dynamics of such solutions. In

addition, we will determine a spot self-replication bifurcation that will be triggered as the radius of the sphere grows adiabatically in time.

3.1 Localized spot patterns on the sphere

The specific system that we shall study in detail is the approximate system that results from (3.1) in the asymptotic regime for which $D_v \ll 1$ and $D_u = O(D_v^{-1}) \gg 1$. To derive this system, we let $\mathcal{V} = v/D_v$ and $\mathcal{U} = D_v u$ in (3.1) to obtain that

$$v_t = D_v \Delta_s v + b D_v - v + uv^2, \qquad D_v u_t = D_u D_v \Delta_s u + a - \frac{1}{D_v} uv^2 \,. \quad (3.5)$$

We then label $D_v \equiv \varepsilon^2$ with $\varepsilon \to 0$. Moreover, we define D by $D = D_u D_v$, and we assume that $D = O(1)$ as $\varepsilon \to 0$. In this way, we can neglect the bD_v and $D_v u_t$ terms in (3.5) and obtain the following elliptic-parabolic limit of the original Schnakenburg system (3.1):

$$v_t = \varepsilon^2 \Delta_s v - v + uv^2 \,, \qquad 0 = D\Delta_s u + a - \varepsilon^{-2} uv^2. \quad (3.6)$$

Morever, by a simple re-scaling of ε^2 and D by the square of the radius L of the sphere, it sufficies to consider (3.6) on the surface of the unit sphere, and so without loss of generality Δ_s now denotes the usual Laplace-Beltrami operator on the unit sphere. The key bifurcation parameters in (3.6) are $a > 0$ and $D > 0$.

Although this parabolic-elliptic limiting system of the original Schnakenburg model does not admit spot patterns that undergo Hopf bifurcations, there are two other instability mechanisms that occur and will be analyzed.

3.1.1 The quasi-equilibrium multi-spot pattern

In the limit of small diffusivity $\varepsilon \to 0$, we will first use the method of matched asymptotic expansions to construct a quasi-equilibrium solution of (3.6) with spots located at $\{x_1, \ldots, x_N\}$ on the surface of the sphere.

In the inner region near the j-th spot we introduce the local variables

$$y = \varepsilon^{-1}(x - x_j)\,, \qquad \rho = |y|\,, \qquad U_j = D^{-1/2}u\,, \qquad V_j = D^{1/2}v\,, \quad (3.7)$$

where $V_j(\rho)$ and $U_j(\rho)$ are radially symmetric. Upon substituting (3.7) into (3.6) we are effectively making a tangent plane approximation to the surface of the sphere at $x_j \in \Omega$. We obtain that U_j and V_j satisfy the following (so-called) core problem on $0 < \rho < \infty$:

$$\begin{aligned} &V_j'' + \frac{1}{\rho}V_j' - V_j + U_j V_j^2 = 0\,, \qquad U_j'' + \frac{1}{\rho}U_j - U_j V_j^2 = 0, \\ &U_j'(0) = V_j'(0) = 0; \quad V_j \to 0 \text{ and } U_j \sim S_j \log\rho + \chi(S_j) + o(1) \text{ as } \rho \to \infty. \end{aligned} \quad (3.8)$$

Upon integrating the equation for U_j on $0 < \rho < \infty$ we obtain the identity that

$$S_j = \int_0^\infty \rho U_j V_j^2 d\rho\,. \quad (3.9)$$

We can solve (3.8) for a range of values of S_j, and then at each S_j output the constant $\chi(S_j)$ defined by the limiting process $\lim_{\rho\to\infty}(U_j - S_j\log\rho) = \chi(S_j)$.

This core problem is solved numerically on a large but finite domain, and in this way we obtain an approximation to $\chi(S_j)$, as shown in Figure 3.1. Our numerical results show that there is a unique solution to this system at least on the range $0 < S_j < 7.5$.

Next, we determine a nonlinear algebraic system for the source strengths $S_1, \ldots, S_N$.

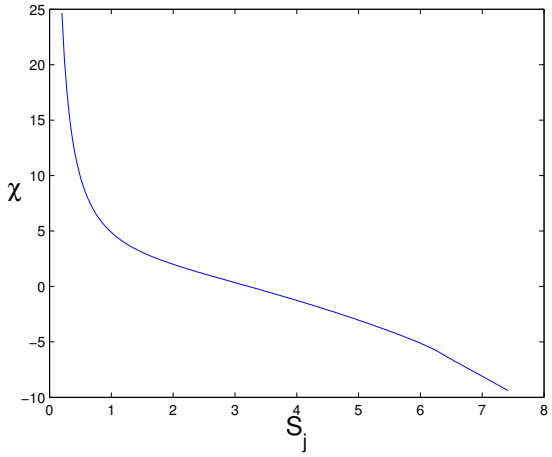

Figure 3.1: Numerical estimation of $\chi(S_j)$ by solving the core problem (3.8)

This is done by asymptotically matching the inner solutions near each spot to a global outer solution for u valid away from the spot locations. The determination of the S_j for $j = 1, \ldots, N$ then specifies the inner solution near each spot.

To formulate the outer problem for the inhibitor variable u, we first estimate in the sense of distributions the term proportional to ε^{-2} in the u-equation of (3.6). We calculate that

$$\varepsilon^{-2} u v^2 \to \left(\int_{\mathbb{R}^2} \frac{1}{\sqrt{D}} U_j(DV_j^2) dy \right) \delta(x - x_j) = 2\pi\sqrt{D} S_j \delta(x - x_j).$$

Thus, the outer problem for u on the surface of the sphere is

$$\Delta_s u = -\frac{a}{D} + \frac{2\pi}{\sqrt{D}} \sum_{i=1}^{N} S_i \delta(x - x_i), \tag{3.10}$$

subject to the N matching conditions that

$$u \sim \frac{1}{\sqrt{D}} \left[S_j \log|x - x_j| + \frac{S_j}{\nu} + \chi(S_j) \right] \quad \text{as} \quad x \to x_j, \quad j = 1, \ldots, N\,, \tag{3.11}$$

where $\nu = -1/\log\varepsilon$.

To solve this problem for u, we define the Neumann Green's function $G(x;x_0)$ as the unique solution to

$$\Delta_s G = \frac{1}{4\pi} - \delta\,(x - x_0), \qquad x \in \Omega, \qquad \int_\Omega G(x;x_0)\,dx = 0\,, \tag{3.12}$$

with G being 2π periodic in ϕ, and smooth at $\theta = 0, \pi$. The exact solution is

$$G(x;x_0) = -\frac{1}{2\pi}\log|x - x_0| + R, \qquad R = \frac{1}{4\pi}[2\log 2 - 1]. \tag{3.13}$$

Then, the solution to (3.10) and (3.11) can be represented as

$$u(x) = -\frac{2\pi}{\sqrt{D}}\left(\sum_{i=1}^{N} S_i G(x;x_i) + u_c\right), \tag{3.14}$$

where u_c is a constant to be found.

The divergence theorem, as applied to (3.10) and (3.11), yields that

$$\sum_{i=1}^{N} S_i = \frac{2a}{\sqrt{D}}. \tag{3.15}$$

Then, upon expanding the solution in (3.14) as $x \to x_j$ and using the matching condition (3.11) we obtain that

$$-\frac{2\pi}{\sqrt{D}}\left[-\frac{S_j}{2\pi}\log|x - x_j| + S_j R + \sum_{i\neq j}^{N} S_j G_{ji} + u_c\right] \sim \frac{1}{\sqrt{D}}\left[S_j \log|x - x_j| + \frac{S_j}{\nu} + \chi(S_j)\right],$$

for each $j = 1, \ldots, N$.

The singular terms in these matching conditions agree automatically, while the

matching of the constant terms leads to the N nonlinear algebraic equations

$$\frac{S_j}{\nu} + 2\pi \left(S_j R + \sum_{i \neq j}^{N} S_i G_{ji} \right) + \chi(S_j) = -2\pi u_c \,, \qquad j = 1, \ldots N,$$

coupled to the scalar constraint (3.15). Here $G_{ji} = G(x_j; x_i) = G(x_i; x_j)$. This yields an $N+1$ dimensional nonlinear algebraic system for the determination of the unknowns $S_1, \ldots, S_N$ and u_c. In this way, we obtain that $S_1, \ldots, S_N$ and u_c satisfy the matrix system

$$\begin{gathered} (I + 2\pi\nu(\mathcal{G} + RE))\,\vec{S} + \nu\chi(\vec{S}) = -2\pi u_c \nu \vec{e}, \\ e^{\vec{T}}\vec{S} = \frac{2a}{\sqrt{D}}, \quad \mathcal{G} = \begin{pmatrix} 0 & & L_{ij} \\ & \ddots & \\ L_{ji} & & 0 \end{pmatrix}, \quad \vec{\chi} = \begin{pmatrix} \chi(S_1) \\ \ddots \\ \chi(S_N) \end{pmatrix}, \quad E = \frac{1}{N}\vec{e}\vec{e}^{T}, \end{gathered} \tag{3.16}$$

where $\vec{e} = (1, \ldots, 1)^T$, and $L_{ij} = -\frac{1}{2\pi}\log|x_i - x_j|$.

From the system we can eliminate u_c and obtain a set of N nonlinear algebraic equations for the unknowns $\vec{S} = (S_1, \ldots, S_N)^T$. We summarize our main result for the construction of the quasi-equilibrium N-spot solution as follows:

Principal Result 3.1.1 *In the limit $\varepsilon \to 0$, an N-spot quasi-equilibrium solution to* (3.6) *is characterized by*

$$\begin{aligned} v_e &\sim \sum_{j=1}^{N} \sqrt{\mathcal{D}} V_j(\varepsilon^{-1}|x - x_j|), \\ u_e &\sim \begin{cases} \frac{1}{\sqrt{\mathcal{D}}} U_j(\varepsilon^{-1}|x - x_j|) & \text{for } |x - x_j| = O(\varepsilon) \\ -\frac{2\pi}{\sqrt{D}} \left(\sum_{i=1}^{N} S_i G(x; x_i) + u_c \right) & \text{for } |x - x_j| \gg O(\varepsilon). \end{cases} \end{aligned} \tag{3.17}$$

Here U_j and V_j satisfy the core problem (3.8). *In addition, the vector $\vec{S}$ of source*

strengths $S_1, \ldots, S_N$ satisfies the nonlinear algebraic system

$$\vec{S} + \nu(I - E)(\vec{\chi} + 2\pi(\mathcal{G} + RE)\vec{S}) = \frac{2a}{N\sqrt{D}}, \qquad E = \frac{1}{N}\vec{e}\vec{e}^T, \quad \nu = \frac{-1}{\log \varepsilon}. \tag{3.18}$$

Remark

(i) Suppose that $\{x_1, \ldots, x_N\}$ are such that $\mathcal{G}$ is a cyclic matrix. This always occurs for two spot patterns, for spots equally spaced on a ring of constant latitude, and for other such symmetric patterns (see §3.4 below). However, this condition imposes a restriction on the spot locations for general multi-spot patterns. In the cyclic case, we have that

$$\mathcal{G}\vec{e} = k_1\vec{e}.$$

Therefore, we can look for a solution to (3.18) of the form $S = S_c\vec{e}$, so that $\vec{\chi} = \chi(S_c)\vec{e}$. From (3.18) we obtain using $(I - E)\vec{e} = 0$ that

$$(I - E)\left(\vec{\chi} + 2\pi(\mathcal{G} + RE)\vec{S}\right) = \chi(S_c)(I - E)\vec{e} + 2\pi S_c(I - E)(k_1 + R)\vec{e} = 0.$$

Therefore, for the cyclic case we conclude that to all orders in ν there exists a solution to (3.18) with a common source strength S_c where

$$S_c = \frac{2a}{N\sqrt{D}}. \tag{3.19}$$

3.2 The spot self-replication threshold

In this section we study a linear instability mechanism for the local deformation of a spot. This peanut-type instability is the trigger for a nonlinear spot self-replication event. Such an instability mechanism was first analyzed for the Schnakenberg system in a planar domain in [24]. Since this instability is a lo-

cal instability, the analysis of peanut-splitting instabilities for a spot on the sphere parallels that of the planar case. We now briefly outline this analysis.

We linearize (3.6) around the quasi-equilibrium solution of (3.17) by writing

$$v = v_e + e^{\lambda t}\phi\,, \qquad u = u_e + e^{\lambda t}\eta\,. \tag{3.20}$$

By substituting (3.20) into (3.6) and linearizing, we obtain the following eigenvalue problem for ϕ and η:

$$\begin{aligned} \varepsilon^2\Delta_s\phi - \phi + 2u_e v_e\phi + v_e^2\eta = \lambda\phi, \\ D\Delta_s\eta - 2\varepsilon^{-2}u_e v_e\phi - \varepsilon^{-2}v_e^2\eta = 0. \end{aligned} \tag{3.21}$$

In the j-th inner region we have

$$u_e = \frac{1}{\sqrt{D}}U_j, \qquad v_e = \sqrt{D}V_j, \qquad y = \varepsilon^{-1}(x - x_j), \tag{3.22}$$

where U_j and V_j satisfy the core problem (3.8). In the inner region near x_j we seek an $\mathcal{O}(1)$ time-scale instability associated with the local angular integer mode m satisfies $m \geq 2$. We introduce the new variables $\hat{N}_j(\rho)$ and $\hat{\Phi}_j(\rho)$ by

$$\eta = \frac{1}{D}e^{im\omega}\hat{N}_j(\rho)\,, \qquad \phi = e^{im\omega}\hat{\Phi}_j(\rho)\,, \qquad \rho = |y|\,, \qquad \omega = \arg y\,. \tag{3.23}$$

Upon substituting (3.22) and (3.23) into (3.21), we obtain the following radially symmetric eigenvalue problem where the integer mode $m \geq 2$ is a parameter:

$$\begin{aligned} \Delta_\rho\hat{\Phi}_j - \hat{\Phi}_j - \frac{m^2}{\rho^2}\hat{\Phi}_j + 2U_jV_j\hat{\Phi}_j + V_j^2\hat{N}_j = \lambda\hat{\Phi}_j, \quad \hat{\Phi}_j \to 0, \text{ as } \rho\to\infty, \\ \Delta_\rho\hat{N}_j - \frac{m^2}{\rho^2}\hat{N}_j - 2U_jV_j\hat{\Phi}_j - V_j^2\hat{N}_j = 0, \quad \hat{N}_j \to 0, \text{ as } \rho\to\infty. \end{aligned} \tag{3.24}$$

Since $m \geq 2$ we can impose the decay condition for $\hat{N}_j$ as $\rho \to \infty$.

The eigenvalue problem (3.24) was solved numerically in §2.3 of [24]. We label λ_0 to be the eigenvalue of this problem with the largest real part. Since the core solution depends on S_j from (3.8), then $\lambda_0 = \lambda_0(S_j, m)$. To determine the onset of any instabilities, the threshold value $S_j = \Sigma_m$ where $\mathrm{Re}(\lambda_0(\Sigma_m, m)) = 0$ was computed. In the computations of [24], only the modes $m = 2, 3, 4, \ldots$ were considered, since $\lambda_0 = 0$ for any value of S_j for the translational mode $m = 1$.

For $m \geq 2$, the computations of [24] showed that $\lambda_0(S_j, m)$ is real and that $\lambda_0(S_j, m) > 0$ when $S_j > \Sigma_m$, and that $\Sigma_2 < \Sigma_3 < \Sigma_4$ etc.. Therefore, the smallest value of S_j where an instability is triggered occurs for the "peanut-splitting" instability $m = 2$. The numerical value for this threshold was found to be $\Sigma_2 \approx 4.3$. We conclude that there is a peanut-splitting instability for the j-th spot if and only if $S_j > \Sigma_2 \approx 4.3$.

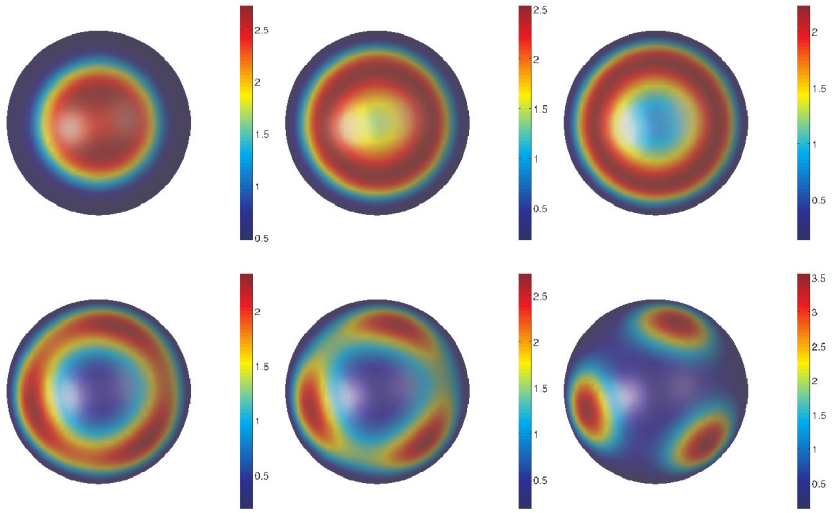

Figure 3.2: Spot-splitting in the Schnakenberg model ($u(\vec{x})$). The same dynamics occurs in the lower hemisphere in this example, as the initial configuration consisted of two spots. The parameters were $D = 1, \varepsilon = 0.1, R = 1.5$, and a similar initial condition with $R = 1$ will does not split.

With regards to the effect of domain growth on spot-splitting, we predict that spot self-replication will occur once the radius of a sphere becomes greater than some critical value. To show this qualitatively, suppose that we have an initial configuration of N spots for which the Green's matrix is cyclic. Then, the common source strength S_c from (3.19) is $S_c = \frac{2a}{N\sqrt{D}}$. We conclude that $S_c > \Sigma_2 \approx 4.3$, when

$$D < \left(\frac{2a}{N\Sigma_2}\right)^2 .$$

Since D is inversely proportional to the square of the radius L of the sphere, we conclude that spot self-replication will occur when L exceeds a critical value L_N. Further spot self-replication events will occur when L increases past a further threshold. We conclude that spot self-replication is an under-crowding type of instability.

3.2.1 The competition instability threshold

In this subsection we obtain a new explicit two-term result for the competition instability threshold for an N-spot quasi-equilibrium pattern with spots at $\{x_1, \ldots, x_N\}$ for the special case where $\mathcal{G}$ is a cyclic matrix. We will find that the stability threshold is $D = O(1/\nu) + O(1)$, with $\nu = -1/\log\varepsilon$, where both terms are calculated analytically.

Similarly to our analysis of the Brusselator model, in our stability analysis we will "freeze" the locations of the spots, since they evolve on a much longer time-scale of order $O(\varepsilon^{-2})$ than the $O(1)$ time-scale needed to initiate a competition instability. The calculation of the competition instability threshold proceeds in three distinct steps.

1. For the fully coupled core problem (3.8), we determine a two-term approximation to this system for $S_j \to 0$. In particular, we determine a two-term asymptotic expansion for $\chi(S_j)$ as $S_j \to 0$. Then, when $\mathcal{G}$ is a cyclic ma-

trix, so that $\mathcal{G}\vec{e} = k_1\vec{e}$, there exists a quasi-equilibrium pattern with a common source strength S_c, where S_c is given in (3.19) and is $O(\nu^{1/2})$ when $D = O(\nu^{-1})$. This motivates the need for the small S analysis of the solution to the core problem.

2. By linearizing around the quasi-equilibrium N-spot solution we formulate a globally coupled nonlocal eigenvalue problem (NLEP). We then write the condition for $\lambda = 0$ to be an eigenvalue of this problem. The threshold condition will involve $\chi'(S_c)$ in a central way.

3. From the information obtained in step 1 and step 2, we finally eliminate S_c to determine a two-term asymptotic result for the stability threshold in terms of D.

Step 1: Asymptotics as $S \to 0$ of the solution to the core problem

For the core problem (3.8), we replace $U_j \to U$, $V_j \to V$, and $S_j \to S$, and write the radially symmetric core problem as

$$\begin{aligned} \Delta_\rho V - V + UV^2 = 0, \qquad V \to 0, \quad \text{as} \quad \rho \to \infty, \\ \Delta_\rho U = UV^2, \qquad U \sim S\log\rho + \chi(S), \quad \text{as} \quad \rho \to \infty. \end{aligned} \tag{3.25}$$

We now give a formal scaling analysis for the limit $S \to 0$. Let $U = uS^{-P}$, $V = S^P v$, so that $UV^2 = O(UV)O(V) = O(V)$. Hence, the V equation is invariant, whereas for the U equation we have

$$\Delta_\rho u = S^{2p}uv^2, \qquad u \sim S^{1+p}\log\rho + S^p\chi.$$

In order to obtain a distinguished limit, we require that $2p = p + 1$, and $\chi = O(S^{-p})$. This yields that $p = 1$. Hence, for $S \to 0$, we have $U \sim u/S$, $V \sim Sv$, and $\chi \sim \hat{\chi}/S$.

In a systematic way, we can now expand the solution to the core problem using

the previous scaling. We write

$$U = \frac{1}{S}\hat{U}, \qquad V = S\hat{V}, \qquad \chi = \frac{1}{S}\hat{\chi}\,. \tag{3.26}$$

Then, (3.25) transforms to

$$\begin{aligned} \Delta_\rho \hat{V} - \hat{V} + \hat{U}\hat{V}^2 = 0, \qquad \hat{V} \to 0, \quad \text{as} \quad \rho \to \infty, \\ \Delta_\rho \hat{U} = \hat{U}\hat{V}^2 S^2, \qquad \hat{U} \sim \hat{\chi} + S^2 \log\rho, \quad \text{as} \quad \rho \to \infty. \end{aligned} \tag{3.27}$$

Since we will need a two-term asymptotic result for $\chi(S)$ as $S \to 0$, we will expand

$$\begin{aligned} \hat{V} &= \hat{V}_0 + S^2\hat{V}_1 + S^4\hat{V}_2 + \cdots, \\ \hat{U} &= \hat{U}_0 + S^2\hat{U}_1 + S^4\hat{U}_2 + \cdots, \\ \hat{\chi} &= \hat{\chi}_0 + S^2\hat{\chi}_1 + S^4\hat{\chi}_2 + \cdots. \end{aligned}$$

We substitute this expansion into (3.27) and equate powers of S^2 to obtain

$$\begin{aligned} \Delta_\rho \hat{V}_0 - \hat{V}_0 + \hat{U}_0\hat{V}_0^2 = 0, \qquad \hat{V}_0 \to 0, \quad \text{as} \quad \rho \to \infty, \\ \Delta_\rho \hat{U}_0 = 0, \qquad \hat{U}_0 \sim \hat{\chi}_0, \quad \text{as} \quad \rho \to \infty, \end{aligned} \tag{3.28}$$

and

$$\begin{aligned} \Delta_\rho \hat{V}_1 - \hat{V}_1 + 2\hat{U}_0\hat{V}_0\hat{V}_1 = -\hat{U}_1\hat{V}_0^2, \qquad \hat{V}_1 \to 0, \quad \text{as} \quad \rho \to \infty, \\ \Delta_\rho \hat{U}_1 = \hat{U}_0\hat{V}_0^2, \qquad \hat{U}_1 \sim \hat{\chi}_1 + \log\rho, \quad \text{as} \quad \rho \to \infty. \end{aligned} \tag{3.29}$$

At one higher order the problem for $\hat{U}_2$ is

$$\Delta_\rho \hat{U}_2 = \hat{U}_1\hat{V}_0^2 + 2\hat{U}\hat{V}_0\hat{V}_1, \qquad \hat{U}_2 \quad \text{bounded as} \quad \rho \to \infty. \tag{3.30}$$

The solution to (3.28) is

$$\hat{U}_0 = \hat{\chi}_0, \qquad \hat{V}_0 = \frac{w}{\hat{\chi}_0},$$

where w is the radially symmetric ground-state solution satisfying $\Delta_\rho w - w + w^2 = 0$. Then (3.29) becomes

$$\begin{aligned} \mathrm{L}_0\hat{V}_1 \equiv \Delta_\rho \hat{V}_1 - \hat{V}_1 + 2w\hat{V}_1 = -\frac{\hat{U}_1}{\hat{\chi}_0^2} w^2, \qquad \hat{V}_1 \to 0, \quad \text{as} \quad \rho \to \infty, \\ \Delta_\rho \hat{U}_1 = \frac{1}{\hat{\chi}_0} w^2, \qquad \hat{U}_1 \sim \log\rho + \hat{\chi}_1, \quad \text{as} \quad \rho \to \infty. \end{aligned} \tag{3.31}$$

Upon integrating the $\hat{U}_1$ equation over $0 < \rho < \infty$, we obtain that

$$\hat{\chi}_0 = b, \qquad b = \int_0^\infty \rho w^2 d\rho.$$

Since we require a two-term expansion in order to obtain our stability threshold below, we must calculate $\hat{\chi}_1$. To do so, we decompose $\hat{U}_1$ and $\hat{V}_1$ as

$$\hat{U}_1 = \hat{\chi}_1 + \frac{1}{\hat{\chi}_0}\hat{U}_{1p}, \qquad \hat{V}_1 = -\frac{\hat{\chi}_1}{\hat{\chi}_0^2} w + \frac{1}{\hat{\chi}_0^3}\hat{V}_{1p}. \tag{3.32}$$

Upon using the identity that $\mathrm{L}_0 w = w^2$, we readily derive from (3.29) that $\hat{U}_{1p}$ and $\hat{V}_{1p}$ satisfy

$$\begin{aligned} \mathrm{L}_0\hat{V}_{1p} = -w^2\hat{U}_{1p}, \qquad 0 < \rho < \infty; \qquad \hat{V}_{1p} \to 0, \quad \text{as} \quad \rho \to \infty, \\ \Delta_\rho \hat{U}_{1p} = w^2, \qquad 0 < \rho < \infty\,; \qquad \hat{U}_{1p} \sim b\log\rho + o(1), \quad \text{as} \quad \rho \to \infty. \end{aligned} \tag{3.33}$$

We remark that there exists a unique solution to (3.33) since we have imposed that $\hat{U}_{1p} - b\log\rho \to 0$ as $\rho \to \infty$.

Finally, to obtain $\hat{\chi}_1$ we integrate the $\hat{U}_2$ equation in (3.30). Since $\hat{U}_2$ is bounded at infinity we obtain that

$$\int_0^\infty \left(\rho\hat{U}_1\hat{V}_0^2 + 2\rho\hat{U}_0\hat{V}_0\hat{V}_1\right) d\rho = 0. \tag{3.34}$$

Upon using (3.32), we obtain

$$\int_0^\infty \rho\left(\hat{\chi}_1+\frac{1}{\hat{\chi}_0}\hat{U}_{1p}\right)\frac{1}{\hat{\chi}_0^2}w^2d\rho=-2\int_0^\infty \rho w\left(-\frac{\hat{\chi}_1}{\hat{\chi}_0^2}w+\frac{1}{\hat{\chi}_0^3}\hat{V}_{1p}\right)d\rho,$$

which reduces to

$$\hat{\chi}_1=\frac{1}{\hat{\chi}_0 b}\int_0^\infty \rho\left(\hat{U}_{1p}w^2+2w\hat{V}_{1p}\right)d\rho.$$

Finally, since $\hat{\chi}_0=b$ and $2w\hat{V}_{1p}+\hat{U}_{1p}w^2=-\Delta_\rho\hat{V}_{1p}+\hat{V}_{1p}$, the formula above for $\hat{\chi}_1$ can be written compactly as

$$\hat{\chi}_1=\frac{1}{b^2}\int_0^\infty \rho\hat{V}_{1p}d\rho,\qquad \text{with}\quad b=\int_0^\infty \rho w^2d\rho.$$

We summarize our result as follows.

In the limit $S\to 0$, the solution to the core problem (3.25) has the following asymptotic behaviour:

$$\begin{aligned}U&\sim\frac{1}{S}\left(\hat{\chi}_0+S^2\left(\hat{\chi}_1+\frac{1}{\hat{\chi}_0}\hat{U}_{1p}\right)+\cdots\right),\\ V&\sim S\left(\frac{w}{\hat{\chi}_0}+S^2\left(-\frac{\hat{\chi}_1}{\hat{\chi}_0^2}+\frac{1}{\hat{\chi}_0^3}\hat{V}_{1p}\right)+\cdots\right).\end{aligned}\tag{3.35}$$

Here $\hat{\chi}_0=b=\int_0^\infty \rho w^2d\rho$, $\hat{\chi}_1=\frac{1}{b^2}\int_0^\infty \rho\hat{V}_{1p}d\rho$, and $\hat{U}_{1p}$, $\hat{V}_{1p}$ are the unique solutions to (3.33).

The function $\chi(S)$ in (3.25) has the following two-term asymptotics for $S\to 0$:

$$\chi\sim\frac{1}{S}\left(\hat{\chi}_0+S^2\hat{\chi}_1+\cdots\right)=\frac{b}{S}+S\hat{\chi}_1+\cdots.\tag{3.36}$$

Therefore, for $S\to 0$, we have

$$\chi'(S)\sim-\frac{b}{S^2}+\hat{\chi}_1+o(1)\quad\text{as}\quad S\to 0,\qquad \hat{\chi}_1=\frac{1}{b^2}\int_0^\infty \rho\hat{V}_{1p}d\rho.\tag{3.37}$$

This ends step 1.

Step 2: Formulation of the globally coupled eigenvalue problem

Next, we linearize (3.6) around the quasi-equilibrium solution of (3.17) to obtain on the surface of the sphere that the perturbation satisfies (3.21).

In the j-th inner region we have

$$u_e = \frac{1}{\sqrt{D}} U_j, \qquad v_e = \sqrt{D} V_j, \qquad y = \varepsilon^{-1}(x - x_j).$$

To analyze competition instabilities, we look for a locally radially symmetric eigenfunction. In the j-th spot inner region, we let $\eta = \frac{1}{D} N_j(\rho)$ and $\phi = \Phi_j(\rho)$ to obtain from (3.21) that on $0 < \rho < \infty$,

$$\begin{aligned} \Delta_\rho \Phi_j - \Phi_j + 2U_j V_j \Phi_j + V_j^2 N_j &= \lambda \Phi_j, \\ \Delta_\rho N_j - 2U_j V_j \Phi_j - V_j^2 N_j &= 0. \end{aligned}$$

We must impose that N_j has logarithmic growth as $\rho \to \infty$.

We then set $\Phi_j = c_j \hat{\Phi}_j$, $N_j = c_j \hat{N}_j$, where c_j is an arbitrary constant, to obtain that

$$\begin{aligned} &\Delta_\rho \hat{\Phi}_j - \hat{\Phi}_j + 2U_j V_j \hat{\Phi}_j + V_j^2 \hat{N}_j = \lambda \hat{\Phi}_j, \qquad \hat{\Phi}_j \to 0, \quad \text{as} \quad \rho \to \infty, \\ &\Delta_\rho \hat{N}_j - 2U_j V_j \hat{\Phi}_j - V_j^2 \hat{N}_j = 0, \qquad \hat{N}_j \sim \log \rho + \hat{B}_j, \quad \text{as} \quad \rho \to \infty. \end{aligned} \tag{3.38}$$

Here $\hat{B}_j = \hat{B}_j(S_j, \lambda)$ must be computed numerically. By integrating the equation for $\hat{N}_j$ over $0 < \rho < \infty$, and recalling that $N_j = c_j \hat{N}_j$, we obtain the following identity that is needed below:

$$c_j = \int_0^\infty \left(2U_j V_j \Phi_j + V_j^2 N_j \right) \rho d\rho. \tag{3.39}$$

We note that $\hat{B}_j = \hat{B}_j(S_j, \lambda)$. Upon differentiating the core problem (3.8) with respect to S_j, and then comparing the resulting system with (3.38), we conclude when $\lambda = 0$ that

$$\hat{B}_j(S_j, 0) = \chi'(S_j). \tag{3.40}$$

Here $\chi(S_j)$, as defined in (3.25), must be computed from the core problem.

Next, we determine the matching condition and we formulate the problem for the outer solution for η. The far field of the inner solution for η, when written in outer variables, yields the following matching condition for the outer solution:

$$\eta \sim \frac{1}{D} c_j \left[\log|x - x_j| + \frac{1}{\nu} + \hat{B}_j \right], \quad \text{as} \quad x \to x_j \,. \tag{3.41}$$

In order to derive the outer problem for η we must estimate, in the sense of distributions, the terms proportional to ε^{-2} in the η equation in (3.21). We calculate that

$$2\varepsilon^{-2} u_e v_e \phi \to 2 \left(\int_{\mathbb{R}^2} \Phi_j U_j V_j dy \right) \delta(x - x_j),$$
$$\varepsilon^{-2} v_e^2 \eta \to \left(\int_{\mathbb{R}^2} D V_j^2 \frac{1}{D} N_j dy \right) \delta(x - x_j).$$

Upon combining these expressions, we get

$$2\varepsilon^{-2} u_e v_e \phi + \varepsilon^{-2} v_e^2 \eta \to 2\pi \left[\int_0^\infty \left(2\Phi_j U_j V_j + V_j^2 N_j \right) \rho d\rho \right] \delta(x - x_j).$$

Therefore, upon using the identity (3.39), and the matching condition (3.41), we obtain that the outer solution for η on the surface of the unit sphere satisfies

$$\begin{aligned} \Delta\eta &= \frac{2\pi}{D} \sum_{i=1}^{N} c_j \delta(x - x_i), \\ \eta &\sim \frac{1}{D} c_j \left[\log|x - x_j| + \frac{1}{\nu} + \hat{B}_j \right], \text{ as } x \to x_j, \quad j = 1, \ldots, N. \end{aligned} \tag{3.42}$$

From the divergence theorem we get

$$\sum_{i=1}^{N} c_i = 0.$$

The solution η is then represented as

$$\eta = -\frac{2\pi}{D}\sum_{i=1}^{N} c_j G(x;x_i) + \frac{\bar{\eta}}{\nu D},$$

where $\bar{\eta}$ is a constant to be determined and G is the Neumann Green's function of (3.12).

Upon expanding η as $x \to x_j$ and then comparing the result with the required singularity behaviour in (3.42), we obtain that $c_1, \ldots, c_N$ and $\bar{\eta}$ satisfy the homogeneous linear system

$$c_j + 2\pi\nu\left(c_j R + \sum_{i\neq j}^{N} c_j G_{ji}\right) + c_j\hat{B_j}\nu = \bar{\eta}, \quad j = 1,\ldots,N; \quad \sum_{i=1}^{N} c_i = 0. \tag{3.43}$$

To write this system more conveniently in matrix form, we introduce

$$\vec{c} = \begin{pmatrix} c_1 \\ \vdots \\ c_N \end{pmatrix}, \qquad \mathcal{B} \equiv \begin{pmatrix} \hat{B_1} & & 0 \\ & \ddots & \\ 0 & & \hat{B_N} \end{pmatrix}, \qquad \vec{e} = \begin{pmatrix} 1 \\ \vdots \\ 1 \end{pmatrix},$$

so that (3.43) becomes

$$\vec{c} + 2\pi\nu(\mathcal{G} + RE)\vec{c} + \nu\mathcal{B}\vec{c} = \bar{\eta}\vec{e}, \qquad \vec{e^T}\vec{c} = 0, \tag{3.44}$$

where $\mathcal{G}$ is the usual Neumann Green's matrix of (3.16). Upon multiplying this system with $\vec{e^T}$ we can then eliminate the scalar $\bar{\eta}$. In this way, we obtain the

following homogeneous linear system for $\vec{c}$:

$$[I + 2\pi\nu(I - E)(\mathcal{G} + RE) + \nu(I - E)\mathcal{B}]\,\vec{c} = 0.$$

We conclude that any discrete eigenvalues corresponding to a locally radially symmetric perturbation near each spot must satisfy

$$\det \mathcal{M} = 0,$$

where $\mathcal{M} = \mathcal{M}(\lambda)$ is the $N \times N$ matrix defined by

$$\mathcal{M}\vec{c} = 0, \qquad \mathcal{M} \equiv I + 2\pi\nu(I - E)(\mathcal{G} + RE) + \nu(I - E)\mathcal{B}. \tag{3.45}$$

Therefore, we must find conditions that guarantee the existence of a non-trivial $\vec{c}$. We refer to this eigenvalue problem as the *globally coupled extended nonlocal eigenvalue problem (NLEP)*.

Remark

(i) In order to find the stability threshold in terms of D we will look for conditions for which $\det \mathcal{M} = 0$ when $\lambda = 0$.

(ii) Recall that when $\mathcal{G}$ is cyclic, then to all orders in ν, there exists a solution with a common source strength S_c as given in (3.19).

(iii) We also recall from (3.40) that when $\lambda = 0$, then $\hat{B}_j(S_j, 0) = \chi'(S_j)$. Therefore, when the spots have a common source strength S_c, the matrix $\mathcal{B}$ in (3.45) is simply $\mathcal{B} = \chi'(S_c)I$ at the threshold $\lambda = 0$, where I is the identity matrix.

Therefore, in the cyclic case we calculate at $\lambda = 0$ that $\vec{c}$ must be a nontrivial

solution to

$$2\pi\nu(I-E)(\mathcal{G}+RE)\vec{c} = -\left[I+\nu\chi'(S_c)(I-E)\right]\vec{c}. \tag{3.46}$$

This completes step 2 of the analysis.

Step 3: Calculation of the stability threshold

We now look for conditions on D for which there exists a nontrivial solution $\vec{c}$ to (3.46). We label k_1 and k_j, for $j = 2, \ldots, N$, to be the eigenvalues of $\mathcal{G}$. The matrix spectrum of $\mathcal{G}$ is simply

$$\begin{aligned} &&&\mathcal{G}\vec{e} = k_1\vec{e}, && \text{synchronous mode,} \\ \mathcal{G}\vec{q_j} = k_j\vec{q_j}, \qquad &\vec{e}^T\vec{q_j} = 0, \quad &j = 2, \ldots, N, \qquad & \text{competition modes.} \end{aligned}$$

For the **synchronous mode**, we replace $\vec{c} = \vec{e}$ in (3.46), and use $\mathcal{G}\vec{e} = k_1\vec{e}$, and $(I-E)\vec{e} = 0$. This leads to

$$2\pi\nu(I-E)(\mathcal{G}+RE)\vec{e} = -\left[I+\nu\chi'(S_c)(I-E)\right]\vec{e},$$

which reduces to the contradictory statement that $\vec{0} = \vec{e}$. Therefore, as expected, we conclude that there is no instability threshold associated with the synchronous mode.

For the **competition modes**, we let $\vec{c} = \vec{q_j}$ for $j = 2, \ldots, N$ where $\vec{q_j}^T\vec{e} = 0$. Then, we calculate $\mathcal{G}\vec{q_j} = k_j\vec{q_j}$, and $E\vec{q_j} = 0$. Thus, (3.46) becomes

$$\begin{aligned} 2\pi\nu(I-E)(\mathcal{G}+RE)\vec{q_j} &= -\left[I+\nu\chi'(S_c)(I-E)\right]\vec{q_j}, \\ k_j 2\pi\nu(I-E)\vec{q_j} &= -\vec{q_j} - \nu\chi'(S_c)\vec{q_j}, \\ 2\pi\nu k_j\vec{q_j} &= -(1+\nu\chi'(S_c))\vec{q_j}. \end{aligned}$$

We conclude that $\det \mathcal{M}(0) = 0$ when

$$2\pi\nu k_j = -1 - \nu\chi'(S_c), \qquad j = 2, \ldots, N.$$

Therefore, for the competition modes, there are $N-1$ distinct thresholds where $\lambda = 0$. In terms of D they are given by the roots of the transcendental equations

$$\frac{1}{2\pi}\left(\chi'(S_c) + \frac{1}{\nu}\right) = -k_j, \qquad j = 2, \ldots, N. \tag{3.47}$$

Finally, we use $S_c = \frac{2a}{N\sqrt{D}}$, and the two-term asymptotics $\chi'(S_c) \sim -\frac{b}{S_c^2} + \hat{\chi_1}$ as $S_c \to 0$ as given in (3.37) to solve (3.47) asymptotically for D. Substituting these results into (3.47) we obtain

$$-\frac{b}{S_c^2} + \hat{\chi_1} + \frac{1}{\nu} \sim -2\pi k_j,$$

so that

$$S_c^2 \sim \frac{b}{\nu^{-1} + \hat{\chi_1} + 2\pi k_j}.$$

Then, upon recalling that $S_c^2 = \frac{4a^2}{N^2 D}$ from (3.19), we solve for D to obtain that

$$D = \frac{4a^2}{bN^2\nu}\left(1 + \nu(2\pi k_j + \hat{\chi_1})\right).$$

This completes the final step 3.

We summarize our main result for competition instabilities as follows:

Principal Result 3.2.1 *Suppose that the configuration $\{x_1, \ldots, x_N\}$ of spots are such that $\mathcal{G}$ is a cyclic matrix. Then, there exists an N-spot quasi-equilibrium solution with common source strengths, i.e., $S_j = S_c$ for all $j = 1, \ldots N$. For this solution, the globally coupled extended NLEP has a zero eigenvalue corresponding to a sign-fluctuating instability of the spot amplitudes at the critical values D_j for*

$j = 2, \ldots, N$ *of the inhibitor diffusivity* D*, given by*

$$D_j = \frac{4a^2}{bN^2\nu} + \frac{4a^2}{bN^2}\left(2\pi k_j + \hat{\chi}_1\right) + o(1), \quad \textit{as} \quad \nu \to 0. \tag{3.48}$$

Here k_j *for* $j = 2, \ldots, N$ *are the eigenvalues of the Green's matrix* $\mathcal{G}$ *in the* $N-1$ *dimensional subspace perpendicular to* $\vec{e}$*, i.e.* $\mathcal{G}\vec{q_j} = k_j\vec{q_j}$ *for* $\vec{e}^T q_j = 0$ *and* $j = 2, \ldots, N$*. In addition,* $b = \int_0^\infty \rho w^2 d\rho$*, where* w *is the ground-state solution,* $\nu = -1/\log\varepsilon$*, and* $\hat{\chi}_1$ *is determined from a correction to the leading-order core solution as*

$$\hat{\chi_1} = \frac{1}{b^2}\int_0^\infty \rho \hat{V}_{1p} d\rho,$$

where $\hat{V_{1p}}$ *is the unique solution to* (3.33)*.*

Remark

(i) The instability threshold is then $D_{th} = \min_{2\le j\le N} D_j$, which involves the minimum of the k_j.

(ii) Our analysis was based on reducing the Schnakenberg system to the unit sphere. For a sphere of adiabatically slowly increasing radius L, our competition instability result can still be used if we identify that D and ε^2 have both decreased by a factor of L^2. Therefore, competition instabilities become increasingly less prominent as the radius of the sphere increases. This is in direct contrast to the occurrence of spot self-replication instabilities, which become more prominent as the sphere radius increases. In a nutshell, a competition instability is an over-crowding instability, whereas, as discussed earlier, a spot self-replication instability is an under-crowding instability.

3.3 Slow spot dynamics on the surface of the sphere

In this section we derive a differential algebraic system (DAE) of ODE's characterizing the slow motion of a collection of spots. For a planar domain, such an analysis has been previously given in [24]. However, on the surface of the sphere, the analysis needed to derive the DAE system is rather more intricate in that we must retain certain new higher order terms in the inner solution near each spot related to the curvature of the sphere. As such, we must exercice care in working with the Laplacian in the spherical coordinate system. The DAE system characterizes slow spot motion in the absence of any spot self-replication or competition instability.

On the unit sphere, the Laplacian in spherical coordinates is

$$\Delta_{\theta,\phi} = \frac{1}{\sin\theta}\frac{\partial}{\partial\theta}\left(\sin\theta\,\frac{\partial}{\partial\theta}\right) + \frac{1}{\sin^2\theta}\frac{\partial^2}{\partial\phi^2} = \partial_{\theta\theta} + \cot\theta\,\partial_\theta + \frac{1}{\sin^2\theta}\partial_{\phi\phi}. \tag{3.49}$$

We introduce the local coordinate system near the j-th spot as $s_1 = \varepsilon^{-1}(\theta - \theta_j(\tau))$, $s_2 = \varepsilon^{-1}\sin\theta_j(\phi - \phi_j(\tau))$, where $\tau = \varepsilon^2 t$. Upon substituting this into (3.49) we obtain that

$$\begin{aligned}\Delta_{s_1,s_2} &= \frac{1}{\varepsilon^2}\partial_{s_1s_1} + \frac{1}{\varepsilon}\cot(\theta_j + \varepsilon s_1)\partial_{s_1} + \frac{1}{\varepsilon^2}\frac{\sin^2\theta_j}{\sin^2(\theta_j+\varepsilon s_1)}\partial_{s_2s_2}\\ &\simeq \frac{1}{\varepsilon^2}\partial_{s_1s_1} + \frac{1}{\varepsilon}\cot\theta_j\partial_{s_1} + \frac{1}{\varepsilon^2}\frac{1}{(1+2\varepsilon s_1\cot\theta_j)}\partial_{s_2s_2}\\ &\simeq \frac{1}{\varepsilon^2}(\partial_{s_1s_1}+\partial_{s_2s_2}) + \frac{1}{\varepsilon}\cot\theta_j\partial_{s_1} - \frac{2}{\varepsilon}s_1\cot\theta_j\partial_{s_2s_2}.\end{aligned} \tag{3.50}$$

This result is used below to identify key correction terms in the inner region that are crucial for the analysis of spot motion.

The Schnakenberg model (3.6) on the surface of the sphere when written in spherical coordinates is

$$v_t = \varepsilon^2\,\Delta_{\theta,\phi}v - v + uv^2, \qquad 0 = D\Delta_{\theta,\phi}u + a - \varepsilon^{-2}uv^2,$$

where $\Delta_{\theta,\phi}$ is written explicitly in (3.49).

In the j-th inner region, we perform the local change of variables to s_1 and s_2, as written explicitly above, and we introduce U and V by $u = D^{-1/2}U$ and $v = \sqrt{D}V$. In this way, we obtain that

$$\begin{aligned} V_t &= \big(V_{s_1 s_1} + V_{s_2 s_2} + \varepsilon\, \cot\theta_j V_{s_1} - 2\varepsilon\, s_1 \cot\theta_j V_{s_2 s_2} + O(\varepsilon^2)\big) - V + UV^2, \\ 0 &= D\,\big(U_{s_1 s_1} + U_{s_2 s_2} + \varepsilon\, \cot\theta_j U_{s_1} - 2\varepsilon\, s_1 \cot\theta_j U_{s_2 s_2} + O(\varepsilon^2)\big) \\ &\qquad - UV^2 + \varepsilon^2 \sqrt{D} a. \end{aligned} \tag{3.51}$$

Next, the time derivative V_t on the left hand side of (3.51) is calculated as

$$\begin{aligned} \frac{\mathrm{d}}{\mathrm{d}t} &= \frac{\partial}{\partial s_1}\frac{\partial s_1}{\partial \theta_j}\frac{\partial \theta_j}{\partial \tau}\frac{\partial \tau}{\partial t} + \frac{\partial}{\partial s_2}\frac{\partial s_2}{\partial \phi_j}\frac{\partial \phi_j}{\partial \tau}\frac{\partial \tau}{\partial t} = -\varepsilon\, V_{s_1}\theta_j' - \varepsilon\, \sin\theta_j V_{s_2}\phi_j' \\ &= -\varepsilon\,(V_{s_1}, V_{s_2}) \cdot (\theta_j', \sin\theta_j \phi_j'). \end{aligned} \tag{3.52}$$

Here the primes indicate derivatives with respect to the slow time variable τ given by $\tau = \varepsilon^2 t$. The key point, which suggested the asymptotic order in ε of the slow time-scale, is that the time-derivative term must balance the $O(\varepsilon)$ order of the spatial correction terms on the right hand-sides of (3.51). This balance is achieved when $\tau = \varepsilon^2 t$.

As such, the explicit form of the $O(\varepsilon)$ correction terms suggests that we expand

$$U = U_0 + \varepsilon\, U_1 + \cdots, \qquad V = V_0 + \varepsilon\, V_1 + \cdots.$$

We substitute this expansion together with (3.52) into (3.51) and collect powers of ε.

At leading order we recover the core problem

$$V_{0_{s_1,s_1}} + V_{0_{s_2,s_2}} - V_0 + U_0 V_0^2 = 0\,, \qquad U_{0_{s_1,s_1}} + U_{0_{s_2,s_2}} - U_0 V_0^2 = 0. \tag{3.53}$$

Upon collecting the $O(\varepsilon)$ terms we get

$$\begin{aligned} -(V_{0_{s_1}}, V_{0_{s_2}}) \cdot (\theta'_j, \sin\theta_j \phi'_j) = V_{1_{s_1,s_1}} + V_{1_{s_2,s_2}} + \cot\theta_j (V_{0_{s_1}} - 2s_1 V_{0_{s_2,s_2}}) \\ - V_1 + U_1 V_0^2 + 2U_0 V_0 V_1 \\ 0 = U_{1_{s_1,s_1}} + U_{1_{s_2,s_2}} + \cot\theta_j (U_{0_{s_1}} - 2s_1 U_{0_{s_2,s_2}}) \\ - U_1 V_0^2 - 2U_0 V_0 V_1. \end{aligned} \tag{3.54}$$

We then rewrite (3.54) in a convenient matrix form as

$$\Delta_s W_1 + \mathcal{A} W_1 = f. \tag{3.55}$$

Here $\Delta_s \equiv \partial_{s_1,s_1} + \partial_{s_2,s_2}$, and we have defined the vectors W_1 and f, and the matrix $\mathcal{A}$, by

$$\begin{aligned} W_1 \equiv \begin{pmatrix} V_1 \\ U_1 \end{pmatrix}, \qquad \mathcal{A} = \begin{pmatrix} -1 + 2U_0 V_0 & V_0^2 \\ -2U_0 V_0 & -V_0^2 \end{pmatrix}, \\ f \equiv \begin{pmatrix} -\cot\theta_j (V_{0_{s_1}} - 2s_1 V_{0_{s_2,s_2}}) - (V_{0_{s_1}}, V_{0_{s_2}}) \cdot (\theta'_j, \sin\theta_j \phi'_j) \\ -\cot\theta_j (U_{0_{s_1}} - 2s_1 U_{0_{s_2,s_2}}) \end{pmatrix}. \end{aligned} \tag{3.56}$$

The ODE system for the spot locations is obtained from imposing a solvability condition on (3.56). However, we must first determine the correct far-field behaviour for the solution W_1 before invoking this condition. The required far-field condition on W_1 is now determined from an asymptotic matching procedure with the outer solution.

The outer solution for u was given in (3.14) as

$$\begin{aligned} u(x) = \frac{2\pi}{\sqrt{D}} \left(\sum_{i=1}^{N} S_i G(x; x_i) + u_c \right), \\ G(x; x_0) = -\frac{1}{2\pi} \log|x - x_0| + \frac{1}{4\pi}(2\log 2 - 1). \end{aligned}$$

On the unit sphere, both $|x| = |x_0| = 1$, and by the law of cosines $|x - x_0|^2 = 2 - 2\cos\omega$, with ω denoting the angle between x and x_0. In terms of spherical coordinates we can write $G(x; x_0) = G(\phi, \theta\,; \phi_0, \theta_0)$ explicitly as

$$\begin{aligned} G &= -\frac{1}{4\pi}\log(1 - x\cdot x_0) + \frac{1}{4\pi}(\log 2 - 1) \\ &= -\frac{1}{4\pi}\log(1 - \sin\theta\,\sin\theta_0\cos\phi\cos\phi_0 - \sin\theta\,\sin\theta_0\sin\phi\sin\phi_0 - \cos\theta\,\cos\theta_0) \\ &\quad + \frac{1}{4\pi}(\log 2 - 1). \end{aligned} \tag{3.57}$$

From this expression we can readily compute the partial derivatives $\partial G/\partial\phi$ and $\partial G/\partial\theta$ at the spot location ϕ_0, θ_0.

We can now use this result to find a matching condition for the inner problem. We Taylor expand the outer problem as $x \to x_j$, and write the resulting expression in terms of local coordinates to obtain

$$\begin{aligned} u(x) \sim -\frac{2\pi}{\sqrt{D}}\left[-\frac{S_j}{2\pi}\log|x - x_j| + S_j R + \sum_{i\neq j}^{N} S_j G_{ji} + u_c\right] \\ - \frac{2\pi\varepsilon}{\sqrt{D}}\sum_{i\neq j}^{N} S_i\left(\frac{\partial G^j}{\partial\theta}s_1 + \frac{\partial G^j}{\partial\phi}\frac{s_2}{\sin\theta_j}\right) + O(\varepsilon^2). \end{aligned} \tag{3.58}$$

Here we have defined $\frac{\partial G^j}{\partial\theta}$ and $\frac{\partial G^j}{\partial\phi}$ to be the partial derivatives of G evaluated at the j-th spot location $\theta = \theta_j$ and $\phi = \phi_j$. These terms can be calculated explicitly from (3.57).

Hence, in terms of the local variables associated with the inner problem, the $O(\varepsilon)$ term in (3.58) gives the required far-field behaviour of the inner solution. Since the inner expansion $u = D^{-1/2}(U_0 + \varepsilon U_1 + \cdots)$, we obtain from (3.58) that U_1 must have the far-field behaviour

$$U_1 \sim -2\pi\sum_{i\neq j}^{N} S_i\left(\frac{\partial G^j}{\partial\theta}s_1 + \frac{\partial G^j}{\partial\phi}\frac{s_2}{\sin\theta_j}\right) = \vec{\alpha}\cdot\vec{s}. \tag{3.59}$$

Here we have defined $\vec{s} = (s_1, s_2)^T$ and $\vec{\alpha} = (\alpha_1, \alpha_2)$ as

$$\vec{\alpha} \equiv -2\pi \sum_{i \neq j}^{N} S_i \left(\frac{\partial G^j}{\partial \theta}, \frac{\partial G^j}{\partial \phi} \frac{1}{\sin\theta_j} \right) . \tag{3.60}$$

Therefore, the required far-field behaviour of the inner problem for W_1, given by (3.55) is

$$W_1 \sim \begin{pmatrix} 0 \\ \vec{\alpha} \cdot \vec{s} \end{pmatrix}, \qquad \text{as} \quad |\vec{s}| \to \infty. \tag{3.61}$$

The final step in the determination of an ODE system for the dynamics of the spots is to impose a solvability condition on the solution to the inner problem (3.55) subject to the far-field behaviour (3.61).

The homogeneous adjoint problem for (3.55) is

$$\Delta_s P + \mathcal{A}^T P = 0, \qquad \vec{s} \in \mathbb{R}^2, \qquad P \equiv \begin{pmatrix} \Phi \\ \Psi \end{pmatrix}. \tag{3.62}$$

Let $\hat{P}$ satisfy the radially-symmetric problem, with the far-field condition that $(\hat{\Phi}, \hat{\Psi})^T \to (0,0)^T$ as $\rho \to \infty$. The precise asymptotic behaviour of $\hat{P}$ is readily seen to be $\hat{P} \sim (0, \rho^{-1})^T$ as $\rho \to \infty$. Then, we seek solutions to (3.62) of the form $P_c \equiv \hat{P}\cos\Theta$, or $P_s \equiv \hat{P}\sin\Theta$, where Θ is the polar angle for $\vec{s}$. In order to apply the solvability condition below, we need to define the inner product $(u, v) = \iint_{\mathbb{R}^2} (u^T v) d\vec{s}$, where $d\vec{s} \equiv ds_1 ds_2$. Moreover, we define the operator $\mathcal{L}F \equiv \Delta_s F + \mathcal{A}F$ and its adjoint $\mathcal{L}^* F \equiv \Delta_s F + \mathcal{A}^T F$.

By combining the problems satisfied by W_1 and P_c we get

$$\begin{aligned} &(P_c, \mathcal{L}W_1) - (W_1, \mathcal{L}^* P_c) = \\ &\iint_{\mathbb{R}^2} \left[P_c^T (\Delta_s W_1 + \mathcal{A}W_1) - W_1^T (\Delta_s P_c + \mathcal{A}^T P_c) \right] d\vec{s} = \iint_{\mathbb{R}^2} P_c^T f \, d\vec{s} \\ &\iint_{\mathbb{R}^2} \left(P_c^T \Delta_s W_1 - W_1^T \Delta_s P_c \right) ds_1 ds_2 = \int_0^\infty \int_0^{2\pi} \hat{P}^T \cos\Theta \, f \rho \, d\rho d\Theta \, . \end{aligned} \tag{3.63}$$

Next, we use Green's second identity to the left hand-side of this expression to derive

$$\begin{aligned}
&\iint_{\mathbb{R}^2} \left(P_c^T \Delta_s W_1 - W_1^T \Delta_s P_c\right) d\vec{s} = \lim_{\sigma\to\infty} \int_0^{2\pi} \left(P_c^T \frac{\partial W_1}{\partial \rho} - W_1^T \frac{\partial P_c}{\partial \rho} \right)\Big|_{\rho=\sigma} \sigma d\Theta \\
&= \lim_{\sigma\to\infty} \int_0^{2\pi} \left(\hat{P}^T \cos\Theta \frac{\partial W_1}{\partial \rho} - W_1^T \frac{\partial \hat{P}}{\partial \rho} \cos\Theta \right)\Big|_{\rho=\sigma} \sigma \, d\Theta \\
&= \int_0^{2\pi} \Bigg(\frac{1}{\sigma} \cos\Theta \left(\alpha_1 \cos\Theta + \alpha_2 \sin\Theta\right) \\
&\qquad\qquad -\sigma(\alpha_1 \cos\Theta + \alpha_2 \sin\Theta) \frac{-1}{\sigma^2} \cos\Theta \Bigg) \sigma \Big|_{\infty} \, d\Theta \\
&= \int_0^{2\pi} 2\alpha_1 \cos^2\Theta \, d\Theta = 2\pi\alpha_1.
\end{aligned} \tag{3.64}$$

To calculate the right hand-side of the last expression in (3.63) we use the expression for f from (3.56). Then, since $(\theta'_j, \sin\theta_j \phi'_j) = -\varepsilon(s'_1, s'_2)$, we get

$$\begin{aligned}
&\int_0^{\infty} \int_0^{2\pi} \hat{P}^T \cos\Theta \, f \rho \, d\rho \, d\Theta = \int_0^{\infty} \int_0^{2\pi} (\hat{\Phi}, \hat{\Psi})^T f \cos\Theta \, \rho \, d\rho \, d\Theta \\
&= \iint_{\mathbb{R}^2} \hat{\Phi} \left(-\cot\theta_j (V_{0_{s_1}} - 2s_1 V_{0_{s_2,s_2}}) + \varepsilon(V_{0_{s_1}}, V_{0_{s_2}}) \cdot (s'_1, s'_2) \right) \cos\Theta \, d\vec{s} \\
&\qquad + \iint_{\mathbb{R}^2} \hat{\Psi} \left(-\cot\theta_j (U_{0_{s_1}} - 2s_1 U_{0_{s_2,s_2}}) \right) \cos\Theta \, d\vec{s}.
\end{aligned} \tag{3.65}$$

Recall that both U_0 and V_0 are radially symmetric, as well as the two components $\hat{\Phi}$ and $\hat{\Psi}$ of the adjoint solution $\hat{P}$. In addition, we note that $\partial_{s_1} = \partial_\rho \cos\Theta$, $\partial_{s_2} = \partial_\rho \sin\Theta$. Furthermore, we observe that since the terms $U_{0_{s_2,s_2}}$ and $V_{0_{s_2,s_2}}$ are even functions of s_1, so that when they are multiplied by s_1 they become odd, and hence they integrate to zero over $\mathbb{R}^2$. With these considerations, the left-hand

side of (3.65) reduces to

$$\iint_{\mathbb{R}^2} \left(-\hat{\Phi} \cot\theta_j V_{0_\rho} + \varepsilon\, \hat{\Phi} V_{0_\rho} s_1' - \hat{\Psi} \cot\theta_j U_{0_\rho} \right) \cos^2\Theta \; d\vec{s} = 2\pi\alpha_1. \quad (3.66)$$

Therefore, the solvability condition for P_c provides an ODE for s_1:

$$\varepsilon\, s_1' = -\theta_j' = \frac{2\alpha_1 + \cot\theta_j \int_0^\infty \left(\hat{\Phi} V_{0_\rho} + \hat{\Psi} U_{0_\rho} \right) \rho\, d\rho}{\int_0^\infty \hat{\Phi} V_{0_\rho} \rho\, d\rho} = -\left(\alpha_1 + \frac{\beta}{2} \cot\theta_j \right) \gamma\,, \quad (3.67)$$

where $\gamma \equiv -2/\int_0^\infty \hat{\Phi} V_{0_\rho} \rho\, d\rho$, and $\beta \equiv \int_0^\infty \left(\hat{\Phi} V_{0_\rho} + \hat{\Psi} U_{0_\rho} \right) \rho\, d\rho$ are two functions of the local spot strength S_j involving the core solution and the two components of the solution to the homogeneous adjoint problem. The function γ appeared in the derivation of [24] for spot dynamics in a planar domain, and it is plotted as a function of S_j in Figure 3 of [24]. For spot dynamics on the sphere, the new integral term β arises and must be computed as a function of S_j.

Upon repeating the same procedure with $P_s = \hat{P} \sin\Theta$, the left hand-side of the resulting expression is completely analogous and we get $2\pi\alpha_2$. For the right hand-side, all the $\partial_{s_1} = \partial_\rho \cos\Theta$ terms integrate to zero, as well as the terms involving second derivatives by using the same symmetry argument as with P_c. In this way, we get

$$\varepsilon\, s_2' = -\phi_j' \sin\theta_j = \frac{2\alpha_2}{\int_0^\infty \hat{\Phi} V_{0_\rho} \rho\, d\rho} = -\alpha_2 \gamma\,. \quad (3.68)$$

We summarize our result as follows:

Principal Result 3.3.1 *Consider a collection of N spots on the surface of the sphere at spherical coordinates ϕ_j and θ_j for $j = 1, \ldots, N$. Then, provided that the quasi-equilibrium pattern is stable to any $O(1)$ time-scale instability, the slow motion on the time-scale $\tau = \varepsilon^2 t$ of these collection of spots satisfies a DAE system. For this DAE system, the dynamics $(\theta_j', \sin\theta_j \phi_j') = -\varepsilon\,(s_1', s_2')$ of the*

spots is given by

$$\varepsilon\, s_1' = -\theta\,'_j = \frac{2\alpha_1 + \cot\theta_{\,j} \int_0^\infty \left(\hat{\Phi} V_{0_\rho} + \hat{\Psi} U_{0_\rho}\right) \rho\, d\rho}{\int_0^\infty \hat{\Phi} V_{0_\rho} \rho\, d\rho}, \tag{3.69}$$

$$\varepsilon\, s_2' = -\phi_j' \sin\theta_{\,j} = \frac{2\alpha_2}{\int_0^\infty \hat{\Phi} V_{0_\rho} \rho\, d\rho}, \tag{3.70}$$

for $j = 1, \ldots, N$ with primes denoting derivatives with respect to τ and

$$\vec{\alpha} = (\alpha_1, \alpha_2)^T \equiv -2\pi \sum_{i \neq j}^{N} S_i \left(\frac{\partial G^j}{\partial \theta}\,, \frac{\partial G^j}{\partial \phi} \frac{1}{\sin\theta_{\,j}} \right).$$

The constraints in the DAE system consist of the nonlinear algebraic system (3.18) *for the source strengths $S_1, \ldots, S_N$ defined in terms of the Neumann Green's matrix, which involves the instantaneous spot locations.*

Remark

(i) In the DAE system the spot strengths evolve slowly in time as a result of the slow motion of the collection of spots. The DAE system is valid provided that that the spots strengths are below the spot-splitting threshold, i.e. $S_j < 4.3$ for $j = 1, \ldots, N$.

(ii) The ODE dynamics involves two separate integral terms that must be computed as a function of the local source strength S_j. In a (practical) numerical implementation of spot dynamics these functions can be tabulated numerically in advance.

It is beyond the scope of this thesis to investigate the consequences of this DAE system for spot evolution, such as the presence of stable stationary patterns or orbits. However, we remark that this system is vaguely related to, but seemingly more complicated than, the well-studied ODE systems characterizing the motion of Eulerian fluid point vortices on the surface of the sphere ([40], [9]).

3.4 Quasi-equilibria and the cyclic matrix structure

Solving the quasi-equilibrium problem for a collection of N spots on a sphere implies finding the locations $\{x_1, \ldots, x_N\}$ and source strengths $S_1, \ldots, S_N$ that satisfy (3.18)

$$(I + 2\pi\nu(\mathcal{G} + RE))\vec{S} + \nu\vec{\chi} = -2\pi\nu u_c e; \qquad \vec{e}^T\vec{S} = \frac{2a}{\sqrt{D}}, \tag{3.71}$$

with I the identity matrix, and

$$\vec{S} \equiv \begin{pmatrix} S_1 \\ \vdots \\ S_N \end{pmatrix}, \qquad \vec{e} \equiv \begin{pmatrix} 1 \\ \vdots \\ 1 \end{pmatrix}, \qquad \vec{\chi} \equiv \begin{pmatrix} \chi(S_1) \\ \vdots \\ \chi(S_N) \end{pmatrix},$$

$$\mathcal{G} \equiv \begin{pmatrix} 0 & \cdots & -\frac{\log|x_1 - x_N|}{2\pi} \\ -\frac{\log|x_2 - x_1|}{2\pi} & & \\ \vdots & \ddots & \vdots \\ & & -\frac{\log|x_{N-1} - x_N|}{2\pi} \\ -\frac{\log|x_N - x_1|}{2\pi} & \cdots & 0 \end{pmatrix},$$

with $R = \frac{1}{4\pi}(2\log 2 - 1)$ and $E = \frac{1}{N}\vec{e}\vec{e}^T$.

The nonlinear term $\vec{\chi}$ makes it impossible to solve the problem in the general case, but we can solve a reduced case where by prescribing the source strengths for all the N spots. The problem becomes that of finding the locations of the spots. Similarly, a second approach would be to prescribe the location of the spots and solve to find the source strengths. In the related problem of point vortices on a rotating sphere [18], this approach was used to categorize collections of point vortices on a sphere located at the vertices of platonic solids.

We will follow the first approach and consider the problem where $\vec{S}$ is an eigenvector of the cyclic matrix $\mathcal{G}$, say with corresponding eigenvector λ. We will simplify things further by assuming that all the spots have a common source strength

S_c, therefore $\vec{S} = S_c\vec{e}$ and $\vec{\chi} = \chi(S_c)\vec{e}$.

This particular choice of $\vec{S}$, together with the assumption that $\mathcal{G}$ is a cyclic matrix, allows us to decouple (3.71) into

$$\begin{aligned} u_c &= -\frac{(1 + 2\pi\nu(\lambda + R)2a/\sqrt{D} - \nu e^T\chi(S_c)}{2\pi\nu N} \\ S_c &= \frac{2a}{N\sqrt{D}}, \end{aligned} \tag{3.72}$$

The problem has now been reduced to finding spot configurations that make $\mathcal{G}$ into a cyclic matrix. We remark that since the matrix is real symmetric, all of its eigenvalues are real. For a cyclic matrix $\mathcal{G}$, it must have a constant row sum, and thus it has the eigenvector $\vec{e}$ with corresponding eigenvalue

$$\lambda = \frac{-1}{2\pi}\log\left(\prod_{\substack{j=1 \\ j\neq i}}^{N}|x_i - x_j|\right), \tag{3.73}$$

for any row i. Since all the non diagonal terms in $\mathcal{G}$ are negative, by use of the Gershgorin circle theorem we can see that λ is the most negative eigenvalue in $\mathcal{G}$.

More importantly, requiring that $\vec{e}$ is an eigenvector of $\mathcal{G}$ is a geometrical restriction on the position of the spots. The fact that all the rows in the matrix have to add to λ implies that the net effect of all the spots on each other is the same. The simplest way for this to happen is if the spots are the same distance apart from each other, i.e., $|x_i - x_j| = C$ for all rows and $i \neq j$. This condition can be true for at most 4 spots in a sphere, at the vertices of an equilateral pyramid (or 3 equally spaced spots along a latitudinal ring, or 2 spots anywhere on the sphere.

A second way to distribute the spots so that $\vec{e}$ is an eigenvector of $\mathcal{G}$ is by arranging them in rings. Without loss of generality, the idea is to arrange the spots in latitudinal rings, with the spots equally-space on the ring. There are results on the stability of point vortices arranged in latitudinal rings ([8], [9]), including

a famous result that limits the number of spots in such a configuration to ensure stability. The notion of stability in this point vortex problem is stability with respect to small perturbations of the locations of the vortices on the ring.

We emphasize that in our context of spot patterns for reaction-diffusion systems, there are two different classes of eigenvalues governing the stability of the pattern. Our analysis has focused exclusively on the stability of the spot profile through our study of spot-replication, competition, and oscillatory instabilities. These spot amplitude-type instabilities, are "fast" instabilities as they result from $O(1)$ unstable eigenvalues, and they appear to have no direct counterpart in the point-vortex fluid problem. For spot patterns, there are also weak translational-type instabilities associated with eigenvalues that are $O(\varepsilon^2)$. These eigenvalues can in principle be obtained by linearizing the DAE system in Principal Result 3.3.1 around an equilibrium configuration of spots, and determining the matrix spectrum of the associated Jacobian. It is the study of such "small" eigenvalue instabilities that has a more direct counterpart with the notion of stability of point vortices on the sphere. We have not analyzed any such small eigenvalue instability for spot patterns in this thesis, but we do expect that there should be a result similar to ([8] and [9] for the maximum number of "stable" spots that can be placed on a ring of constant latitude. In fact, for the case of a planar unit disk containing a ring of concentric equally-spaced spots, it was observed numerically for the Schnakenburg system in [24] that this system can support a maximum number of spots, beyond which some spots are pushed off the ring due to a small eigenvalue instability.

With this digression, we now return to discussing configurations of spots for which $\mathcal{G}$ is a cyclic matrix. For more than 4 points, and not considering a ring, the points will have to be distributed in a less trivial way. We can no longer have an arrangement in which all the points are an equal distance from each other. We have to distribute the points in such a way that the sum of the contributions over each are the same. In geometrical terms, this is related to the symmetry of the configuration. Since the rows of $\mathcal{G}$ are all the same, there have to be rotations of the sphere that maintain the same configuration.

Similarly to when we were looking for equally-spaced points, there is a finite number of point distributions that exactly satisfy that condition, namely, the platonic solids. We can arrange 4, 6, 8, 12, and 20 points in a sphere such that their corresponding matrix $\mathcal{G}$ will also have e as an eigenvector.

For homogeneous configurations with a different number of spots, $\vec{e}$ will cease to be an eigenvector. However, what we have observed is that by arranging the points in the most homogeneous possible distribution, the first eigenvector of $\mathcal{G}$ will be close to e (see table 3.1). A condition on a homogeneous distribution of N points on a sphere is that it maximizes the minimal distance between the points. A collection of these optimal point distributions, numerically computed, is available for up to 130 points, and can be found at Neil Sloane's webpage [55].

Interestingly enough, maximizing the minimal distances does not necessarily correspond to platonic solids. For 8 and 20 nodes the minimizing configurations do not correspond to either a cube, or a dodecahedron, respectively. This was also empirically observed in [61].

Configurations of points that are the most homogeneously distributed on a sphere for a given number of points are called elliptic Fekete point distributions. Mathematically, Fekete points maximize the product of the distances between all pairs of points,

$$J = \prod_{\substack{j=1 \\ j\neq i}}^{N} |x_i - x_j| \,, \qquad V = \sum_{\substack{j=1 \\ j\neq i}}^{N} \log |x_i - x_j|. \tag{3.74}$$

Since $\log$ is monotonic, then maximizing J is equivalent to maximizing V. Notice how close that equation is to the eigenvalue equation in (3.73).

As mentioned earlier, an alternative description is that of a group of equally charged particles that repel each other on the surface of the sphere. Minimizing the electrostatic potential yields the Fekete problem, and in this context is known as

the Thomson problem [58]

The Fekete points can be numerically computed by considering V to be a spring-like potential, adding a relaxation term (friction), and using Lagrange multipliers. We solved the system with a symplectic numerical scheme, following the description in [51].

For various optimal spot locations from the numerical Fekete configurations, we computed the difference between the eigenvector corresponding to the smallest eigenvalue of $\mathcal{G}$ and $\vec{e}$.

Number of points n	$\|\|x_n - e_n\|\|$
4	$3.8459e-16$
6	$1.8626e-10$
8	$6.0301e-16$
10	0.0216
12	$2.9374e-16$
20	0.0050
20_p	$8.5142e-16$
50	0.0029
100	0.0029
120	0.0015
130	0.0027

Table 3.1: The norm of the difference between the first eigenvector and e, both normalized, for different spot configurations.

Although, as can be seen in table 3.1, we can no longer expect to find $\vec{e}$ as an eigenvector of the distribution of points, the first eigenvector of distributions with minimal distances between points maximized is in fact close to $\vec{e}$. Notice too, that in the 8 point case (a rotated cube), the difference in norm is within machine error, despite the fact that we no longer have a platonic solid. However, the optimal distribution in the sense of maximal minimal distances for 20 points yields a result accurate only to 3 decimals. The result 20_p corresponds to a true dodecahedral distribution of 20 points, and instead we have $||x_n - e_n|| = 8.5142e - 16$. For

comparison, a random distribution of 100 points has a norm difference of 0.2512.

3.5 Numerical method for reaction-diffusion patterns on the sphere

To validate our asymptotic stability theory for the Brusselator and the Schnakenberg reaction-diffusion models, we need to compare our results with full numerical simulations of these PDE systems on the surface of the sphere.

Previous work on reaction-diffusion systems on spheres can be found in [61], [10], [16], [17]. The first work that we are aware of is that of [61]. In this study, they numerically solved a generic reaction-diffusion system on a sphere and were able to obtain spotted and striped stationary solutions, depending on the the strength of the cubic and quadratic terms respectively.

The numerical method they used was to write the Laplacian in spherical coordinates, and integrate in (θ, ϕ) space explicitly with an Euler method after an appropriate patching of the boundary. This approach was also used in [17] where they also considering growing spheres, although the method was implicit-explicit. The disadvantage of this method is that the finite difference method subdivides the $(\theta\,, \phi)$ domain into equal subsections, and on the full sphere this corresponds to a majority of the grid points being close to the poles. Since the maximum time step in two dimensions for an explicit time integration scales as $(\Delta x)^2$, with Δx being the smallest distance between points, the integration time will reflect the scale at the poles, making it very numerically intensive to resolve events that happen elsewhere, such as in the vicinity of localized spots.

The work by [10] involved simulating a reaction-diffusion system that modelled tumour growth. The numerical method used was a method of lines with a spectral component in the reaction terms that was generalized for any reaction terms. Our previous experience with spectral methods on systems with localized

patterns was limited by the small number of grid points and their distribution. Although these methods typically have a high degree of accuracy and very fast convergence rates, the large number of points needed to resolve the structures made them unreliable, at least in our implementation.

The approach that we chose to implement is the recently-developed Closest Point Method (see [50]). The basic idea of this method is to solve the PDE system on a grid on an embedding domain of dimension greater than the system. The method works by propagating the values of the solution on the embedded domain to the grid, iterating the solution on the grid to the next timestep, and propagating back to the embedded domain via a suitable interpolation algorithm ([7], [46]). Instead of working with the full 3-D space, it is sufficient to restrict the problem to a narrow band around the embedded domain, with the width of the band thick enough to contain enough points to make the interpolation of the same order as the differentiation scheme. This approach has the advantage that the problem is solved on the grid using basic Laplacian operators, and the geometry of the system is handled through the way the solution is propagated to and from the grid. Other than the closest point algorithm, the rest of the approach is standard explicit or implicit solvers, plus an interpolation algorithm in 3-D.

For the problem of simulating spot dynamics for either the Brusselator or the Schnakenberg model on the surface of the sphere, we need to be perform very long-time integrations since the time-scale for the motion of the spots is $O(1/\varepsilon^2)$. To be able to take large time steps the method has to be implicit, or at least implicit-explicit, as the CFL condition limits explicit methods to time steps of order $O((\Delta x)^2)$. For a simulation with 81 grid points in each direction, we have that $\Delta t = 0.0005$. Currently in our full numerical simulations we typically use $\varepsilon = 0.1$ as a trade-off between computational difficulty and reasonable accuracy of the asymptotic theory. To fully validate the asymptotic theory we would need to use somewhat smaller values of ε. However, this has a detrimental effect on the stability of the computations, as the discretized diffusion term becomes stiffer. As a result of this computational challenge, we were not able to validate our asymptotic results for the dynamics of spots for the Schnakenberg model, nor were we

able to numerically realize a "chaotic attractor", consisting of intermittent spot self-replication and annhilation events, for the Brusselator model. However, as we discussed, the stability theory that we undertook for the Brusselator model did strongly suggest that such an attractor should exist.

Therefore, our numerical experiments for the full Schnakenberg and Brusselator system were undertaken only to exhibit spot self-replication and competition instabilities for moderate values of ε, since it is these instabilities that occur on a fast $O(1)$ time-scale. In addition, the explicit version of this method that we implemented was sufficient to validate the results obtained in [17] on stationary spheres. As observed also in [61], and predicted in the asymptotic analysis, the number of spots that can stabilize on a sphere depends on the radius of the sphere, or equivalently on the value of the inhibitor diffusivity.

Closest Point Method. One of the main authors of this method [49] graciously shared with us a basic explicit code that solved a linear diffusion problem on a sphere. We improved it by changing the interpolation method, which was a basic divided-differences approach, to a barycentric interpolation method (see [7]), which is about an order of magnitude more efficient. Interpolation an a 3-D lattice (N^3 points) was done by first interpolating in the z direction N^2 times, then using those values to interpolate in the y direction N times, and finally do a single interpolation on the x direction ([46]). Integrating to $T = 100$, on a grid of $40 \times 40 \times 40$ takes around half an hour on a computer with an Intel T9400 processor (2.5 Ghz).

We now briefly summarize the Closest Point Method [50]. The key idea of the Closest Point Method lies in the closest point extension. If the intrinsic gradient and divergence operators on the surface are denoted ∇_s, and $\nabla_s \cdot$, by mapping the points in the grid to their closest point on the surface, we have on the grid that

$$\nabla_s u(x) = \nabla u(CP(x)), \qquad \nabla_s \cdot u(x) = \nabla \cdot u(CP(x)).$$

This is intuitively easy to see, as it all depends on the fact that $u(CP(x))$

is constant in directions that are normal to the surface. This can be generalized to higher order operators too, and for our purposes we used that $\nabla_s \cdot (\nabla_s u(x)) = \nabla \cdot (\nabla u(CP(x))) = \Delta u(CP(x))$, for the Laplace-Beltrami operator on the surface of the sphere.

When the embedded domain is a unit sphere, centred at the origin, the closest point algorithm is simply

```
cp_x = closest_point(x)
   d = sqrt(x(1)^2 + x(2)^2 + x(3)^2)
   cp_x = x/d
```

The following pseudo-code represents an explicit algorithm for updating $w^{(n)}$ to $w^{(n+1)}$ in a differential equation of the form $w_t = \text{rhs}(w)$:

```
for i=1 to num_points
   x = domain_border + dx*i
   cp_x = closest_point(x)
   w_temp(x) = interpolate(w(n),cp_x)
end

for i=1 to num_points
   w(x,n+1) = w_temp(x) + dt*(rhs(w_temp)))
end
```

With more complicated domains, the part of the algorithm that finds the closest point can get significantly more computationally expensive. However, this computation only needs to be done once, and this is the only part of the code that has to be adjusted for different domains. In that sense, a very powerful feature of the Closest Point Method is that it can deal with general domains independently from the discretization or interpolation algorithms.

Chapter summary

In this chapter we derived a localized spot-type solution for the Schnakenberg model, and we analyzed its stability. By employing a full nonlinear derivation that results in a DAE system similar to the one obtained for the Brusselator in the previous chapter, we obtained the threshold for a self-replication instability.

We analyzed in detail the possible spot distributions that would result in solutions with equal spot strengths, and connected it with the Fekete problem, as was also the case in the Brusselator problem.

We did full numerics using a specialized algorithm for solving PDEs in general surfaces called the Closest Point Method, thus verifying the analytic results.

Furthermore, we considered the case of the spots motion on the surface of the sphere and derived differential equations for the dynamics of the full system.

In the next chapter we will discuss 1D mesa solutions for the GMS system, derive solutions and study their stability.

Chapter 4

Case study: mesa patterns on the GMS system

4.1 Model formulation and Turing stability analysis

One of the first models for a Turing system was introduced by Alfred Gierer and Hans Meinhardt in 1972 [15]. This model was constructed as a simplified representation of an activator-inhibitor reaction with sources, and can give rise to a large number of patterns. It was first used as a simple model for biological morphogenesis, and used to model patterns on sea shells [34].

The standard GM model has been shown to exhibit spike-type solutions [63]. On the other hand, an extension on the GM model that adds saturation to the reaction kinetics can exhibit mesa-type patterns [22], i.e., truncated spikes with wide flat tops, separated by two sharp interfaces from a quasi-constant solution.

In this section we will study the dimensionless Gierer-Meinhardt model with

saturation, which in non-dimensional form can be written as

$$\begin{aligned} u_t &= \varepsilon^2 \Delta u + f(u,v) = \varepsilon^2 \Delta u - u + \frac{u^2}{v(1+ku^2)} \\ \tau v_t &= D\Delta v + g(u,v) = D\Delta v - v + u^2, \end{aligned} \tag{4.1}$$

on $x \in [-1,1]$, with homogeneous Neumann boundary conditions. Here $k > 0$ is the saturation parameter. We consider the singular limit where $\varepsilon \ll 1$, and we will study the solutions that arise for various parameter regimes.

We will consider the case of a growing domain, both dynamically $L = L(t)$, and adiabatically, and discuss the modifications that need to be made in the dynamic growth case. In the splitting regime we will analyze the effect of varying the growth rate.

4.1.1 Turing stability analysis

A spatially homogeneous stationary solution to (4.1) occurs when

$$\frac{u^2}{v(1+ku^2)} = u, \qquad u^2 = v,$$

which involves solving the cubic equation $u + ku^3 - 1 = 0$. We will consider positive values of k only, therefore the curve $h(u) = u + ku^3 - 1$ is monotonically increasing, thus guaranteeing that there will only be one homogeneous solution. For example, when $k = 2.5$, which was the used for most of the numerical calculations below , the stationary homogeneous solution is $u_s \simeq 0.5603, v_s = u_s^2$. Starting close to the homogeneous solution, the evolution of the $u(x)$ solution can be seen in Figure 4.1. The mesa profiles appear relatively quickly, and over a much longer time-scale they rearrange to occupy the domain equally distributed, as can be seen in the solution at $t = 50,000$.

According to Turing theory (see [60], [37]), when the ratio of the diffusion

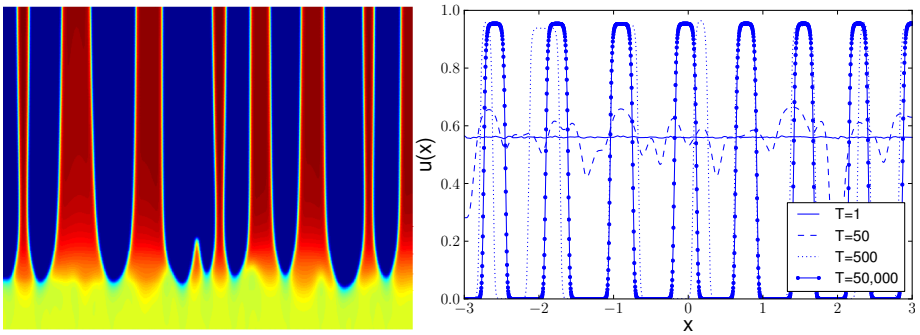

Figure 4.1: Solution profiles for various integration times starting close to the homogeneous solution. The figure on the left has the time evolution of the solution for $u(x)$ up to $t = 500$, with time in the y-axis. The figure on the left represents four different snapshots, at $t = 1$, $t = 50$, $t = 500$, and $t = 50,000$. We used $\kappa = 2.5$, $D = 10$, $\tau = 1$, and $\varepsilon = 0.01$ on (4.1), with a random initial condition close to $u = 0.5603$, $v = u^2$. The numerical method we utilized was an implicit-explicit scheme.

coefficients is large ($D/\varepsilon^2 \gg 1$), the homogeneous solution becomes unstable and a stable heterogeneous solution develops. By linearizing around the homogeneous solution it is possible to determine the domain length L at which the new solution appears, as well as to derive general conditions on the existence of heterogeneous solutions.

The linearized problem around the equilibrium solutions previously computed is

$$\begin{aligned} u_t &= \varepsilon^2 \Delta u + f_u(u_{eq}, v_{eq})u + f_v(u_{eq}, v_{eq})v \\ \tau v_t &= D\Delta v + g_u(u_{eq}, v_{eq})u + g_v(u_{eq}, v_{eq})v. \end{aligned} \tag{4.2}$$

Using separation of variables, $w(x,t) \equiv (u,v)^T = \mathbf{w}(t)\mathbf{W}(x)$, the spatial component leads to the eigenvalue problem

$$\Delta \mathbf{W} + k^2 \mathbf{W} = 0, \qquad (\hat{\mathrm{n}} \cdot \nabla)\mathbf{W} = 0.$$

For the 1-D domain $[0, L]$ we have that the eigenvalues are $k = n\pi/L$, and the corresponding eigenvectors are $W \propto \cos(kx)$, for $n \in \mathbb{N}$.

Likewise, the purely temporal solution of the linearized system is $\mathbf{w} \propto e^{\lambda t}$. The full solution to the linearized problem is then given by

$$w(x,t) = \sum_k c_k e^{\lambda t} \mathbf{W}_k(x) = \sum_k c_k e^{\lambda t} \cos(kx),$$

with the constants c_k defined by the initial condition. Upon substituting into (4.2), we get the system

$$\begin{gathered} \lambda \mathbf{W}_k = -\mathcal{D}k^2 \mathbf{W}_k + \mathbf{A}\mathbf{W}_k, \\ \mathcal{D} = \begin{bmatrix} \varepsilon^2 & 0 \\ 0 & D/\tau \end{bmatrix} \qquad \mathbf{A} = \begin{bmatrix} f_u(u_{eq}, v_{eq}) & f_v(u_{eq}, v_{eq}) \\ g_u(u_{eq}, v_{eq})/\tau & g_v(u_{eq}, v_{eq})/\tau \end{bmatrix}. \end{gathered} \tag{4.3}$$

Nontrivial $\mathbf{W}_k$ solutions will exist for values of λ determined by the roots of the characteristic polynomial of the matrix $\mathbf{A} - \mathcal{D}k^2$. Since the equilibrium solutions are constant, we have a 2×2 constant matrix, and thus we have that the characteristic polynomial for λ is

$$\begin{aligned} &\lambda^2 + \lambda(k^2(D/\tau + \varepsilon^2) - f_u - g_v/\tau) + h(k^2) = 0 \\ &h(k^2) = k^4\varepsilon^2 D/\tau - k^2(\varepsilon^2 g_v/\tau + f_u D/\tau) + f_u g_v/\tau - f_v g_u/\tau. \end{aligned}$$

We are looking for solutions that are stable in the absence of diffusion, therefore if $k = 0$ we require $f_u + g_v/\tau < 0$ ($\text{tr}(A) < 0$) and $f_u g_v - f_v g_u > 0$ ($\det(A) > 0$).

The particular solutions we are interested in become unstable when spatial effects are taken into account ($k \neq 0$).

Spatially heterogeneous solutions will appear when the real part of $\lambda(k^2)$ becomes positive. A necessary condition for this to happen is $h(k^2) < 0$, hence we

require the additional condition that $\varepsilon^2 g_v + f_u D > 0$.

To satisfy a sufficient condition we must also require that $h(k^2) < 0$ for some k^2. By differentiation we find that the critical value is $k^2_{min} = \frac{\varepsilon^2 g_v + f_u D}{2\varepsilon^2 D}$, and

$$h(k^2_{min}) = \det(A) - \frac{(\varepsilon^2 g_v + f_u D)^2}{4\varepsilon^2 D\tau}.$$

Together, we have four conditions that need to be satisfied in order for the system to have a bifurcation to non-homogeneous solutions. These are

$$\begin{aligned} f_u + g_v/\tau &< 0, \\ f_u g_v - f_v g_u &> 0, \\ \varepsilon^2 g_v + f_u D &> 0, \\ \det(A) - \frac{(\varepsilon^2 g_v + f_u D)^2}{4\varepsilon^2 D\tau} &< 0. \end{aligned} \tag{4.4}$$

The values of L at which heterogeneous solutions appear, for various eigenmodes n, are shown in Table 4.1.

Eigenmode n	L
1	0.3729
2	0.7458
4	1.4917
8	2.9833

Table 4.1: Some domain length values at which non-homogeneous solutions appear, according to Turing theory. The values were computed using the constants $\tau = 1, \varepsilon = 0.02, D = 1$. The eigenmodes correspond to one, two, four, and eight peaks. These values can be seen overlapped in the full bifurcation diagram of Figure 4.4.

When considering systems with domains that grow dynamically, the standard

Turing equations need to be modified accordingly.

When considering the extended reaction-difusion equations (RDE) system in (4.10), we considered very small growth rates r, say $r \ll 1$. As a first approximation, assuming $t = O(1)$, the only thing that changes in the Turing conditions is that the eigenvalues shift to the left. Instead of (4.3), the $-r\mathbf{W}$ term appears in the diagonal as

$$\lambda_r \mathbf{W}_k = -\mathcal{D}k^2 \mathbf{W}_k + \mathbf{A}\mathbf{W}_k - rI,$$

and the eigenvalues for this case are $\lambda_r = \lambda_s - r$, with respect to the λ_s eigenvalues of the stationary system. In § 4.2 we will discuss recent analytical results that describe in more detail the effect of growing domains on the four Turing conditions (4.4).

4.2 Domain growth extension

It has long been speculated that domain growth is one of the mechanisms that influences pattern selection. In the work by Kondo and Asai [25], a domain length-dependent term in a reaction-diffusion system was introduced, and the resulting patterns successfully mimicked the characteristics exhibited by growing fish. Further work ([12], [13], [3]) specifically addressed the effect that domain growth had on patterning, and recent research has generalized the formalisms of Turing analysis to account for domain growth, both numerically ([27],[17]), and analytically ([45], [35], [28]).

Moreover, one of the main criticisms to Turing's postulation of RDE as models for pattern formation has been that mode selection appears to not be robust enough when compared to naturally occurring patterns. Adding domain growth to the equations has shown in some cases to increase the robustness of patterns [45], and in itself works as a mechanism for pattern selection.

A general system of RDE for a fixed domain Ω, in one or more dimensions, can

be extended to account for growing domains. The following derivation was based on Plaza et al.'s work [45].

Consider a parameter (spatial) $s \in [0,1]$, defined for each time t, which is used to parametrize the mapping ψ_t, such that for every time $t \geq 0$,

$$\psi_t : [0,1] \longrightarrow \mathbb{R}^3, \qquad \psi_t \equiv X(s,t) = \begin{pmatrix} x(s,t) \\ y(s,t) \\ z(s,t) \end{pmatrix} \tag{4.5}$$

It is required that $\psi_t : \Omega_0 \subset \mathbb{R} \longrightarrow \mathbb{R}^3$ be C^2 for every $t \geq 0$, and continuously differentiable with respect to t. Thus, (4.5) defines a regular curve $\mathcal{C}_t$ embedded in $\mathbb{R}^3$, with the characteristic that for every $s \in [0,1]$, and $t \geq 0$

$$X_s(s,t) \neq 0.$$

The arclength $\sigma(s,t)$ of the mapping ψ_t, as a function of s and t, and its derivative with respect to s, are:

$$\begin{aligned} \sigma &= \int_0^s |X_s(s',t)| \mathrm{d}s', \\ \sigma_s &= |X_s(s,t)|. \end{aligned} \tag{4.6}$$

Let ϕ be the concentration (mols per unit length) of the chemicals $\phi = (\phi_1, \phi_2, ...)^T$. Assuming that the chemicals diffuse according to Fick's law, the flux vector J of the chemicals, proportional to the concentration gradient, is:

$$J = -\mathcal{D}\nabla\phi,$$

for a particular diagonal diffusion matrix $\mathcal{D}$ (no cross diffusion terms are considered). Given that the rate of change in the chemicals' concentration is proportional to the flow through the boundary $\partial\Omega$, for any outer unit normal $\hat{\mathrm{n}}$, the volume that

exits Ω through the element dS is $-J \cdot \hat{\mathrm{n}}\mathrm{d}S$.

$$\frac{\mathrm{d}}{\mathrm{d}t}\int_{\Omega(t)} \phi \mathrm{d}X = -\mathcal{D}\int_{\partial\Omega(t)} J \cdot \hat{\mathrm{n}}\mathrm{d}S = \mathcal{D}\int_{\partial\Omega(t)} \nabla\phi \cdot \hat{\mathrm{n}}\mathrm{d}S. \tag{4.7}$$

By rewriting (4.7), and using the parametrization from (4.5), making a change of variables, using (4.6), and integrating in a segment $[s_1, s_2]$ of the curve $\mathcal{C}_t$, defined by $\psi_t([s_i, s_2], t)$, with $[s_1, s_2] \in [0, 1]$, the left hand side yields:

$$\frac{\mathrm{d}}{\mathrm{d}t}\int_{\Omega(t)} \phi \mathrm{d}X = \frac{\mathrm{d}}{\mathrm{d}t}\int_{s_1}^{s_2} \phi(X(s,t),t)\sigma_s(s,t)\mathrm{d}s.$$

Notice that since Ω is a line, $\partial\Omega$ corresponds to the two endpoints of the interval.

Doing the same change of variables for the right hand side of (4.7) results in:

$$\mathcal{D}\int_{\partial\Omega(t)} \nabla\phi\cdot\hat{\mathrm{n}}\mathrm{d}S = \mathcal{D}\nabla_X\phi\Big|_{s_1}^{s_2} = \mathcal{D}\int_{s_1}^{s_2} \partial_s\left(\nabla_X\phi\cdot\frac{|X_s|}{|X_s|}\right)\mathrm{d}s = \mathcal{D}\int_{s_1}^{s_2}\partial_s\left(\frac{\phi_s}{\sigma_s}\right)\mathrm{d}s.$$

Dropping the integral sign on both sides (as it's valid on any interval $[s_1, s_2] \subset (0,1), t \geq 0$), the generalized RDE on a growing 1-D domain is obtained:

$$\phi_t = \frac{\mathcal{D}}{(\sigma_s)^2}\left(\phi_{ss} - \frac{\sigma_{ss}}{\sigma_s}\phi_s\right) - \frac{\sigma_{st}}{\sigma_s}\phi,$$

or, equivalently

$$\phi_t = \frac{\mathcal{D}}{\sigma_s}\partial_s\left(\frac{\phi_s}{\sigma_s}\right) - \partial_t(\ln\sigma_s)\phi\,. \tag{4.8}$$

For the standard pattern-formation problem with two reactants, $\phi \equiv \mathbf{w} = (u, v)^T$, (4.8) corresponds to the uncoupled portion of the equations. The coupling comes from the reaction term $F(\mathbf{w}) = (f(u,v), g(u,v))^T$, as seen in models such as the Schnakenberg, Barrio-Varea-Aragón-Maini model (BVAM), Gierer-Meinhardt, etc.

The full model, for two interacting chemicals $\mathbf{w} = (u, v)^T$, in non-dimensional

form, with $\mathcal{D} = \left(\begin{smallmatrix} D_u & 0 \\ 0 & D_v \end{smallmatrix}\right)$, is

$$\mathbf{w}_t = \frac{\mathcal{D}}{\sigma_s^2}\left(\mathbf{w}_{ss} - \frac{\sigma_{ss}}{\sigma_s}\mathbf{w}_s\right) - \frac{\sigma_{st}}{\sigma_s}\mathbf{w} + F(\mathbf{w}) \tag{4.9}$$

In 1-D, a number of simplifying assumptions can be made that make the problem much more analytically tractable, while keeping it physically meaningful.

Assuming that the system grows isotropically, it is possible to separate the growth term from the manifold parametrization, $X(x,t) = \rho(t)X_0(s)$. Moreover, a straight line domain, characterized by $X_0(s) = (s,0,0)^T$, with $s \in [0,1]$, results in $\sigma_s = 1,\ \ \sigma_{ss} = 0$.

The system can be further simplified by assuming slow exponential growth ($\rho(t) = \exp(rt)$), hence

$$\frac{\sigma_{st}}{\sigma_s} = \frac{\rho_t}{\rho} = r.$$

With all of the above assumptions, the simplified version of (4.9) is, then

$$\mathbf{w}_t = \frac{\mathcal{D}}{\rho^2}\mathbf{w}_{ss} - r\mathbf{w} + F(\mathbf{w}) \tag{4.10}$$

The effect that domain growth has on the four conditions necessary for a diffusion-driven instability was recently studied [28]. Even in the simplified case of exponential growth in (4.10), the effective diffusion coefficients become non-autonomous, invalidating the standard linear approach. Asymptotic analysis showed that the conditions for patterning on growing domains are less strict, i.e., it is possible to observe patterns on systems with activators on both components, and similarly for short-range inhibition and long-range activation systems.

In terms of bifurcation theory, systems with domain growth exhibit delayed self-replication events when compared to solutions obtained by adiabatically varying the domain length parameter L (integrating for each value of L until equilibrium is achieved). This behaviour was encountered in [3] for the 1-d Schnakenberg system (figure 5a), although the delayed bifurcation phenomena was not discussed.

4.3 Stability of 1-d mesa patterns for the Gierer-Meinhardt model with saturation (GMS) model when D = O(1)

In the previous section we derived a set of Turing conditions for the existence of non-homogeneous patterns in the GMS model. We also extended the reaction diffusion system to account for growing domains. We will now use the previous results to investigate numerically the effect of domain growth on mesa patterns, as well as the difference between domains that grow adiabatically versus dynamically. We will use results from numerical bifurcation theory, and perform analytical continuation on stable solutions in order to obtain a global picture of the bifurcation diagram. Our computations are for the parameter range where $D = O(1)$.

4.3.1 Construction of a single mesa

Solving the GMS system numerically reveals that the solutions past the Turing thresholds have a mesa profile (see Figure 4.2). A single mesa is essentially a saturated pulse solution with a symmetric flat profile in the centre of the domain, separated from a quasi-zero solution by sharp interfaces located at $x = \pm l$. Analogously to pulse systems such as the Schnakenberg system (cf. [52]), in this parameter regime increasing the domain length will split the solution into images of the single mesa.

The mesa solutions can tought of as two back-to-back heteroclinic solutions that are separated by a plateau regio. This characteristic can be exploited to obtain a first asymptotic approximation of the system. This approach was done originally in [23], and we outline the construction here.

We start by looking for an asymptotic solution near the interface $x = l$ to the

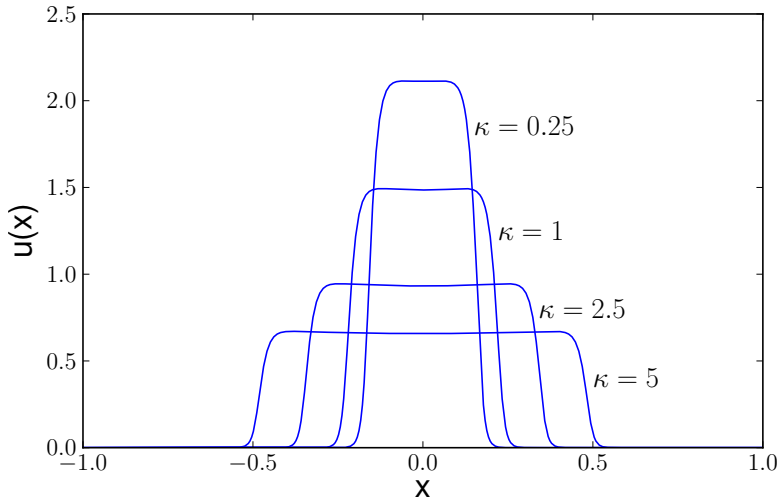

Figure 4.2: Mesa profiles for various values of κ, obtained by numerically solving (4.1). The other parameters used are $D = 10$ and $L = 1$. The system was integrated using an implicit explicit scheme on a 500 point grid.

steady state problem $u_t = v_t = 0$:

$$u = U_0(y) + \varepsilon\, U_1(y) + \ldots, \qquad v = V_0(y) + \varepsilon\, V_1(y) + \ldots, \qquad y = \frac{x - l}{\varepsilon}.$$

To $O(1)$, since $D_u = O(\varepsilon^{\,2})$, the system is

$$U_0'' = U_0 - \frac{U_0^2}{V_0(1 + kU_0^2)}$$
$$V_0'' = 0.$$

From the boundary conditions we have that V_0 is a constant. To determine its value, we use the Maxwell line condition [31], which states that in order to have a heteroclinic connection between $x = 0$ and $x = L$, there has to be a value v_c, such that the area under the roots of $a(u, v_c) = -u + \frac{u^2}{v_c(1+ku^2)}$ is zero. The three roots of

$a(u,v)$ occur at $u=0$ and at $u=u_{\pm}(v)=\frac{1\pm\sqrt{1-4kv^2}}{2kv}$, with $0<u_-(v)<u_+(v)$. The non-zero roots can be expressed as $v=h(u)=\frac{u}{1+ku^2}$ for $0<v<v_m$, with $v=v_m$ the value at which both roots coalesce. Hence, the solution to the $O(1)$ equation is $V_0=v_c$, with v_c the value that satisfies the Maxwell line condition

$$\int_0^{u_c} a(u,v_c)=0, \qquad u_c\equiv u_+(v_c), \tag{4.11}$$

and U_0 the unique heteroclinic connection satisfying $U_0(-\infty)=u_+(v_c)=u_c$ and $U_0(\infty)=0$.

To $O(\varepsilon)$ we have the system

$$\begin{aligned}\mathcal{L}(U_1)=U_1''+a_u(U_0,V_0)U_1&=-a_v(U_0,V_0)V_1\\ V_1''&=0.\end{aligned}$$

The solution to the second equation is $V_1=V_{11}y+V_{12}$. Since $\mathcal{L}(U_0')=0$, we can derive a solvability condition to determine V_{12} in terms of V_{11},

$$V_{12}\int_{-\infty}^{\infty} a_v(U_0,v_c)U_0'dy=V_{11}\int_{-\infty}^{\infty} a_v(U_0,v_c)yU_0'dy.$$

Furthermore, matching to the outer solution yields that $V_{11}=v'(l^{\pm})$.

There are two outer solutions, to the left and right of the internal layer at $x=l$, that when matched will determine the value for $v'(l^{\pm})$. The problem to the left of the layer, $0<x<l$, is

$$D_v v''=b(u,h(u))=g(u), \qquad v(l)=v_c, \qquad v'(0)=0, \qquad u=u_+(v), \tag{4.12}$$

whereas the outer problem on the right side of the layer, $l<x<L$, is defined as

$$D_v v''=b(0,v), \qquad v(l)=v_c, \qquad v'(L)=0. \tag{4.13}$$

Since V_{11} is a constant, the matching condition is that $v'(l^-) = v'(l^+)$

Multiplying (4.12) by $v' = h'(u)u'$ and integrating yields the following equations for u_x and v_x,

$$\frac{dv}{dx} = -\sqrt{\frac{2F(u;u_0)}{D}}, \qquad \frac{du}{dx} = -\sqrt{\frac{2F(u;u_0)}{Dh'(u)}},$$

with $F(u;u_0) = \int_{u_0}^{u} g(s)h'(s)ds$. Upon integrating between $u_0 = u(0)$ and $u(l) = u_c$, we obtain the following relationship:

$$-\frac{l}{\sqrt{D}} = \int_{u_0}^{u_c} \frac{h'(u)}{\sqrt{2F(u;u_0)}}du = \frac{\sqrt{2F(u_c;u_0)}}{g(u_c)} + \int_{u_0}^{u_c} \frac{g'(u)}{(g(u))^2}\sqrt{2F(u;u_0)}du. \tag{4.14}$$

The exact solution on the outer region given in (4.13) can be calculated analytically as

$$v(x) = v_c\left(\frac{\cosh\left[(L-x)/\sqrt{D}\right]}{\cosh\left[(L-l)/\sqrt{D}\right]}\right), \qquad v'(l^+) = -\frac{v_c}{\sqrt{D}}\tanh\left[(L-l)/\sqrt{D}\right]. \tag{4.15}$$

Finally, since $v'(l^+) = v'(l^-)$, we can solve for l in (4.15) and substitute it into (4.14) to obtain the critical points at which the domain will split,

$$\frac{L}{\sqrt{D}} = \tanh^{-1}\left(\frac{\sqrt{2F(u_c;u_0)}}{v_c}\right) - \frac{\sqrt{2F(u_c;u_0)}}{g(u_c)} - \int_{u_0}^{u_c} \frac{g'(u)}{(g(u))^2}\sqrt{2F(u;u_0)}du. \tag{4.16}$$

From a practical point of view, the u_c, v_c values can be found using a quadrature, and a simple numerical integration will then yield the three terms in (4.16). In the next section we will calculate this threshold and compare it with numerical results of systems with growing domains. The remainder of this chapter will consist of numerical experiments based on numerical bifurcation theory.

4.3.2 Bifurcation analysis

In the previous section we derived a solution for the $D = O(1)$ case by treating the mesa solution as two back-to-back heteroclinic curves. Equation (4.16) determines a critical value in terms of L or D, beyond which the heteroclinic cannot exist. This provided us with an analytical estimate of the domain length at which splitting or self-replication will occur.

We now want to study the splitting behaviour as the domain increases both adiabatically (when stationary solutions are recomputed at each domain length value), and dynamically (when the domain length itself is a dynamic variable). We start by focusing on how solutions change numerically as the domain length increases. The boundary conditions were homogeneous Neumann, and the values of the constants were $k = 2.5, \tau = 1, D = 1$, and $\varepsilon = 0.02$.

In the adiabatic growth case, numerical solutions to the full 1-D problem were computed for increasing values of L. An initial solution was iterated until convergence for some domain length $L = L_0$; the stationary solution thus obtained then became the initial solution for an increased domain length $L = L_1$, and so forth for increasing values of L. Typical solutions for three different values of L are given in figure 4.3, while on the two-mesa regime. The three solutions all occur for varying values of the domain length. They were all obtained through numerical continuation on the L parameter. We started by obtaining a stationary solution from random initial data, and from it we used the numerical continuation package AUTO-07P [14] to follow the curve of solutions for varying L, using $\max(V)$ as the bifurcation parameter.

Solution I is essentially the leading eigenvector $\phi = A\cos(2n\pi x/L)$, first estimated through linear stability analysis, and as expected from Turing theory, unstable. Going up on the branch beyond solution I leads to the homogeneous Turing solution $u = 0.5603$, $v = u^2$, and traversing the branch in the other direction leads to the stable mesa branch.

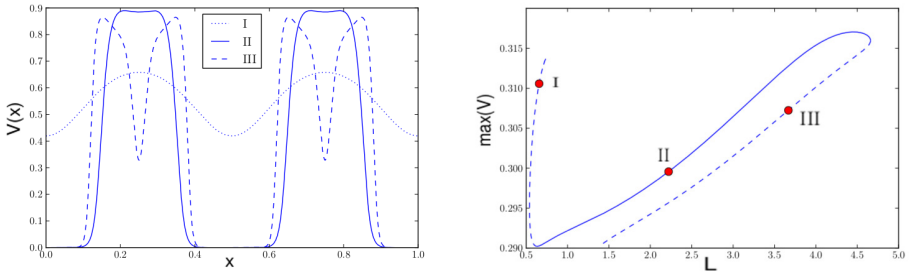

Figure 4.3: Three distinct two-mesa solutions to the GMS system. Solution I is close to the Turing instability, II is the stable mesa solution, and III is the unstable solution that develops when the domain length is increased past a critical point. The image on the right is the bifurcation diagram for the branch of two-mesa solutions.

Solution II lies in the stable branch. This is a characteristic mesa structure, and it is far from the Turing equilibrium. Continuing on the branch along increasing L eventually leads to a fold point, beyond which we reach the unstable branch characterized by solution III. Going beyond the fold point causes the solution to drop to the next branch of solutions, which will have double the number of mesas.

The bifurcation diagram for one, two, four, and eight mesa solutions is given in figure 4.4. The thickest line is a stable solution that is recomputed for increasing values of L. It traverses the stable branches from left to right, and at each fold point it falls to the next branch, which manifests in the solutions as a doubling in the number of mesas. Since each successive branch doubles the number of mesas, the critical value L_c at which the new set of mesas will split doubles with each iteration, hence $L_c(n) = L_c(1) \times 2^{n-1}$. This exponential relationship can be readily seen in the symmetry of the bifurcation diagram of figure 4.4, which was plotted on a logarithmic scale.

This numerical results show that there will always be a stable solution in the $(D, \tau) = O(1)$ parameter regime, for all domain lengths. The asymptotic formula (4.16) provides us an estimate of the critical values $L_c(n)$ at which an n mesa

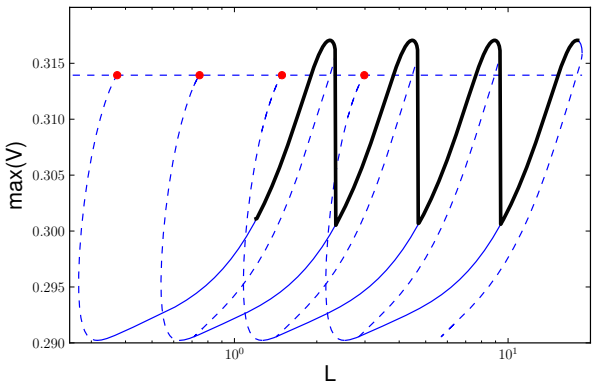

Figure 4.4: Four branches of the GMS system, with an overlay of the family of stable solutions obtained by traversing it left to right . When reaching the fold point of each branch the solutions fall to the next branch, effectively doubling the number of mesas. The upper horizontal unstable line are the unstable Turing solutions, and the red points on it are the values shown on table 4.1.

solution splits into $2n$ mesas.

In order to numerically compute the value, we first found the u_c, v_c values that satisfy the Maxwell line condition, shown in (4.11), via a quadrature. It was then straightforward to numerically integrate $F(u_c; u_0)$ and the third term in (4.16).

The resulting value was $L_c = 2.1010$ for $-L < x < L$, or half that for $0 < x < L$ (as shown in Figures 4.3, 4.4). The location of the fold point in the 1-mesa branch was then calculated by solving the full system, using $\varepsilon = 0.002$ and 1500 grid points. The value thus obtained was $L_c = 2.1325$.

Furthermore, the system exhibits hysteresis, traversing the bifurcation diagram left to right produces a very different picture. Traversing left to right shows the splittings occurring at the points predicted in (4.16), whereas traversing in the opposite direction results in in the solution staying in the 8-mesa branch until the left edge of the stable branch, beyond which the solution will jump either to the 4-

mesa branch, or to the 2-mesa branch. In principle, estimating those points should involve very similar analysis as was done in Section § 4.3.1. The differences between the bifurcation structure of $u(x)$ when traversed in either direction are shown in Figure 4.5.

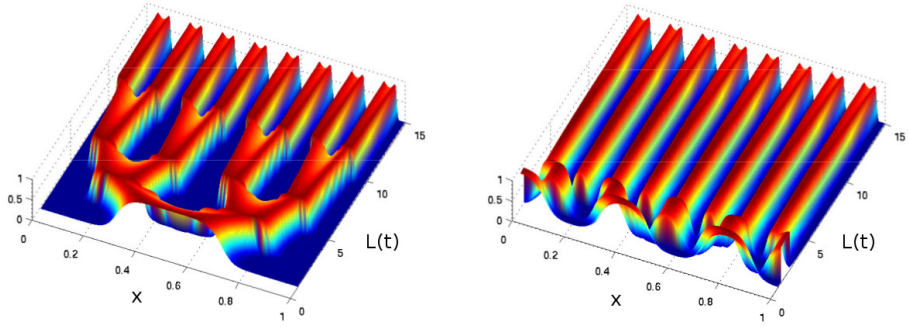

Figure 4.5: The full solution curve for $u(x)$ as the bifurcation branches in Figure 4.4 are traversed from left to right (image on the left), and from right to left (image on the right). The solutions are all plotted on a normalized domain, and the proper domain length L is represented on the y-axis.

All of the work above was done with the domain length L fixed; when a stable solution was attained it was used as the starting point for the next computation at a slightly changed L. When considering dynamically varying domains, i.e., making $L \equiv L(t)$, the system needs to be modified. A general framework on how to extend stationary equations into growing domains was discussed earlier in § 4.2. The extended system for isotropic exponential growth is relatively simple,

$$\begin{aligned} u_t &= \frac{\varepsilon^2}{L^2}\Delta u - \rho u - u + \frac{u^2}{v(1+ku^2)} \\ \tau v_t &= \frac{D}{L^2}\Delta v - \rho v - v + u^2 \\ L_t &= \rho L, \end{aligned}$$

with ρ the rate of domain growth.

We solved the system by discretizing in space using centred differences, with second order boundary conditions, and Matlab's ode15s routine was used for time integration. The solution curves for various values of ρ were obtained, and when overlapping them in the bifurcation diagram of Figure 4.4 we can see a delayed bifurcation effect in the left image of Figure 4.6. Notice the sharp transitions of the static solutions in Figure 4.5, compared to the soft dynamic transitions on the right image in Figure 4.6. The stability of the branches highlighted in the above

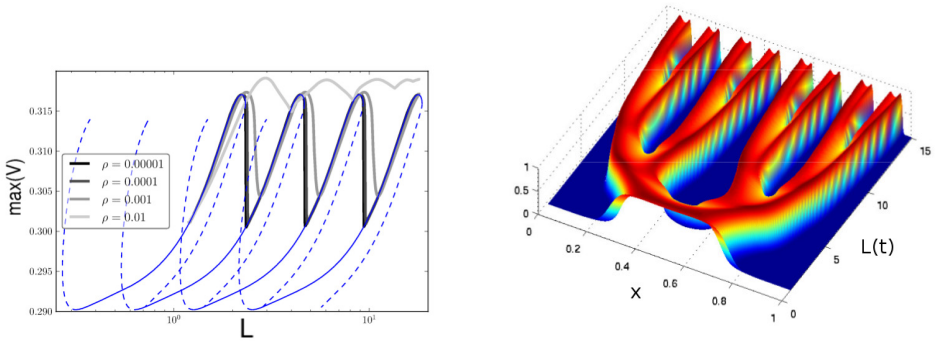

Figure 4.6: Solution curves for systems with growing domains, $L(t) = e^{\rho t}$. Notice the delay in the bifurcation (jump between branches) as ρ gets larger. The figure on the right shows the effect on Figure 4.5 (left) when adding domain growth, with $\rho = 0.002$. The y-axis represents $L(t)$, and $L = 15$ is reached when $t = 1354$.

figures had to be obtained independently from the continuation software used to generate the bifurcation the diagram. The package that we used (AUTO-07P [14]) is designed primarily for finite dimensional systems; stability can be established in a straightforward way for systems of ordinary differential equations (ODE). When extended to dealing with parabolic partial differential equations (PDE)s this capability is lost. We performed the eigenvalue analysis separately by saving the stationary solutions obtained while traversing the branches, and using them as the basis of a Taylor expansion on a perturbation to the solutions. The algorithm in AUTO utilizes non-uniform grids, a spline on the output was used to generate a uniformly spaced grid amenable with the discrete Jacobian.

In order to study stability we introduce the perturbation

$$u(x) = u_s(x) + e^{\lambda t}\phi(x), \qquad v(x) = v_s(x) + e^{\lambda t}\psi(x), \tag{4.17}$$

with u_s, v_s the stationary solutions and $\phi \ll 1$, $\psi \ll 1$. Substituting this into (4.1), we get

$$\lambda\phi = \varepsilon^2\Delta\phi + a_u(u_s, v_s)\phi + a_v(u_s, v_s)\psi$$
$$\lambda\tau\psi = D\Delta\psi + b_u(u_s, v_s)\phi + b_v(u_s, v_s)\psi.$$

This can be written as an eigenvalue problem in matrix form, $Aw = \lambda w$, with $w = (\phi, \psi)^T$, and A as

$$A = \begin{bmatrix} \varepsilon^2\Delta + a_u(u_s, v_s) & a_v(u_s, v_s) \\ b_u(u_s, v_s)/\tau & D\Delta/\tau + b_v(u_s, v_s)/\tau \end{bmatrix}. \tag{4.18}$$

Plotting the eigenvalue with largest real part versus the corresponding L value for the stationary solutions reveals the stable and unstable manifolds in the branches. In Figure 4.7 we show such a curve for the full range of stationary solutions along the one-mesa branch. The labelling regarding stability on all the previous figures was based on this calculation, and due to the symmetry of the system, the curves for the different branches are essentially identical. The region in Figure 4.7 where the eigenvalues have negative values is roughly a straight line of magnitude $O(\varepsilon)$. This was expected from the estimates done on [24].

4.3.3 Hopf bifurcations of 1D mesa patterns

So far we have examined the instabilities that occur for increasing L, which typically result in the splitting of solutions. A second mechanism for generating instabilities is when the value of τ increases. In all previous calculations we've worked with $\tau = O(1)$, and the difference in difusivities marks the $v(x)$ equation

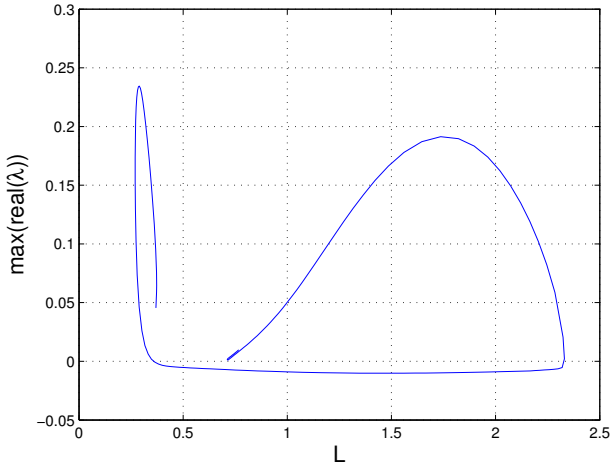

Figure 4.7: Stability curve of the maximum eigenvalue vs L for solutions on the 1-mesa branch.

as the fast component in the system. However, if τ grows to be $O(1/\varepsilon)$, or even to $O(1/\varepsilon^2)$, the v equation will slow down and approach the time scale of the u equation. When this happens, feedback will happen between the two equations, and phenomena characteristic of delay differential equations such as oscillatory instabilities will occur.

During oscillations it is even possible that the width of the mesa might exceed the splitting threshold, which would result in a mesa splitting bifurcation.

We start by doing a perturbation analysis with τ as a parameter, similar to what was done in (4.18). We start at a stationary solution on the stable part of the one-mesa branch, and we vary τ until we find a zero eigenvalue, using Newton's method. The critical value for a stable solution originating at $L = 2.02$ is $\tau = 278$. Plotting the eigenvalues with largest real part as τ increases shows how a set of complex conjugate eigenvalues becomes unstable, as depicted in Figure 4.8.

The type of instability generated by large values of τ are oscillations on the

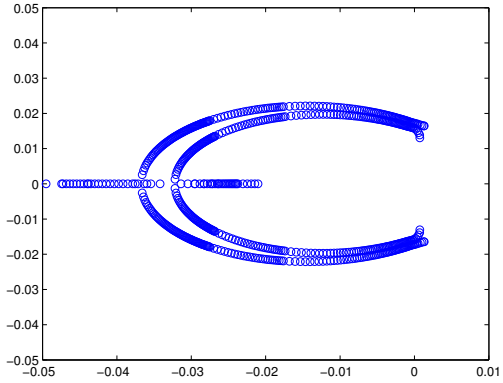

Figure 4.8: Real part of eigenvalues as τ approaches critical value. The x and y axis are the real and imaginary components of the eigenvalues, respectively.

width of the mesa. We computed full numerical solutions for two different cases beyond the Hopf threshold, and these can be seen in Figure 4.8. In the first case, the domain length of the original stationary solution was small enough, that even with τ beyond the threshold the mesa doesn't split. The complex pairs have largest real part, so stable oscillations develop. This type of instability is called a breather type instability, and we will study it in more detail when we discuss systems with $D = O(1/\varepsilon)$ in § 4.4.

The second case involves a single mesa on a slightly larger initial domain. When τ grows, the oscillations bring it beyond the splitting threshold, and this causes the mesa to split into two mesas. The two new mesas now have domain lengths that are half the length of the original one, so they quickly stabilize. This case highlights a dynamic splitting bifurcation.

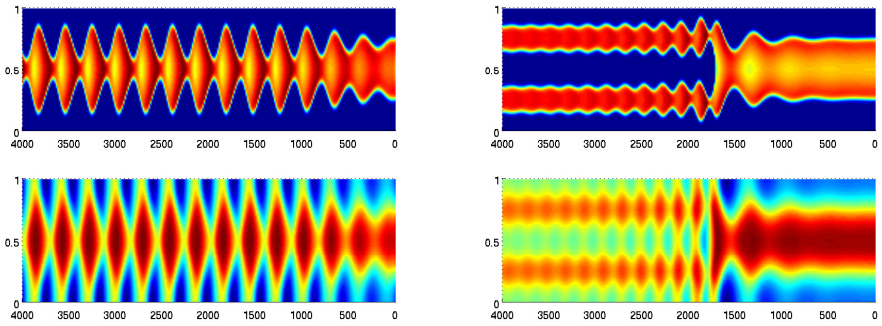

Figure 4.9: Solution graphs for both $u(x)$ (top), and $v(x)$ (bottom), for large τ. Both numerical computations were done for $\tau = 380$, the ones on the left with a domain length $L = 1.6$ and the ones on the right had $L = 2.02$. The horizontal axis is time, and the vertical axis is the domain length.

4.4 Mesa patterns in the near-shadow limit

When considering the GMS model with a diffusion coefficient $D = O(1)$, we have shown in the previous sections numerical results highlighting the existence of both splitting and oscillatory instabilities, and an instance of an oscillatory-triggered splitting instability (Figure 4.9).

We now want to extend the results obtained previously to the near-shadow limit, i.e., $D = \mathcal{D}/\varepsilon$ with $\mathcal{D} = O(1)$. We will show that this limit is more tractable analytically. We will observe that the behaviour that we observed in the numerical experiments of the previous section is amenable to asymptotic analysis when working in this regime.

We want to construct a $K-$stripe stationary solution on $x \in [0, 1]$, with $L = 1/K$ the period of the solution, and l the length of each individual mesa, as shown in Figure (4.10).

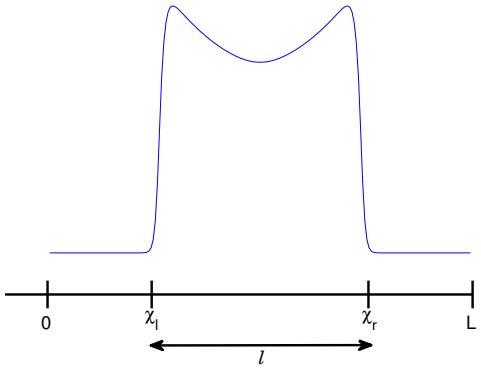

Figure 4.10: A typical mesa profile in the stationary solution $v(x)$. The left and right edges of the mesa are labelled as χ_l and χ_r respectively; and the length of the mesa section is l.

The stationary system

$$\begin{aligned} 0 &= \varepsilon^2 u_{xx} - u + \frac{u^2}{v(1+ku^2)}, & u_x(0) = u_x(L) = 0, \\ 0 &= \frac{\mathcal{D}}{\varepsilon} v_{xx} - v + u^2, & v_x(0) = v_x(L) = 0. \end{aligned} \tag{4.19}$$

Beyond the stability of 1D mesas, we will extend the mesas in the y-direction to form stripes, and derive conditions on the parameters to guarantee stability with respect to transverse perturbations.

4.4.1 Construction of a multi-stripe pattern

To leading order, we have that $v_{xx} = 0$. Applying the Neumann boundary condition, we have then that $v \sim \mathcal{V}$, and the value of the constant can be estimated by

integrating over the whole domain,

$$\mathcal{V} = \frac{1}{L}\int_0^L u^2 dx. \tag{4.20}$$

In the inner region near the left boundary of the mesa we have that $v = \mathcal{V}$, and we do a change of variables for $u = \mathcal{V}w$ and $y = \varepsilon^{-1}(x - \chi_l)$. The resulting equation is

$$w_{yy} + f(w) = 0, \qquad -\infty < y < \infty, \qquad f(w) = -w + \frac{w^2}{1 + bw^2}, \tag{4.21}$$

with $b = k\mathcal{V}^2$. Now, we are looking for a heteroclinic connection in u as the transition mechanism that generates the mesa, one for each side of the mesa. For a heteroclinic connection to exist in (4.21), it has to satisfy the Maxwell line condition [31].

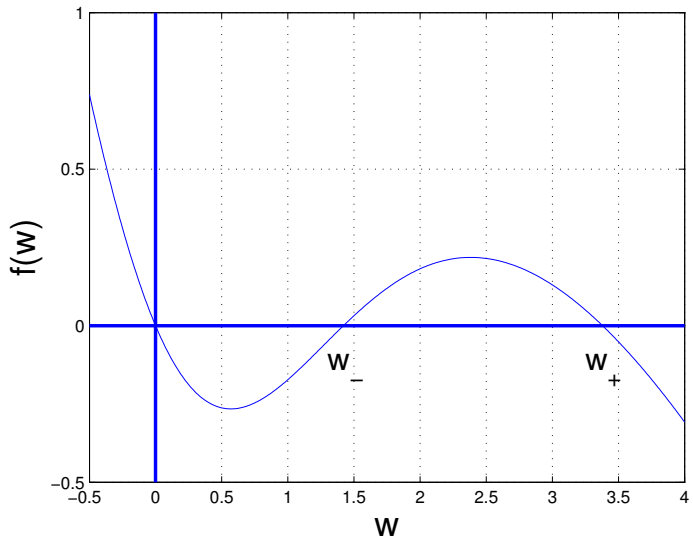

Figure 4.11: A plot of the function $f(w)$ given in (4.21).

The function $f(w) = 0$ has zeros at $w = 0$ and $w_\pm = \frac{1\pm\sqrt{1-4b}}{2}$, with distinct real values for $w_\pm$ existing in the range $0 \leq b < 1/4$. The profile of the curve in that range can be seen in Figure (4.11). The Maxwell line condition states that a heteroclinic connection will exist for the value $b = b_0$ such that $\int_0^{w_+} f(w)dw = 0$. Integrating $f(w)$ we get

$$\begin{aligned}\int_0^{w_+} f(w)dw &= \left(-\frac{w^2}{2} + \frac{w}{b} - \frac{1}{b^{3/2}}\arctan(b^{1/2}w)\right)\Bigg|_0^{w_+}, \\ &= -\frac{w_+^2}{2} + \frac{w_+}{b_0} - \frac{1}{b_0^{3/2}}\arctan(b_0^{1/2}w_+),\end{aligned}$$

and since we have that $b_0 = \frac{w_+-1}{w_+^2}$, the Maxwell line condition will be satisfied if

$$b_0 = \frac{w_+ - 1}{w_+^2}, \qquad \sqrt{w_+ - 1}(w_+ + 1) = 2w_+ \arctan(\sqrt{w_+ - 1}). \tag{4.22}$$

This can be solved numerically to obtain the critical values $b_0 = 0.211376$, and $w_+ = 3.295209$. For use later in Section §4.4, we need to compute

$$\beta = \int_{-\infty}^{\infty} w'^2 dy$$

Next, we multiply (4.21) by w' to get

$$\frac{d}{dy}\left(\frac{w'^2}{2}\right) = \frac{d}{dy}\mathcal{F}(w) \qquad \rightarrow \qquad w'^2 = 2\mathcal{F},$$

with $\mathcal{F} = -\int_0^w f(s)ds$. We then obtain

$$\beta = \int_{-\infty}^{\infty} w'^2 dy = \int_0^{w_+} w'^2 \frac{1}{w'} dw = \int_0^{w_+} \sqrt{2\mathcal{F}(w)}dw. \tag{4.23}$$

This can be numerically calculated using the previously computed value for w_+, to get $\beta \sim 1.49882$.

Linearizing around $w = 0$ for $y \to -\infty$, and for $w = w_+$ for $y \to \infty$, we get that for $b = b_0$ we have a heteroclinic solution

$$\begin{aligned} &w'' + f(w) = 0, && -\infty < y < \infty, \quad f(w) = -w + \frac{w^2}{1 + b_0 w^2}, \\ &w \sim d_- e^y, && \text{as } y \to -\infty, \\ &w \sim w_+ - d_+ e^{-\nu_+ y}, && \text{as } y \to \infty, \end{aligned}$$

for $\nu_+ = \sqrt{1 - 2/w_+}$. To break translation invariance we take $w(0) = w_+/2$, in order to guarantee uniqueness.

A full mesa solution will consist of two back-to-back heteroclinic curves, and can be constructed as

$$u \sim \mathcal{V}[w_l + w_r - w_+], \quad \text{with} \quad w_l \sim w\left(\frac{x - \chi_l}{\varepsilon}\right), \quad w_r \sim w\left(\frac{\chi_r - x}{\varepsilon}\right).$$

Integrating (4.20), we get that to first order $\mathcal{V} \sim \frac{1}{L}\mathcal{V}^2 w_+^2 l$, with $l = \chi_r - \chi_r$ the width of the mesa. We then have, since $b_0 = k\mathcal{V}^2$, that

$$\mathcal{V} w_+^2 \sim \frac{L}{l} + O(\varepsilon), \qquad l \sim \frac{L\sqrt{k}}{\sqrt{b_0} w_+^2} < L.$$

Therefore, a necessary condition for a $K-$stripe solution to exist is that

$$\frac{\sqrt{k}}{\sqrt{b_0} w_+^2} < 1.$$

To refine the solution, it is necessary to further expand $u(x)$ and $v(x)$. In the outer region we expand u and v as

$$v \sim \mathcal{V} + \varepsilon\, v_1 + \varepsilon^{\,2} v_2 + \cdots.$$

Since outside of the mesa u is exponentially small, and in the plateau region $u \sim \mathcal{V} w_+ + O(\varepsilon)$, by substituting into (4.19), we get that

$$\mathcal{D} v_{1,xx} = \begin{cases} \mathcal{V} & \text{for } 0 < x < \chi_l \\ \mathcal{V}(1 - \mathcal{V} w_+^2) = \mathcal{V}(1 - L/l) & \text{for } \chi_l < x < \chi_r \\ \mathcal{V} & \text{for } \chi_r < x < L \end{cases} \tag{4.24}$$

with $v_{1,x}(0) = v_{1,x}(L) = 0$. In order to find the conditions on v_1 at the transition layers χ_l and χ_r, we expand u as $u \sim \mathcal{V} w_+ + \varepsilon \mathcal{U}_1 + ...$ on $\chi_l < x < \chi_r$.

Substituting into (4.19), we get that

$$-\mathcal{U}_1 + g_u(\mathcal{V} w_+, \mathcal{V}) \mathcal{U}_1 + g_v(\mathcal{V} w_+, \mathcal{V}) v_1 = 0,$$

with

$$g(u, v) = \frac{u^2}{v(1 + k u^2)}$$

Since $1 + b_0 w_+^2 = w_+$, the linearization terms simplify to

$$\begin{aligned} g_u(\mathcal{V} w_+, \mathcal{V}) &= \frac{2 w_+}{(1 + b_0 w_+^2)^2} = \frac{2}{w_+}, \\ g_v(\mathcal{V} w_+, \mathcal{V}) &= \frac{-w_+^2}{1 + b_0 w_+^2} = -w_+, \end{aligned} \tag{4.25}$$

and this yields

$$-\mathcal{U}_1 + \frac{2}{w_+} \mathcal{U}_1 - w_+ v_1 = 0, \qquad \Rightarrow \qquad \mathcal{U}_1 = \frac{w_+^2}{2 - w_+} v_1.$$

We now expand u and v near the left transition point $x = \chi_l$ (zooming in $y = \varepsilon^{-1}(x - \chi_l)$) as

$$u = u_0 + \varepsilon\, u_1 + \varepsilon^2 u_2 + \cdots, \qquad v = \mathcal{V} + \varepsilon\, \mathcal{V}_1 + \varepsilon^2 \mathcal{V}_2 + \cdots,$$

with $u_0 = \mathcal{V} w_+$. Substituting into (4.19), the $O(\varepsilon)$ system is

$$\begin{aligned} \mathcal{L}u_1 : &\equiv u_1'' - u_1 + g_u(u_0, \mathcal{V}) u_1 = -g_v(u_0, \mathcal{V}) \mathcal{V}_1 \\ \mathcal{V}_1'' &= 0. \end{aligned} \tag{4.26}$$

For $\mathcal{V}_1$ we get that $\mathcal{V}_1 = \mathcal{V}_{10} + \mathcal{V}_{11} y$. We also have that $\mathcal{L}u_0' = 0$.

The solvability condition on (4.26) is that

$$\int_{-\infty}^{\infty} g_v(u_0, \mathcal{V}) \mathcal{V}_1 u_0' dy = \int_{-\infty}^{\infty} \frac{w^2}{1 + bw^2} w' \mathcal{V}_1 dy = 0. \tag{4.27}$$

Substituting in $\mathcal{V}_1 = \mathcal{V}_{10} + \mathcal{V}_{11} y$, the condition from (4.27) implies that

$$\mathcal{V}_{10} \int_{-\infty}^{\infty} \frac{w^2 w'}{1 + bw^2} dy + \mathcal{V}_{11} \int_{-\infty}^{\infty} \frac{w^2 w' y}{1 + bw^2} dy = 0.$$

Since $\mathcal{V}_1 = O(\varepsilon)$, $\mathcal{V}_{11}$ has to be zero, as otherwise for $|y| \gg 1$ we would have $\mathcal{V}_1 = O(1)$. Consequently, $\mathcal{V}_{10}$ also has to be zero, and the conclusion is that $\mathcal{V}_1 = 0$. We have then that $\mathcal{L}u_1 = 0$, and therefore we also have $u_1 = 0$.

This result yields that

$$v_1(\chi_l) = v_1(\chi_r) = 0,$$

and now we have enough conditions to solve uniquely for v_1.

Using the fact that $\chi_r - \chi_l = l$, and that $\mathcal{V} w_+^2 = L/l$, the full solution to (4.24) is

$$v_1 = \begin{cases} \frac{\mathcal{V}}{2\mathcal{D}}(x^2 - \chi_l^2) & \text{for } 0 < x < \chi_l \\ \frac{\mathcal{V}(l-L)}{2\mathcal{D}l}[(x - \chi_l)^2 - l(x - \chi_l)] & \text{for } \chi_l < x < \chi_r \\ \frac{\mathcal{V}}{2\mathcal{D}}[(L - x)^2 - (L - \chi_r)^2] & \text{for } \chi_r < x < L \end{cases}$$

It is possible now to calculate $v_{1,x}$ close to the transition layers. We have

$$\begin{aligned} v_{1,x}(\chi_l^-) &= \frac{\mathcal{V}\chi_l}{\mathcal{D}}, \qquad & v_{1,x}(\chi_l^+) &= \frac{\mathcal{V}(L-l)}{2\mathcal{D}}, \\ v_{1,x}(\chi_r^-) &= -\frac{\mathcal{V}(L-l)}{2\mathcal{D}}, \qquad & v_{1,x}(\chi_r^+) &= -\frac{\mathcal{V}(L-\chi_r)}{\mathcal{D}}, \end{aligned} \tag{4.28}$$

This suggests that there is a term to next order, as $\mathcal{V}_2 \sim v_{1,x}(\chi_l)$. Expanding to next order in the inner region, as $u = u_0 + \varepsilon^2 u_2$ and $v = \mathcal{V} + \varepsilon^2 \mathcal{V}_2$, and defining $g_0(w) = \frac{w^2}{1+b_0 w^2}$, we have the system

$$\begin{aligned} \mathcal{L}u_2 = u_2'' - u_2 + g_0'(w)u_2 = g_0(w)\mathcal{V}_2, \\ \mathcal{V}_2'' = 0. \end{aligned}$$

We have then that $\mathcal{V}_2 = \mathcal{V}_{20} + y\mathcal{V}_{21}$.

We can derive a solvability condition from $\mathcal{L}u_2 = g_0(w)\mathcal{V}_2$, since $\mathcal{L}w' = 0$. We get

$$\int_{-\infty}^{\infty} \mathcal{V}_2 g_0(w) w' dy = \int_{-\infty}^{\infty} (\mathcal{V}_{20} + y\mathcal{V}_{21}) g_0(w) w' dy = 0,$$

We can now match the inner solution to the outer solution evaluated at the interface, to determine $\mathcal{V}_{20}$ and $\mathcal{V}_{21}$. We get that

$$\mathcal{V} + \varepsilon^2(\mathcal{V}_{20} + y\mathcal{V}_{21}) + \cdots = \mathcal{V} + \varepsilon\, v_1(\chi_l) + \varepsilon\, v_{1,x}(\chi_l^-)(x - \chi_l) + \varepsilon^2 v_2(\chi_l) + \cdots$$

From this we can conclude that $\mathcal{V}_{21} = v_{1,x}(\chi_l^-)$, and that $\mathcal{V}_{20} = v_2(\chi_l)$. This last value, for both the inner and outer solutions, can be calculated from the solvability condition given that we now know $\mathcal{V}_{21}$.

Furthermore, repeating the matching procedure with $x \to \chi_l^+$ yields the same value, as the outer solution has no ambiguity. From this we get that $v_{1,x}(\chi_l^+) =$

$v_{1,x}(\chi_l^-)$. Repeating the procedure yet again at the right boundary χ_r, we get the same result, i.e., $v_{1,x}(\chi_r^+) = v_{1,x}(\chi_r^-)$. Since we already knew from (4.28) that $v_{1,x}(\chi_l^+) = -v_{1,x}(\chi_r^-)$, we can solve for χ_l and χ_r to get that the position of the boundaries of the mesa on $[0, L]$ are

$$\chi_l = \frac{L-l}{2}, \qquad \chi_r = \frac{L+l}{2},$$

with l the length of the plateau. A corollary from this result is that stationary mesa solutions have to be centred.

We can find a second solvability condition that will be of use later on. Differentiating with respect to y, we have

$$\mathcal{L}u_2' = -g_0''(w)u_2w' + g_0(w)\mathcal{V}_2' + g_0'(w)\mathcal{V}_2w',$$

and using the fact that $\mathcal{L}w' = 0$, the solvability condition we get is

$$\begin{aligned} -\mathcal{V}_{21}\int_{-\infty}^{\infty} g_0(w)w'dy &= \int_{-\infty}^{\infty}(g_0'(w)\mathcal{V}_2 - g_0''(w)u_2)w'^2dy, \\ v_{1,x}(\chi_r)\int_{-\infty}^{\infty} g_0(w)w'dy &= \int_{-\infty}^{\infty}(g_0'(w)\mathcal{V}_2 - g_0''(w)u_2)w'^2dy, \end{aligned} \tag{4.29}$$

since $\mathcal{V}_2' = \mathcal{V}_{21} = -v_{1,x}(\chi_r)$.

4.4.2 Transverse stability in the near-shadow limit to perturbations in the y direction

We will now extend the solutions obtained in the previous section for a 1D mesa to $\mathbb{R}^2$ by extending the mesas along the y-direction to form stripes. We will study the stability to perpendicular perturbations, which can give rise to buckling in the solutions.

We assume that the solutions exist in a rectangular domain $[0, 1] \times [0, d_0]$, with

Neumann boundary conditions on all sides. We introduce a perturbation on the equilibrium solution (u_e, v_e) of the form

$$u = u_e + e^{\lambda t + imy}\phi(x), \qquad v = v_e + e^{\lambda t + imy}\psi(x); \quad m = \frac{k\pi}{d_0},\ k = 1, 2, \ldots,$$

with $|\phi| \ll 1$, and $|\psi| \ll 1$.

Substituting into (4.1), we get the following eigenvalue problem

$$\bar{\lambda}\phi = \mathcal{L}_\varepsilon\,\phi + g_v(u_e, v_e)\psi = \varepsilon^{\,2}\phi_{xx} - \phi + g_u(u_e, v_e)\phi + g_v(u_e, v_e)\psi, \quad \text{(4.30a)}$$

$$\frac{\varepsilon}{\mathcal{D}}(1 + \tau\lambda)\psi = \psi_{xx} - m^2\psi + \frac{2\varepsilon}{\mathcal{D}}u_e\phi, \quad \text{(4.30b)}$$

with $\bar{\lambda} = \lambda + \varepsilon^{\,2}m^2$, and Neumann conditions $\phi_x(0) = \phi_x(1) = \psi_x(0) = \psi_x(1) = 0$.

As shown in (4.25), in the plateau region we have that $g_u(u_e, v_e) = 2/w_+$, and $g_v(u_e, v_e) = -w_+$. Substituting into (4.30a), we have that, to first order and when $\bar{\lambda} \ll 1$, the asymptotic form of ϕ on the plateau region is

$$\phi = \mu\psi, \qquad \text{with} \quad \mu \equiv \frac{w_+^2}{2 - w_+}, \qquad \chi_l < x < \chi_r.$$

Near the boundary region ϕ is asymptotically small, therefore, near the transition layers located at χ_l, χ_r, ϕ is proportional to the derivative w' of the heteroclinic connection. We have then the following asymptotic form for ϕ

$$\phi \sim \begin{cases} c_{li}(w'(\varepsilon^{\,-1}(x - \chi_{li})) + O(\varepsilon)) & \text{for } x \sim \chi_{li} \\ c_{ri}(w'(\varepsilon^{\,-1}(x - \chi_{ri})) + O(\varepsilon)) & \text{for } x \sim \chi_{ri} \\ \phi_i = \mu\psi & \text{for } x \in (\chi_{li}, \chi_{ri}), \quad i = 1, \ldots, K, \end{cases}$$

with the constants c_{li}, c_{ri} to be found.

Since ϕ is localized near the transition layers, we can estimate it in the sense

of distributions, approximating u_e as $u_e \sim \mathcal{V}w$

$$\frac{2\varepsilon\, u_e\phi}{\mathcal{D}} \sim \sum_{i=1}^{K}\left(\frac{2\varepsilon^{\,2}\mathcal{V}c_l}{\mathcal{D}}\int_{-\infty}^{\infty} w_l w_l' dy\delta\left(x-\chi_{li}\right) \right.$$
$$\left. +\frac{2\varepsilon^{\,2}\mathcal{V}c_r}{\mathcal{D}}\int_{-\infty}^{\infty} w_r w_r' dy\delta\left(x-\chi_{ri}\right) + \frac{2\varepsilon\,\mathcal{V}}{\mathcal{D}} w_+\mu\psi H_{[\chi_{li},\chi_{ri}]}\right),$$

with $H_{[\chi_{li},\chi_{ri}]} = 1$ on $x \in (\chi_{li},\chi_{ri})$, and zero elsewhere.

This then yields

$$\frac{2\varepsilon\, u_e\phi}{\mathcal{D}} \sim \sum_{i=1}^{K}\left(\frac{\varepsilon^{\,2}\mathcal{V}c_l w_+^2}{\mathcal{D}}\delta\left(x-\chi_{li}\right) + \frac{\varepsilon^{\,2}\mathcal{V}c_r w_+^2}{\mathcal{D}}\delta\left(x-\chi_{ri}\right) \right.$$
$$\left. +\ \frac{2\varepsilon\,\mathcal{V}w_+\mu\psi H_{[\chi_{li},\chi_{ri}]}}{\mathcal{D}}\right)$$

Substituting into (4.30b), we get that ψ satisfies

$$\psi_{xx} - \theta^{\,2}\psi = -\frac{\varepsilon^{\,2}\mathcal{V}w_+^2}{\mathcal{D}}\left[\sum_i (c_{li}\delta\left(x-\chi_{li}\right) + c_{ri}\delta\left(x-\chi_{ri}\right))\right], \tag{4.31}$$

with θ the piecewise constant function

$$\theta = \begin{cases} \theta_- \equiv \left(m^2 + \frac{\varepsilon\,(1+\tau\lambda)}{\mathcal{D}}\right)^{1/2}, & \text{for } x \notin \cup_{i=1}^{K}[\chi_{li},\chi_{ri}] \\ \theta_+ \equiv \left(m^2 + \frac{\varepsilon}{\mathcal{D}}\left(1+\tau\lambda+\frac{2w_+}{l(w_+-2)}\right)\right)^{1/2}, & \text{for } x \in \cup_{i=1}^{K}[\chi_{li},\chi_{ri}] \end{cases} \tag{4.32}$$

Since w' is localized, we can define $w_{li}' = w'(x-\chi_{li})$ and $w_{ri}' = w'(x-\chi_{ri})$, and multiply it into (4.30a), to obtain the matrix eigenvalue problems

$$c_{li}(w_{li}', \mathcal{L}_\varepsilon\, w_{li}') + (w_{li}', g_v(u_e,v_e)\psi) = c_{li}\bar{\lambda}(w_{li}', w_{li}'), \tag{4.33a}$$
$$c_{ri}(w_{ri}', \mathcal{L}_\varepsilon\, w_{ri}') + (w_{ri}', g_v(u_e,v_e)\psi) = c_{ri}\bar{\lambda}(w_{ri}', w_{ri}'), \tag{4.33b}$$

where $(f,g) = \int_0^1 fg dx$.

The second term in (4.33a) and (4.33b) can be readily estimated, using the fact that $w'' - w = g_0(w)$, and that $g_v = -g_0$, with $g_0(w) = \frac{w^2}{1+b_0 w^2}$, as

$$\begin{aligned}(w'_{li}, g_v(u_e, v_e)\psi) &= \int_0^1 w'_{li}\psi g_v(u_e, v_e)dx = -\varepsilon \sum_{i=1}^{K} \psi(\chi_{li}) \int_{-\infty}^{\infty} w' g_0(w)dy \\ &= -\varepsilon \sum_{i=1}^{K} \psi(\chi_{li}) \int_{-\infty}^{\infty} w'(w'' - w)dy = -\varepsilon \sum_{i=1}^{K} \psi(\chi_{li}) \frac{w_+^2}{2},\end{aligned}$$

and similarly,

$$(w'_{ri}, g_h(u_e, v_e)\psi) = -\varepsilon \sum_{i=1}^{K} \psi(\chi_{ri}) \frac{w_+^2}{2}.$$

The third term can be estimated straight from the definition of β in (4.23). We get

$$(w'_{li}, w'_{li})) \sim \varepsilon \int_{-\infty}^{\infty} (w')^2 dy = \varepsilon\, \beta.$$

The first term can be estimated using some of the results previously obtained. We have that

$$\mathcal{L}_\varepsilon\, w'_l = (w'_l)'' - w'_l + g_u(u_e, v_e)w'_l.$$

We can approximate $g_u(u_e, v_e)$ as

$$g_u(u_e, v_e) \sim g_u(w\mathcal{V}, \mathcal{V}) + \varepsilon^2 (g_{uu}(w\mathcal{V}, \mathcal{V}) + g_{uv}(w\mathcal{V}, \mathcal{V})) + \cdots .$$

The derivatives can be related to $g_0(w) = \frac{w^2}{1+b_0 w^2}$ in the following way:

$$
\begin{aligned}
g_u(u,v) &= \frac{2u}{v(1+ku^2)^2} \sim \frac{2w}{(1+b_0w^2)^2} = g_0'(w),\\
g_{uu}(u,v) &= \frac{1}{v}\frac{2-6ku^2}{(1+ku^2)^3} \sim \frac{1}{\mathcal{V}}\frac{2-6b_0w^2}{(1+b_0w^2)^3} = \frac{1}{\mathcal{V}}g_0''(w),\\
g_{uv}(u,v) &= -\frac{2u}{v^2(1+ku^2)^2} \sim -\frac{2w}{\mathcal{V}(1+b_0w^2)^2} = -\frac{1}{\mathcal{V}}g_0'(w).
\end{aligned}
$$

Substituting them in, we get

$$
\begin{aligned}
g_u(u_e,v_e) &\sim g_0'(w) + \frac{\varepsilon^2}{\mathcal{V}}(g_0''(w)u_2 - g_0'(w)\mathcal{V}_2) + \cdots,\\
\mathcal{L}_\varepsilon w_{li}' &\sim \frac{\varepsilon^2}{\mathcal{V}}(g_0''(w_{li})u_2 - g_0'(w_{li})\mathcal{V}_2)w_{li}'.
\end{aligned}
$$

We can now express the first term as

$$
\begin{aligned}
(w_{li}', \mathcal{L}_\varepsilon w_{li}') &\sim \frac{\varepsilon^2}{\mathcal{V}}\int_0^1 \left(g_0''(w_{li})u_2 - g_0'(w_{li})\mathcal{V}_2\right) w_{li}'^2 dx\\
&= \frac{\varepsilon^3}{\mathcal{V}}\int_{-\infty}^{\infty} \left(g_0''(w_{li})u_2 - g_0'(w_{li})\mathcal{V}_2\right) w_{li}'^2 dy
\end{aligned}
$$

Using the solvability condition in (4.29),

$$
\mathcal{V}_2'\int_{-\infty}^{\infty} g_0(w)w'dy = \int_{-\infty}^{\infty}(g_0'(w)\mathcal{V}_2 - g_0''(w)u_2)w'^2 dy,
$$

we get

$$
\begin{aligned}
(w_{li}', \mathcal{L}_\varepsilon w_{li}') &\sim \frac{\varepsilon^3}{\mathcal{V}}\mathcal{V}_2'\int_{-\infty}^{\infty} g_0(w)w'dy = \frac{\varepsilon^3}{\mathcal{V}}\mathcal{V}_2'\int_{-\infty}^{\infty}(w-w'')w'dy\\
&= \frac{\varepsilon^3\mathcal{V}_2'}{2\mathcal{V}}w_+^2 = \frac{\varepsilon^3 v_{1x}(\chi_{li})w_+^2}{2\mathcal{V}}
\end{aligned}
$$

Similarly, on the other side of the plateau the process is identical, except for a sign change in the slope,

$$(w'_{ri}, \mathcal{L}_\varepsilon\, w'_{ri}) \sim -\frac{\varepsilon^{\,3} v_{1x}(\chi_{ri}) w_+^2}{2\mathcal{V}}$$

Putting everything together results in the following $2K \times 2K$ system

$$\begin{aligned}
\varepsilon\, \bar{\lambda} c_{li} \beta &\sim \frac{\varepsilon^{\,3}}{2\mathcal{V}} c_{li} v_{1x}(\chi_{li}) w_+^2 - \frac{\varepsilon}{2}\psi(\chi_{li}) w_+^2, \\
\varepsilon\, \bar{\lambda} c_{ri} \beta &\sim -\frac{\varepsilon^{\,3}}{2\mathcal{V}} c_{ri} v_{1x}(\chi_{ri}) w_+^2 - \frac{\varepsilon}{2}\psi(\chi_{ri}) w_+^2,
\end{aligned}$$

and since from (4.28) we know that

$$v_{1x}(\chi_{li}) = v_{1x}(\chi_{ri}) = \frac{\mathcal{V}(L-l)}{2\mathcal{D}},$$

the above system can be simplified to

$$\begin{aligned}
\bar{\lambda}\beta c_{li} &\sim \varepsilon^{\,2} \frac{(L-l) w_+^2}{4\mathcal{D}} c_{li} - \frac{w_+^2}{2}\psi(\chi_{li}), \\
\bar{\lambda}\beta c_{ri} &\sim -\varepsilon^{\,2} \frac{(L-l) w_+^2}{4\mathcal{D}} c_{ri} - \frac{w_+^2}{2}\psi(\chi_{ri}).
\end{aligned} \tag{4.34}$$

This equation, together with (4.31) constitutes a system for $\bar{\lambda}$ and $\vec{c} = [c_{li}, c_{ri}]$.

The system given in (4.34) depends on $\psi(\chi_{ri})$ and $\psi(\chi_{li})$. Solving (4.31) explicitly, we get

$$\psi(x) = \begin{cases}
\psi(\chi_{l1}) \frac{\cosh(\theta_-(x))}{\cosh(\theta_-\chi_{l1})}, & \text{for } 0 < x < \chi_{l1} \\
\psi(\chi_{li}) \frac{\sinh(\theta_+(\chi_{ri}-x))}{\sinh(\theta_+(\chi_{ri}-\chi_{li}))} + \psi(\chi_{ri}) \frac{\sinh(\theta_+(x-\chi_{li}))}{\sinh(\theta_+(\chi_{ri}-\chi_{li}))}, & \text{for } \chi_{li} < x < \chi_{ri} \\
\psi(\chi_{ri}) \frac{\sinh(\theta_-(\chi_{l(i+1)}-x))}{\sinh(\theta_-(\chi_{l(i+1)}-\chi_{ri}))} + \psi(\chi_{l(i+1)} \frac{\sinh(\theta_-(x-\chi_{ri}))}{\sinh(\theta_-(\chi_{l(i+1)}-\chi_{ri}))}, & \text{for } \chi_{ri} < x < \chi_{l(i+1)} \\
\psi(\chi_{rK}) \frac{\cosh(\theta_-(1-x))}{\cosh(\theta_-(1-\chi_{rK}))}, & \text{for } \chi_{rK} < x < 1
\end{cases} \tag{4.35}$$

for $i = 1, \ldots, K$.

We have that $\chi_{ri} - \chi_{li} = l$; similarly, we define $d \equiv \chi_{l(i+1)} - \chi_{ri} = \frac{1}{K} - l$, and the constants

$$\begin{aligned} c_l &= \cosh(\theta_+ l), \qquad & s_l &= \sinh(\theta_+ l), \\ c_d &= \cosh(\theta_- d), \qquad & s_d &= \sinh(\theta_- d) \end{aligned}$$

Additionally, the jump conditions that solution (4.35) has to satisfy are given by

$$\begin{aligned} -[\psi_x(\chi_{li}^+) - \psi_x(\chi_{li}^-)] &= \frac{\varepsilon^2 \mathcal{V} w_+^2}{\mathcal{D}} c_{li} \equiv b_{li}, \\ -[\psi_x(\chi_{ri}^+) - \psi_x(\chi_{ri}^-)] &= \frac{\varepsilon^2 \mathcal{V} w_+^2}{\mathcal{D}} c_{ri} \equiv b_{ri}, \end{aligned} \tag{4.36}$$

for $i = 1, \ldots, K$.

This results in a linear system, with b_{li} defined as

$$\begin{aligned} b_{li} &= \psi_{r(i-1)} \theta_- \left(s_d - \frac{c_d^2}{s_d} \right) - \psi_{ri} \frac{\theta_+}{s_l} + \psi_{li} \left(\theta_- \frac{c_d}{s_d} + \theta_+ \frac{c_l}{s_l} \right) \\ &= -\psi_{r(i-1)} \frac{\theta_-}{s_d} - \psi_{ri} \frac{\theta_+}{s_l} + \psi_{li} \left(\theta_- \frac{c_d}{s_d} + \theta_+ \frac{c_l}{s_l} \right), \end{aligned}$$

and similarly,

$$b_{ri} = -\psi_{l(i+1)} \frac{\theta_-}{s_d} - \psi_{li} \frac{\theta_+}{s_l} + \psi_{ri} \left(\theta_+ \frac{c_l}{s_l} + \theta_- \frac{c_d}{s_d} \right),$$

for $i = 2, \ldots, K-1$. The values at the boundaries are slightly different and have to be derived separately. Using the identity

$$\frac{\sinh(x/2)}{\cosh(x/2)} = \frac{\cosh(x) - 1}{\sinh(x)},$$

we finally have that

$$b_{l1} = \psi_{l1}\left(\theta_- \frac{c_d}{s_d} - \frac{\theta_-}{s_d} + \theta_+ \frac{c_l}{s_l}\right) - \psi_{r1}\frac{\theta_+}{s_l}$$
$$b_{rK} = \psi_{rK}\left(\theta_- \frac{c_d}{s_d} - \frac{\theta_-}{s_d} + \theta_+ \frac{c_l}{s_l}\right) - \psi_{lK}\frac{\theta_+}{s_l}.$$

We can now write the $2K \times 2K$ system of equations in matrix form as $M\vec{\psi} = \vec{b}$, with M the tridiagonal matrix

$$M = \begin{bmatrix} a+c & b & & & & & & & \\ b & c & a & & & & & & \\ & a & c & b & & & & & \\ & & & \ddots & & & & & \\ & & & & b & c & a & & \\ & & & & & a & c & b & \\ & & & & & & b & c+a \end{bmatrix},$$

and where

$$a = -\frac{\theta_-}{s_d}, \qquad b = -\frac{\theta_+}{s_l}, \qquad c = \frac{c_d}{s_d}\theta_- + \frac{c_l}{s_l}\theta_+.$$

The eigenpairs of M can be found explicitly (appendix B in [48]), and for the reader's convenience we will reproduce the calculation.

The M matrix can be simplified into $M = Q + cI$, with

$$Q = \begin{bmatrix} a & b & & & & & & \\ b & 0 & a & & & & & \\ & a & 0 & b & & & & \\ & & & \ddots & & & & \\ & & & & b & 0 & a & \\ & & & & & a & 0 & b \\ & & & & & & b & a \end{bmatrix}.$$

We use the property that $\text{eig}(M) = c + \text{eig}(Q)$. We start by looking for an eigenvector $\vec{q} = [z, tz^2, z^3, tz^4, \ldots, tz^{2K}]^T$, with $t, z \in \mathbb{C}$, $|z| = 1$, and corresponding eigenvalue σ. From the second equation to the second to last we get the following system,

$$\begin{aligned} atz^{1-l} + btz^{1+l} &= \sigma z^l, \qquad \text{if } l \text{ is odd,} \\ bz^{1-l} + az^{1+l} &= \sigma tz^l, \qquad \text{if } l \text{ is even.} \end{aligned} \tag{4.37}$$

Since $z\bar{z} = 1$, hence $1/z = \bar{z}$, we can solve for t in the above system to get

$$t = \pm \frac{az + b\bar{z}}{|az + b\bar{z}|},$$

which implies that $|t| = 1$.

In order to satisfy the first and last equations, we look at the extended system $Q(Ah + B\bar{h}) = \sigma(Ah + B\bar{h})$, with $h = [t, \vec{q}, tz^{2K+1}]^T$. The first and last equations are

$$\begin{gathered} a(At + B\bar{t}) + b(Az + B\bar{z}) = \sigma(At + B\bar{t}), \\ b(Atz^{2K} + B\bar{t}\bar{z}^{2K}) + a(Az^{2K+1} + B\bar{z}^{2K+1}) = \sigma(Az^{2K+1} + B\bar{z}^{2K+1}). \end{gathered}$$

The first and last equations will then be satisfied if

$$At + B\bar{t} = Az + B\bar{z},$$
$$Atz^{2K} + B\bar{t}\bar{z}^{2K} = Az^{2K+1} + B\bar{z}^{2K+1}.$$

Nontrivial solutions for A and B exist if

$$(z-t)(1-\bar{t}\bar{z})\bar{z}^{2K} = (\bar{z}-\bar{t})(1-tz)z^{2K}$$

is satisfied. Since $|z| = |t| = 1$, we have then that $z^{4K} = 1$. If we write z in polar form, we have that the roots of $z^{4K} = 1$ are $z = e^{i\frac{2\pi(j-1)}{2K}}$, with $j = 1, 2, \ldots, 2K$. Substituting it into (4.37), we get

$$\sigma = \pm|az + b\bar{z}| = \pm\sqrt{a^2 + b^2 + 2ab\cos(\theta)},$$

with $\theta = \frac{2\pi(j-1)}{2K}$. Since we have both positive and negative values, we are counting twice when ranging $j = 1, \ldots, 2K$; therefore the range can be restricted to obtain the following set of distinct eigenvalues

$$\sigma_{j\pm} = \pm\sqrt{a^2 + b^2 + 2ab\cos\theta_j}, \qquad \text{with } \theta_j = \frac{\pi j}{K}, \qquad j = 1, \ldots, K-1,$$
$$\sigma_{K\pm} = a \pm b.$$

Going back to (4.36), we can express the jump condition as the following system,

$$\vec{\psi} = M^{-1}\vec{b} = \frac{\varepsilon^2 \mathcal{V} w_+^2}{D} M^{-1}\vec{c},$$

and we can use it to substitute $\vec{\psi}$ in (4.34), resulting in the system

$$\bar{\lambda}\beta\vec{c} = \varepsilon^2 \left(\frac{(L-l)w_+^2}{4\mathcal{D}} I - \frac{\mathcal{V} w_+^4}{2\mathcal{D}} M^{-1} \right) \vec{c}. \tag{4.38}$$

Since $\bar{\lambda} = \lambda + \varepsilon^2 m^2$, and $M^{-1}\vec{c} = \hat{\sigma}^{-1}\vec{c}$, with $\hat{\sigma} = c + \sigma$, we have then that

in the limit when $\varepsilon \to 0$,

$$\lim_{\varepsilon \to 0} \frac{\lambda_{j\pm}}{\varepsilon^2} = -m^2 + \frac{(L-l)w_+^2}{4\mathcal{D}\beta} - \frac{\mathcal{V}w_+^4}{2\mathcal{D}\beta}\hat{\sigma}_{j\pm}^{-1}, \qquad j = 1, \ldots, K.$$

To establish the stability of the system, we want to establish conditions that guarantee that the eigenvalues will be negative, hence stable.

The largest eigenvalue corresponds to the largest $\hat{\sigma}$ value; since both a and b are negative, the largest σ values corresponds to $j = 1$; and as the number of mesas increases the largest eigenvalue tends to $c + |a + b|$.

On the other end of the spectrum, we have that the smallest eigenvalue is always positive,

$$c+a+b = c-|a+b| = \frac{c_d\theta_-}{s_d} + \frac{c_l\theta_+}{s_l} - \frac{\theta_-}{s_d} - \frac{\theta_+}{s_l} = \frac{s_l\theta_-(c_d-1) + s_d\theta_+(c_l-1)}{s_d s_l},$$

since $\cosh(x) > 1$ for $x \neq 0$.

From (4.32) we have that to leading order both $\theta_-, \theta_+ \sim m$. Let

$$\hat{a} = \frac{-1}{\sinh(md)}, \qquad \hat{b} = \frac{-1}{\sinh(ml)}, \qquad \hat{c} = \coth(md) + \coth(ml),$$

the stability condition is, then

$$\begin{aligned}\frac{(L-l)w_+^2}{4\mathcal{D}\beta} &< m^2 + \frac{\mathcal{V}w_+^4}{2\mathcal{D}\beta}\hat{\sigma}_{j\pm}^{-1} \\ &= m^2 + \frac{Lw_+^2}{2\mathcal{D}\beta lm}\left[\frac{1}{\hat{c} \pm \sqrt{\hat{a}^2 + \hat{b}^2 + 2\hat{a}\hat{b}\cos\left(\frac{\pi j}{K}\right)}}\right],\end{aligned}$$

for all $j = 1, \ldots, K-1$, and $m = \frac{k\pi}{d_0}$, $k = 1, \ldots$.

A sufficient condition for stability is as follows: if

$$\mathcal{D} > \frac{(L-l)w_+^2 d_0^2}{4\pi^2\beta}$$

then the $K-$stripe system will be stable.

For the $m = 0$ mode, and to first order, we approximate a, b, and c as

$$a = -\frac{1}{d} + O(\varepsilon), \qquad b = -\frac{1}{l} + O(\varepsilon), \qquad c = \frac{1}{d} + \frac{1}{l} + O(\varepsilon),$$

Since $\hat{\sigma}_{K+} = a + b + c$ would be zero to first order, we can approximate c to second order for that particular case, resulting in

$$c = \frac{1}{d} + \frac{1}{l} + \frac{1}{2}(d\theta_-^2 + l\theta_+^2) + O(\varepsilon^2).$$

We have then that

$$\begin{aligned}
\hat{\sigma}_{j\pm} &\sim \frac{1}{d} + \frac{1}{l} \pm \sqrt{\frac{1}{d^2} + \frac{1}{l^2} + \frac{2}{dl}\cos(\theta_j)}, \qquad j = 1, \ldots, K-1, \\
\hat{\sigma}_{K+} &\sim \frac{1}{2}(d\theta_-^2 + l\theta_+^2), \\
\hat{\sigma}_{K-} &\sim \frac{2}{l}.
\end{aligned}$$

Similarly, we have that the eigenvalues $\lambda_{j\pm}$ for the full system, for the $m = 0$

mode, are

$$\lambda_{K+} = \varepsilon^2 \left(\frac{(L-l)w_+^2}{4\mathcal{D}\beta} - \frac{Lw_+^2}{2\mathcal{D}\beta l}\sigma_{K+}^{-1} \right), \tag{4.39a}$$

$$= -\varepsilon \frac{Lw_+^2}{\beta l}\left[\frac{1}{K} - \frac{2w_+}{2-w_+} \right]^{-1} + O(\varepsilon^2) < 0,$$

$$\lambda_{K-} = \varepsilon^2 \left(\frac{(L-l)w_+^2}{4\mathcal{D}\beta} - \frac{Lw_+^2}{2\mathcal{D}\beta l}\frac{l}{2} \right) = -\varepsilon^2 \frac{lw_+^2}{4\mathcal{D}\beta} < 0, \tag{4.39b}$$

$$\lambda_{j\pm} = \varepsilon^2 \left(\frac{(L-l)w_+^2}{4\mathcal{D}\beta} - \frac{Lw_+^2}{2\mathcal{D}\beta l}\sigma_{j\pm}^{-1} \right), \qquad j = 1, \ldots, K-1, \tag{4.39c}$$

$$< \varepsilon^2 \left(\frac{(L-l)w_+^2}{4\mathcal{D}\beta} - \frac{Lw_+^2}{2\mathcal{D}\beta l}\left[\frac{2}{d} + \frac{2}{l} \right]^{-1} \right),$$

$$= \varepsilon^2 \left(\frac{(L-l)w_+^2}{4\mathcal{D}\beta} - \frac{Lw_+^2}{2\mathcal{D}\beta l}\left[\frac{l(L-l)}{2L} \right] \right) = 0,$$

with (4.39a) being negative resulting from the previous numerical estimation $w_+ \sim 3.30$ in (4.22).

This shows that for the mode $m = 0$, all the eigenvalues λ_j, $j = 1, \ldots, K$ are negative. Hence, a 1-D $K-$stripe mesa pattern with $D = O(\varepsilon^{-1})$ is a stable solution to the GMS system.

For the GMS system, we computed the eigenvalues of a two-mesa solution. Of the four possible eigenvalues, their corresponding eigenvectors show that the instabilities will lead to either two breather stripes, or two zigzag stripes (using the notation from [22]). In the Figures 4.12 we have the four eigenvalues as a function of the mode m. The most unstable pair corresponds to a zigzag-type instability, and the other two correspond to a breather instability.

We also found the critical value where $\frac{d\lambda}{dm} = 0$ and $\lambda = 0$ for one of the breather and zigzag eigenvalues.

Using these results we simulated the full system on a 2D domain $(-1, 1) \times (0, d_0)$. Varying the length of the domain d_0, we observed mode-one and mode-

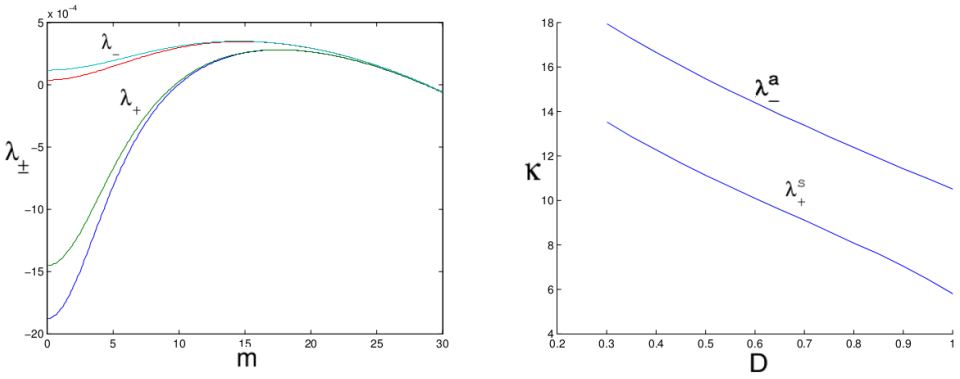

Figure 4.12: Eigenvalues for a two mesa solution. The parameters are $D = 0.5$, $\varepsilon = 0.001$ and $\kappa = 3$ for the Figure on the left. The λ_- eigenvalues are the zigzag ones, while λ_+ are the breather ones. The Figure on the right has the critical (κ, D) values for instability.

two instabilities develop over time (Figures 4.13). Since the mode $m = \frac{k\pi}{d_0}$, it

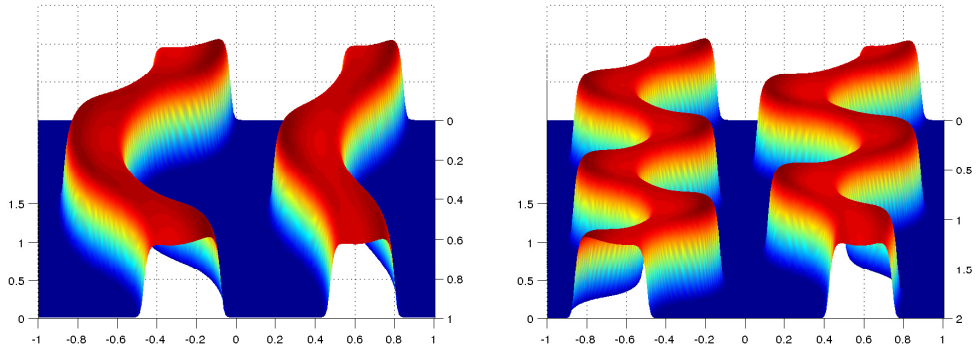

Figure 4.13: Full 2D simulation with parameters $\varepsilon = 0.01$, $D = 0.5$, $\kappa = 1.5$. The solutions were integrated using an IMEX algorithm. The solution on the left has $d_0 = 1.5$, and the solution on the right has $d_0 = 2$.

is immediate from the formula in (4.38) that increasing the domain width will destabilize the system.

Both solutions were integrated until $T = 10,000$ from an initial condition that had previously converged to two mesa stripes, and that had a small amount of noise added. When integrating the same system for $d_0 = 1$ no transverse instabilities were observed up to $T = 20,000$.

Chapter summary

In this chapter we analyzed mesa-type solutions to the GMS system. We started by analyzing the Turing-type solutions and considering the case of domain growth. We used numerical continuation to extend the Turing solutions to the fully nonlinear regime, where we observed the solutions split as the domain length was increased. We studied the cases of both a dynamically growing domain and adiabatic growth.

We next constructed a matched asymptotic solution for the fully nonlinear regime by joining two heteroclinic solutions. Studying its stability we were able to corroborate the splitting thresholds observed numerically in the splitting regime. Upon extending the mesas into stripes on the plane, we were able to derive analytic thresholds for the stability to perpendicular perturbations of multiple mesas, and verified it with full numerics.

In the next chapter we will extend the theory developed for the GMS system to general mesa systems, and apply the model to a Predator-Prey model.

Chapter 5

The stability of mesa stripes in general reaction-diffusion systems

We have previously studied the stability of mesa stripes in the GMS model in both one and two dimensions, and considered the parameter regimes $D = O(1)$ and $D = O(\varepsilon^{-1})$. In this chapter we will extend this previous analysis and obtain analytical results for the stability of a mesa stripe pattern for a general reaction-diffusion system when $D = \mathcal{D}/\varepsilon$, with $\mathcal{D} = O(1)$. At the end of the chapter we will apply the results to a predator-prey RDE.

The general system that we will study is the following two-component set of reaction diffusion equations:

$$\begin{aligned} u_t &= \varepsilon^2 \Delta u + f(u,v) \\ \tau v_t &= \frac{\mathcal{D}}{\varepsilon}\Delta v + g(u,v), \end{aligned} \tag{5.1}$$

with homogeneous Neumann boundary conditions on $x \in [0,1] \times [0,d_0]$. We

consider the limit where $\varepsilon \ll 1$, and regard all the other constants as being $O(1)$. Some conditions on f and g are needed for the existence of a mesa pattern (see below),

5.1 Construction of the solution in the near-shadow limit

The following analysis is based on work done by Kolokolnikov and McKay [32]. We will use their results to extend the analysis done earlier for the GMS model to consider the transverse stability of a general stripe pattern.

We want to construct a $K-$stripe stationary mesa solution on $x \in [0,1]$. A mesa structure is characterized as a function $u(x) \sim u_+$ on $-l < x < l$, and $u(x) \sim u_-$ on $l < |x| < L$; with $u_+ > u_-$, and both values joined by a sharp interface.

The mesa pattern will be formed by two back-to-back interfaces. We will start by constructing a solution on $[0, L]$, with the interface centred at $x = l$. A full mesa solution can then be constructed by adding an even reflection, and a $K-$mesa solution will simply be K copies, with $2K$ interfaces. The stationary equation we want to solve is

$$\begin{aligned} 0 &= \varepsilon^2 u_{xx} + f(u,v), & u_x(-L) = u_x(L) = 0, \\ 0 &= \frac{\mathcal{D}}{\varepsilon} v_{xx} + g(u,v), & v_x(-L) = v_x(L) = 0. \end{aligned} \tag{5.2}$$

To first order, we have $v_{xx} = 0$. Applying the Neumann boundary condition, we have then that $v \sim \mathcal{V}$, and the value of the constant can be estimated by integrating over the whole domain. The resulting equation is

(5.3)

with $v = \mathcal{V}$ constant.

Now, we are looking for a heteroclinic connection in u as the transition mechanism connecting $u = u_+$ to $u = u_-$. This imposes the algebraic constraint that $f(u_+, \mathcal{V}) \equiv f_+ = 0$, and $f(u_-, \mathcal{V}) \equiv f_- = 0$, which has to be satisfied together with the Maxwell line condition [31] $\int_{u_-}^{u_+} f(w, \mathcal{V})dw = 0$. For both branches to be stable we also require $f_u(u_\pm, \mathcal{V}) < 0$. Solving the algebraic system determines $u_\pm$, and $v_0 = \mathcal{V}$.

In the inner region near the interface of the mesa, we have that $v \sim \mathcal{V}$, and we do a change of variables for $y = \varepsilon^{-1}(x - l)$, and $u(x) \sim U_0(\frac{x-l}{\varepsilon})$. Integrating (5.3) in two parts across the interface yields the following result

$$
\begin{aligned}
0 = \frac{D}{\varepsilon}\int_0^l v_{xx} + \int_0^l g(u, \mathcal{V})dx \qquad &\Rightarrow \qquad \frac{D}{\varepsilon}v_x(l^-) = -lg_+, \\
0 = \frac{D}{\varepsilon}\int_l^L v_{xx} + \int_l^L g(u, \mathcal{V})dx \qquad &\Rightarrow \qquad \frac{D}{\varepsilon}v_x(l^+) = (L - l)g_-.
\end{aligned}
$$

Since the v solution doesn't have sharp interfaces, we obtain to leading order that

$$
l = \frac{g_-}{g_- - g_+}L + O(\varepsilon). \tag{5.4}
$$

Furthermore, since $0 < l < L$, we require that the following consistency condition be satisfied:

$$
0 < \frac{g_-}{g_- - g_+} < 1, \tag{5.5}
$$

Here, as with $f_\pm$, we have defined $g_\pm \equiv g(u_\pm, \mathcal{V})$.

We will divide the half-mesa branch into three regions: the outer part on the mesa plateau, $0 < x < l$; the outer part of the mesa beyond the plateau, $x > l$; and the internal layer around $x = l$ bridging the two outer regions.

To zoom into the inner layer we let $y = \frac{x-l}{\varepsilon}$, $u(\varepsilon\, y + l) \equiv U(y)$, $v(\varepsilon\, y + l) \equiv$

$V(y)$, which when substituted into (5.2) result in

$$\begin{aligned} &U_{yy} + f(U,V) = 0, && \infty < y < \infty, && U \to U_{\pm} \text{ as } y \to \mp\infty, \\ &V_{yy} + \frac{\varepsilon}{\mathcal{D}}^3 g(U,V) = 0, && \infty < y < \infty, && V \to V_{\pm} \text{ as } y \to \mp\infty. \end{aligned} \tag{5.6}$$

In the outer region, $0 < x < l$, we have

$$\begin{aligned} &f(u,v) = 0, && u_x(0) = 0, \\ &v_{xx} + \frac{\varepsilon}{\mathcal{D}} g(u,v) = 0, && v_x(0) = 0. \end{aligned}$$

with the boundary conditions stemming from the even symmetry imposed on the mesas. Similarly, for the region $x > l$ we have

$$\begin{aligned} &f(u,v) = 0, && u_x(L) = 0, \\ &v_{xx} + \frac{\varepsilon}{\mathcal{D}} g(u,v) = 0, && v_x(L) = 0. \end{aligned} \tag{5.7}$$

Performing an asymptotic expansion $u = u_- + \frac{\varepsilon}{\mathcal{D}} u_1 + \cdots$, $v = \mathcal{V} + \frac{\varepsilon}{\mathcal{D}} v_1 + \cdots$, and substituting into a Taylor expansion of $f(u,v)$ in (5.7), we obtain

$$f(u_-, \mathcal{V}) + \frac{\varepsilon}{\mathcal{D}}(f_u^- u_1 + f_v^- v_1) + \cdots = 0.$$

Therefore, $u_1 = -\frac{f_v^-}{f_u^-} v_1$, where $f_v^{\pm} = f_v(u_{\pm}, \mathcal{V})$, and $f_u^{\pm} = f_u(u_{\pm}, \mathcal{V})$.

From (5.7) we also obtain that

$$\begin{aligned} &v_{1xx} = -g_-, && \text{on } l < x < L, && \text{with } g_- = g(u_-, \mathcal{V}), \\ &v_{1x}(L) = 0, && v_1(l^+) = v_{1-}, \end{aligned} \tag{5.8}$$

where we have imposed the boundary condition $v_1(l^+) = v_{1-}$ in terms of an unknown constant v_{1-} to be calculated later.

The solution in this region is

$$v_1(x) = -g_- \left(\frac{1}{2}(x-L)^2 - \frac{1}{2}(L-l)^2 \right) + v_{1-}. \tag{5.9}$$

Therefore, we have that in the outer region $l < x < L$

$$\begin{aligned} u &\sim u_- + \frac{\varepsilon}{\mathcal{D}} \left(-\frac{f_v^-}{g_u^-} v_1(x) \right), \\ v &\sim \mathcal{V} + \frac{\varepsilon}{\mathcal{D}} v_1(x). \end{aligned} \tag{5.10}$$

Either by taking the derivative of(5.10), or integrating (5.8) over $l < x < L$ we get that $v_{1x}(l^+) \equiv v'_{1-} = g_-(L-l)$.

An analogous calculation in the outer region $0 < x < l$ yields

$$\begin{aligned} &u \sim u_+ + \frac{\varepsilon}{\mathcal{D}} \left(-\frac{f_v^+}{g_u^+} v_1(x) \right), \\ &v \sim \mathcal{V} + \frac{\varepsilon}{\mathcal{D}} v_1(x), \quad \text{with} \quad v_1(x) = -g_+ \left(\frac{1}{2}x^2 - \frac{l^2}{2} \right) + v_{1+}, \end{aligned}$$

again with a boundary condition $v_1(l^-) = v_{1+}$ in terms of an unknown constant to be found.

Threfore, for both sides of the interface, we have

$$\begin{aligned} v_{1x}(l^-) &\equiv v'_{1+} = -g_+ l, \\ v_{1x}(l^+) &\equiv v'_{1-} = g_-(L-l). \end{aligned} \tag{5.11}$$

Taylor expanding both solutions near $x = l^{\pm}$ provides matching conditions for the inner solution. The problem for the inner layer, in terms of the variable

$y = \varepsilon^{-1}(x-l)$, is

$$U_{yy} + f(U,V) = 0, \quad -\infty < y < \infty, \quad U \sim u_{\pm} - \frac{\varepsilon}{\mathcal{D}} \frac{f_v^{\pm}}{f_u^{\pm}} v_{1\pm} \text{ as } y \to \mp\infty,$$
$$V_{yy} = -\frac{\varepsilon^3}{\mathcal{D}} g(U,V), \quad -\infty < y < \infty, \quad V \sim \mathcal{V} + \frac{\varepsilon}{\mathcal{D}}(V_{1\pm} + \varepsilon\, y V_{1\pm}') \text{ as } y \to \mp\infty.$$

Expanding the inner solution, $U = U_0 + \frac{\varepsilon}{\mathcal{D}} U_1 + \cdots$, $V = V_0 + \frac{\varepsilon}{\mathcal{D}} V_1 + \cdots$, we get

$$\mathcal{L}(U_1) = U_{1yy} + f_U(U_0,V_0)U_1 = -f_V(U_0,V_0)V_1,$$
$$V_{1yy} = 0.$$

The matching condition for $V_1 = h_1 y + h_2$ is $V_1 \sim v_{1\pm}$ as $y \to \mp\infty$. Thus, we must have that $h_1 = 0$, and $h_2 = v_{1+} = v_{1-} = V_1$.

A solvability condition can be obtained, since by translational invariance we have that $\mathcal{L}(U_0') = 0$. Hence

$$\int_{-\infty}^{\infty} (U_0' \mathcal{L} U_1 - U_1 \mathcal{L} U_0') dy = -V_1 \int_{-\infty}^{\infty} U_0' f_V(U_0,V_0) dy = 0.$$

We can conclude then that if $f_V \neq 0$, then $V_1 = 0$, thus $V_{1\pm} = 0$. We also have then that $U_1 = cU_0'$, and without loss of generality we take $c = 0$.

To $O(\varepsilon)$ we have then

$$v(x) = \begin{cases} \mathcal{V} + \frac{\varepsilon}{2\mathcal{D}} \left(g_-(x-L)^2 + g_-(L-l)^2 \right), & l < x < L, \\ \mathcal{V} - \frac{\varepsilon}{2\mathcal{D}} g_+(x^2 - l^2), & 0 < x < l. \end{cases}$$
$$u(x) = \begin{cases} u_- + O(\frac{\varepsilon^2}{\mathcal{D}}), & l < x < L, \\ u_+ + O(\frac{\varepsilon^2}{\mathcal{D}}), & 0 < x < l. \end{cases} \tag{5.12}$$

In the inner region we expand to second order, $u = U_0 + \frac{\varepsilon^2}{\mathcal{D}} U_2 + \cdots$ and $v = \mathcal{V} + \frac{\varepsilon^2}{\mathcal{D}} V_2 + \cdots$, to get

$$\begin{aligned} \mathcal{L}(U_2) = U_{2yy} + f_U(U_0, V_0) U_2 &= -f_V(U_0, V_0) V_2, \\ V_{2yy} &= 0, \end{aligned}$$

with the matching condition that $V_2 \sim y v'_{1\pm}$ as $y \to \mp\infty$, and v_1 the $O(\varepsilon/\mathcal{D})$ term for $v(x)$ in (5.12).

We must have then that $V_2(y) = H_{20} + y H_{21}$, and we can conclude that $H_{21} = V'_{1+} = V'_{1-}$. Using (5.11), we can now recover the result from (5.4):

$$g_-(L - l) = -g_+ l \qquad \to \qquad l = \frac{g_-}{g_- - g_+} L.$$

The constant H_{20} can be found in terms of H_{21} via a solvability condition, since $\mathcal{L} U'_0 = 0$, and

$$\mathcal{L} U_2 = U_{2yy} + f_U(U_0, V_0) U_2 = -f_V(U_0, V_0)(H_{20} + y H_{21}),$$

We have then that

$$\begin{aligned} \int_{-\infty}^{\infty} (H_{20} + y H_{21}) U'_0 f_V(U_0, V_0) dy &= 0, \\ \text{hence} \quad H_{20} = -V'_{1\pm} \frac{\int_{-\infty}^{\infty} y U'_0 f_V(U_0, V_0) dy}{\int_{-\infty}^{\infty} U'_0 f_V(U_0, V_0) dy} & \end{aligned}$$

In the outer expansion, $v(x) = \mathcal{V} + \frac{\varepsilon}{\mathcal{D}} v_1 + \frac{\varepsilon^2}{\mathcal{D}} v_2$, we require then that $v_2(l) = H_{20}$.

5.2 Transverse stability of the K-mesa solution to perturbations along the y-axis

We will now use the general mesa construction outlined in the previous section to study the stability of mesa stripes to transverse perturbations.

We start by considering a one-mesa steady-state solution in the domain $[-L, L]\times[0, d_0]$. We consider small perturbations of the form

$$u(x,y) = u_e(x) + e^{\lambda t}e^{imy}\phi(x),$$
$$v(x,y) = v_e(x) + e^{\lambda t}e^{imy}\psi(x),$$

which yield the eigenvalue problem

$$\begin{aligned}\lambda\phi &= \varepsilon^2\phi_{xx} - \varepsilon^2 m^2\phi + f_u(u_e,v_e)\phi + f_v(u_e,v_e)\psi,\\ \tau\lambda\psi &= \frac{\mathcal{D}}{\varepsilon}\psi_{xx} - \frac{\mathcal{D}}{\varepsilon}m^2\psi + g_u(u_e,v_e)\phi + g_v(u_e,v_e)\psi.\end{aligned} \tag{5.13}$$

We now multiply the ϕ equation in (5.13) by u_x, and integrate it by parts on $[0, L]$. Given that the equilibrium problem satisfies $\varepsilon^2 u_{xx} + f(u,v) = 0$, we have then

$$\varepsilon^2(u_x)_{xx} + f_u u_x + f_v v_x = 0.$$

We define the operator $\mathcal{L}_\varepsilon u$ by

$$\mathcal{L}_\varepsilon u \equiv \varepsilon^2 u_{xx} + f_u u,$$

and we have that the equilibrium problem satisfies

$$\mathcal{L}_\varepsilon u_x = \varepsilon^2(u_x)_{xx} + f_u u_x = -f_v v_x,$$

and from (5.13) we get

$$\mathcal{L}_\varepsilon\phi + f_v\psi = \bar{\lambda}\phi.$$

Integrating first on $-L < x < 0$, we have

$$\int_{-L}^{0} (u_x \mathcal{L}_\varepsilon \, \phi - \phi \mathcal{L}_\varepsilon \, u_x) dx = \varepsilon^{\,2} [u_x \phi_x - \phi u_{xx}] \Big|_{-L}^{0}.$$

The two terms on the left side of the integral each equate to

$$\int_{-L}^{0} u_x \mathcal{L}_\varepsilon \, \phi dx = \bar{\lambda} \int_{-L}^{0} u_x \phi dx - \int_{-L}^{0} u_x f_v \psi dx$$
$$\int_{-L}^{0} \phi \mathcal{L}_\varepsilon \, u_x dx = - \int_{-L}^{0} \phi f_v v_x.$$

Putting it all together leads to

$$\bar{\lambda} \int_{-L}^{0} u_x \phi dx - \int_{-L}^{0} u_x f_v \psi dx + \int_{-L}^{0} \phi f_v v_x = \varepsilon^{\,2} [u_x \phi_x - \phi u_{xx}] \Big|_{-L}^{0}.$$

We now make use of the following facts: $u_x(-L) = u_x(0) = 0$ from Neumann boundary conditions and even symmetry considerations, respectively. Both $\psi(x)$ and $v_x(x)$ are approximately constant, hence $\psi(x) \cong \psi(-l)$, $v_x(x) \cong v_x(-l)$. Since $u_x(x)$ is localized near the interface, we have that

$$\int_{-L}^{0} u_x \phi dx = c_- \int_{-L}^{0} u_x^2 dx.$$

This reduces the equation to

$$\bar{\lambda} c_- \int_{-L}^{0} u_x^2 dx \cong \psi(-l) \int_{-L}^{0} u_x f_v dx - v_x(-l) c_- \int_{-L}^{0} f_v u_x dx - \varepsilon^{\,2} [\phi u_{xx}] \Big|_{-L}^{0},$$
$$\bar{\lambda} c_- \int_{-L}^{0} u_x^2 dx \cong [\psi(-l) - v_x(-l) c_-] \int_{-L}^{0} u_x f_v dx - \varepsilon^{\,2} [\phi u_{xx}] \Big|_{-L}^{0},$$

We now estimate

$$\phi\Big|_{x=-L} = O(1), \qquad \phi\Big|_{x=0} = O(1), \text{ as well as}$$
$$u_{xx}\Big|_{x=-L} = O(\varepsilon), \quad u_{xx}\Big|_{x=0} = O(\varepsilon),$$

therefore we have that $\varepsilon^2(\phi u_{xx})\Big|_{-L}^{0} = O(\varepsilon^3)$.

Changing variables to $y = \varepsilon^{-1}(x+l)$, we have that

$$\int_{-L}^{0} u_x f_v dx \sim \int_{-\infty}^{\infty} U_0'(y) f_v dy = \int_{u_-}^{u_+} f_v du,$$

since $u \to u_\pm$ when $y \to \pm\infty$. Similarly, we can make the same change of variables to have

$$\int_{-L}^{0} u_x^2 dx \sim \int_{-L}^{0} \frac{1}{\varepsilon^2}(U_0')^2 dx = \frac{1}{\varepsilon}\int_{-\infty}^{\infty}(U_0')^2 dy.$$

This yields the simplified equation

$$\bar{\lambda} c_- \int_{-\infty}^{\infty}(U_0')^2 dy \sim \varepsilon\,[\psi(-l) - c_- v_x(-l)]\int_{u_-}^{u_+} f_v du + O(\varepsilon^4).$$

We now define

$$\kappa_0 \equiv \frac{\int_{-\infty}^{\infty}(U_0')^2 dy}{\int_{u_-}^{u_+} f_v du}.$$

The integral in the numerator, $\int_{-\infty}^{\infty}(U_0')^2 dy$, can be further estimated by integrating the U equation in (5.6)

$$\int_{-\infty}^{\infty} U_{0y}^2(y) dy \sim \int_0^{u_+} U_{0y}^2 \frac{1}{U_{0y}} dU_0 = \int_0^{u_+} \sqrt{2\mathcal{F}(u)} du,$$

with $\mathcal{F}(u) = -\int_0^u f(s)ds$.

Then,

$$\bar{\lambda}\kappa_0 c_- \sim \varepsilon \left[\psi(-l) - v_x(-l)c_-\right].$$

Repeating the procedure for the $0 < x < L$ region, we obtain the analogous equation

$$\bar{\lambda}\kappa_0 c_+ \sim \varepsilon \left[-\psi(l) + v_x(l)c_+\right],$$

with the sign change from the fact that with a change of variables $y = \varepsilon^{-1}(x - l)$ and the transition layer at $x = l$, in this region we have $u \to u_\pm$ when $y \to \mp\infty$.

We recall from (5.9) and (5.10) that $v_x(l) \sim \frac{\varepsilon}{\mathcal{D}} g_-(L - l)$, and we also know from (5.4) that $l = \frac{g_- L}{g_- - g_+}$, therefore

$$v_x(l) = -\left(\frac{\varepsilon}{\mathcal{D}}\right)\frac{g_- g_+ L}{g_- - g_+}.$$

Furthermore, since $v(x)$ is an even function, we have that $v_x(-l) = -v_x(l)$.

We can collect both equations into the following linear system

$$\begin{aligned}\varepsilon^{-1}\bar{\lambda}\kappa_0 \begin{pmatrix} c_+ \\ c_- \end{pmatrix} &\cong \begin{pmatrix} -\psi(l) \\ \psi(-l) \end{pmatrix} + v_x(l) \begin{pmatrix} c_+ \\ c_- \end{pmatrix} \\ &\cong \begin{pmatrix} -\psi(l) \\ \psi(-l) \end{pmatrix} - \left(\frac{\varepsilon}{\mathcal{D}}\right)\frac{g_- g_+ L}{g_- - g_+} \begin{pmatrix} c_+ \\ c_- \end{pmatrix}\end{aligned} \tag{5.14}$$

Remark

(i) The goal is to find λ; to establish the conditions under which the system is lin-

early stable or unstable it is sufficient to determine the sign of λ. To fully solve the system in (5.14) we need to find $\psi(\pm l)$, and this has to be done by finding the equilibrium solution for the second equation in (5.13):

$$\psi_{xx} - m^2\psi + \frac{\varepsilon}{\mathcal{D}}(g_u\phi + g_v\psi) = 0. \tag{5.15}$$

(ii) At this point we want to consider solutions consisting of $K-$mesas. The one mesa problem in $-L < x < L$ can be extended to the $K-$mesa case on $-L < x < (2K-1)L$ by means of Floquet theory. This can be accomplished for the ψ equation by using the following boundary conditions:

$$\psi((2j-1)L) = z^j\psi(-L), \qquad \psi'((2j-1)L) = z\psi'(-L), \qquad \text{for } j = 1, \cdots, K.$$

At the boundary of the whole interval $[-L, (2K-1)L]$, we have $\psi((2K-1)L) = z^K\psi(-L)$. We can get standard periodic boundary conditions then by choosing $z^K = 1$.

(iii) Systems with homogeneous Neumann boundary conditions can be extended to periodic boundary conditions by adding an even reflection on one of the boundaries, yielding a system on twice the original domain. By the same token, a system with periodic boundary conditions, with even symmetry, can be folded in half into an equivalent system with Neumann boundary conditions. Applying this idea to the extended $K-$mesa system implies that we have to consider $2K$ mesas in the periodic case, and thus $z = e^{2\pi ik/2K}, \quad k = 0, \ldots, K-1$.

The case for $K = 1$ has to be considered separately, and will be discussed in detail in § 5.2.1.

Since $u(x)$ is approximately constant except at the interfaces, we can approximate the eigenfunction $\phi \sim c_\pm u_x$, and similarly $\psi \sim \psi(\pm l)$ when $x \sim \pm l$.

In the flat regions $|x| < l$ and $l < |x| < L$ we have that $f_u\phi + f_v\psi = \lambda\phi$. We will show later that $\lambda \ll 1$, and this can be used to approximate

$$\begin{aligned} \phi &\sim -\frac{f_v^+}{f_u^+}\psi \qquad \text{for } |x| < l, \\ \phi &\sim -\frac{f_v^-}{f_u^-}\psi \qquad \text{for } l < |x| < L. \end{aligned}$$

Substituting it into (5.15), we end up with the ODE

$$\psi_{xx} - \sigma_\pm^2\psi = 0, \tag{5.16}$$

which is defined everywhere except at the interfaces, and where

$$\begin{aligned} \sigma_\pm^2 &= m^2 + \frac{\varepsilon}{\mathcal{D}}\kappa_\pm + \frac{\varepsilon\,\tau\lambda}{\mathcal{D}}, \text{ with} \\ \kappa_+ &\equiv -\left(g_v^+ - \frac{f_v^+}{f_u^+}g_u^+\right) > 0, \qquad \text{when } |x| < l \\ \kappa_- &\equiv -\left(g_v^- - \frac{f_v^-}{f_u^-}g_u^-\right) > 0, \qquad \text{when } l < |x| < L, \end{aligned} \tag{5.17}$$

and as before, we are using the notation $f_v^+ \equiv \frac{\partial f}{\partial v}(u^+, \mathcal{V})$.

Remark

(i) We will eventually show that for $m \neq 0$ we have that $\lambda = O(\varepsilon^{\,2})$, and that $\lambda = O(\varepsilon\,)$ for $m = 0$. It is tempting to disregard the $\tau\lambda\varepsilon$ term in (5.13), however, we will keep this term in order to analyze the case when $\tau \to \infty$.

Since ψ is smooth, the jump across $x = \pm l$ can be estimated in the sense of distributions through the term $g_u\phi$. We start with the jump across $x = l$, with the

standard inner change of variables $y = \varepsilon^{-1}(x - l)$,

$$g_u\phi \sim g_u c_+ u_x \to c_+ \int_{l^-}^{l^+} g_u u_x dx\delta(x-l) \sim c_+ \int_{-\infty}^{+\infty} g_{U_0} U_{0y} dy\delta(x-l)$$
$$\sim c_+ \int_{u_+}^{u_-} g_{U_0} dU_0 \delta(x-l) \sim c_+(g_- - g_+)\delta(x-l). \tag{5.18}$$

Similarly, for the jump across $x = -l$, with $y = \varepsilon^{-1}(x + l)$, we have

$$g_u\phi \sim g_u c_- u_x \to c_- \int_{-l^+}^{-l^-} g_u u_x dx\delta(x+l) \sim c_- \int_{-\infty}^{+\infty} g_{U_0} U_{0y} dy\delta(x+l)$$
$$\sim c_- \int_{u_-}^{u_+} g_{U_0} dU_0 \delta(x+l) \sim c_-(g_+ - g_-)\delta(x+l). \tag{5.19}$$

Therefore, we have

$$g_u\phi \sim c_+(g_- - g_+)\delta\left(x-l\right) + c_-(g_+ - g_-)\delta\left(x+l\right),$$

effectively taking into account the contributions from both interfaces.

We can now write (5.16) defined on the whole interval $-L < x < L$ as

$$\psi_{xx} - \sigma_\pm^2\psi = \frac{\varepsilon}{\mathcal{D}}(g_- - g_+)\big[c_+\delta\left(x-l\right) - c_-\delta\left(x+l\right)\big],$$

with the added conditions that the solution has to be continuous across the interfaces at $x = \pm l$; that the jump conditions $\psi_x\Big|_{-l^+}^{-l^-} = c_- s$, and $\psi_x\Big|_{l^-}^{l^+} = c_+ s$ are satisfied; and that the Floquet boundary conditions $\psi(L) = z\psi(-L)$, and $\psi'(L) = z\psi'(-L)$ are satisfied as well.

For the jump conditions we have $s = \frac{\varepsilon}{\mathcal{D}}(g_- - g_+)$

A solution to the system with prescribed continuity across the interfaces is

$$\psi(x) = \begin{cases} \psi(-l)\dfrac{\cosh[\sigma_-(x+L)]}{\cosh[\sigma_-(L-l)]} + A_L \sinh[\sigma_-(x+l)], & -L < x < -l, \\ \psi(-l)\dfrac{\sinh[\sigma_+(l-x)]}{\cosh(2\sigma_+ l)} + \psi(l)\dfrac{\sinh[\sigma_+(x+l)]}{\sinh(2\sigma_+ l)}, & -l < x < l, \\ \psi(l)\dfrac{\cosh[\sigma_-(L-x)]}{\cosh[\sigma_-(L-l)]} + A_R \sinh[\sigma_-(x-l)], & l < x < L, \end{cases} \tag{5.20}$$

the four unknowns $A_L, A_R, \psi(l), \psi(-l)$ can be determining by enforcing all four boundary and jump conditions.

We start with the Floquet boundary conditions. The four relevant terms are

$$\begin{aligned} \psi(L) &= \frac{\psi(l)}{\cosh[\sigma_-(L-l)]} + A_R \sinh[\sigma_-(L-l)], \\ z\psi(-L) &= \frac{z\psi(-l)}{\cosh[\sigma_-(L-l)]} - zA_L \sinh[\sigma_-(L-l)], \\ \psi'(L) &= A_R \sigma_- \cosh[\sigma_-(L-l)], \\ z\psi'(-L) &= zA_L \sigma_- \cosh[\sigma_-(L-l)]. \end{aligned}$$

From the condition on $\psi'(L) = z\psi'(-L)$, it can immediately be seen that $zA_L = A_R$.

From the condition that $\psi(L) = z\psi(-L)$, we get

$$\frac{\psi(l) - z\psi(-l)}{\cosh[\sigma_-(L-l)]} = -2zA_L \sinh[\sigma_-(L-l)],$$

hence

$$\psi(l) - z\psi(-l) = -zA_L \sinh[2\sigma_-(L-l)] \tag{5.21}$$

For the jump conditions, the four relevant terms are

$$\begin{aligned}
\psi_x(l^+) &= -\psi(l)\sigma_- \tanh[\sigma_-(L-l)] + A_R\sigma_-, \\
\psi_x(l^-) &= \psi(l)\sigma_+ \coth(2\sigma_+ l) - \psi(-l)\sigma_+ \mathrm{csch}\,(2\sigma_+ l), \\
\psi_x(-l^+) &= \psi(l)\sigma_+ \mathrm{csch}\,(2\sigma_+ l) - \psi(-l)\sigma_+ \coth(2\sigma_+ l), \\
\psi_x(-l^-) &= -\psi(-l)\sigma_- \tanh[\sigma_-(L-l)] + A_L\sigma_-.
\end{aligned}$$

The two jump conditions, $\psi(l^+) - \psi(l^-) = c_+ s$ and $\psi(-l^+) - \psi(-l^-) = -c_- s$, yield

$$\begin{aligned}
&-\psi(l)\sigma_- \tanh[\sigma_-(L-l)] + A_R\sigma_- - \\
&\qquad \psi(l)\sigma_+ \coth(2\sigma_+ l) + \psi(-l)\sigma_+ \mathrm{csch}\,(2\sigma_+ l) = c_+ s, \\
&\psi(-l)\sigma_- \tanh[\sigma_-(L-l)] + A_L\sigma_- - \\
&\qquad \psi(l)\sigma_+ \mathrm{csch}\,(2\sigma_+ l) + \psi(-l)\sigma_+ \coth(2\sigma_+ l) = c_- s
\end{aligned}$$

Simplifying things slightly, and using $A_R = zA_L$, we get

$$\begin{aligned}
-\psi(l)\big(\sigma_- \tanh[\sigma_-(L-l)] + \sigma_+ \coth(2\sigma_+ l)\big) + \psi(-l)\sigma_+ \mathrm{csch}\,(2\sigma_+ l) &= c_+ s - zA_L\sigma_-, \\
-\psi(l)\sigma_+ \mathrm{csch}\,(2\sigma_+ l) + \psi(-l)\big(\sigma_- \tanh[\sigma_-(L-l)] + \sigma_+ \coth(2\sigma_+ l)\big) &= c_- s - A_L\sigma_-
\end{aligned} \tag{5.22}$$

Putting together (5.22) and (5.21), we can express $\psi(\pm l)$ as the solution to the linear system

$$\begin{aligned}
\begin{pmatrix} d & e \\ e & d \end{pmatrix} \begin{pmatrix} \psi(l) \\ -\psi(-l) \end{pmatrix} &= -s \begin{pmatrix} c_+ \\ c_- \end{pmatrix} + \sigma_- A_L \begin{pmatrix} z \\ 1 \end{pmatrix}, \\
\begin{pmatrix} z \\ 1 \end{pmatrix}^T \begin{pmatrix} \psi(l) \\ -\psi(-l) \end{pmatrix} &= -A_L z \sinh[2\sigma_-(L-l)]
\end{aligned}$$

with

$$d \equiv \sigma_- \tanh[\sigma_-(L-l)] + \sigma_+ \coth(2\sigma_+ l),$$
$$e \equiv \sigma_+ \mathrm{csch}\,(2\sigma_+ l).$$

Solving for A_L in the second equation, and substituting it into the first one yields

$$G\vec{r} = -s\vec{c} + \vec{b}_0 \left(\frac{-\vec{b}_1^T \vec{r}}{z\chi} \right),$$

with

$$G = \begin{pmatrix} d & e \\ e & d \end{pmatrix}, \quad r = \begin{pmatrix} \psi(l) \\ -\psi(-l) \end{pmatrix}, \quad c = \begin{pmatrix} c_+ \\ c_- \end{pmatrix},$$
$$\vec{b}_0 = \begin{pmatrix} z \\ 1 \end{pmatrix}, \qquad \vec{b}_1 = \begin{pmatrix} 1 \\ z \end{pmatrix}, \qquad \chi = \frac{\sinh[2\sigma_-(L-l)]}{\sigma_-}.$$

This yields the matrix problem

$$(G+B)\vec{r} = -s\vec{c}, \tag{5.23}$$

where

$$B = \frac{1}{z\chi}\vec{b}_0\vec{b}_1^T = \frac{1}{z\chi}\begin{pmatrix} z & z^2 \\ 1 & z \end{pmatrix} = \frac{1}{\chi}\begin{pmatrix} 1 & z \\ \bar{z} & 1 \end{pmatrix},$$

since $z\bar{z} = 1$.

Recall that the eigenvalue system that we want to solve, from (5.14), is

$$\varepsilon^{-1}\bar{\lambda}\kappa_0 \begin{pmatrix} c_+ \\ c_- \end{pmatrix} = \begin{pmatrix} -\psi(l) \\ \psi(-l) \end{pmatrix} + v_x(l) \begin{pmatrix} c_+ \\ c_- \end{pmatrix},$$

or, using compact notation

$$\varepsilon^{-1}\bar{\lambda}\kappa_0\vec{c} = \vec{r} + v_x(l)\vec{c}. \tag{5.24}$$

Solving for $\vec{r}$ in (5.23), and substituting it into (5.24) yields

$$\frac{\varepsilon^{-1}\bar{\lambda}\kappa_0}{s}\vec{c} = (G+B)^{-1}\vec{c} + \frac{v_x(l)}{s}\vec{c}. \tag{5.25}$$

Now,

$$\frac{v_x(l)}{s} = -\frac{\varepsilon}{\mathcal{D}}\frac{g_-g_+L}{g_- - g_+}\frac{\mathcal{D}}{\varepsilon\,(g_+ - g_-)} = \frac{g_-g_+L}{(g_+ - g_-)^2}.$$

And since

$$l = \frac{g_-}{g_- - g_+}L \qquad \rightarrow \qquad \frac{g_+}{g_-} = 1 - \frac{L}{l},$$

we can then calculate

$$\frac{v_x(l)}{s} = \frac{l^2}{L}\left(1 - \frac{L}{l}\right) = \left(1 - \frac{L}{l}\right)\frac{l^2}{L^2}L. \tag{5.26}$$

Similarly,

$$\frac{\varepsilon^{-1}\bar{\lambda}\kappa_0}{s} = \frac{\varepsilon^{-1}\bar{\lambda}\kappa_0}{\varepsilon\,(g_+ - g_-)/\mathcal{D}} = -\frac{\mathcal{D}}{\varepsilon^{\,2}}\frac{\bar{\lambda}\kappa_0}{g_-}\frac{l}{L}.$$

Substituting into (5.25), with $\bar{\lambda} = \lambda + \varepsilon^{\,2}m^2$, we obtain

$$(G+B)^{-1}\vec{c} + \left(1 - \frac{L}{l}\right)\frac{l^2}{L^2}L\vec{c} - m^2\alpha\bar{c} = \frac{\alpha}{\varepsilon^{\,2}}\lambda\bar{c}, \tag{5.27}$$

with $\alpha = -\frac{\mathcal{D}}{g_-}\kappa_0\left(\frac{l}{L}\right)$.

The eigenpairs λ and $\bar{c}$ of (5.27) are given in terms of the spectrum of the two-by-two matrix $(G+B)^{-1}$,

$$(G+B)^{-1}\vec{\nu}_\pm = \omega_\pm\vec{\nu}_\pm,$$

they are given as

$$\begin{aligned} \vec{c} = \vec{\nu}_+, \qquad \text{and} \qquad \lambda_+ &= \frac{\varepsilon^2}{\alpha}\left[\omega_+ + \left(1 - \frac{L}{l}\right)\frac{l^2}{L^2}L - m^2\alpha\right], \\ \vec{c} = \vec{\nu}_-, \qquad \text{and} \qquad \lambda_- &= \frac{\varepsilon^2}{\alpha}\left[\omega_- + \left(1 - \frac{L}{l}\right)\frac{l^2}{L^2}L - m^2\alpha\right]. \end{aligned} \tag{5.28}$$

This will yield two eigenpairs for each value of z. Thus we only need to find the spectrum of $(G+B)^{-1}$, and this can be done by first calculating the eigenpairs of $G+B$, and then taking the reciprocals of the eigenvalues.

Since the matrix

$$G + B = \begin{pmatrix} d & e \\ e & d \end{pmatrix} + \frac{1}{\chi}\begin{pmatrix} 1 & z \\ \bar{z} & 1 \end{pmatrix}$$

is a Hermitian matrix, then all the eigenvalues must be real, and it is possible to find an orthonormal basis.

We let $(G+B)\vec{\nu} = \sigma\vec{\nu}$, and we have

$$\det\begin{pmatrix} d + \frac{1}{\chi} - \sigma & e + \frac{z}{\chi} \\ e + \frac{\bar{z}}{\chi} & d + \frac{1}{\chi} - \sigma \end{pmatrix} = 0.$$

Thus

$$\begin{aligned} \left(d + \frac{1}{\chi} - \sigma\right)^2 &= \left(e + \frac{z}{\chi}\right)\left(e + \frac{\bar{z}}{\chi}\right), \\ &= e^2 + \frac{1}{\chi^2} + \frac{e}{\chi}(z + \bar{z}), \end{aligned}$$

and we have used the fact that $z\bar{z} = 1$.

Thus

$$d+\frac{1}{\chi}-\sigma=\pm\left(e^2+\frac{1}{\chi^2}+\frac{2e}{\chi}\mathrm{Re}(z)\right)^{1/2},$$

and we can conclude that the eigenvalues of $(G+B)^{-1}$, needed in (5.28), are simply

$$\omega_\pm=\frac{1}{d+\frac{1}{\chi}\pm\left(e^2+\frac{1}{\chi^2}+\frac{2e}{\chi}\mathrm{Re}(z)\right)^{1/2}}.$$

Now, in order to calculate the eigenvectors we first notice that

$$d+\frac{1}{\chi}-\sigma=\pm|f|,\qquad\text{where}\quad f=e+\frac{z}{\chi},\quad\text{and}\quad|f|=(f\bar{f})^{1/2}$$

is the length of the complex vector f.

Thus, for ω_+ we have

$$\begin{pmatrix}d+\frac{1}{\chi}-\sigma & e+\frac{z}{\chi}\\ e+\frac{\bar{z}}{\chi} & d+\frac{1}{\chi}-\sigma\end{pmatrix}\vec{\nu}_+=\begin{pmatrix}|f| & f\\ \bar{f} & |f|\end{pmatrix}\vec{\nu}_+=\vec{0},\quad\text{therefore}\quad\vec{\nu}_+=\begin{pmatrix}|f|\\ -\bar{f}\end{pmatrix}.$$

Similarly, for ω_- we have

$$\begin{pmatrix}-|f| & f\\ \bar{f} & -|f|\end{pmatrix}\vec{\nu}_-=\vec{0},\quad\text{hence}\quad\vec{\nu}_-=\begin{pmatrix}|f|\\ \bar{f}\end{pmatrix}.$$

Notice that in a generalized dot product defined as

$$\vec{a}\cdot\vec{b}=\vec{a}^\dagger\vec{b},\quad\text{where}\quad\vec{a}=\begin{pmatrix}a_1\\ \vdots\\ a_N\end{pmatrix},\quad\vec{a}^\dagger=(\bar{a}_1,\cdots,\bar{a}_N),$$

then

$$\vec{\nu}_+ \cdot \vec{\nu}_- = (|f|, -f) \begin{pmatrix} |f| \\ \bar{f} \end{pmatrix} = 0.$$

Therefore $\vec{\nu}_+, \vec{\nu}_-$ are orthogonal with respect to this inner product.

Lemma 5.1 *The spectrum of* $(G+B)^{-1}\vec{\nu}_\pm = \omega_\pm \vec{\nu}_\pm$ *is as follows:*

$$\begin{aligned} \omega_+ &= \frac{1}{d + \frac{1}{\chi} + |f|} \qquad & \vec{\nu}_+ &= \begin{pmatrix} |f| \\ -\bar{f} \end{pmatrix}, \\ \omega_- &= \frac{1}{d + \frac{1}{\chi} - |f|} \qquad & \vec{\nu}_- &= \begin{pmatrix} |f| \\ \bar{f} \end{pmatrix}, \end{aligned} \tag{5.29}$$

where

$$\begin{aligned} f &= e + \frac{z}{\chi}, & e &= \sigma_+ \mathrm{csch}\,(2\sigma_+ l), \\ \chi &= \frac{\sinh[2\sigma_-(L-l)]}{\sigma_-}, & d &= \sigma_- \tanh[\sigma_-(L-l)] + \sigma_+ \coth(2\sigma_+ l). \end{aligned}$$

Then, we have that

$$|f| = \left(e^2 + \frac{1}{\chi^2} + \frac{2e}{\chi} \mathrm{Re}(z) \right)^{1/2}, \qquad z = e^{i\theta}.$$

Lemma 5.2 *Consider a steady-state solution of* $K-$*mesas on an interval of length* $2KL$ *with Neumann boundary conditions. Then the linearized problem admits* $2K$ *eigenvalues.*

The eigenvalues are given by

$$\lambda_{\pm_j} = \frac{\varepsilon^2}{\alpha} \left[\omega_{\pm_j} + \left(1 - \frac{L}{l} \right) \frac{l^2}{L^2} L - m^2 \alpha \right] \qquad \textit{for } j = 1, \cdots, K-1,$$

where

$$\omega_{\pm_j} = \frac{1}{d + \frac{1}{\chi} \pm \left(e^2 + \frac{1}{\chi^2} + \frac{2e}{\chi}\cos(\pi j/K)\right)^{1/2}}, \qquad j = 1, \cdots, K-1.$$

Finally, the two remaining eigenvalues are

$$\lambda_{\pm K} = \frac{\varepsilon^{\,2}}{\alpha}\left[\omega_{\pm K} + \left(1 - \frac{L}{l}\right)\frac{l^2}{L^2}L - m^2\alpha\right],$$

with

$$\omega_{+K} = \frac{1}{d+e}, \qquad \omega_{-K} = \frac{1}{d-e}.$$

These are the eigenvalues that correspond to a $K-$mesa pattern generated by gluing together K mesas.

The various quantities are:

$$\begin{aligned} d &= \sigma_- \tanh[\sigma_-(L-l)] + \sigma_+ \coth(2\sigma_+ l), \\ e &= \sigma_+ \mathrm{csch}\,(2\sigma_+ l), \\ \chi &= \sigma_-^{-1} \sinh[2\sigma_-(L-l)], \\ \sigma_\pm^2 &= m^2 - \frac{\varepsilon}{\mathcal{D}}\left(g_v^\pm - \frac{f_v^\pm}{f_u^\pm} g_u^\pm\right) + \frac{\varepsilon\,\tau\lambda}{\mathcal{D}}. \end{aligned}$$

Now, we calculate with a little algebra

$$\begin{aligned} d + e &= \sigma_- \tanh[\sigma_-(L-l)] + \sigma_+ \coth(\sigma_+ l), \\ d - e &= \sigma_- \tanh[\sigma_-(L-l)] + \sigma_+ \tanh(\sigma_+ l), \\ d + \frac{1}{\chi} &= \sigma_-(\tanh[\sigma_-(L-l)] + \sigma_+ \mathrm{csch}\,[2\sigma_-(L-l)]) + \sigma_+ \coth(2\sigma_+ l). \end{aligned}$$

In addition,

$$\left(e^2+\frac{1}{\chi^2}+\frac{2e}{\chi}\cos(2\pi j/K)\right)^{1/2}=\left[\left(e+\frac{1}{\chi}\right)^2-\frac{4e}{\chi}\sin^2\left(\frac{\pi j}{2K}\right)\right]^{1/2},$$

and

$$\begin{aligned}e+\frac{1}{\chi}&=\sigma_+\mathrm{csch}\,(2\sigma_+ l)+\sigma_-\mathrm{csch}\,[2\sigma_-(L-l)],\\ \frac{4e}{\chi}&=4\sigma_+\sigma_-\mathrm{csch}\,(2\sigma_+ l)\mathrm{csch}\,[2\sigma_-(L-l)].\end{aligned}$$

Thus

$$\omega_{\pm_j}=\frac{1}{d+\frac{1}{\chi}\pm\left[\left(e+\frac{1}{\chi}\right)^2-\frac{4e}{\chi}\sin^2\left(\frac{\pi j}{2K}\right)\right]^{1/2}},\qquad j=1,\cdots,K-1.$$

Finally,

$$\alpha=-\frac{\mathcal{D}}{g_-}\kappa_0\left(\frac{l}{L}\right),\qquad \kappa_0\equiv\frac{\int_{-\infty}^{\infty}(U_0')^2dy}{\int_{u_-}^{u_+}f_v du},\qquad \frac{l}{L}=\frac{g_-}{g_--g_+}$$

In order to find the eigenvalues for a specific RD system, the key elements that need to be determined are $u_+, u_-, \mathcal{V}$, which are obtained through the heteroclinic Maxwell line condition

$$\begin{aligned}f(u_+,\mathcal{V})&\equiv f_+=0,\\ f(u_-,\mathcal{V})&\equiv f_-=0,\\ \int_{u_-}^{u_+}f(w,\mathcal{V})dw&=0.\end{aligned}$$

Regarding the stability of the heteroclinic, we also require that $f_u(u_\pm,\mathcal{V})<0$.

The mesa half-width l can then be determined in terms of the domain half-width L,

$$l = \frac{g_-}{g_- - g_+} L,$$

with $g_\pm \equiv g(u_\pm, \mathcal{V})$, and similarly $f_\pm \equiv f(u_\pm, \mathcal{V})$.

Lastly, in order to determine κ_0 we need $\int_{-\infty}^{\infty} (U_0')^2 dy$, and this can be determined in the following way,

$$\int_{-\infty}^{\infty} (U_0')^2 dy = \int_0^{u_+} \sqrt{2\mathcal{F}(u)} du, \text{ with } \mathcal{F}(u) = -\int_0^u f(s) ds.$$

The rest of the terms necessary to determine the breather and zigzag eigenvalues can be trivially calculated from these results.

5.2.1 The one-mesa special case

The case of the stability of a one-mesa solution with Neumann boundary conditions will now be considered. This has to be done separately, as the Floquet theory used in the $K-$ mesa case is for $j = 1, \cdots, K-1$, and therefore excludes the case $K = 1$.

Since the analysis is analogous to what was previously done for $K-$mesas, we will start at (5.14), which we write as

$$\varepsilon^{-1} \bar{\lambda} \kappa_0 \begin{pmatrix} c_+ \\ c_- \end{pmatrix} = \begin{pmatrix} -\psi(l) \\ \psi(-l) \end{pmatrix} + v_x(l) \begin{pmatrix} c_+ \\ c_- \end{pmatrix}, \tag{5.30}$$

with

$$v_x(l) = \left(\frac{\varepsilon}{\mathcal{D}}\right) \frac{g_- g_+ L}{g_- - g_+},$$

and $\psi(x)$ satisfies

$$\begin{aligned}\psi(x)_{xx} - \sigma^2\psi = \frac{c_+\varepsilon}{\mathcal{D}}(g_+ - g_-)\delta\left(x-l\right) - \frac{c_-\varepsilon}{\mathcal{D}}(g_+ - g_-)\delta\left(x+l\right),\\ \psi'(-L) = \psi'(L) = 0.\end{aligned} \tag{5.31}$$

Analogous with (5.20), we obtain that

$$\psi(x) = \begin{cases} \psi(-l)\dfrac{\cosh[\sigma_-(x+L)]}{\cosh[\sigma_-(L-l)]}, & -L < x < -l,\\ \psi(-l)\dfrac{\sinh[\sigma_+(l-x)]}{\sinh(2\sigma_+ l)} + \psi(l)\dfrac{\sinh[\sigma_+(x+l)]}{\sinh(2\sigma_+ l)}, & -l < x < l,\\ \psi(l)\dfrac{\cosh[\sigma_-(L-x)]}{\cosh[\sigma_-(L-l)]}, & l < x < L,\end{cases}$$

with $s = \frac{\varepsilon}{\mathcal{D}}(g_+ - g_-)$.

The unknowns $\psi(\pm l)$ are to be found by satisfying the jump conditions $\psi_x\Big|_{-l^-}^{-l^+} = -c_- s$, and $\psi_x\Big|_{l^-}^{l^+} = c_+ s$. Hence, we get

$$\begin{aligned}\psi(l)\left[\sigma_-\tanh[\sigma_-(L-l)] + \sigma_+\coth(2\sigma_+ l)\right] - \psi(-l)\sigma_+\mathrm{csch}\left(2\sigma_+ l\right) = -c_+ s,\\ \psi(l)\sigma_+\mathrm{csch}\left(2\sigma_+ l\right) - \psi(-l)\left[\sigma_+\coth(2\sigma_+ l) + \sigma_-\tanh[\sigma_-(L-l)]\right] = -c_- s.\end{aligned}$$

We can write this as the linear system

$$\begin{pmatrix} d & e\\ e & d\end{pmatrix}\begin{pmatrix}\psi(l)\\ -\psi(-l)\end{pmatrix} = -s\begin{pmatrix}c_+\\ c_-\end{pmatrix}, \qquad G \equiv \begin{pmatrix} d & e\\ e & d\end{pmatrix},$$

where

$$\begin{aligned} d &\equiv \sigma_-\tanh[\sigma_-(L-l)] + \sigma_+\coth(2\sigma_+ l),\\ e &\equiv \sigma_+\mathrm{csch}\left(2\sigma_+ l\right).\end{aligned}$$

Inverting G and substituting into (5.31), we get

$$\frac{\varepsilon^{-1}\bar{\lambda}\kappa_0}{s}\begin{pmatrix}c_+\\c_-\end{pmatrix} = \frac{v_x(l)}{s}\begin{pmatrix}c_+\\c_-\end{pmatrix} + G^{-1}\begin{pmatrix}c_+\\c_-\end{pmatrix},$$

with $v_x(l)/s$ as in (5.26),

$$\frac{v_x(l)}{s} = \frac{\varepsilon}{\mathcal{D}}\frac{g_-g_+L}{g_+-g_-}\frac{\mathcal{D}}{\varepsilon\,(g_+-g_-)} = \frac{g_-g_+L}{(g_+-g_-)^2} = \left(1-\frac{L}{l}\right)\frac{l^2}{L^2}L,$$

and similarly,

$$\frac{\varepsilon^{-1}\bar{\lambda}\kappa_0}{s} = \frac{\varepsilon^{-1}\bar{\lambda}\kappa_0}{(\varepsilon/\mathcal{D})(g_+-g_-)} = -\frac{\mathcal{D}}{\varepsilon^{\,2}g_-}\bar{\lambda}\kappa_0\left(\frac{l}{L}\right).$$

Putting it all together, we conclude that

$$G^{-1}\begin{pmatrix}c_+\\c_-\end{pmatrix} + \left(1-\frac{L}{l}\right)\frac{l^2}{L^2}L\begin{pmatrix}c_+\\c_-\end{pmatrix} = -\frac{\mathcal{D}}{\varepsilon^{\,2}g_-}\bar{\lambda}\kappa_0\left(\frac{l}{L}\right)\begin{pmatrix}c_+\\c_-\end{pmatrix}, \qquad (5.32)$$

with

$$G^{-1} = \frac{1}{d^2-e^2}\begin{pmatrix}d & -e\\-e & d\end{pmatrix}.$$

Thus, the stability of a single mesa is governed by (5.32).

Remark

(i) As a sanity check, we need to show that (5.32) evaluated for the GMS system yields an equivalent equation as the matrix problem in equation (5.15) of [22].

(ii) Similarly, we also need to show that the general $K-$mesa matrix problem given in (5.27) is also equivalent in the GMS case to the previously computed system in (4.38).

We have from (5.15) of [22] that

$$\left[\frac{L}{2}(1-L)I - \hat{G}^{-1}\right]\hat{c} = \frac{\alpha}{\varepsilon^{\,2}}\bar{\lambda}\hat{c}, \qquad \text{with } \hat{c} = \begin{pmatrix} c_l \\ c_r \end{pmatrix}, \tag{5.33}$$

where L is the width of the mesa, and the domain has constant length 1; and

$$\hat{G}^{-1} = \frac{1}{d^2 - e^2}\begin{pmatrix} d & e \\ e & d \end{pmatrix}, \qquad \alpha \equiv \frac{2\beta L\mathcal{D}}{w_+^2}, \qquad \beta = \int_{-\infty}^{\infty} w'^2 dy.$$

Remark

(i) Notice that in the formulation for $\vec{c}$ in (5.18) and (5.19), when compared to $\hat{c}$, we have that $c_l = c_-$, but $c_r = -c_+$.

Rewriting (5.33) in the notation we have been using, we have that $L = 2l$ is the width of the mesa, and we have

$$\left[\hat{G}^{-1} - l(1-2l)I\right]\hat{c} = -\frac{\alpha}{\varepsilon^{\,2}}\bar{\lambda}\hat{c}, \tag{5.34}$$

with $\alpha = \frac{2\beta(2l)\mathcal{D}}{w_+^2}$.

Now, in our formulation, if we restrict it to the case $L = 1/2$ (domain length 1), we obtain

$$\left[G^{-1} - l(1-2l)I\right]\vec{c} = -\frac{\mathcal{D}\kappa_0(2l)}{\varepsilon^{\,2}g_-}\bar{\lambda}\vec{c}. \tag{5.35}$$

For the left hand side, we expand (5.34) as

$$\begin{aligned} -\frac{1}{d^2-e^2}\left[dc_l + ec_r\right] + l(1-2l)c_l &= \frac{\alpha}{\varepsilon^{\,2}}\bar{\lambda}c_l, \\ \frac{1}{d^2-e^2}\left[dc_r + ec_l\right] - l(1-2l)c_r &= -\frac{\alpha}{\varepsilon^{\,2}}\bar{\lambda}c_r. \end{aligned}$$

Interchanging the rows, we can write this as

$$\frac{1}{d^2-e^2}\begin{pmatrix} d & -e \\ -e & d \end{pmatrix}\begin{pmatrix} c_r \\ -c_l \end{pmatrix} - l(1-2l)\begin{pmatrix} c_r \\ -c_l \end{pmatrix} = -\frac{\alpha}{\varepsilon^{\,2}}\bar{\lambda}\begin{pmatrix} c_r \\ -c_l \end{pmatrix},$$

and since $c_r = -c_+$, and $c_l = c_-$, this system is equivalent to (5.35), provided that the right hand sides match, and that the d and e values are consistent.

Thus, we only need to show that

$$\alpha = \frac{4\beta l\mathcal{D}}{w_+^2} = \frac{2l\kappa_0\mathcal{D}}{g_-},$$

or, more succinctly, that

$$\frac{2\beta}{w_+^2} = \frac{\kappa_0}{g_-},$$

where

$$\beta = \int_{-\infty}^{\infty} w'^2 dy, \quad U_0 = \mathcal{V}w(y), \quad \kappa_0 = \frac{\int_{-\infty}^{\infty}(U_0')^2 dy}{\int_{u_-}^{u_+} f_v du}, \quad g_- = g(u_-, \mathcal{V}).$$

For the GMS model, we have that

$$\begin{aligned} g(u,v) &= -v + u^2, \\ f(u,v) &= -u + \frac{u^2}{v(1+\kappa u^2)}, \qquad \text{and } u_- = 0. \end{aligned}$$

When $v = \mathcal{V}$, we integrate

$$\int_{u_-}^{u_+} f_v du = -\int_0^{u_+} \frac{u^2}{\mathcal{V}^2(1+\kappa u^2)} du.$$

Now, we substitute $u = \mathcal{V}w$, $u_+ = \mathcal{V}w_+$, and get

$$\int_{u_-}^{u_+} f_v du = -\mathcal{V} \int_0^{w_+} \frac{w^2}{1 + b_0 w^2} dw, \qquad \text{with } b_0 = \kappa \mathcal{V}^2.$$

From the definition of the system in (4.21), we have that

$$w'' - w + \frac{w^2}{1 + b_0 w^2} = 0.$$

Multiplying by w' and integrating from $y = -\infty$ to $y = \infty$, we get

$$\begin{aligned} \frac{w'^2}{2}\Big|_{-\infty}^{\infty} - \frac{w^2}{2}\Big|_{-\infty}^{\infty} + \int_{-\infty}^{\infty} \frac{w^2}{1 + b_0 w^2} \frac{dw}{dy} dy = 0, \\ - \frac{w_+^2}{2} + \int_0^{w_+} \frac{w^2}{1 + b_0 w^2} dw = 0. \end{aligned}$$

Hence

$$\int_0^{w_+} \frac{w^2}{1 + b_0 w^2} dw = \frac{w_+^2}{2},$$

and we can conclude that

$$\int_{u_-}^{u_+} f_v du = -\mathcal{V} \frac{w_+^2}{2}.$$

We also calculate that

$$\int_{-\infty}^{\infty} (U_0')^2 dy = \mathcal{V}^2 \int_{-\infty}^{\infty} (w')^2 dy, \qquad g_- = g(u_-, \mathcal{V}) = -\mathcal{V}.$$

We conclude that

$$\frac{\kappa_0}{g_-} = \frac{\mathcal{V}^2 \int_{-\infty}^{\infty} (w')^2 dy}{-\mathcal{V}(-\mathcal{V} w_+^2/2)} = \frac{2}{w_+^2} \int_{-\infty}^{\infty} (w')^2 dy.$$

Now, the only thing remaining to ensure compatibility between our result and (5.15) of [22] is to show that the decay rates $\sigma_\pm$ and $\theta_\pm$ are the same.

We have from (5.17) that

$$\begin{aligned}
&\sigma_\pm^2 = m^2 + \frac{\varepsilon}{\mathcal{D}}(\kappa_\pm + \tau\lambda), \text{ with} \\
&\kappa_+ \equiv -\left(g_v^+ - \frac{f_v^+}{f_u^+} g_u^+\right) > 0, \\
&\kappa_- \equiv -\left(g_v^- - \frac{f_v^-}{f_u^-} g_u^-\right) > 0,
\end{aligned}$$

and from (4.32) that $\theta_\pm$ is

$$\theta = \begin{cases} \theta_- \equiv \left(m^2 + \frac{\varepsilon(1+\tau\lambda)}{\mathcal{D}}\right)^{1/2}, \\ \theta_+ \equiv \left(m^2 + \frac{\varepsilon(1+\tau\lambda)}{\mathcal{D}}\left(1 + \frac{2w_+}{l(w_+-2)}\right)\right)^{1/2} \end{cases}$$

We have then, that for the GMS system,

$$u_- = 0 \quad u_+ = \mathcal{V} w_+, \quad v = \mathcal{V}, \quad \text{where } \mathcal{V} = \frac{1}{w_+^2 2l}.$$

Now, we have that $g_u^- = 0$, and $g_v^- = -1$, hence $\kappa_- = 1$, and thus $\theta_- = \sigma_-$.

Similarly, since u_+ satisfies $f(u_+, \mathcal{V}) = 0$, and thus

$$u_+ = \mathcal{V}(1 + \kappa u_+^2),$$

we have,

$$\begin{aligned}
&g_u^+ = 2u_+, \quad f_u^+ = -1 + \frac{2u_+}{\mathcal{V}(1+\kappa u_+^2)^2} = -1 + \frac{2}{1+\kappa u_+^2} = -1 + \frac{2\mathcal{V}}{u_+}, \\
&g_v^+ = -1, \quad f_v^+ = -\frac{u_+^2}{\mathcal{V}^2(1+\kappa u_+^2)} = -\frac{u_+}{\mathcal{V}}.
\end{aligned}$$

We have then

$$\kappa_+ = -\left(g_v^+ - \frac{f_v^+}{f_u^+} g_u^+\right) = -\left(-1 + \frac{u_+/\mathcal{V}}{\frac{2\mathcal{V}-u_+}{u_+}} 2u^+\right) = 1 + \frac{2u_+^3}{\mathcal{V}u_+ - 2\mathcal{V}^2}$$
$$= 1 + \frac{2\mathcal{V}w_+^3}{w_+ - 2} = 1 + \frac{w_+}{l(w_+ - 2)}.$$

This shows that $\sigma_\pm = \theta_\pm$, hence the GMS results in (5.15) of [22] are consistent with ours general result. Thus, the GMS results constitute a particular case of our general framework.

Our final result is that on a domain $[-L, L]$, with mesa width $2l$, we have

$$G^{-1}\begin{pmatrix} c_+ \\ c_- \end{pmatrix} + \left(1 - \frac{L}{l}\right)\frac{l^2}{L^2} L \begin{pmatrix} c_+ \\ c_- \end{pmatrix} = -\frac{\mathcal{D}}{\varepsilon^2 g_-}\bar{\lambda}\kappa_0 \left(\frac{l}{L}\right)\begin{pmatrix} c_+ \\ c_- \end{pmatrix}, \qquad (5.36)$$

where

$$G^{-1} = \frac{1}{d^2 - e^2}\begin{pmatrix} d & -e \\ -e & d \end{pmatrix},$$
$$d = \sigma_- \tanh[\sigma_-(L-l)] + \sigma_+ \coth(2\sigma_+ l),$$
$$e = \sigma_+ \mathrm{csch}\,(2\sigma_+ l),$$
$$\sigma_\pm^2 = m^2 + \frac{\varepsilon}{\mathcal{D}}(\kappa_\pm + \tau\lambda),$$
$$\kappa_+ = -\left(g_v^+ - \frac{f_v^+}{f_u^+} g_u^+\right) > 0,$$
$$\kappa_- = -\left(g_v^- - \frac{f_v^-}{f_u^-} g_u^-\right) > 0,$$
$$\bar{\lambda} = \lambda + \varepsilon^2 m^2,$$
$$g_- = g(u_-, \mathcal{V}),$$
$$\kappa_0 = \frac{\int_{-\infty}^{\infty} (U_0')^2 dy}{\int_{u_-}^{u_+} f_v du}.$$

It is now convenient to define

$$\alpha = -\frac{\mathcal{D}}{g_-}\kappa_0\left(\frac{l}{L}\right).$$

Then, with I the identity matrix, we can rewrite (5.36) as

$$\left(G^{-1} + \left(1 - \frac{L}{l}\right)\frac{l^2}{L^2}LI - m^2\alpha I\right)\vec{c} = \frac{\alpha}{\varepsilon^2}\lambda\vec{c}$$

The eigenpairs of the system are then

$$\begin{aligned}\lambda_\pm &= \frac{\varepsilon^2}{\alpha}\left[\omega_\pm + \left(1 - \frac{L}{l}\right)\frac{l^2}{L^2}L - m^2\alpha\right],\\ \vec{c}_\pm &= \begin{pmatrix}1\\ \mp 1\end{pmatrix},\end{aligned} \tag{5.37}$$

with $\omega_\pm$ the eigenvalues of G^{-1}, given by

$$\begin{aligned}\omega_+ &= \frac{1}{d-e} = [\sigma_- \tanh[\sigma_-(L-l)] + \sigma_+ \tanh(l\sigma_+)]^{-1},\\ \omega_- &= \frac{1}{d+e} = [\sigma_- \tanh[\sigma_-(L-l)] + \sigma_+ \coth(l\sigma_+)]^{-1}.\end{aligned}$$

The $(\lambda_+, \vec{c}_+)$ eigenpair corresponds then to the breather mode, and the $(\lambda_-, \vec{c}_-)$ is the zigzag mode.

Two cases are worth considering,

- The case $m \neq 0$, $\tau = O(1)$:

  We have that, irrespective of the sign of α, and for m sufficiently large, we will have that $\lambda_\pm < 0$, i.e., the stripe is stable to short wavelength perturbations in the y-direction.

  We have that $\omega_\pm > 0$, and in fact as $L \to \infty$ we have $\omega_\pm \sim \frac{1}{2m}$. Given that

$1 - L/l < 0$, with the ratio L/l remaining constant when only the domain length L is increased, we have that on a small enough domain the stripe will always be stable, and that there will be a critical length L beyond which the stripe will become unstable.

- The case $m = 0$, $\tau = O(1)$:

  When $\varepsilon \to 0$ we have that $\sigma_\pm \to 0$. For the zigzag mode (λ_-), we have that

$$\sigma_+ \coth(\sigma_+ l) = \frac{\sigma_+}{\tanh(\sigma_+ l)} \sim \frac{1}{l(1 - \frac{\sigma^2 l^2}{3})} \sim \frac{1}{l} + O(\sigma_+^2),$$

  and since $\sigma_- \tanh[\sigma_-(L-l)] \sim \sigma_-^2 (L-l)$, we have

$$\omega_- \sim \left[\sigma_-^2 (L-l) + \frac{1}{l} + O(\sigma_+^2)\right]^{-1} = l + O(\sigma_+^2, \sigma_-^2).$$

  We conclude that for $m = 0$ we have

$$\lambda_- \simeq \frac{\varepsilon^2}{\alpha}\left[\left(1 - \frac{L}{l}\right)\frac{l^2}{L^2} L + l + O(\sigma_+^2, \sigma_-^2)\right] \sim \frac{\varepsilon^2}{\alpha}\left[\left(\frac{l^2}{L^2}\right) L + O(\sigma_+^2, \sigma_-^2)\right],$$

  and stability is guaranteed for this mode when $\alpha < 0$.

Remark

(i) When $\tau \gg 1$ this analysis is consistent provided that the term in $\omega_\pm$, $\varepsilon\,\tau\lambda \ll 1$. Since this shows that $\lambda = O(\varepsilon^2)$, the condition for self-consistency is that $\tau \ll O(1/\varepsilon^3)$.

Now, for the breather mode λ_+, we have that

$$\omega_+ \sim \frac{1}{\sigma_-^2 (L-l) + \sigma_+^2 l} = \frac{1}{\sigma_-^2 L + l(\sigma_+^2 - \sigma_-^2)}.$$

Since $\sigma_-^2 = \frac{\varepsilon}{\mathcal{D}}(\kappa_- + \tau\lambda)$, and $\sigma_+^2 - \sigma_-^2 = \frac{\varepsilon}{\mathcal{D}}(\kappa_+ - \kappa_-)$, we have that

$$\omega_+^2 \sim \frac{\mathcal{D}}{\varepsilon\, L\left[(\kappa_- + \tau\lambda) + \frac{l}{L}(\kappa_+ - \kappa_-)\right]}.$$

In terms of the breather eigenvalue, this yields that

$$\lambda_+ = \frac{\varepsilon^2}{\alpha}\left[\omega_+ + \left(1 - \frac{L}{l}\right)\frac{l^2}{L^2}L\right] \sim \frac{\varepsilon\mathcal{D}}{L\alpha}\frac{1}{(\kappa_- + \tau\lambda) + \frac{l}{L}(\kappa_+ - \kappa_-)}.$$

Notice again that since $l/L < 1$ we have stability of this mode provided that $\alpha < 0$.

Remark

(i) Notice that the breather eigenvalue $\lambda_+ = O(\varepsilon)$, while the zigzag eigenvalue $\lambda_- = O(\varepsilon^2)$.

(ii) The consistency condition for the breather case is that $0 < \tau < O(\varepsilon^{-1})$, since $\lambda_+ = O(\varepsilon, \tau\lambda)$.

5.3 Hopf bifurcation on 1-d mesa patterns in the shadow limit

In the previous section we studied in detail the breather and zigzag instabilities that arise from transverse perturbations. We will now use the estimates on the eigenvalues for the $m = 0$ case to consider the possibility of a Hopf instability giving rise to oscillatory instabilities.

The eigenvalues of 1-d mesa patterns are given by (5.37) when considering the case $m = 0$,

$$\begin{aligned}\lambda_+ &= \frac{\varepsilon^2}{\alpha}\left[\omega_+ + \left(1 - \frac{L}{l}\right)\frac{l^2}{L^2}L\right],\\ \lambda_- &= \frac{\varepsilon^2}{\alpha}\left[\omega_- + \left(1 - \frac{L}{l}\right)\frac{l^2}{L^2}L\right],\end{aligned} \tag{5.38}$$

where

$$\omega_+ = \frac{1}{d-e} = [\sigma_- \tanh[\sigma_-(L-l)] + \sigma_+ \tanh(l\sigma_+)]^{-1},$$
$$\omega_- = \frac{1}{d+e} = [\sigma_- \tanh[\sigma_-(L-l)] + \sigma_+ \coth(l\sigma_+)]^{-1},$$

with

$$\sigma_\pm = \sqrt{\frac{\varepsilon}{\mathcal{D}}(\kappa_\pm + \tau\lambda)}, \qquad \alpha = -\frac{\mathcal{D}}{g_-}\kappa_0 \frac{l}{L},$$
$$\kappa_\pm = -\left(g_v^\pm - \frac{f_v^\pm}{f_u^\pm} g_u^\pm\right), \qquad \kappa_0 = \frac{\int_{-\infty}^{\infty}(U_0')^2 dy}{\int_{u_-}^{u_+} f_v du}. \tag{5.39}$$

Remark

(i) There are several distinguished limits in τ that are relevant.

Case I: The natural distinguished limit is when $\lambda_\pm = O(\varepsilon^{\,2})$. In this limit we need both ω_+ and ω_- to satisfy $\omega_\pm = O(1)$, and thus we require that $\sigma_\pm = O(1)$ (we showed earlier that ω_+ and ω_- have different limits as $\sigma_\pm \to 0$).

To satisfy this condition we require that $\frac{\varepsilon\tau\lambda}{\mathcal{D}} = O(1)$ in order to have $\sigma_\pm = O(1)$. Given that $\lambda = O(\varepsilon^{\,2})$, this means that $\tau = O(\varepsilon^{\,-3})$.

The equations can be simplified by eliminating some constants via a suitable change of variables. Let τ_0 and Λ be defined as

$$\lambda = -\frac{\varepsilon^{\,2}}{\alpha}\Lambda, \qquad \tau = -\frac{1}{\varepsilon^{\,3}}\alpha\mathcal{D}\tau_0.$$

From (5.39) we obtain

$$\sigma_\pm = \sqrt{\tau_0\Lambda} + O(\varepsilon),$$

and the equations in (5.38) become

$$\begin{aligned}\Lambda &= -\frac{1}{\sqrt{\tau_0\Lambda}\left[\tanh(\sqrt{\tau_0\Lambda}(L-l))+\tanh(\sqrt{\tau_0\Lambda}l)\right]} - \left(1-\frac{L}{l}\right)\frac{l^2}{L^2}L,\\ \Lambda &= -\frac{1}{\sqrt{\tau_0\Lambda}\left[\tanh(\sqrt{\tau_0\Lambda}(L-l))+\coth(\sqrt{\tau_0\Lambda}l)\right]} - \left(1-\frac{L}{l}\right)\frac{l^2}{L^2}L,\end{aligned} \tag{5.40}$$

for the zigzag and breather eigenvalues, respectively.

In order to find the Hopf bifurcation values, we let $\Lambda = i\delta/\tau_0$, and for the zigzag case we get

$$F_+ = \frac{i\delta}{\tau_0} + \frac{1}{\sqrt{i\delta}\left[\tanh(\sqrt{i\delta}\,(L-l))+\tanh(\sqrt{i\delta}\,l)\right]} + \left(1-\frac{L}{l}\right)\frac{l^2}{L^2}L = 0.$$

We must now find values for δ and τ such that

$$F_+ = \text{Re}[F_+] + i\text{Im}[F_+] = 0,$$

hence we require both $\text{Re}[F_+] = 0$ and $\text{Im}[F_+] = 0$.

We have then that the Hopf bifurcation values in (5.38) are the roots of

$$\text{Re}\left[\frac{1}{\sqrt{i\delta}\left[\tanh(\sqrt{i\delta}\,(L-l))+\tanh(\sqrt{i\delta}\,l)\right]}\right] + \left(1-\frac{L}{l}\right)\frac{l^2}{L^2}L = 0, \tag{5.41a}$$

$$\text{Im}\left[\frac{1}{\sqrt{i\delta}\left[\tanh(\sqrt{i\delta}\,(L-l))+\tanh(\sqrt{i\delta}\,l)\right]}\right] + \frac{\delta}{\tau_0} = 0. \tag{5.41b}$$

This setup decouples the system in terms of finding δ and τ_0. To find both values one must start by solving (5.41a) in terms of δ, and then substitute the

values into (5.41b) in order to find τ_0

$$\tau_0 = -\frac{\delta}{\mathrm{Im}\left[\frac{1}{\sqrt{i\delta}\left[\tanh(\sqrt{i\delta}\,(L-l))+\tanh(\sqrt{i\delta}\,l)\right]}\right]}$$

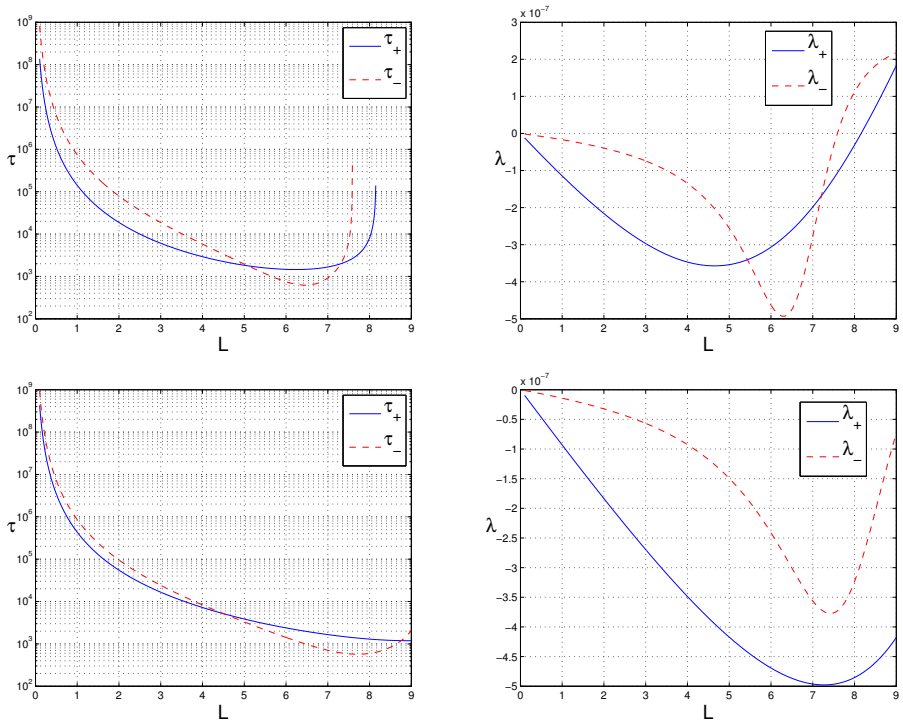

Figure 5.1: Plots of both the critical τ and λ_I at which a Hopf bifurcation occurs, as a function of the domain length L for the GMS model. The parameters used in the computations are $D = 50$, $\varepsilon = 0.01$. The two top figures are for $\kappa = 1$, and the bottom figures are for $\kappa = 0.65$.

Using a straightforward Newton method the system can be easily solved, Figure 5.1 shows the Hopf curves for both the imaginary part of λ and τ. At the point where the eigenvalues become positive, the critical value of τ becomes discontinuous. Throughout the range where $\lambda_\pm$ remains negative, the breather eigenvalue

will always be smaller for small values of L.

Plotting the critical τ values provides the Hopf bifurcation threshold, as seen in the two bottom images in figure 5.1. We will later do a numerical simulation of an RD model when considering τ in the Hopf regime.

5.3.1 ODE-PDE system

We will now compute a full time-dependent solution for the case where $\tau = O(\varepsilon^{-3})$, and $\lambda = O(\varepsilon^{2})$.

We start again with the full system (5.1),

$$\begin{aligned} u_t &= \varepsilon^2 \Delta u + f(u,v) \\ \tau v_t &= \frac{\mathcal{D}}{\varepsilon} \Delta v + g(u,v), \end{aligned}$$

where we look for a time-dependent mesa solution on the domain $[-L, L]$, with the two interfaces located at $x = l_1$ and $x = l_2$. Since $\lambda = O(\varepsilon^{2})$, the proper time scale of the interfaces is

$$l_1 \equiv l_1(\varepsilon^2 t); \qquad l_2 \equiv l_2(\varepsilon^2 t).$$

We also let $\tau = \tilde{\tau}_0/\varepsilon^3$, and we define $T = \varepsilon^2 t$.

We have then that (5.1) becomes

$$\begin{aligned} \varepsilon^2 u_T &= \varepsilon^2 \Delta u + f(u,v) \\ \frac{\tilde{\tau}_0}{\varepsilon} v_T &= \frac{\mathcal{D}}{\varepsilon} \Delta v + g(u,v). \end{aligned} \tag{5.42}$$

We now do an asymptotic expansion near around the right layer (a similar

expansion will also have to be computed for the leftmost layer), with

$$u = U_0(y_1) + \varepsilon\, U_{1R}(y_1) + \cdots,$$
$$v = V_0 + \varepsilon\, V_{1R} + \varepsilon^{\,2} V_{2R} + \cdots,$$

where $y = \varepsilon^{\,-1}(x - l_1(T))$, and therefore $u_T = -\varepsilon^{\,-1} U_0' l_1'$. Substituting into (5.42), we obtain that

$$-\varepsilon^{\,-1} U_0' l_1' = U_0'' + \varepsilon\, U_{1R}'' + f(U_0, V_0) + \varepsilon\, f_U^0 U_{1R} + \varepsilon\, f_V^0 V_{1R} + \cdots$$

As before, we take $V_0 =$ constant, and define u_+, u_-, V_0 in terms of the heteroclinic Maxwell line condition

$$\int_{u_-}^{u_+} f(u, V_0) du = 0, \qquad f(u_\pm, V_0) = 0, \qquad f_u(u_\pm, V_0) < 0.$$

Thus, around the right transition layer we have

$$U_{1R}'' + f_u^0 U_{1R} = -f_V^0 V_{1R} - l_1' U_0', \qquad -\infty < x < \infty.$$

Similarly, for the V equation we have

$$\tilde{V}_0 V_{1T} = \frac{\mathcal{D}}{\varepsilon^{\,3}}(V_0'' + \varepsilon\, V_1'' + \cdots) + g(U_0, V_0) + \cdots$$

Since $V_0 =$ constant we have that

$$O(1) = \frac{1}{\varepsilon^{\,2}} \mathcal{D} V_{1R}'' + O(1),$$

therefore $V_{1R}'' = 0$. We also have that $V \sim V_0$ on the entire interval, therefore in the internal region we cannot have V_{1R} growing at infinity, hence

$$V_{1R} = V_{1R}(T),$$

independent of y.

The inner problem on the rightmost layer is

$$\mathcal{L}U_1 \equiv U_1'' + f_u^0 U_1 = -f_v^0 V_{1R} - l_1' U_0'.$$

Since $\mathcal{L}U_0' = 0$, the solvability condition is

$$-l_1' \int_{-\infty}^{\infty} U_0'^2 dy - V_{1R} \int_{-\infty}^{\infty} f_v^0 U_0' dy = 0,$$

and as we did before, since U_0 is a heteroclinic connection,

$$\int_{-\infty}^{\infty} f_v^0 U_0' dy = \int_{u_+}^{u_-} f_v^0 dU_0 = -\int_{u_-}^{u_+} f_v^0 dU_0.$$

Thus, the ODE for the rightmost layer is

$$l_1' = \frac{dl_1}{dT} = V_{1R}(T) \frac{\int_{u_-}^{u_+} f_v^0 dU_0}{\int_{-\infty}^{\infty} U_0'^2 dy}. \tag{5.43}$$

The same procedure on the leftmost layer at $x = l_2$ yields that

$$l_2' = -V_{1L}(T) \frac{\int_{u_-}^{u_+} f_v^0 dU_0}{\int_{-\infty}^{\infty} U_0'^2 dy}. \tag{5.44}$$

To find values for V_{1L} and V_{1R} we need to match with the outer solution.

Now, in the outer region we expand $V = V_0 + \varepsilon V_1 + \cdots$, and we obtain from substituting into (5.42) that

$$\tilde{\tau_0} V_{1T} = \mathcal{D} V_{1xx} + \begin{cases} g_+ & \text{if } l_2 < x < l_1 \\ g_- & \text{if } l_1 < x < L \text{ or } -L < x < l_2. \end{cases}$$

The matching condition is that

$$V_{1L}(T) = v_1(l_2, T),$$
$$V_{1R}(T) = v_1(l_1, T).$$

We now define w by

$$v_1 = \frac{g_-}{\tilde{\tau}} w,$$

and recall that $\frac{g_+ - g_-}{g_-} = -\frac{L}{l_e}$, with l_e the equilibrium half-length of the mesa.

We can now write an ODE-PDE system that can be solved to obtain the location of the mesa interfaces as a function of time,

$$\begin{aligned} w_T &= \mathcal{D}_0 w_{xx} + 1 + \frac{L}{l_e}\left[H(x - l_1) - H(x - l_2)\right], \\ w_x &= 0 \text{ at } x = \pm L, \\ \frac{dl_1}{dT} &= \mu w(l_1, t), \\ \frac{dl_2}{dT} &= -\mu w(l_2, T), \end{aligned} \tag{5.45}$$

where

$$\mathcal{D}_0 \equiv \frac{\mathcal{D}}{\tilde{\tau}_0}, \qquad \mu \equiv \frac{1}{\kappa_0}\frac{g_-}{\tilde{\tau}_0}, \qquad H(z) = \begin{cases} 1 & \text{if } z > 0 \\ 0 & \text{if } z < 0 \end{cases}.$$

Remark

(i) By performing linear stability analysis on (5.45) it is possible to recover (5.31).

(ii) Numerically solving (5.45) has the complication that it is necessary to discretize a Heaviside function. Doing this directly will introduce errors of order h, with h the mesh spacing. This limitation can be mitigated by using a differentiable approximation to $H(z)$.

In our numerical calculation we used the following discretization,

$$H(z) \sim \begin{cases} H(z) & \text{if } |z| \geq \delta \\ \frac{1}{2} + \frac{z}{2\delta} + \frac{1}{2\pi}\sin\left(\frac{\pi z}{\delta}\right) & \text{if } |z| \leq \delta \end{cases},$$

with $\delta = O(h)$.

To illustrate the theory, we solved (5.45) for the GMS system, and compared it with a full numerical simulation. We chose parameters similar to those in Figure 5.1, specifically $\kappa = 1$. From the top figures we can see that for a domain half-length $L = 2.5$, the solution will become unstable first to a breather instability. The critical τ for the breather and zigzag instabilities is $\tau \sim 10,000$ and $\tau \sim 40,000$, respectively. We can see from Figure 5.2 that the full numerical solution compares well with the ODE-PDE approximation. As expected from the threshold values, the solution became unstable to a breather instability, and the ODE-PDE system matches well the period and amplitude of the full solution.

When choosing a τ value that is above both the breather and zigzag instabilities, it is possible to get solutions where the mesa walls collide with each other. This is not an issue in the ODE-PDE system, however, attempting to solve the full system will result in the solution collapsing, as can be seen in Figure 5.2 on the right. A similar result was studied in more detail in [33], although they worked in the parameter regime $\tau = O(\varepsilon^{-2})$, whereas in our system we consider $\tau = O(\varepsilon^{-3})$.

5.3.2 Stability proof for the breather case

In order to prove that the system is stable before the Hopf point, we will utilize the Nyquist stability criteria. The argument principle states a complex function $f(z)$, analytic in a simply connected domain G except for at most a finite number of poles satisfies

$$Z - P = \frac{1}{2\pi}\Delta\arg(f)|_C,$$

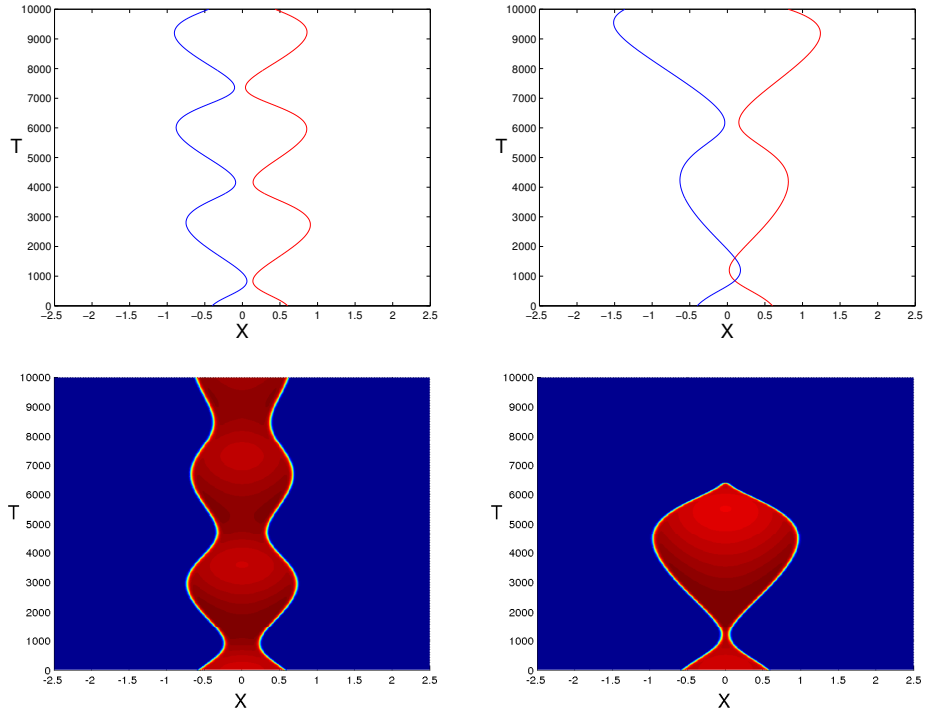

Figure 5.2: A comparison between the ODE-PDE system (5.45) and the full numerical simulation for a system beyond the Hopf threshold. The figures in the left correspond to $\tau = 25,000$, and the images in the right to $\tau = 65,000$. The rest of the parameters are $D = 50, \varepsilon = 0.01$. The solution was integrated until $T = 10,000$, with an IMEX scheme with 800 grid points.

with Z and P the number of zeroes and poles of $f(z)$ in G, respectively; C a closed contour in G not passing through any of the poles or zeroes; and $\Delta\arg(f)|_C$ the change in $\arg(f)|_C$ as C is traversed counter-clockwise.

The Nyquist stability criteria is an application of the argument principle on a contour that encompasses the right half-plane. If a dynamical system represented by a function $f(z)$, with no poles on the right half plane is thus shown to have $\Delta\arg(f)|_C = 0$, then the solutions to the system will be stable.

We will focus on equations (5.40); with $\Lambda = z/\tau_0$ we have that $f(z)$ is

$$\begin{aligned} f_+(z) &= \frac{z}{\tau_0} + \frac{1}{\sqrt{z}\left[\tanh(\sqrt{z}(L-l)) + \tanh(\sqrt{z}l)\right]} + \left(1 - \frac{L}{l}\right)\frac{l^2}{L}, \\ f_-(z) &= \frac{z}{\tau_0} + \frac{1}{\sqrt{z}\left[\tanh(\sqrt{z}(L-l)) + \coth(\sqrt{z}l)\right]} + \left(1 - \frac{L}{l}\right)\frac{l^2}{L}, \end{aligned} \tag{5.46}$$

If we approach $z = 0$ along the imaginary axis, as $z \to 0$ we have that

$$\begin{aligned} f_+(z) &\simeq \frac{1}{Lz}, \\ f_-(z) &\simeq \frac{z}{\tau_0} + \frac{l}{z(L-l)+1} + \left(1 - \frac{L}{l}\right)\frac{l^2}{L} \simeq \frac{l^2}{L} \end{aligned}$$

therefore $f_+(z)$ has a simple pole at the origin, whereas $f_-(z)$ has a removable singularity instead.

Taking this into consideration, we will check the Nyquist criterion on $f_+(z)$ on the contour given in Figure 5.3, whereas for f_- it would only be necessary to use C_R and the full imaginary axis.

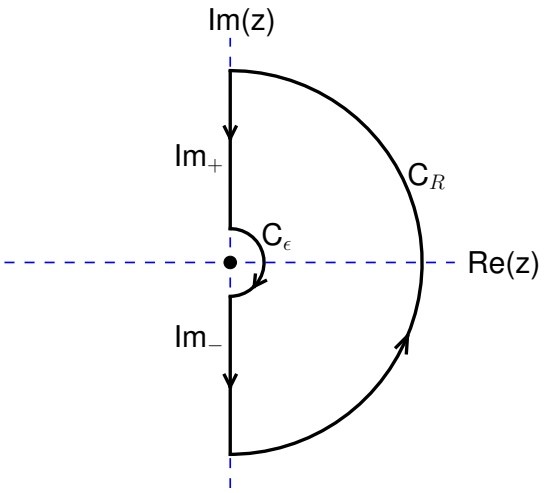

Figure 5.3: The contour on which to check the Nyquist stability criterion.

The four sections on the contour are given by

$$\begin{aligned} C_R &: z = Re^{i\theta}, \quad -\pi/2 < \theta < \pi/2, \\ C_\varepsilon &: z = \varepsilon\, e^{i\theta}, \quad \pi/2 > \theta > -\pi/2, \\ \mathrm{Im}_+ &: z = te^{i\pi/2}, \quad R > t > \varepsilon\,, \\ \mathrm{Im}_- &: z = te^{i\pi/2}, \quad -\varepsilon > t > -R, \end{aligned}$$

and we consider the limit when $\varepsilon \to 0$ and $R \to \infty$.

On C_R, we expand $\tanh(z)$ as

$$\tanh(a+ib) = \frac{\tanh(a)+\tanh(ib)}{1+\tanh(a)\tanh(ib)} = \frac{\sinh(a)\cos(b)+i\cosh(a)\sin(b)}{\cosh(a)\cos(b)+i\sinh(a)\sin(b)}. \tag{5.47}$$

In this case we have that $a+ib = \sqrt{R}e^{i\theta/2}(L-l)$, hence $a = \sqrt{R}(L-l)\cos(\theta/2)$, and $b = \sqrt{R}(L-l)\sin(\theta/2)$, with $-\pi/2 < \theta < \pi/2$. Since for $x \to \infty$ we have that $\sinh(x) \simeq \cosh(x)$, we have that on C_R $\tanh(z) \to 1$, and

$$f(z) = \frac{Re^{i\theta}}{\tau_0} + O(R^{-1/2}) + O(1) \simeq \frac{Re^{i\theta}}{\tau_0}.$$

Thus, the change in argument in C_R is $\Delta\arg(f)|_{C_R} = \pi/2 - -\pi/2 = \pi$.

On C_ε, we can see from (5.47) that when $a, b \to 0$

$$\tanh(a+ib) \simeq \frac{a+ib}{1+iab} \simeq a+ib,$$

therefore, we have that

$$f(z) \simeq \frac{\varepsilon\, e^{-i\theta}}{\tau_0} + \frac{e^{i\theta}}{L\varepsilon} + \left(1-\frac{L}{l}\right)\frac{l^2}{L} \simeq \frac{e^{i\theta}}{L\varepsilon},$$

for $\varepsilon \to 0$.

Therefore, the change in argument in C_ε is also $\Delta\arg(f)|_{C_\varepsilon} = \pi$.

On Im_+, we have $z = it$, on $R > t > \varepsilon$. We have that

$$f_+(it) = \frac{it}{\tau_0} + \frac{1}{\sqrt{it}\left[\tanh(\sqrt{it}(L-l)) + \tanh(\sqrt{it}l)\right]} + \left(1 - \frac{L}{l}\right)\frac{l^2}{L}.$$

When $t \to \infty$ we have

$$\begin{aligned}\mathrm{Re}[f_+(it)] &\simeq \left(1 - \frac{L}{l}\right)\frac{l^2}{L} < 0,\\ \mathrm{Im}[f_+(it)] &\simeq \frac{t}{\tau_0} \to \infty.\end{aligned}$$

Therefore, since the contour is traversed counterclockwise, we have $\arg(f)|_{i\infty} = -\pi/2$.

Similarly, when $t \to 0$, we approximate $\tanh(x) \simeq x - \frac{x^3}{3}$, and upon expanding f_+ we get

$$f_+(it) \simeq \frac{\frac{t^2 L}{3}(L^2 - 3Ll + 3l^2) - itL}{t^2L^2 + \frac{t^4L^2}{9}(L^2 - 3Ll + 3l^2)^2} + \left(1 - \frac{L}{l}\right)\frac{l^2}{L},$$

and upon cancelling the fourth order term in the denominator, we get that the real and imaginary components are

$$\mathrm{Re}[f_+(it)] \simeq \frac{L^2 - 6Ll + 6l^2}{3L}, \tag{5.48a}$$

$$\mathrm{Im}[f_+(it)] \simeq -\frac{1}{tL}, \tag{5.48b}$$

with the real part independent of t.

Equation (5.48a) defines a new condition on the existence of a Hopf bifurcation for the breather eigenvalue. If (5.48a) is negative, then the change in argument in both imaginary axis segments will be of -2π combined, cancelling the contributions from C_R and C_ε, and thus guaranteeing that solutions will be sta-

ble. However, if the domain length L satisfies that either $L < (3-\sqrt{3})l$, or that $(3+\sqrt{3})l < L$, then (5.48a) will be positive at one point. If it so happens that f_+ is positive while crossing the real axis, then the change in argument will have the opposite sign, and by the argument theorem we will have two positive real-valued zeros, hence instability.

Therefore, solutions will be stable provided that

$$\frac{L^2 - 6Ll + 6l^2}{3L} < 0. \tag{5.49}$$

Since the change from negative to positive in the real part doesn't necessarily have to happen at the two endpoints we approximated, it is best to estimate it numerically in order to get an idea of the dependence on τ_0.

It would be interesting to explore the conditoin (5.49) on a numerical simulation.

5.4 Case study: the predator-prey model

We will apply the mesa theory developed in §5 to a spatio-temporal predator-prey model. We will focus on the transverse stability of a K-mesa solution in the near-shadow regime $D = O(1/\varepsilon)$, and we will present some numerical results in the mesa-splitting regime $D = O(1)$.

The specific model we will study is a ratio-dependent predator-prey system with a Michaelis-Menten type functional response. The spatially homogeneous model was originally posited in [64], and the full spatio-temporal model was discussed in [2], and [62].

The model in question is

$$\begin{aligned}\frac{\partial N}{\partial t} &= D_1\nabla^2 N + rN\left(1-\frac{N}{K}\right) - \frac{\alpha NP}{P+\alpha\beta N},\\ \frac{\partial P}{\partial t} &= D_2\nabla^2 P - \gamma P + \frac{e\alpha NP}{P+\alpha\beta N},\end{aligned} \tag{5.50}$$

where N, P are the prey and predator densities, respectively; D_1, D_2 are their diffusion coefficients; r is the maximal growth rate for the prey, K is the carrying capacity, α is the capture rate, β is the handling time, e is the conversion efficiency, and γ is the predator death rate.

By nondimensionalizing time (see [2]), the system can be simplified to

$$\begin{aligned}U_t &= D_U\nabla^2 U + U(1-U) - \frac{AUV}{U+V}\\ V_t &= D_V\nabla^2 V - CV + \frac{BUV}{U+V},\end{aligned} \tag{5.51}$$

and the parameter values used in the paper were $D_U = 1,\ D_V = 8,\ A = 1.1,\ B = 0.9$, and $C = 0.1$; and with V and U the populations of predators and prey, respectively.

It is possible to simplify the model a bit more. By letting $\hat{x} = x/L$, and rescaling in the domain length, for 1D we get, after dropping the hats,

$$\begin{aligned}u_t &= \varepsilon^2 u_{xx} + u(1-u) - \frac{auv}{u+v} = \varepsilon^2 u_{xx} + f(u,v)\\ \tau v_t &= Dv_{xx} - v + \frac{buv}{u+v} = Dv_{xx} + g(u,v).\end{aligned} \tag{5.52}$$

In terms of the original parameters in (5.50), we have that $a = \alpha/r$, $b = \frac{e}{\gamma\beta}$, $\tau = r/\gamma$, $\varepsilon^2 = \frac{D_1}{rL^2}$, and $D = \frac{D_2}{\gamma L^2}$. The parameter τ, for instance, represents the ratio between the maximal prey growth rate and the predator death rate.

We will discuss two distinguished regimes: the near-shadow regime where

$D = O(1/\varepsilon)$, and the splitting regime where $D = O(1)$.

5.4.1 Preliminaries

There are three possible homogeneous steady-state solutions, however, the only non-trivial one that can yield a Turing instability is given by

$$u_h = 1 - a\left(1 - \frac{1}{b}\right),$$
$$v_h = u_h(b-1)$$

The Turing space associated with the system, as a function of the parameters a and b, is given by Figure 5.4.

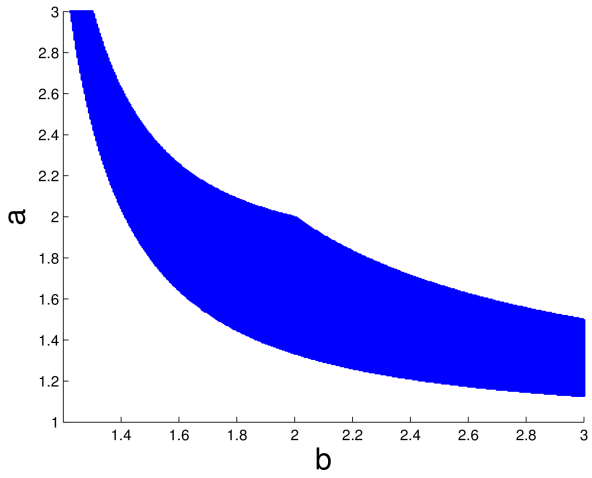

Figure 5.4: Turing space for the system given by 5.52, in term of the parameters a and b.

In the near-shadow limit, when $D = \mathcal{D}/\varepsilon$, with $\mathcal{D} = O(1)$, the width of the mesa can be established in a straightforward manner. Integrating over half of the stationary v equation in 5.52, and from the Neumann boundary conditions and the

symmetry at the centre of the mesa we have that

$$\int_0^L g(u,\mathcal{V})dx = 0.$$

Furthermore, splitting the integral in two, at the location of the interface, yields

$$\begin{aligned}
0 &= \int_0^{l^-} \left(\frac{\mathcal{D}}{\varepsilon}v_{xx} + g(u,\mathcal{V})\right) dx + \int_{l^+}^{L} \left(\frac{\mathcal{D}}{\varepsilon}v_{xx} + g(u,\mathcal{V})\right) dx,\\
0 &= \frac{\mathcal{D}}{\varepsilon}v_x(l^-) + g(u_+,\mathcal{V})l - \frac{\mathcal{D}}{\varepsilon}v_x(l^+) + g(u_-,\mathcal{V})(L-l),\\
l &= \frac{g(u_-,\mathcal{V})}{g(u_-,\mathcal{V}) - g(u_+,\mathcal{V})}L = \frac{u_+ + \mathcal{V}}{bu_+}L,
\end{aligned}$$

with $v_x(l^-) = v_x(l^+)$ from the fact that $v(x)$ is a smooth function.

Plotting the half-mesa width versus the parameter a yields the result shown in Figure 5.5. Notice that for much of the parameter space which satisfies the Turing conditions the mesa width would be very close or above the domain length L.

For these two specific choices in b we get the consistency conditions that $a > 1.45$ for $b = 3$, and $a > 1.2$ for $b = 2$. The stationary $u(x)$ solution with a wide mesa depicted in Figure 5.5 corresponds to parameter values that fall squarely in the Turing regime. The parameters that give rise to the narrower mesa ($a = 3, b = 2$) are outside of the Turing space.

The bifurcation diagram for the solution as the domain length L increases, as a function of the L2 norm of the solution, is shown in Figure 5.6. The branch of solutions connects with the Turing solution, and eventually with the homogeneous solution, at the lowest part of the branch, on one edge with the 1-mode Turing solution, and on the unstable side with the 2-mode Turing solution.

Past the cusp we have the unstable solutions that lead to the splitting of the solution. As in the GMS case, there will be a family of identical branches for larger

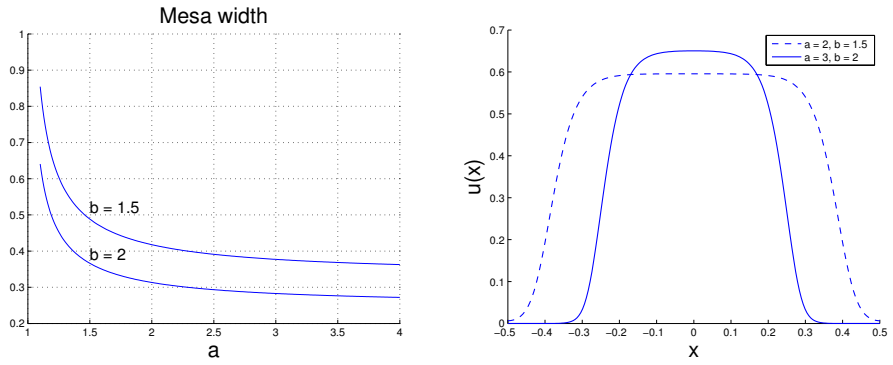

Figure 5.5: The figure on the left shows the projected half-width of a mesa versus the parameter a, for two values of b, and for $L = 0.5$. Notice that there is a consistency requirement on a, given that we must satisfy $l < L$. The second figure shows two stationary solutions for different values of the parameters that illustrates the change in mesa width.

L values representing the 2^n mesa branch.

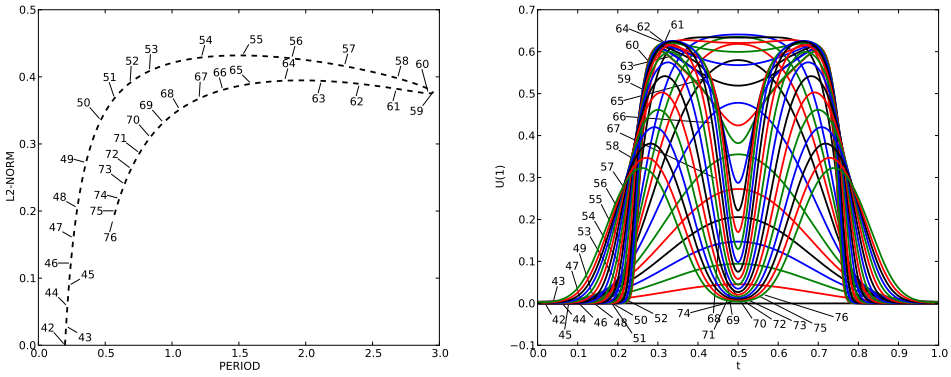

Figure 5.6: The bifurcation diagram for the one mesa solution, and solutions corresponding to various points along the branch. The bifurcation diagram was computed using AUTO [14]. The parameters used were $a = 3, b = 2, \tau = 1, D = 1$, with the asymptotic term $\varepsilon = 0.02$.

5.4.2 Stability in the near-shadow regime, $D = O(\varepsilon^{-1})$

We now study the stability of mesa stripes to transverse perturbations. We will apply the general results from § 5 and test the theory in a different model. This type of analysis was previously computed for the GMS model in § 4.4.2.

From the general mesa theory developed in § 5.2, we need to first compute the heteroclinic Maxwell line parameters u_+ and $\mathcal{V}$ (it is straightforward to check that $u_- = 0$). These will be the key elements necessary to determine the zigzag and breather eigenvalues. We need to find u_+ and $\mathcal{V}$ such that

$$\begin{aligned} f(u_+, \mathcal{V}) &= f(0, \mathcal{V}) = 0, \\ \int_0^{u_+} f(u, \mathcal{V}) du &= 0. \end{aligned} \tag{5.53}$$

Computing the values was done using a Newton method. The results are shown in Figure 5.7, where we show the numerical values for u_+ and $\mathcal{V}$, as well as for $\beta_{pp} = \int_{-\infty}^{\infty} (U_0')^2 dy$. This last value was constant for the GMS model, but depends on the parameter a in the Predator-Prey model. These are the building blocks that

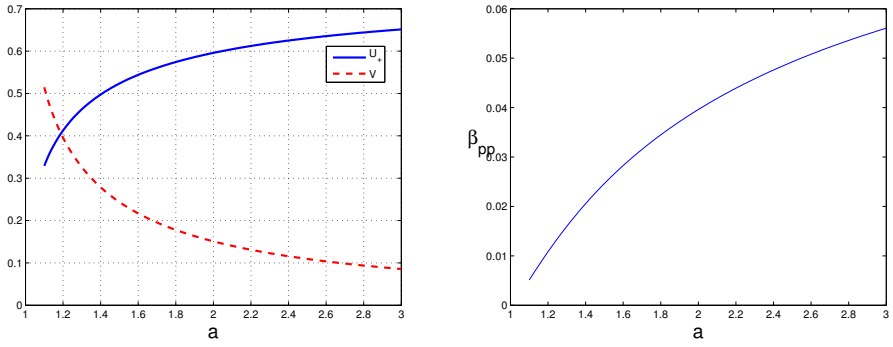

Figure 5.7: The values of u_+ and $\mathcal{V}$ that satisfy the heteroclinic connection as a function of the parameter a (right figure), and the parameter $\beta_{pp} = \int_{-\infty}^{\infty} (U_0')^2 dy$.

are required to establish the stability of a K-mesa solution. From lemma 5.2 we have:

A steady-state solution of K mesas admits $2K$ eigenvalues, and these are given by the following formula

$$\lambda_{\pm_j} = \frac{\varepsilon^2}{\alpha}\left[\omega_{\pm_j} + \left(1 - \frac{L}{l}\right)\frac{l^2}{L^2}L - m^2\alpha\right] \qquad \text{for } j = 1, \cdots, K-1,$$

for the first $2K-2$ eigenvalues, and where

$$\omega_{\pm_j} = \frac{1}{d + \frac{1}{\chi} \pm \left(e^2 + \frac{1}{\chi^2} + \frac{2e}{\chi}\cos(\pi j/K)\right)^{1/2}}, \qquad j = 1, \cdots, K-1.$$

Finally, the two remaining eigenvalues are

$$\lambda_{\pm K} = \frac{\varepsilon^2}{\alpha}\left[\omega_{\pm K} + \left(1 - \frac{L}{l}\right)\frac{l^2}{L^2}L - m^2\alpha\right],$$

with

$$\omega_{+K} = \frac{1}{d+e}, \qquad \omega_{-K} = \frac{1}{d-e}.$$

The various quantities are:

$$\begin{aligned}
d &= \sigma_- \tanh[\sigma_-(L-l)] + \sigma_+ \coth(2\sigma_+ l),\\
e &= \sigma_+ \mathrm{csch}\,(2\sigma_+ l),\\
\chi &= \sigma_-^{-1}\sinh[2\sigma_-(L-l)],\\
\sigma_\pm^2 &= m^2 - \frac{\varepsilon}{\mathcal{D}}\left(g_v^\pm - \frac{f_v^\pm}{f_u^\pm}g_u^\pm\right) + \frac{\varepsilon\,\tau\lambda}{\mathcal{D}},\\
m &= \frac{k\pi}{d_0}, \text{ for } k = 1, \ldots,\\
l &= \frac{g_-}{g_- - g_+}L + O(\varepsilon).
\end{aligned}$$

It is worth noting that in the regime with $\tau = 0(1)$, the term $\frac{\varepsilon\tau\lambda}{\mathcal{D}}$ in $\sigma_{\pm}$ can be discarded, as we have that $\lambda = O(\varepsilon^2)$.

Implementing this in software was very straightforward. We started by choosing a value of a, and computing the eigenvalues for the two-mesa case for a range of values in the parameter b. We wanted to find a set of parameters that enabled us to observe a transverse instability, so we next chose a b value that resulted in $\lambda > 0$, specifically for the zigzag eigenvalue λ_{-}. With this set of values for (a, b), we next ranged on the mode M, as this would determine the type of instability (mode one, mode two, etc.)

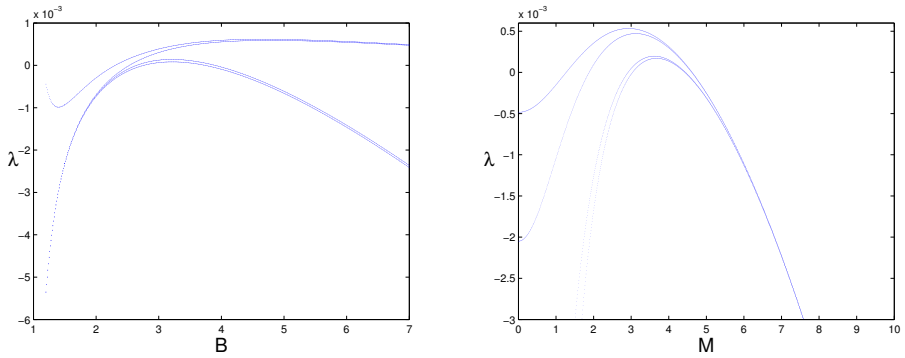

Figure 5.8: The four eigenvalues of a two mesa solution, as a function of b (left), and as a function of M (right). The parameters are $D = 3, A = 1.6, \varepsilon = 0.01, L = 1,$, and $M = \pi$ for the figure on the left, and $B = 3.5$ for the figure on the right.

The results from the eigenvalue calculation are shown in Figure 5.8. With the parameter choice $(a, b) = (1.6, 3.5)$ we expect to have a solution that becomes unstable to mode-one on a domain with width $d_0 = 1$, while remaining stable to mode-two instabilities. If the domain width were to increase to $d_0 = 2$, we could expect to see mode-two instabilities as well (since $m = k\pi/d_0$, with $k = 1, 2, \ldots$).

Armed with the parameters previously computed, we proceeded to run a full

numerical simulation of the Predator-Prey model on a 2D lattice. We used a very similar scheme as the one used for the GMS simulation, although this model has a less diagonally-dominant matrix, necessitating higher numerical accuracy.

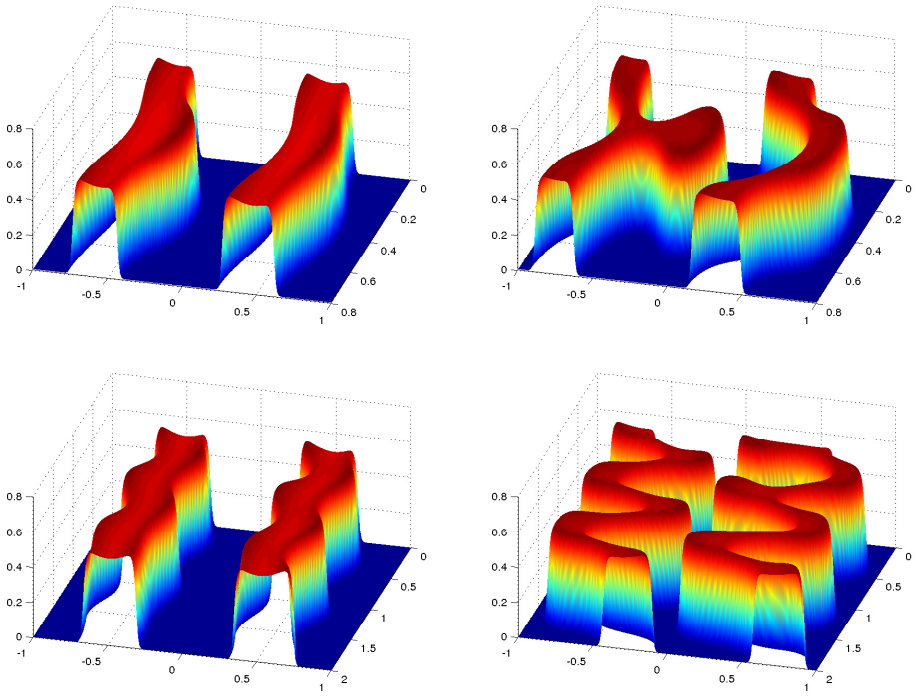

Figure 5.9: Full numerical simulation of the Predator-Prey model on a 2D lattice. We used $\varepsilon = 0.01, D = 0.4, a = 1.6, b = 3.5, \tau = 1$. Both lattices were $-1 < x < 1$, and the lattice on the left had $0 < y < 0.8$, while the lattice on the right had $0 < y < 2$. The figures on the left were integrated until $T = 5,000$, and the figures on the right until $T = 10,000$.

We integrated until $T = 10,000$ (Figure 5.9), and chose the domain width to allow for a mode-one instability (left), and a mode-two instability (right), and recorded an image at $T = 5,000$. Both mesas started from a stationary solution with a small amount of noise added. As expected, the solution on the smaller

domain became unstable to a mode-one instability, and when extending the domain we saw the emergence of a mode-two instability.

Chapter summary

In this chapter we extend the results obtained for the GMS system to general mesa systems. We start by constructing a solution and then derive thresholds for the transverse stability of multiple mesa stripes on the shadow regime.

Furthermore, we study the stability to Hopf bifurcations and derive an ODE-PDE system that reduces the problem to that of finding the location of the mesa interfaces as a function of time. The system is compared to full numerics and found to be in good agreement. We study the analytic stability for the breather case by means of the Nyquist stability criteria.

The general model is then verified by applying it on a Predator-Prey model and analyzing its stability to transverse perturbations. In the splitting regime we generate a bifurcation diagram by means of numerical continuation, and in the near-shadow regime we compare the results of the theory on a two stripe system with full numerics.

Chapter 6

Future directions

The following is a list of topics that we think would be interesting to explore in more detail.

1. The instabilities that we studied in the Brusselator model, particularly the self-replication and the competition instabilities, could interact with each other and give rise to complicated dynamics.

   We observed that as $f \to 1$, the stable region where the real part $\mathrm{Re}[\lambda] < 0$ decreases. we suspect that it is possible to find a regime where the splitting and competition instability thresholds are close enough that when one of the instabilities is triggered the system lands in the unstable regime for the other instability, and vice versa. A train of events could occur with the instabilities alternating. This is close in spirit to the work by Painter et al [44] on a chemotaxis model.

   The main hurdle to studying this problem is that it is computationally expensive to integrate for long enough time to observe multiple events. The time scale for the slow motion of the spots is $O(\varepsilon^{-2})$, hence an efficient numerical solver would be key.

2. The problem of the slow motion of the spots was addressed for the case of the Schnakenberg model on the sphere, and a similar calculation should yield similar results for the Brusselator model.

   From what we can tell, the dynamical system that we obtained is new; it would be interesting to determine the existence of stationary solutions and stable orbits, and how they relate to the quasi-stationary solutions and the Fekete problem.

3. While most of the work we did was in the fully nonlinear regime, it would be interesting to connect the results we obtained with the wide body of literature that exists on Turing systems in the weakly nonlinear regime. There are two approaches where the tools of weakly nonlinear analysis would be beneficial:

   - To obtain a global bifurcation picture for solutions on the sphere by connecting both regimes by means of a numerical continuation. This could throw light on the existence of asymmetric solutions, as well as clarifying the picture of the degenerate solutions on the sphere.
   - The particle-like solutions we obtained in our analysis were useful in determining bifurcation thresholds, however the technique did not allow us to determine analytically the type of bifurcations, although from numerical experimentation it seems they were subcritical. Performing a weakly nonlinear stability analysis on the particle-like solutions would be useful to get a more complete picture of the bifurcation structure.

4. Beyond non spherical domains, the problem for a general surface has yet to be addressed. Three possible avenues for study are possible:

   - The case of perturbations on the sphere.
   - Other structures where a Green's function can be obtained, such as spherical hemispheres, or paraboloids.
   - General surfaces, where the problem is that of obtaining a Green's function. As far as we can tell this hasn't been done yet.

5. Back to the Brusselator case, we established the Hopf bifurcation threshold numerically but for lack of time were not able to study it in detail. Full numerical analysis is necessary to complete the picture, and it is possible that it can interact with the other two instabilities in a complicated dynamical system.

6. As was done for the mesa case, where a general theory was developed, it should be possible to obtain a general theory for systems with spot solutions on the sphere, both for the stability of the solutions, and for the slow motion of the spots.

Bibliography

[1] E. L. Altschuler and A. Prez-Garrido. Global minimum for thomsons problem of charges on a sphere. *Physical Review E*, 71(4):047703, 2005. URL http://pre.aps.org/abstract/PRE/v71/i4/e047703. → pages 5

[2] M. Banerjee. Self-replication of spatial patterns in a ratio-dependent predator-prey model. *Mathematical and Computer Modelling*, 51(1-2):4452, 2010. → pages 2, 216, 217

[3] I. Barrass, E. J. Crampin, and P. K. Maini. Mode transitions in a model reaction–diffusion system driven by domain growth and noise. *Bulletin of Mathematical Biology*, 68:981–995, 2006. → pages 3, 131, 134

[4] B. P. Belousov. A periodic reaction and its mechanism. *Compilation of Abstracts on Radiation Medicine*, 147:145, 1959. → pages 1

[5] D. E. Bentil and J. D. Murray. On the mechanical theory for biological pattern formation. *Physica D: Nonlinear Phenomena*, 63(1-2):161190, 1993. → pages 2

[6] B. Bergersen, D. Boal, and P. Palffy-Muhoray. Equilibrium configurations of particles on a sphere: the case of logarithmic interactions. *Journal of Physics A: Mathematical and General*, 27:2579, 1994. URL http://iopscience.iop.org/0305-4470/27/7/032. → pages 5

[7] J. P. Berrut and L. N. Trefethen. Barycentric lagrange interpolation. *Siam Review*, 46(3):501517, 2004. → pages 122, 123

[8] S. Boatto. Curvature perturbations and stability of a ring of vortices. *Discrete and continuous dynamical systems. Series B*, 10(2-3), 2008. → pages 5, 117, 118

[9] S. Boatto and H. E. Cabral. Nonlinear stability of a latitudinal ring of point-vortices on a nonrotating sphere. *SIAM Journal on Applied Mathematics*, 64(1):216230, 2003. → pages 115, 117, 118

[10] M. A. J. Chaplain, M. Ganesh, and I. G. Graham. Spatio-temporal pattern formation on spherical surfaces: numerical simulation and application to solid tumour growth. *Journal of Mathematical Biology*, 42(5):387423, 2001. → pages 3, 121

[11] D. Coombs, R. Straube, and M. J. Ward. Diffusion on a sphere with localized traps: Mean first passage time, eigenvalue asymptotics, and fekete points. *SIAM J. Appl. Math*, 70(1):302332, 2009. → pages 42, 86

[12] E. J. Crampin, E. A. Gaffney, and P. K. Maini. Reaction and diffusion on growing domains: Scenarios for robust pattern formation. *Bulletin of Mathematical Biology*, 61:1093–1120, 1999. → pages 3, 131

[13] E. J. Crampin, W. W. Hackborn, and P. K. Maini. Pattern formation in reaction-diffusion models with nonuniform domain growth. *Bulletin of Mathematical Biology*, 64:747–769, 2002. → pages 3, 131

[14] E. Doedel, A. Champneys, T. Fairgrieve, Y. Kuznetsov, B. Oldeman, R. Paffenroth, B. Sandstede, X. Wang, and C. Zhang. AUTO-07P: continuation and bifurcation software for ordinary differential equations., 2007. *URL http://indy. cs. concordia. ca/auto*. → pages xii, 139, 143, 220

[15] A. Gierer and H. Meinhardt. A theory of biological pattern formation. *Biological Cybernetics*, 12(1):30–39, 1972. → pages 2, 4, 126

[16] J. Gjorgjieva. *Turing pattern dynamics for spatiotemporal models with growth and curvature*. PhD thesis, PhD Thesis, 2006. → pages 4, 87, 121

[17] J. Gjorgjieva and J. Jacobsen. Turing patterns on growing spheres: The exponential case. *Dynamical Systems*, pages 436–445, 2007. → pages 4, 121, 123, 131

[18] M. I. Jamaloodeen and P. K. Newton. The n-vortex problem on a rotating sphere. II. heterogeneous platonic solid equilibria. *Proceedings of the Royal Society A: Mathematical, Physical and Engineering Science*, 462(2075): 32773299, 2006. → pages 5, 116

[19] R. Kidambi and P. K. Newton. Motion of three point vortices on a sphere. *Physica D: Nonlinear Phenomena*, 116(1-2):143175, 1998. → pages 15

[20] R. Kidambi and P. K. Newton. Point vortex motion on a sphere with solid boundaries. *Physics of Fluids*, 12:581, 2000. → pages 15

[21] Y. Kimura and H. Okamoto. Vortex motion on a sphere. *Physical Society of Japan, Journal*, 56:42034206, 1987. → pages 5, 15

[22] T. Kolokolnikov, M. J. Ward, and J. Wei. The stability of a stripe for the gierer-meinhardt model and the effect of saturation. *SIAM J. Appl. Dyn. Sys*, 5:313–363. → pages 6, 126, 167, 195, 196, 199, 200

[23] T. Kolokolnikov, M. J. Ward, and J. Wei. Self-replication of mesa patterns in reaction–diffusion systems. *Physica D: Nonlinear Phenomena*, 236: 104–122, 2007. → pages 6, 135

[24] T. Kolokolnikov, M. J. Ward, and J. Wei. Spot Self-Replication and dynamics for the Schnakenberg model in a Two-Dimensional domain. *Journal of Nonlinear Science*, 19(1):1–56, 2009. → pages 93, 95, 108, 114, 118, 144

[25] S. Kondo and R. Asai. A reaction–diffusion wave on the skin of the marine angelfish pomacanthus. *Nature*, 376:765–768, 1995. → pages 2, 85, 131

[26] H. Levine and W. J. Rappel. Membrane-bound turing patterns. *Physical Review E*, 72(6):61912, 2005. → pages 3

[27] A. Madzvamuse, A. J. Wathen, and P. K. Maini. A moving grid finite element method applied to a model biological pattern generator. *Journal of Computational Physics*, 190(2):478–500, 2003. → pages 131

[28] A. Madzvamuse, E. A. Gaffney, and P. K. Maini. Stability analysis of non-autonomous reaction-diffusion systems: the effects of growing domains. *Journal of Mathematical Biology*, 2009. → pages 3, 131, 134

[29] P. K. Maini, K. J. Painter, and H. N. Chau. Spatial pattern formation in chemical and biological systems. *J. Chem. Soc., Faraday Trans.*, 93(20): 36013610, 1997. → pages 2

[30] P. C. Matthews. Pattern formation on a sphere. *Physical Review E*, 67(3): 036206, 2003. → pages 87

[31] T. O. Maxwell. *Periodic and connecting orbits of Hamiltonian systems*. University of WisconsinMadison, 1994. → pages 136, 149, 172

[32] R. McKay and T. Kolokolnikov. Stability transitions and dynamics of localized patterns near the shadow limit of reaction-diffusion systems. *Discrete and Continuous Dynamical Systems B, to appear*, 2012. → pages 171

[33] R. C. McKay, T. Kolokolnikov, and P. Muir. Interface oscillations in reaction-diffusion systems beyond the hopf bifurcation. *Journal of Dynamics and Differential Equations*, 2011. → pages 211

[34] H. Meinhardt. *The algorithmic beauty of sea shells*. Springer Verlag, 2009. → pages 2, 126

[35] T. Miura, K. Shiota, G. Morriss-Kay, and P. K. Maini. Mixed-mode pattern in doublefoot mutant mouse limbTuring reactiondiffusion model on a growing domain during limb development. *Journal of theoretical biology*, 240(4):562–573, 2006. → pages 3, 131

[36] J. D. Murray. A pre-pattern formation mechanism for animal coat markings. *Journal of Theoretical Biology*, 88(1):161199, 1981. → pages 2

[37] J. D. Murray. *Mathematical biology. Vol. 2: Spatial models and biomedical applications.* Interdisciplinary Applied Mathematics, 2003. → pages 2, 86, 127

[38] W. Nagata, L. G. Harrison, and S. Wehner. Reaction-diffusion models of growing plant tips: bifurcations on hemispheres. *Bulletin of mathematical biology*, 65(4):571–607, 2003. → pages 3, 87

[39] J. C. Neu. Vortices in complex scalar fields. *Physica D: Nonlinear Phenomena*, 43(2-3):385406, 1990. URL http://www.sciencedirect.com/science/article/pii/016727899090143D. → pages 5

[40] P. K. Newton. *The N-vortex problem: analytical techniques*, volume 145. Springer Verlag, 2001. → pages 5, 115

[41] P. K. Newton and G. Chamoun. Vortex lattice theory: A particle interaction perspective. *SIAM review*, 51(3):501, 2009. URL http://www.tims.ntu.edu.tw/download/talk/20110110_1492.pdf. → pages 5

[42] I. L. Novak, F. Gao, Y. S. Choi, D. Resasco, J. C. Schaff, and B. M. Slepchenko. Diffusion on a curved surface coupled to diffusion in the volume: Application to cell biology. *Journal of computational physics*, 226 (2):1271–1290, 2007. → pages 86

[43] H. G. Othmer, K. Painter, D. Umulis, and C. Xue. The intersection of theory and application in elucidating pattern formation in developmental biology. *Mathematical Modelling of Natural Phenomena*, 4(4):3–82, 2009. → pages 85

[44] K. J. Painter and T. Hillen. Spatio-temporal chaos in a chemotaxis model. *Physica D: Nonlinear Phenomena*, 240(4):363375, 2011. URL http://www.sciencedirect.com/science/article/pii/S0167278910002617. → pages 226

[45] R. G. Plaza, F. S. Garduño, P. Padilla, and R. A. Barrio. The effect of growth and curvature on pattern formation. *Journal of Dynamics and Differential Equations*, 16(4):1093–1121, 2004. → pages 131, 132

[46] W. H. Press, B. P. Flannery, S. A. Teukolsky, and W. T. Vetterling. Numerical recipes in c: the art of scientific programming. *Cambridge U. Press, Cambridge, England*, 1992. → pages 122, 123

[47] I. Prigogine and R. Lefever. Symmetry breaking instabilities in dissipative systems. II. *The Journal of Chemical Physics*, 48:1695, 1968. → pages 2, 4, 8

[48] X. Ren and J. Wei. On the spectra of three-dimensional lamellar solutions of the diblock copolymer problem. *SIAM Journal on Mathematical Analysis*, 35:1, 2003. → pages 162

[49] S. J. Ruuth. Private communication. 2010. → pages 123

[50] S. J. Ruuth and B. Merriman. A simple embedding method for solving partial differential equations on surfaces. *Journal of Computational Physics*, 2007. → pages 122, 123

[51] E. B. Saff and A. B. Kuijlaars. Distributing many points on a sphere. *The Mathematical Intelligencer*, 19(1):511, 1997. → pages 120

[52] J. Schnakenberg. Simple chemical reaction systems with limit cycle behaviour. *Journal of Theoretical Biology*, 81(3):389–400, 1979. → pages 4, 85, 135

[53] L. A. Segel and J. L. Jackson. Dissipative structure: an explanation and an ecological example. *Journal of Theoretical Biology*, 37(3):545559, 1972. → pages 2

[54] M. B. Short, M. R. DOrsogna, V. B. Pasour, G. E. Tita, P. J. Brantingham, A. L. Bertozzi, and L. B. Chayes. A statistical model of criminal behavior. *Mathematical Models and Methods in Applied Sciences*, 18(S1):12491267, 2008. → pages 3

[55] N. Sloane. Tables of optimal arrangements of points on a sphere, 2000. → pages 119

[56] W. J. Stortelder, J. J. de Swart, and J. D. Pintr. Finding elliptic fekete points sets: two numerical solution approaches. *Journal of computational and applied mathematics*, 130(1-2):205–216, 2001. → pages 5

[57] D. Thompson. *On growth and form*. Cambridge University Press, 1963. → pages 3

[58] J. J. Thomson, H. Geiger, E. Marsden, E. Rutherford, H. Moseley, and J. Chadwick. On the structure of the atom. *Phylos Mag*, 7:237265, 1904. → pages 5, 31, 120

[59] W. H. Tse, J. Wei, and M. Winter. Spikes for the Gierer-Meinhardt system with many segments of different diffusivities. *Bulletin of the Institute of Mathematics, Academia Sinica*, 3(3-4):525, 2008. → pages 3

[60] A. M. Turing. The chemical theory of morphogenesis. *Phil. Trans. Roy. Soc*, 237:32, 1952. → pages 1, 127

[61] C. Varea, J. L. Aragón, and R. A. Barrio. Turing patterns on a sphere. *Physical Review E*, 60:4588–4592, 1999. → pages 3, 119, 121, 123

[62] W. Wang, Q. Liu, and Z. Jin. Spatiotemporal complexity of a ratio-dependent predator-prey system. *Physical Review E*, 75(5):051913, 2007. → pages 2, 4, 216

[63] J. Wei. On single interior spike solutions of the Gierer-Meinhardt system: uniqueness and spectrum estimates. *European Journal of Applied Mathematics*, 10(4):353378, 1999. → pages 5, 67, 70, 72, 126, 238, 243

[64] D. Xiao and S. Ruan. Global dynamics of a ratio-dependent predator-prey system. *Journal of Mathematical Biology*, 43(3):268ł290, 2001. → pages 216

Appendix A

Spherical coordinate tranformations

Lemma A.1 *Consider a point on the unit sphere*

$$\vec{x}_j = (\cos\phi_j \sin\theta_j, \sin\phi_j \sin\theta_j, \cos\theta_j),$$

with $0 < \phi_j < 2\pi,\ 0 < \theta_j < \pi$. *We will now show that as* $x \to x_j$ *then*

$$|\vec{x} - \vec{x}_j| = |\hat{y}| + \textit{small terms}, \qquad \textit{where } \hat{y} = (\hat{y_1}, \hat{y_2}) = (\sin\theta_j \hat{\phi}, \hat{\phi});$$

and where $\hat{\phi} = \phi - \phi_j$, *and* $\hat{\theta} = \theta - \theta_j$, *with* $\hat{\phi} \ll 1$, *and* $\hat{\theta} \ll 1$.

Proof Using the standard spherical coordinate transformation, we let

$$x = \cos\phi \sin\theta, \qquad y = \sin\phi \sin\theta, \qquad z = \cos\theta.$$

Linearizing $\phi = \phi_j + \hat{\phi}$, $\theta = \theta_j + \hat{\theta}$, we get

$$\begin{aligned} x &= x_j - \sin\phi_j \sin\theta_j \hat{\phi} + \cos\phi_j \cos\theta_j \hat{\theta} + \cdots, \\ y &= y_j + \cos\phi_j \sin\theta_j \hat{\phi} + \sin\phi_j \cos\theta_j \hat{\theta} + \cdots, \\ z &= z_j - \sin\theta_j \hat{\theta} + \cdots. \end{aligned}$$

In matrix form we have

$$\vec{x} = \vec{x_j} + M \begin{pmatrix} \hat{\phi} \\ \hat{\theta} \end{pmatrix}, \quad \text{with } M = \begin{pmatrix} -\sin\phi_j \sin\theta_j & \cos\phi_j \cos\theta_j \\ \cos\phi_j \sin\theta_j & \sin\phi_j \cos\theta_j \\ 0 & -\sin\theta_j \end{pmatrix}$$

with M a 3×2 matrix. We then have

$$|\vec{x} - \vec{x}_j|^2 = (\vec{x} - \vec{x}_j)^T (\vec{x} - \vec{x}_j) = (M_0 \hat{y})^T (M_0 \hat{y}) = \hat{y}^T M_0^T M_0 \hat{y},$$

with

$$\hat{y} = \begin{pmatrix} \hat{y}_1 \\ \hat{y}_2 \end{pmatrix} = \begin{pmatrix} \sin\theta_j \hat{\phi} \\ \hat{\theta} \end{pmatrix}, \text{ and } M_0 = \begin{pmatrix} -\sin\phi_j \sin\theta_j & \cos\phi_j \cos\theta_j \\ \cos\phi_j \sin\theta_j & \sin\phi_j \cos\theta_j \\ 0 & -\sin\theta_j \end{pmatrix}$$

We can now check that $M_0^T M_0 = I$.

Therefore, we conclude that as $\vec{x} \to \vec{x}_j$, we have

$$|\vec{x} - \vec{x}_j| = |\hat{y}| + \text{small terms.} \quad \blacksquare$$

Appendix B

Rigorous properties of NLEPs

The nonlocal eigenvalue problem in (2.100) has the general form

$$\Delta_\rho \tilde{\psi} - \tilde{\psi} + 2w\tilde{\psi} - \gamma w^2 \frac{\int_0^\infty \rho w \tilde{\psi} d\rho}{\int_0^\infty \rho w^2 d\rho} = \lambda \tilde{\psi}, \qquad 0 < \rho < \infty, \tag{B.1}$$

with $\tilde{\psi}'(0) = 0$ and $\tilde{\psi} \to 0$ as $\rho \to \infty$. Here $\gamma = \gamma(\lambda)$ is an analytic function of λ in the right half-plane Re$(\lambda) > 0$, and w is the radially symmetric ground-state solution of $\Delta_\rho w - w + w^2 = 0$ where $\Delta_\rho v \equiv v'' + \rho^{-1} v'$.

Remark

(i) Since this problem is not self-adjoint we must expect that complex eigenvalues are possible. We remark that an NLEP of the form

$$\mathcal{L}_0 \tilde{\Psi} - A(x) \int_{-\infty}^{\infty} B(x) \tilde{\psi} dx = \lambda \tilde{\psi}$$

is self-adjoint if and only if the operator $\mathcal{L}_0$ is self-adjoint, and $A(x) = cB(x)$ for some c independent of x. Since instead we have $w^2(\rho) \int_0^\infty \rho w(\rho) \tilde{\psi} d\rho$, our

NLEP is not self-adjoint. A further complication arises because the multiplier γ also depends on λ.

(ii) The local operator in (B.1) is defined by

$$\mathcal{L}_0\tilde{\psi} \equiv \Delta_\rho\tilde{\psi} - \tilde{\psi} + 2w\tilde{\psi}.$$

It is well-known that the local problem $\mathcal{L}_0\tilde{\psi} = \sigma\tilde{\psi}$ has a unique positive eigenvalue $\sigma_0 > 0$ with even eigenfunction $\tilde{\psi}_0 > 0$ (see [63]). Since the nonlocal term vanishes identically for eigenfunctions that are odd, hence reducing the NLEP to the local problem without nonlocal term, we need only consider the even eigenfunctions of (B.1).

Next, we will convert (B.1) into a transcendental equation in λ. We write (B.1) as

$$(\mathcal{L}_0 - \lambda)\tilde{\psi} - \gamma w^2 J = 0, \qquad \text{where } J \equiv \frac{\int_0^\infty \rho w\tilde{\psi} d\rho}{\int_0^\infty \rho w^2 d\rho},$$

This shows that $\tilde{\psi} = \gamma J(\mathcal{L}_0 - \lambda)^{-1}w^2$, and hence

$$J = \frac{\int_0^\infty \rho w\left(\gamma J[\mathcal{L}_0 - \lambda]^{-1}w^2\right) d\rho}{\int_0^\infty \rho w^2 d\rho} = \gamma J\frac{\int_0^\infty \rho w(\mathcal{L}_0 - \lambda)^{-1}w^2 d\rho}{\int_0^\infty \rho w^2 d\rho}.$$

We need only consider the eigenfunctions for which $J \neq 0$ (since if $J = 0$ the eigenfunctions of the local problem are well known). Therefore, we can cancel J in the equation above and obtain that λ is a root of $g(\lambda) = 0$, where

$$\begin{aligned} g(\lambda) &= \mathbf{C}(\lambda) - \mathcal{F}(\lambda), \\ \mathbf{C}(\lambda) = \frac{1}{\gamma(\lambda)}, &\qquad \mathcal{F}(\lambda) = \frac{\int_0^\infty \rho w(\mathcal{L}_0 - \lambda)^{-1}w^2 d\rho}{\int_0^\infty \rho w^2 d\rho}. \end{aligned} \tag{B.2}$$

In terms of the roots of $g(\lambda) = 0$, our stability criterion is as follows. We have instability if there exists λ with $\text{Re}(\lambda) > 0$ such that $g(\lambda) = 0$. We have stability

if for all roots of $g(\lambda) = 0$ we have $\text{Re}(\lambda) < 0$.

Theorem B.1 *Let λ be real. Then, the properties of $\mathcal{F}(\lambda)$ are as follows:*

- $\mathcal{F}(0) = 1,\ \mathcal{F} \to +\infty$ *as* $\lambda \to \sigma_0^-,\ \mathcal{F} \leq 0$ *for* $\lambda > \sigma_0$.
- $\mathcal{F}'(\lambda) > 0$ *for* $0 < \lambda < \sigma_0$. $\quad \mathcal{F} \to 0$ *as* $\lambda \to +\infty$.

Here $\sigma_0 > 0$ is the unique positive eigenvalue of the local problem $\mathcal{L}_0\tilde{\psi} = \sigma\tilde{\psi}$.

Proof

(i)

- Recall that $\mathcal{L}_0 w = w^2$. In other words, $\mathcal{L}_0 w = \Delta w - w + 2w^2 = w^2$. Thus,
$$\mathcal{F}(0) = \frac{\int_0^\infty \rho w \mathcal{L}_0^{-1} w^2 d\rho}{\int_0^\infty \rho w^2 d\rho} = \frac{\int_0^\infty \rho w(w) d\rho}{\int_0^\infty \rho w^2 d\rho} = 1.$$
- Now, $(\mathcal{L}_0 - \lambda)^{-1}$ does not exist at $\lambda = \sigma_0$ the unique positive eigenvalue of $\mathcal{L}_0$. Hence $(\mathcal{L}_0 - \lambda)^{-1}$ is unbounded at λ approaches σ_0.
$$\mathcal{F} \to +\infty \text{ as } \lambda \to \sigma_0^-; \qquad \mathcal{F} \to -\infty \text{ as } \lambda \to \sigma_0^+.$$
- The proof that $\mathcal{F} < 0$ for $\lambda > \sigma_0$ is more technical and is based on the following lemma:

  Lemma B.1 *Let $\xi(\rho)$ be a solution to*
  $$(\mathcal{L}_0 - \lambda)\xi = v, \qquad \text{on } 0 \leq \rho < \infty,$$
  with $\xi'(0) = 0$ and $\xi \to 0$ as $\rho \to \infty$. Assume that v is smooth, with $v > 0$ on $0 < \rho < \infty$, and $v \to 0$ as $\rho \to \infty$. Then if $\lambda > \sigma_0$ we have $\xi \leq 0$ for $\rho \geq 0$.

Proof Assume to the contrary that there exists $\rho_0 > 0$ with $\xi(\rho_0) > 0$. Then by continuity of ξ, $\xi(\rho) > 0$ on $\rho \in (\rho_1, \rho_2)$, with either

(i) $\xi(\rho_1) = \xi(\rho_2) = 0,\ \xi'(\rho_1) \geq 0,\ \xi'(\rho_2) \leq 0,\ \rho_1 < \rho_2$. Or

(ii) $\rho_1 = 0$ with $\xi(0) \geq 0,\ \xi'(0) = 0,\ \xi(\rho_2) = 0,\ \xi'(\rho_2) \leq 0$.

Let $\mathcal{L}_0\tilde{\psi}_0 = \sigma_0\tilde{\psi}_0$ with $\sigma_0 > 0$ and $\tilde{\psi}_0 > 0$ since it is the first eigenfunction. We then use Green's identity to ξ and $\tilde{\psi}_0$ on the subinterval $\rho_1 < \rho < \rho_2$ to get

$$\int_{\rho_1}^{\rho_2} \left(\tilde{\psi}_0\mathcal{L}_0\xi - \xi\mathcal{L}_0\tilde{\psi}_0\right)\rho d\rho = \rho\left(\tilde{\psi}_0\xi' - \xi\tilde{\psi}_0'\right)\Big|_{\rho_1}^{\rho_2},$$
$$\int_{\rho_1}^{\rho_2} \left(\rho\tilde{\psi}_0[\lambda\xi + v] - \rho\xi\sigma_0\tilde{\psi}_0\right)d\rho = \rho\tilde{\psi}_0\xi'\Big|_{\rho_1}^{\rho_2}.$$

Note that $-\rho\xi\tilde{\psi}_0'\Big|_{\rho_1}^{\rho_1} = 0$ in either (i) or (ii). This becomes

$$\int_{\rho_1}^{\rho_2} \rho\tilde{\psi}_0 v d\rho = (\sigma_0 - \lambda)\int_{\rho_1}^{\rho_2} \rho\tilde{\psi}_0\xi d\rho + \rho\tilde{\psi}_0\xi'\Big|_{\rho_1}^{\rho_2}.$$

We have that the first term is positive since both $\tilde{\psi}_0, v > 0$, whereas the second term is negative since $\lambda > \sigma_0$, and the third term is ≤ 0 by (i) and (ii). This is a contradiction, hence we conclude that $\xi < 0\ \forall\rho$. ∎

As a consequence,

$$\xi = (\mathcal{L}_0 - \lambda)^{-1}w^2 \leq 0 \quad \text{when } \lambda > \sigma_0,$$

which implies that

$$\mathcal{F}(\lambda) = \frac{\int_0^\infty \rho w\left[(\mathcal{L}_0 - \lambda)^{-1}w^2\right]d\rho}{\int_0^\infty \rho w^2 d\rho} < 0 \quad \text{for } \lambda > \sigma_0.$$

(ii) Now $\mathcal{F} \to 0$ as $\lambda \to \infty$ is evident since $(\mathcal{L}_0 - \lambda)^{-1} = O(\lambda^{-1})$ for $\lambda \gg 1$.

Next we use $\mathcal{L}_0 w = w^2$ to write

$$\begin{aligned}\mathcal{F}(\lambda) &= \frac{\int_0^\infty \rho w(\mathcal{L}_0-\lambda)^{-1}w^2 d\rho}{\int_0^\infty \rho w^2 d\rho} = \frac{\int_0^\infty \rho w(\mathcal{L}_0-\lambda)^{-1}\mathcal{L}_0 w d\rho}{\int_0^\infty \rho w^2 d\rho}, \\ &= \frac{\int_0^\infty \rho w(\mathcal{L}_0-\lambda)^{-1}\left[(\mathcal{L}_0-\lambda)w+\lambda w\right] d\rho}{\int_0^\infty \rho w^2 d\rho}, \\ &= \frac{\int_0^\infty \rho w\left(w+\lambda(\mathcal{L}_0-\lambda)^{-1}w\right) d\rho}{\int_0^\infty \rho w^2 d\rho} = 1+\lambda\left(\frac{\int_0^\infty \rho w\lambda(\mathcal{L}_0-\lambda)^{-1}w d\rho}{\int_0^\infty \rho w^2 d\rho}\right).\end{aligned}$$

From this last expression we can readily calculate $\mathcal{F}'(\lambda)$ as

$$\mathcal{F}'(\lambda) = \frac{\int_0^\infty \rho w(\mathcal{L}_0-\lambda)^{-1}w d\rho}{\int_0^\infty \rho w^2 d\rho} + \lambda\frac{\int_0^\infty \rho w(\mathcal{L}_0-\lambda)^{-2}w d\rho}{\int_0^\infty \rho w^2 d\rho}.$$

Then, we can integrate by parts on the second integral to obtain

$$\mathcal{F}'(\lambda) = \frac{\int_0^\infty \rho w(\mathcal{L}_0-\lambda)^{-1}w d\rho}{\int_0^\infty \rho w^2 d\rho} + \lambda\frac{\int_0^\infty \left((\mathcal{L}_0-\lambda)^{-1}w\right)\left((\mathcal{L}_0-\lambda)^{-1}w\right)\rho d\rho}{\int_0^\infty \rho w^2 d\rho},$$

so that

$$\mathcal{F}'(\lambda) = \frac{h(\lambda)}{\int_0^\infty \rho w^2 d\rho} + \lambda\frac{\int_0^\infty \left((\mathcal{L}_0-\lambda)^{-1}w\right)^2 \rho d\rho}{\int_0^\infty \rho w^2 d\rho}, \tag{B.3}$$

where $h(\lambda)$ is defined by $h(\lambda) \equiv \int_0^\infty \rho w(\mathcal{L}_0-\lambda)^{-1}w d\rho$. The second term in $\mathcal{F}'(\lambda)$ is positive for $\lambda > 0$. Therefore, in order to prove that $\mathcal{F}'(\lambda) > 0$ on $0 < \lambda < \sigma_0$ it suffices to prove that $h(\lambda) > 0$ on $0 < \lambda < \sigma_0$.

To establish the positivity of $h(\lambda)$ we will use a simple Calculus argument to show that $h(0) > 0$ and $h'(\lambda) > 0$ on $0 < \lambda < \sigma_0$. We first use the remarkable identity $\mathcal{L}_0^{-1}w = w + \frac{1}{2}\rho w'$ to show that $h(0) = \int_0^\infty \rho w\mathcal{L}_0^{-1}w d\rho > 0$. This identity is readily derived by the direct verification that $\mathcal{L}_0\left(w+\frac{1}{2}\rho w'\right) = w$. We calculate $h(0)$ as

$$h(0) = \int_0^\infty \rho w\left(w+\frac{1}{2}\rho w'\right) d\rho = \int_0^\infty \rho w^2 d\rho + \frac{1}{2}\int_0^\infty \rho^2(ww')d\rho.$$

To determine the sign of this quantity we use integration by parts to get

$$h(0) = \int_0^\infty \rho w^2 d\rho + \frac{1}{4}\int_0^\infty \rho^2 \frac{d}{d\rho}(w^2) d\rho,$$
$$= \int_0^\infty \rho w^2 d\rho + \frac{1}{4}\rho^2 w^2\Big|_0^\infty - \frac{1}{2}\int_0^\infty \rho w^2 d\rho = \frac{1}{2}\int_0^\infty \rho w^2 d\rho > 0.$$

This shows that $h(0) > 0$. Furthermore, we calculate that

$$h'(\lambda) = \int_0^\infty \rho w (\mathcal{L}_0 - \lambda)^{-2} w d\rho = \int_0^\infty \rho \left[(\mathcal{L}_0 - \lambda)^{-1} w\right]^2 d\rho > 0.$$

In addition, $h(\lambda) \to +\infty$ as $\lambda \to \sigma_0^-$. Hence $h(\lambda) > 0$ on $0 < \lambda < \sigma_0$.

Thus, by (B.3), $\mathcal{F}'(\lambda) > 0$ on $0 < \lambda < \sigma_0$. This concludes the proof. ∎

Next, we return to (B.2). We conclude that if $\mathbf{C}(0) > 1$ and $\mathbf{C}$ is analytic in $Re(\lambda) \geq 0$, then the curves $\mathbf{C}(\lambda)$ and $\mathcal{F}(\lambda)$ must cross at some $\lambda > 0$ real on the interval $0 < \lambda < \sigma_0$.

Theorem B.2 *Suppose* $\mathbf{C}(0) > 1$, $\mathbf{C}(\lambda)$ *is analytic in* $Re(\lambda) \geq 0$. *Then there exists an unstable eigenvalue to the NLEP in* $Re(\lambda) > 0$.

Implication Suppose that $\gamma(0) < 1$. Then there exists an unstable eigenvalue on $0 < \lambda < \sigma_0$ that is real. This is precisely the criterion that was used in establishing the principal result (2.110) of §2.5.1.

For instance, consider the competition instability threshold studied in §2.5.1. Then, from (2.108)

$$\gamma(\lambda) = \frac{2[f - (\lambda + 1)]}{f - (\lambda + 1)(1 + \varphi \mathcal{D}_0)}.$$

We calculate

$$\gamma(0) = \frac{2(f-1)}{f-(1-\varphi\mathcal{D}_0)}.$$

Our rigorous result above shows that if $\gamma(0) < 1$ then we have an unstable real eigenvalue. Thus, we obtain such an instability when (see (2.110) of §(2.5.1))

$$\mathcal{D}_0 > \mathcal{D}_{0c} \equiv \frac{4f^2}{N^2(1-f)b}.$$

It is much more difficult to prove the converse, namely that we have stability for the competition modes when $\mathcal{D}_0 < \mathcal{D}_{0c}$. Although we anticipate that such a result is true based on our full numerical simulations of the Brusselator model, we have been unable to prove it from the NLEP. The technical difficulty with completing a rigorous proof is that one must track all the complex eigenvalues of the NLEP. We recall that if γ was a constant, independent of λ, and that $\gamma > 1$, then such a stability proof was given in [63]).